Studies on Stereocomplex Poly(lactic acid) and its Biocomposites

Thesis submitted in the partial fulfilment of the requirements for the degree of

DOCTOR OF PHILOSOPHY

by

Arvind Gupta

(Roll No. 11610713)

Department of Chemical Engineering
Indian Institute of Technology Guwahati
Guwahati-781039, Assam, India

May, 2017

INDIAN INSTITUTE OF TECHNOLOGY GUWAHATI

Guwahati-781039, Assam, India

Department of Chemical Engineering

STATEMENT

This is to certify that the research work in the thesis entitled "**Studies on Stereocomplex Poly(lactic acid) and its Biocomposites**", is carried out by me at CoE-SusPol laboratory, Department of Chemical Engineering, Indian Institute of Technology Guwahati, under the supervision of **Dr. Vimal Katiyar**. The results documented in this thesis achieved by me are reproducible and have not been submitted to any other University or Institute for the award of any degree or diploma.

Arvind Gupta

Roll No. 11610713
Department of Chemical Engineering
Indian Institute of Technology Guwahati
Guwahati-781039, Assam, India.

Guwahati, May 2017.

Dr. Vimal Katiyar

Associate Professor
Department of Chemical Engineering
Indian Institute of Technology Guwahati
Guwahati-781039, Assam, India
Tel: +91-361-258-2278;
Email: vkatiyar@iitg.ernet.in

CERTIFICATE

This is to certify that the thesis entitled "**Studies on Stereocomplex Poly(lactic acid) and its Biocomposites**", submitted by **Mr. Arvind Gupta** for the award of Ph.D. degree has been carried out by him at CoE-SusPol, Department of Chemical Engineering, Indian Institute of Technology Guwahati under my supervision. The work documented in this thesis has not been submitted to any other University or Institute for the award of any degree or diploma.

Guwahati
May, 2017

Dr. Vimal Katiyar
Thesis Supervisor

Dedicated

To

My Family

Acknowledgement

I sincerely express my deepest sense of gratitude to my learned mentor and thesis supervisor Dr. Vimal Katiyar for his valuable guidance and advice throughout my whole research period. He is an embodiment of knowledge, tolerance and perseverance. His true scientific spirit, independence and self-reliance has helped me immensely to develop the quality of my research work. I am extremely fortunate to be involved in a challenging research work assigned by him. It has enriched my life. This work enhanced my thinking abilities and understanding capability. I experienced a feeling of self-satisfaction after completion of my work. Without his continual guidance, this would not have been materialized. I shall remain grateful to him forever.

I would also like to thank my doctoral committee members Professor Parameswar Krishnan Iyer, Dr. Amit Kumar, Dr. Vaibhav V. Goud, and Dr. Anil Varma for their valuable suggestions, comments, encouragement and valuable criticism during all assessments of my Ph.D. programme. I would like to place on record the use of facilities and sophisticated instruments available at Centre of Excellence for Sustainable Polymers (CoE-SusPol) and Central Instruments Facility (CIF), IIT Guwahati for carrying out instrumental analysis part of my research work. I would also like to thank the head and all the authorities of the Department of Chemical Engineering for providing me all research and analytical facilities required for my work. I am extremely thankful to the technical staff (teaching and non-teaching) of the chemical engineering department, particularly Ritumoni Kalita, Harsaraj Biswanath, Dipak Kumar Barman, Jayanta Kumar Mout, Dr. Lukumoni Borah, Debajit Borah, Pankaj Sekhar Baruah, Deep Jyoti Sinha, Sailen Das, Kaustavmoni Deka, Prasun Kumar Bhattacharjee and Bhagya Boro for providing me all help and assistance for the completion of my work.

I express my sincere thanks to Professor E. M. Woo at Department of Chemical Engineering, National Cheng Kung University, Tainan, Taiwan for allowing me to work and learn in his laboratory. I am also thankful to Mr. Yahya Happy Mandela, Dr. Graecia Lugito and Miss Clara (Wan-Ting) for their help during my stay in NCKU Taiwan.

I am thankful to the Ecole Polytechnique Federale De Lausanne (EPFL) Switzerland, Venturelab, Switzerland, Society of Innovation and Entrepreneurship (SINE) hosted by Indian Institute of Technology Bombay and Department of Science and Technology (DST) Government of India for selecting me as one of the ten Indian participants for Academia-Industry Training (AIT) program conducted at Bangalore, India and Lausanne and Zurich, Switzerland and providing me the funding.

I thank Mr. Arbind Prasad for providing me hydroxyapatite and Mr. Akhilesh Kumar Pal for helping me with characterization (TEM and FTIR) of modified chitosan which aided me conduct a part of my research successfully.

I owe my sincere gratitude to Dr. Neelima Tripathi, Dr. Rashmi Rekha Devi, Akhilesh Kumar Pal, Umesh Bhardwaj, Surendra Singh Gaur, Phani Kumar Pentyala, Rahul Patwa, Prodyut Dhar, Gourhari Chakraborty, Medha Mili, Monika, Narendren S., Shasanka Sekhar Borkotoky, Melakuu Tesfaye, Siddhartha Mohan Bhasney, Anup Ashok, Sai Phani Kumar, Dr. Dhruba J. Haloi, Dr. Purabi Bhagabati, Dr. Valapa Ravi Babu, Naba Kumar Kalita, Debashis Tarafdar, Ananya Das, Amit Pandey, Tabli Ghosh, Neha Mulchandani, Parmita Roy, Hena Nasir, Arbind Prasad, Kiran Kumar Gali, Khalid Wani, Unnikrishnan TG, for helping me in every way they could and for making the past couple of years more delightful along with their moral support in the laboratory. I wish to place on record, my thankfulness to my friends Dr. Jay Bhasarkar, Rahul Ramteke, Rupak Kishor for their presence in my life.

Finally, I would like to convey my sincere gratitude to my family members for their sustained help and encouragement in my all academic ventures. I feel deeply indebted to them for whatever I have achieved so far.

Arvind Gupta

Abstract

The current scenario of the world indicates that the consumption of plastics has constantly intensified and laid an impact on the society. However, the disposal of plastics is the prevailing issue of the world which has persuaded the researchers to develop alternatives for a sustainable future. Poly(lactic acid) (PLA) is a biobased plastic which can be considered as promising candidate for replacing petroleum based plastics such as polyethylene, polypropylene, polyethylene terephthalate, etc. PLA has been widely explored by the researchers for its unique characteristics such as the ability to be modified according to the intended applications, its biodegradability and ease in processability. PLA has been explored for its applications ranging from biomedical to textiles, agriculture, electronics, and packaging etc. but suffers from some drawbacks such as relatively low glass transition temperature, low heat deflection temperature, lower melting temperature, slow crystallization, lower melt elasticity and relatively poor gas barrier properties. Enhancing the properties of PLA is a major challenge and several methods such as fabricating biocomposite, polymer blending or formation of stereocomplex, etc. have been adopted by the researchers to improve the properties of PLA.

PLA can be synthesized by polymerization of lactic acid or its derivative i.e. lactide. Lactic acid is a chiral molecule produced in the form of L-lactic acid, D-lactic acid or racemic lactic acid based on the fermentation reaction pathway. It is desired to produce high molecular weight PLA for several applications which is predominantly produced by ring opening polymerization (ROP) of lactide and the purity of lactide affects the molecular weight of the polymer.

Mixing poly(L-lactic acid) (PLLA) and poly(D-lactic acid) (PDLA) in different ratios, a specific type of polymorph called stereocomplex crystallite is formed which significantly enhances the melting temperature of PLA. Formation of stereocomplex crystallites are also responsible for the enhancement of barrier, mechanical and thermal properties. It has also been reported that low molecular weight PLLA and PDLA in 1:1 ratio can easily form stereocomplex crystallites. In case of high molecular weight i.e. more than 100 kDa, homocrystallites form along with stereocomplex crystallites which lead to the relatively poor physical properties of end product. Therefore, it is essential to have high content of stereocomplex crystallites to improve the properties without compromising the molecular weight of the end product.

The present doctoral work demonstrates the effort to develop a novel process for the production of stereocomplex PLA with high content of stereocomplex crystallites and its characterization. Different biomaterials such as cellulose microcrystals, chitosan and hydroxyapatite have been modified by grafting with PLA chains via *in situ* ring opening polymerization of lactide and utilized for the development of high molecular weight stereocomplex poly(lactic acid) biocomposites. The grafting of the fillers allows it to be easily dispersed into the polymer matrix which significantly enhances the molecular contact surface area which in turn increases the stereocomplexation as well as the properties of the end product.

The utilized biomaterial fillers in the current work have their own diverse properties. Use of cellulose as a filler into the polymer matrix is effective for improving several properties. Cellulose contains large number of hydroxyl groups, present in its molecular structure and surface. Similarly, chitosan is one of the promising materials, which has good oxygen barrier properties, biodegradability and nontoxic nature along with its biocompatibility and antibacterial activity. However, due to its hydrophilic nature, its usage in packaging and

engineering applications is limited. Furthermore, hydroxyapatite is a bioactive nontoxic complex form of calcium phosphate which has 60-70% content of mammalian bones. Due to its similarity with mammalian hard tissues, HAP is one of the most investigated synthetic biomaterial.

In this thesis, the production of monomer i.e. lactide, its purification and characterization have been discussed. The purification process has been developed to produce highly purified lactide which results in the production of high molecular weight PLA via ROP. The modification of biomaterials via *in situ* ROP and their use in the production of high molecular weight stereocomplex PLA biocomposites are discussed in detail. The successful modification of the biofillers has been carried out and their presence in the PLA matrix has significantly improved the content of stereocomplex crystallites which in turn significantly enhance the properties of biocomposites. Improvement in the properties such as gas barrier, thermomechanical and thermal properties could be achieved by enhancing the stereocomplexation in the matrix which may be the result of uniform dispersion of the filler. From the processing point of view, a detailed crystallization kinetics and thermal degradation kinetics of the stereocomplex PLA and it biocomposite have been discussed.

This thesis is organized in ten chapters as follows:

In the first and second chapter, the necessity of biobased polymers for the current society and the evolution of biobased polymers have been narrated. Different processes and technologies for the development of Poly(lactic acid) (PLA) are discussed. Literature review focusing the development of PLA and its stereocomplexation is condensed in this chapter.

Third chapter demonstrated the development of precursor i.e. lactide and the process for the synthesis of stereospecific PLA. The synthesis and purification of lactide is discussed

and process development and optimization is executed. Syntheses of enantiomeric PLA i.e. poly(L-lactic acid) (PLLA) and poly(D-lactic acid) (PDLA) are carried out with characterization.

Uniform dispersion of the filler in polymer matrix is always a challenging task towards the preparation of optimum composites. In this context, in the fourth chapter, a novel attempt has been made to improve the dispersion of cellulose microcrystals (CMC) in the PLA matrix. *In situ* polymerization of lactide has been carried out and PLA-CMC biocomposite has been developed. Processes for the fabrication and characterization of stereocomplex PLA biocomposite is discussed in this chapter in detail.

The fifth chapter unfolds the chemical modification of chitosan and its use as a filler in the development of stereocomplex PLA. The fabrication technique to produce modified chitosan (MCH), its characterization and effect on stereocomplex content of PLA is discussed.

As hydroxyapatite (HAP) is a naturally occurring mineral which is bioactive and nontoxic in nature, it can be explored for its use in the biomedical application. The sixth chapter highlights the grafting of HAP with PLA chains wherein HAP is uniformly distributed into the PLA matrix which ultimately improves the properties of PLA and its stereocomplexation. The process of grafting, characterization and fabrication of stereocomplex PLA and its characterization are summarized in this chapter.

As stereocomplexation is a crystalline phase formed by the interaction of PLLA and PDLA chains which is affected by the presence of fillers into the matrix, the effect of fillers on the crystallization behavior of PLA is discussed and detail analysis has been performed in seventh chapter.

Presence of fillers into the PLA matrix affects the formation of stereocomplex crystallites which ultimately affects the degradation behavior of final product. Effect of different fillers such as CMC, MCH and HAP on the degradation behavior of stereocomplex PLA is discussed in eighth chapter.

The applications of developed biomaterials have been demonstrated in the ninth chapter. 3D printed gears and finger bone have been developed by processing the developed biocomposites. Further, cell culture experiments support the biocompatible nature of the fabricated biocomposites.

Tenth chapter highlights the major conclusions drawn from the present doctoral work along with the scope for future studies.

Contents

List of Figures

List of Tables

List of Abbreviations

Abbreviations

3D	three dimensional
c.a.	approximately
PHB	Poly(3-hydroxybutyrate)
PLA	Poly(lactic acid)
PP	Polypropylene
PE	Polyethylene
PET	Polyethylene terephthalate
PBS	Polybutylene succinate
PLLA	Poly(L-lactic acid)
PDLA	Poly(D-lactic acid) (PDLA)
CMC	Cellulose microcrystals
HAP	Hydroxyapatite
MCH	Modified Chitosan
ROP	Ring opening polymerization
LbL	Layer by layer
PEI	Polyethyleneimine
NFC	Nanofibrillated cellulose
MMT	Montmorillonite
HHIC	Hyperthermal hydrogen-induced cross-linking
UV	Ultraviolet
SC	Stereocomplex
sPLA	stereocomplex PLA
T_m	Melting temperature
HDT	Heat deflection temperature
GO	Graphene oxide
NMR	Nuclear magnetic resonance
DSC	Differential scanning calorimetry
XRD	X-ray diffraction

Abbreviations

HFIP	Hexafluoroisopropanol
PVPh	Poly(4-vinyl phenol)
PEG	Poly(ethylene glycol)
PPZn	Zinc phenylphosphonate
FESEM	Field emission scanning electron microscopy
POM	Polarizing optical microscopy
TEM	Transmission electron microscopy
AFM	Atomic force microscopy
FTIR	Fortier transform infrared
KBr	Potassium bromide
$CDCl_3$	Deuterated chloroform
TGA	Thermogravimetric analysis
MS	Mass spectroscopy
UTM	Universal testing machine
ASTM	American Society for Testing and Materials
DMA	Dynamic mechanical analyser
OTR	Oxygen transmission rate
WVTR	Water vapour transmission rate
CA	Contact angle
OP	Optical polarimeter
GPC	Gel permeation chromatography
HPLC	High performance liquid chromatography
MW	Molecular weight
CP	Condensation polymerization
SSP	Solid state polymerization
N_2	Nitrogen
SnO	Tin oxide
^{1}H-NMR	Poroton-Nuclear magnetic resonance
PDI	Polydispersity index
Da	Dalton
ppm	Parts per million

Abbreviations

PDLA-g-CMC	Poly(D-lactic acid) grafted cellulose microcrystals
PTFE	Polytetrafluoroethylene
RH	Relative humidity
T_g	Glass transition temperature
HDT	Heat deflection temperature
LA	Lactic acid
CH	Chitosan
WAXD	Wide angle X-ray diffraction
PMMA	Poly(methyl methacrylate)
HCl	Hydrochloric acid
NaOH	Sodium hydroxide
rpm	Revolutions per minute
EDX	Energy dispersive X-ray spectroscopy
RH	Relative humidity
ΔG	Gibbs free energy
OWF	Ozawa-Flynn-Wall
KAS	Kissinger-Akahira-Sunose

CHAPTER: 1

Introduction

1.1 Introduction

The materials that emerged as long chain macromolecules (polymers) have made their unavoidable presence in the day-to-day activities of human beings. Due to the desired properties such as lightweight, transparency, flexibility, low cost, durability, mechanically strong etc., plastics are now a part of human lifestyle [1]. Plastic has laid its foundation in applications ranging from household to aerospace, packaging to textiles to 3D printing, automobile, healthcare, electronics, biomedical etc. [2]. Plastics are an inseparable part of human life and therefore the present era can be considered to be as "plastic era." These long chain molecules have influenced the development and progress of our society since their inception and aided in solving the social and engineering issues. Approximately, more than 300 million tons of plastic is produced every year worldwide as shown in Figure 1, of which ~9 million tonnes is manufactured in India and it is estimated that the worldwide production may cross 400 million tons by 2050 [3]. For developing countries like India, plastic industries play a vital role in the employment and economic growth of the nation. It is notified by different agencies that approximately 60% of the produced plastic is discarded as waste after use. Although, this plastic waste is reused and recycled, a large amount of it goes for either landfill or incineration [4]. As a consequence, it adds to the carbon footprint as it leads to the generation of environment pollutants along with making us dependent on the petroleum [5]. According to an article published in "*theguardian"* in January 2016 by "Ellen MacArthur" the weight of plastics present as waste in the ocean will overshoot the weight of entire fish present in the ocean by 2050 [6]. Due to such alarming issues, it is the need of the hour to develop alternatives such as biobased plastics for a sustainable and environment friendly planet. The biobased polymers derived from biomass or obtained from the derivatives of biomass which can be processed to finished products are known as biobased plastics [7]. Several biobased polymers such as starch, cellulose or protein based

polymers, poly(3-hydroxybutyrate) (PHB), poly(lactic acid) (PLA), bio-PP, bio-PE, bio-PET, polybutylene succinate (PBS) etc. are commercially available [8]. The varying biomass content in these polymers is responsible for their biodegradability. Among the various biodegradable polymers, PLA has been studied widely by the researchers as it finds its origin in natural materials like corn starch, sugarcane, tapioca roots and the ability to tune its properties according to the desired application.

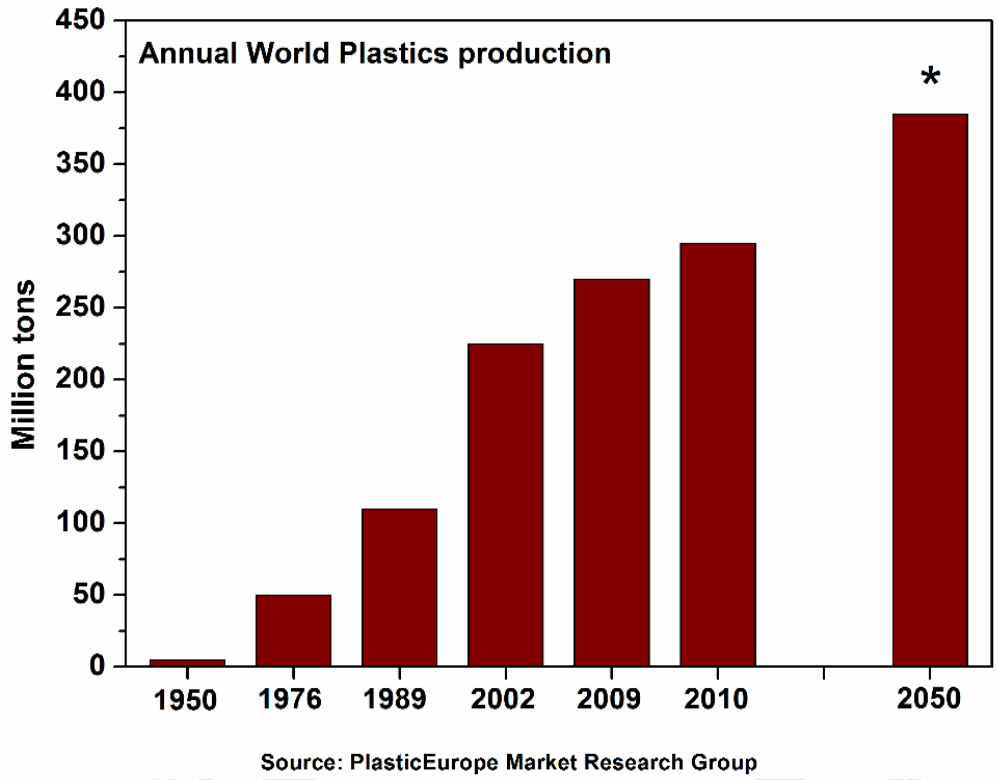

Figure 1.1: Trend for annual plastic production in the world (*Extrapolated data).

PLA is known to have wide number of applications ranging from food packaging to biomedical which exhibits the significance of the material and its impact on the society. However, PLA has some drawbacks such as poor gas barrier properties, low thermomechanical strength, low glass transition temperature which can be enhanced by forming stereocomplex of PLA. Stereocomplexation significantly enhances the gas barrier, thermal and mechanical properties of PLA which allows it to be explored for commercial

applications. The present work aims at developing a biocomposite by *in situ* modification of the fillers such as cellulose, chitosan and hydroxyapatite which leads to the formation of high molecular weight PLA which overcomes the limitation of parent polymer and imparts high mechanical strength which can be explored for several applications. The developed biocomposites are characterized using various techniques to identify the thermal, mechanical, morphological, gas barrier, optical properties so as to use them in the relevant applications. A detailed study of the synthesis of polymer, *in situ* grafting of filler, development of biocomposite and necessary characterization techniques have been reported in the present thesis which gives an essence of the polymer processing, chemistry, degradability and its relevance in the current society.

1.2 Motivation

Biobased and biodegradable polymers are the near future of the polymer industry as they have the properties comparable to that of conventional polymers, though the cost of the production needs to be reduced to make them viable to replace fossil based polymers which are depleting day by day. By ignoring few inherent limitations, poly(lactic acid) is the potential candidate among these biobased polymers. The stereocomplexation is a relatively new area by which properties of PLA can be improved. Extensive research is going on worldwide to overcome these limitations which can be confirmed by the ever increasing published research articles every year as shown in **Figure 1.2** (Scopus Search) **[9]**.

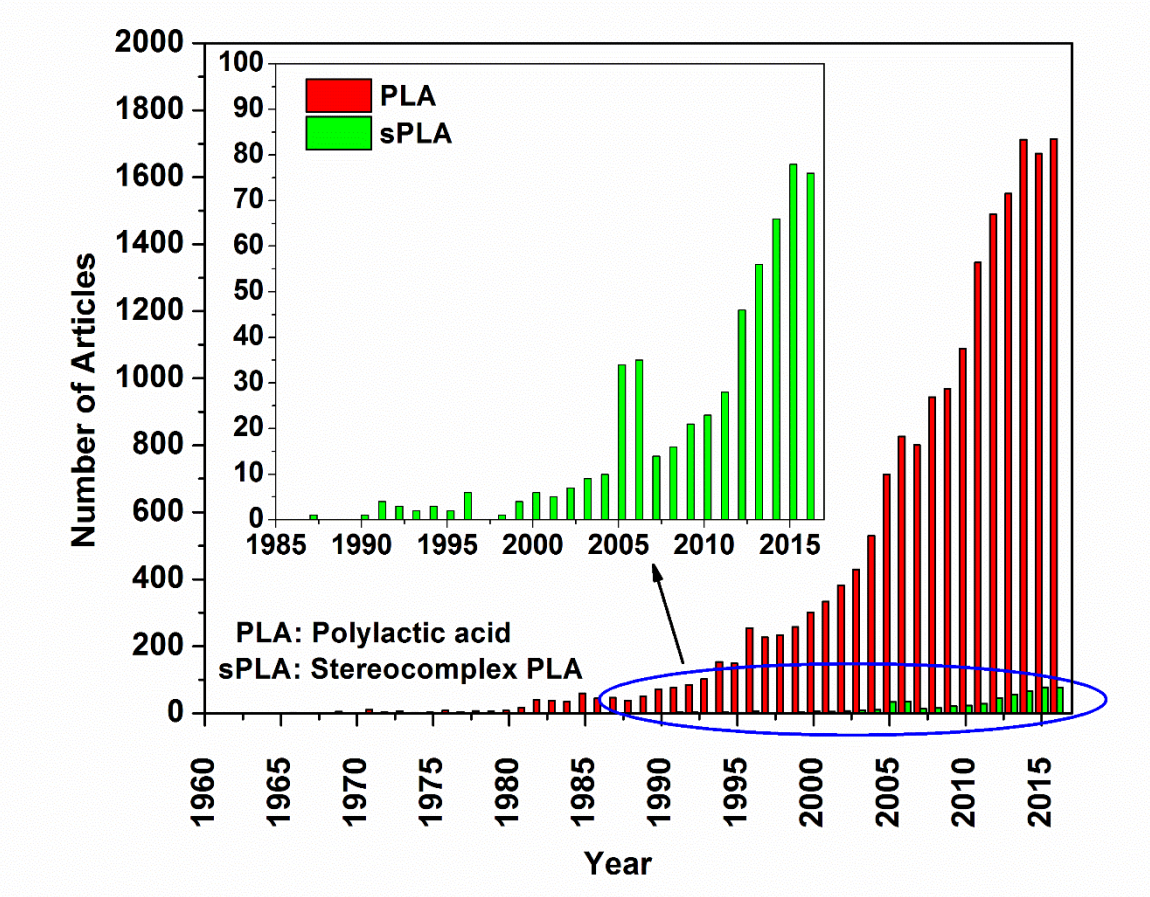

Figure 1.2: Data for the published articles on poly(lactic acid) (PLA) and stereocomplex poly(lactic acid) (sPLA).

It is certainly confirmed from the research carried out by the scientific community that the use of biobased polymers affects the society and environment where we live. This social and environmental impact by the use of biobased polymers motivates us to find the ways to improve the properties of PLA and contribute to the scientific community in the form of technology for the betterment of biobased polymers in order to increase the usefulness for the mankind.

1.3 Organization of Thesis

Chapter 2: Literature review

In this chapter, we discuss that why biobased polymers are the necessity for current society and the evolution of biobased polymers. Different processes and technologies for the development of poly(lactic acid) (PLA) are discussed. Progress in the development of PLA and its stereocomplexation is condensed in this chapter.

Chapter 3: Development of precursors and process for synthesis of stereospecific PLA

Basic ingredient of PLA synthesis is the precursor i.e. lactide. In this chapter, the synthesis and purification of lactide is discussed and process development and some optimization of the process conditions is done. Synthesis of stereospecific PLA i.e. poly(L-lactic acid) (PLLA) and poly(D-lactic acid) (PDLA) is carrier out with its characterization.

Chapter 4: Synthesis and characterization of stereocomplex PLA cellulose microcrystal biocomposite

A novel attempt has been done in order to improve the dispersion of cellulose microcrystals (CMC) in the PLA matrix. *In situ* polymerization of lactide has been carried out and developed the PLA-CMC biocomposite. Processes for the fabrication and characterization of stereocomplex PLA biocomposite is discussed in this chapter in detail.

Chapter 5: Effect of modified chitosan on the properties of stereocomplex PLA

Chitosan is known for having good barrier properties, however, it is a hydrophilic polymer which hinders its use in engineering application. The chitosan is chemically modified and used as filler in the production of stereocomplex PLA. The fabrication technique, characterization and its effect on stereocomplex content of PLA is discussed in this chapter.

Chapter 6: Fabrication and characterization of stereocomplex PLA-hydroxyapatite biocomposite

As hydroxyapatite (HAP) is naturally occurring mineral which is bioactive and nontoxic in nature could be used for the biomedical application. The grafting of the HAP molecules with PLA chains make HAP distributed into the PLA matrix which ultimately improves the properties of PLA and its stereocomplexation. The process of grafting, characterization and fabrication of stereocomplex PLA and its characterization is condensed in this chapter.

Chapter 7: Comparative crystallization kinetics of stereocomplex PLA and its biocomposite

Stereocomplexation is a crystalline phase formed by interaction of PLLA and PDLA chains which is affected by the presence of fillers into the matrix. The effect of fillers on the crystallization behaviour of PLA is discussed and detail analysis is done in this chapter.

Chapter 8: Comparative degradation studies of stereocomplex PLA its biocomposites

Presence of fillers into the PLA matrix affects the formation of stereocomplex crystallites which ultimately affect the degradation behaviour of final product. Effect of different fillers such as CMC, MCH and HAP on the degradation behaviour of stereocomplex PLA is discussed in this chapter.

Chapter 9: Application of Fabricated Stereocomplex PLA Biocomposites

The applications of developed biomaterials have been demonstrated in the ninth chapter. 3D printed gears and finger bone have been developed by processing of the developed biocomposites. Further, cell culture experiments support the biocompatible nature of the fabricated biocomposites.

Chapter 10: Conclusions and future scope

This chapter summarizes the research work carried out and presents an outlook for future studies.

CHAPTER: 2

Literature Review

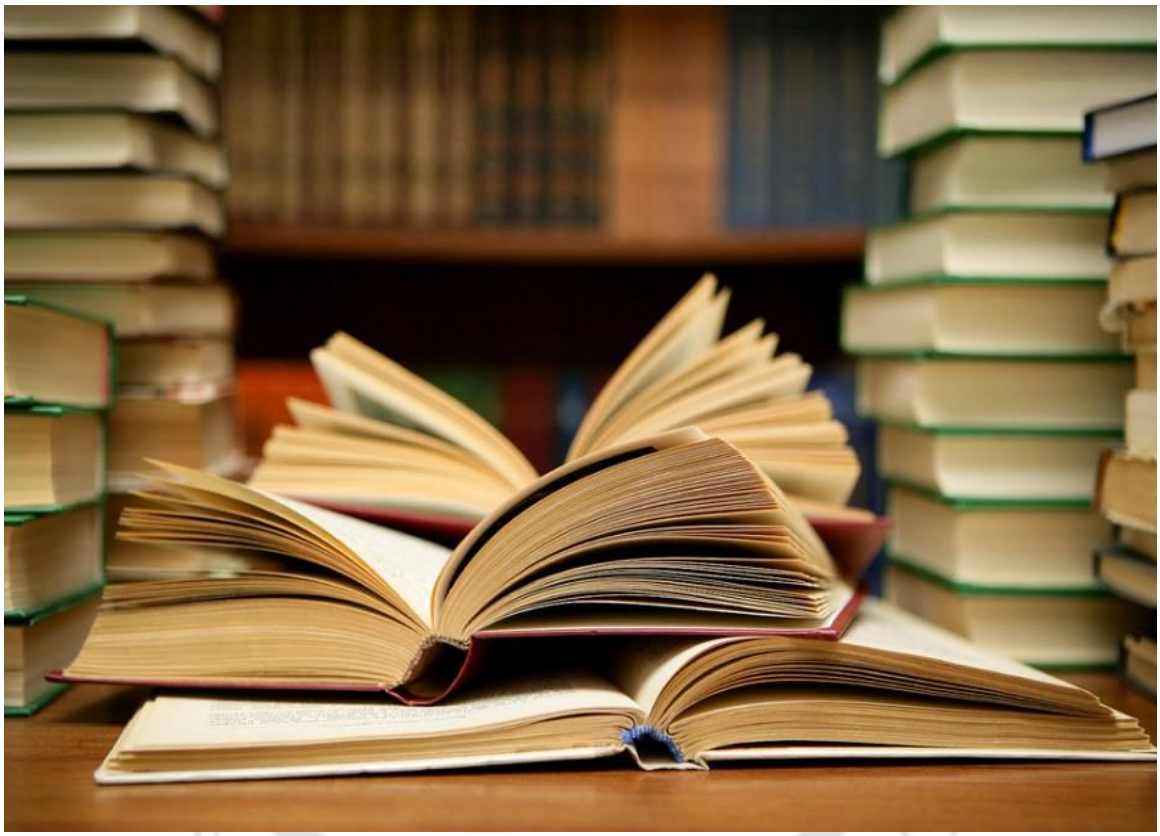

2.1 General Introduction

Plastics have surrounded the mankind in such a way that it is extremely difficult to imagine our life without the use of them. The per capita consumption of plastics in India is 9.7 kg as compared to that of United States of America (USA) which is 109 kg and the current plastic consumption in India is approximately 8 million tonnes which is estimated to be increased to 20 million tonnes by 2020 [10]. The demand breakup of plastics by their types is given in **Figure 2.1** wherein the demand of polypropylene (PP) and polyethylene (PE) is 67% and these commonly used materials along with polyethylene terephthalate (PET) contribute to 79% in flexible packaging applications [10]. Such huge demand of these commercial plastics are evident of the massive growth potential of plastic industries in India and biobased plastics have been proved to be the potential candidates to replace these plastics for, mainly for packaging applications.

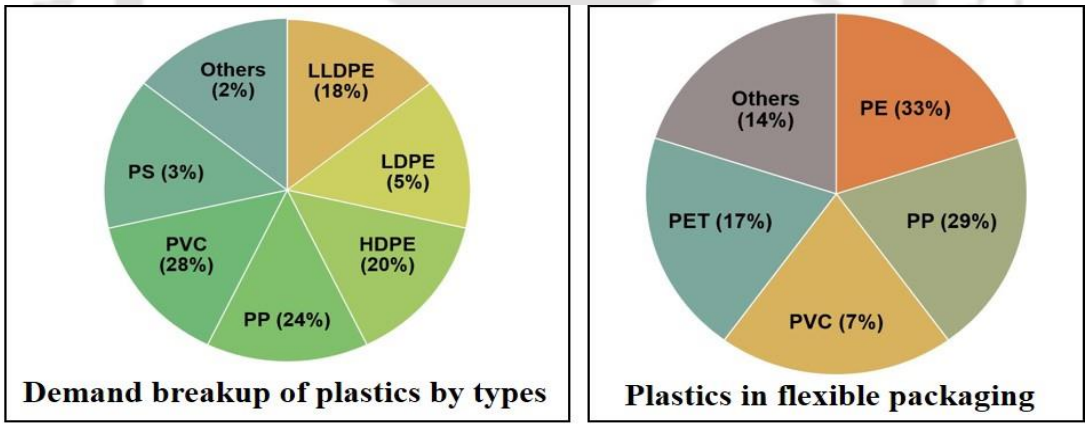

Figure 2.1: Demand breakup of plastics by type and share in flexible packaging.

2.2 Bioplastics

The potential of biobased polymers in various applications have been constantly explored by the researchers. A market survey on biobased polymers was conducted by *Nova Institute for Ecology and Innovation Germany* which reported that, in 2011, approximately 3.5

million tonnes of biobased polymers are produced by 247 companies worldwide which was equivalent to 1.5% of total production of all type of polymers and it is expected that to increase up to 12 million tonnes by 2020 [11]. It is also reported that major industries around the world will invest their capital in Asia and South America due to better access to feedstock and favourable political framework and Asia will have ~55% share of it. Among 247 companies, 25 companies are producing more than 180,000 tonnes per year of biobased material PLA at 30 locations worldwide which is predicted to increase to 800,000 tonnes per year by 2020 (**Figure 2.2**) [11]. These investigations indicate that the production of PLA in a developing country like India will be increase significantly in near future. As per the prior art available, PLA is the most promising candidate to replace the petroleum based polymers. The polymers such as starch, cellulose, chitosan, gums are hydrophilic in nature which limits their use in packaging applications. PLA being the most widely studied biobased polymer can fill the gap for the packaging industry.

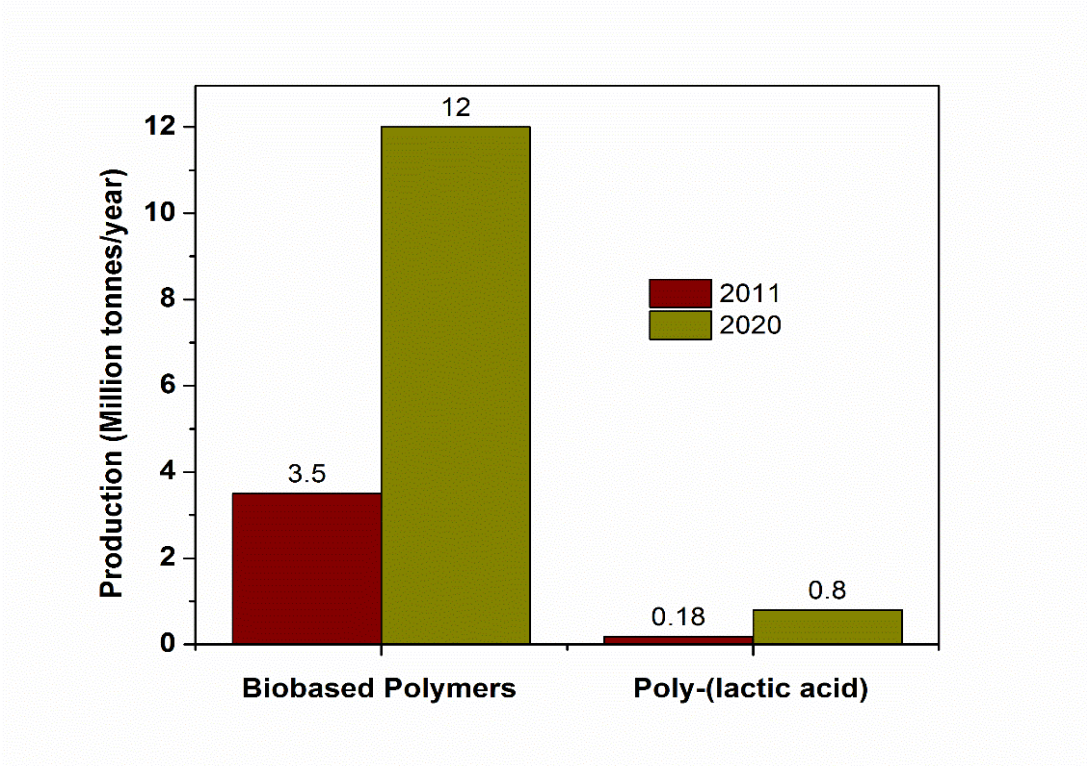

Figure 2.2: Production of biobased polymers and PLA worldwide [11]

PLA is known to be a biodegradable, bioabsorbable, nontoxic, biocompostable polymer, produced by the polymerization of monomer lactic acid which is derived from the plants such as sugar cane, cassava, potato etc. and after its use, can decompose into nontoxic content by composting. Recent developments indicate that PLA is a potential candidate which can replace petroleum based polymers such as PP, PE, and PET. PLA is having 100% biobased content and its properties can be tuned according to the application. General life cycle of PLA is shown in **Figure 2.3**. PLA is synthesized either from lactide or lactic acid which can be produced by fermentation of biomaterials. The subsequent sections will focus on the history and production of lactic acid, lactide and PLA.

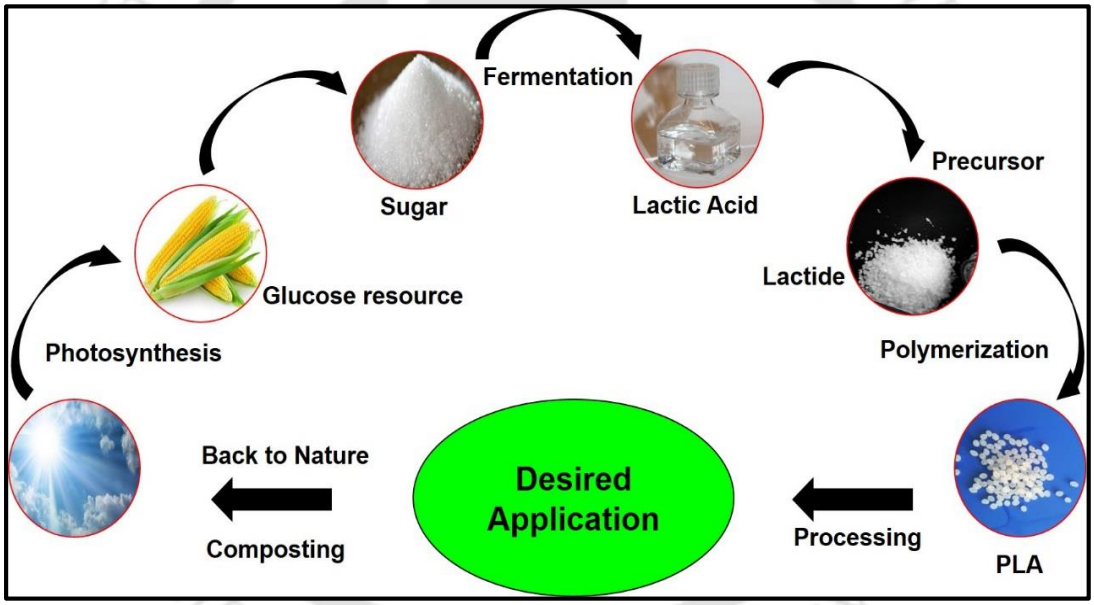

Figure 2.3: Life cycle of poly(lactic acid) [12].

2.3 Poly(lactic acid)

PLA due to its renewable and biodegradable nature is widely substituting various fossil based plastics in a wide variety of applications. Due to its tuneable biodegradability, nontoxicity and biocompatibility, PLA is very widely used in various biomedical applications such as drug delivery, orthopaedic fixation devices, tissue engineering as

scaffolds, etc. PLA and its copolymers are also being used to prepare a range of biomedical devices such as surgical sutures, healing dental wounds, etc. Nowadays, the potential of PLA is also being explored in packaging industries, especially food packaging applications, biodegradable and compostable disposable cups for cold beverages, mugs, etc. Its unique physical properties also make it useful in diverse applications including paper coating, fibres, and films. PLA can also be used in textile industries as woven and non-woven fabrics. Recently, PLA has been also used in 3D printing. Among all the biobased polymers, PLA is the most promising candidate which can replace the conventional polymers [13]. The biggest advantage of PLA is that, after service life, it can go back to the environment in the form of carbon dioxide, methane and water over a period of several months to few years, whereas, other petroleum based polymers take hundreds of year to degrade and go back to the nature [14]. The basic constituent for PLA synthesis is lactic acid which can be produced by fermentation of biomaterial or sugar [15]. In the eighteen century, Swedish chemist Carl Wilhelm Scheele reported the isolation of lactic acid from sour milk [16]. Lactic acid is a chiral molecule which exists in two optical isomeric forms named as L-lactic acid (laevorotatory) and D-lactic acid (dextrorotatory) while the mixture of these two called racemic lactic acid or D,L-lactic acid [17] (**figure 5**).

PLA can be produced using several polymerization techniques such as condensation polymerization, ring opening polymerization (ROP), azeotropic dehydrative condensation polymerization and solid state polymerization [18]. The condensation polymerization and ring opening polymerization are the techniques which are mainly used for the production of high molecular weight PLA [19]. Using condensation polymerization, high molecular weight PLA can be produced after solid state polymerization but it has the limitations of time and energy consumption [20-22]. ROP is the technique which produces high

molecular weight PLA in relatively less time. Lactide is the precursor of ROP which is a dimer of lactic acid as shown in **Figure 2.4** [23].

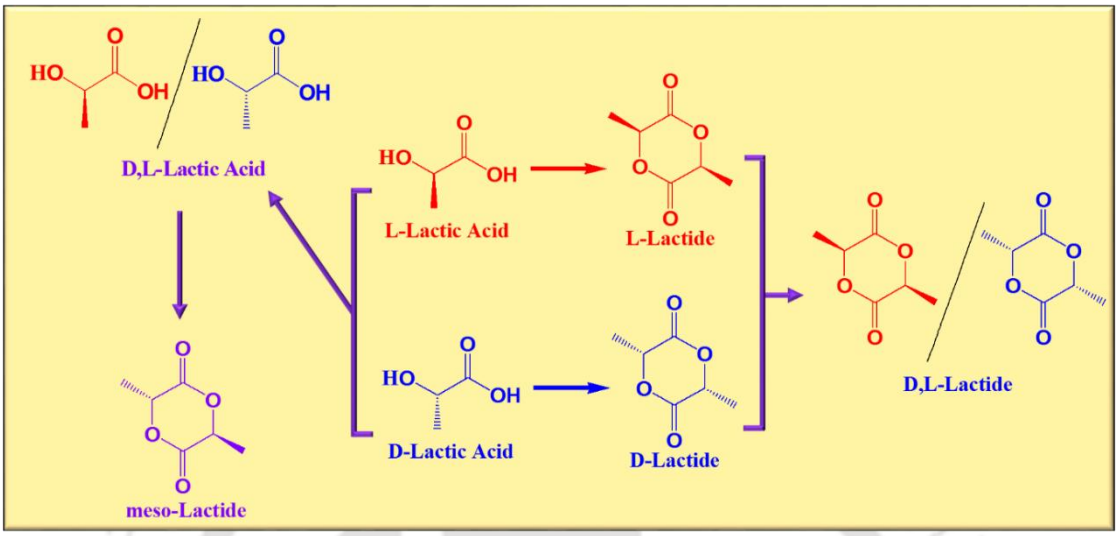

Figure 2.4: Isomers of lactic acid and corresponding lactide.

The process for lactide synthesis was first patented in 1913 by Reinhold Gruter [24] and in 1932, ROP of lactide was reported by Wallace H. Carothers [25]. Earlier, due to the instability in humid condition, PLA was considered to be an undesirable material. In 1966, PLA found its place in biomedical applications due to its biodegradability, bio-absorbability, biocompatibility and nontoxic nature [26]. Since then, the use of PLA in biomedical application increased due to mentioned properties and it also found its place in the other applications such as textile, agriculture, electronics, and packaging etc. in last two to three decades. PLA is known to have comparable thermal, mechanical and barrier properties which makes it more promising candidate to replace petroleum based polymers. Although PLA is known to have significant potential in replacing conventional plastics, it suffers from some drawbacks such as relatively low glass transition temperature, low heat deflection temperature, lower melting temperature, slow crystallization, lower melt elasticity and relatively poor barrier properties [27] and enhancing these properties is a

challenging task for the scientific community. Several methods such as developing biocomposites [28-31], polymer blending [32-36], or formation of stereocomplex [37] etc. have been adopted by researchers to improve the structural and physico-chemical properties of PLA so that it can compete with the properties of petroleum derived polymers.

Development of PLA based biocomposite is an opportunity to fabricate novel biodegradable polymeric films which can effectively improve its intrinsic properties with a potential for commercialization in future. It is proven that mixing PLA with fillers such as cellulose, clays [38-40], graphene [41], chitosan [42], gums [43], cellulose nanocrystals [44], silk [45] or others [46] etc. improves its properties and also leads to a material which is ecological as well as economical [47]. Gas and moisture barrier properties of PLA are very crucial in packaging applications in order to improve its shelf life. Various methods such as layer by layer (LbL), surface treatment, blending etc. can be used for the fabrication of biocomposites. Aulin and his group [48] have used LbL method to prepare multilayer of polyethyleneimine (PEI) and nanofibrillated cellulose (NFC) or carboxymethyl cellulose (CMC) on the surface of PLA substrate and found that PLA films coated with 50 bilayers of PEI/NFC and PEI/CMC exhibited oxygen permeability (~10 cm^3/m^2.day.atm) which was lower (more than an order of magnitude) than uncoated PLA (151.5 cm^3/m^2.day.atm) at 23°C and 50% RH. The coated PLA film became less sensitive to moisture after LbL deposition method. They also found that the film was more than 80% transparent to visible light after coating. The LbL method was employed by Laufer et al. [49] keeping in mind that improving the oxygen permeability of PLA will slow down the oxidative degradation and ultimately improve the shelf life of the food and it successfully reduced the oxygen permeability by four fold. They developed the method in which the PLA film required sequential dip coating with chitosan and montmorillonite (MMT) clay solution followed by drying. After 30 coatings of chitosan and clay, the oxygen permeability of PLA was

reduced from 1.772×10^{-14} $cm^3.cm.cm^{-2}.s^{-1}.Pa^{-1}$ to less than 0.03×10^{-16} $cm^3.cm.cm^{-2}.s^{-1}.Pa^{-1}$. They postulated that layer of clay acted as nanobrick wall film which had built an extremely tortuous path for the oxygen molecules.

The gas or water vapour barrier properties of polymers can also be improved by surface treatment processes such as UV/ozone treatment [50], temperature treatment [51], plasma radiation [52], hyperthermal hydrogen-induced cross-linking (HHIC) technology etc. HHIC technology is used for the selective breaking of C-H or Si-O bond, in absence of any chemical reagents, without affecting other atomic bonds. The breakage of C-H bonds will generate carbon radicals which will lead to cross-linking. The cross linking induced by hyperthermal hydrogen is driven by plasma. Du et al. [53] have used HHIC technology to crosslink the surface molecule of PLA film in order to reduce the water vapour permeability. Due to the hyperthermal hydrogen collision, the C-H bond of PLA molecules selectively cleaves without breaking other bonds which results in cross linking of carbon radicals generated from the organic molecules. The cross-linked layer serves as a gas barrier which reduces the water vapour permeability of PLA from 26.74 to 22.96 $gm/m^2.day$ and improves its hydrophobicity.

Generally, the clays have layered structure which offer a tortuous path for permeation of gas molecules even at a lower loading which reduce the molecular diffusion through matrix. A detailed information is condensed by Cui et al. [54] in the review on the polymer clay composite for gas barrier properties. Blending of polymers is another approach which can significantly improve the gas barrier properties. Armentano et al. [55] have found that 15% addition of PHB into PLA matrix increases its crystallinity due to enhanced crystal packing thereby reducing the oxygen permeability ~35%. In order to improve the barrier properties of PLA, Kakroodi et al. [56] developed a technique to form *in situ* microfibrils of polyamide

(PA) on the surface of PLA by melt blending cum hot stretching process. They found that the addition of ~3wt% of PA leads to significant reduction ~38% in the oxygen permeability. It was found that OTR reduction is directly related to the crystal size and its distribution. In this case, PA microfibrils act as nucleating agents enhancing the nucleation density leading to the production of large amount of small crystals. Ultimately, these small crystals work as constraint to the chain mobility in amorphous region and tight packing of chains leads to the reduction in OTR.

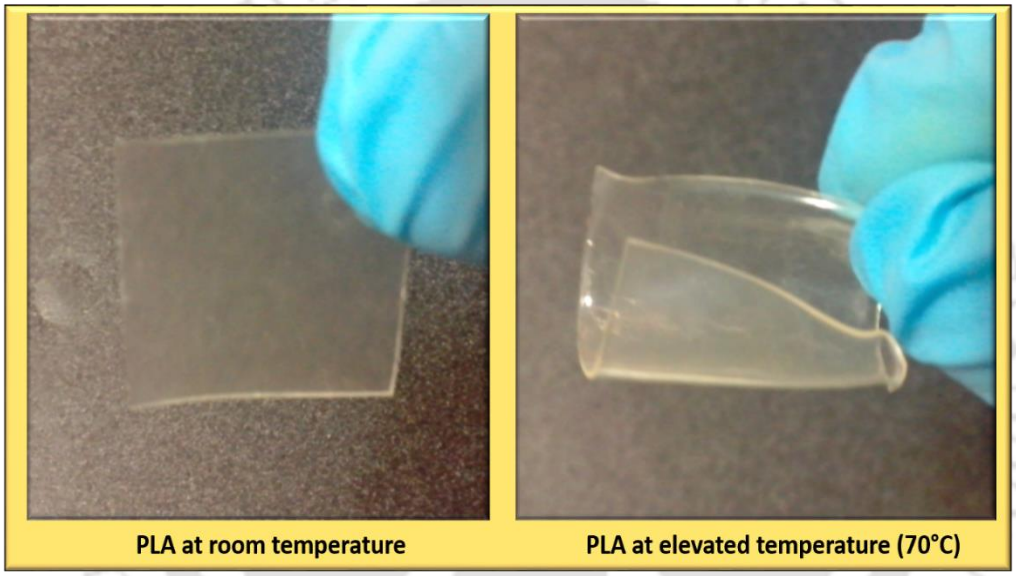

Figure 2.5: Mechanical stability of PLA at elevated temperature.

Along with the gas barrier properties, PLA also lacks in mechanical and thermomechanical properties in comparison to the petroleum based polymers which can be enhanced by the development of biocomposites, polymer blends or other methods. The development of biocomposite is proven to be effective way to prepare relatively mechanically strong PLA. Due to the relatively poor thermomechanical properties, PLA cannot be used for the engineering applications as shown in **Figure 2.5** which presents the poor mechanical stability of PLA at elevated temperature. Subsequently, a new type of crystal called stereocomplex (SC) crystallites was discovered, where the enantiomeric PLA such as

poly(L-lactic acid) (PLLA) and poly(D-lactic acid) (PDLA) are mixed together in 1:1 ratio and subsequently the melting temperature of stereocomplex PLA (sPLA) was found to be 50°C higher than enantiomeric pure PLA [57]. A comparative list of different polymer's thermomechanical properties are described in **Table 2.1**.

Table 2.1: Comparison of the properties of different polymers.

Polymer Name	T_m (°C)	HDT (°C)	Representative Applications
sPLA	200-240	~100-160	Would be suitable for: Electrical, packaging, engineering, medical, etc.
PLLA	155-178	~55	Limited use in packaging & medical
PET	260	120-160	Packaging, textile, electrical
PBT	220	-	Electrical, automobile, tool casing
PS	240	~100	Electrical, packaging, construction

sPLA: Stereocomplex poly(lactic acid), PLLA: poly(L-lactic acid), PET: polyethylene terephthalate, PBT: polybutylene terephthalate, PS: polystyrene, Tm: Melting temperature, HDT: Heat deflection temperature

Detailed schematic about the production and application of PLLA and PDLA is presented as **Figure 2.6.** Stereocomplexation is a special type of crystal formed by the interaction between two enantiomeric PLA chains which is responsible for the improvement in the thermal, mechanical and gas barrier properties of end products. Enantiomeric pure PLA adopts 10_3 helical configuration whereas sPLA has 3_1 helical configuration responsible for the densely packed polymer chains which improves the various properties of PLA. Xu et al. [58] have fabricated graphene oxide (GO) based flexible biopolymer films. They have found that during solution mixing, SC nanospheres are formed and surrounding the GO

sheets lead to act as nucleating sites for spherulite development. Presence of GO in the matrix drove the steady increase in stereocomplex concentration and suppressed the formation of homocrystals. The oxygen permeability of composite films was reduced from 4.869×10^{-15} $cm^3.cm.cm^{-2}.s^{-1}.Pa^{-1}$ to 0.2553×10^{-15} $cm^3.cm.cm^{-2}.s^{-1}.Pa^{-1}$ by the addition of 0.5 wt% GO and further reduced to 0.06264×10^{-15} $cm^3.cm.cm^{-2}.s^{-1}.Pa^{-1}$ after annealing. Presence of GO forms impermeable nano-barrier walls which improves the resistance to diffusing gas molecules and enhancement in the stereocomplex crystallinity in the matrix also play as significant role in the reduction of oxygen solubility.

The production of PLA grafted fillers by *in situ* polymerization is another technique to improve the dispersion of the filler into polymeric matrix. In this method, PLA grafted fillers are synthesized by polymerization of lactide in presence of fillers followed by purification and dispersion into the polymeric matrix. The grafting of PLA chains on the surface of filler influences the interaction between the molecules of matrix and filler which leads to the uniform dispersion. Re and his colleague [59] have demonstrated a dual approach i.e. use of filler and stereocomplexation which significantly overcomes the drawbacks related to properties of the polymeric matrix. They first prepared and purified the PLLA grafted clay (Cloisite 30B) and then melt blended with PDLA to get the uniform dispersion of grafted clay followed by the formation of stereocomplex which leads to 46% reduction in the oxygen permeability of the film. Therefore, from the above discussions it can be concluded that the structural and barrier properties of PLA may be enhanced significantly through various chemical modification approaches which is almost comparable to that of petroleum-derived polymers.

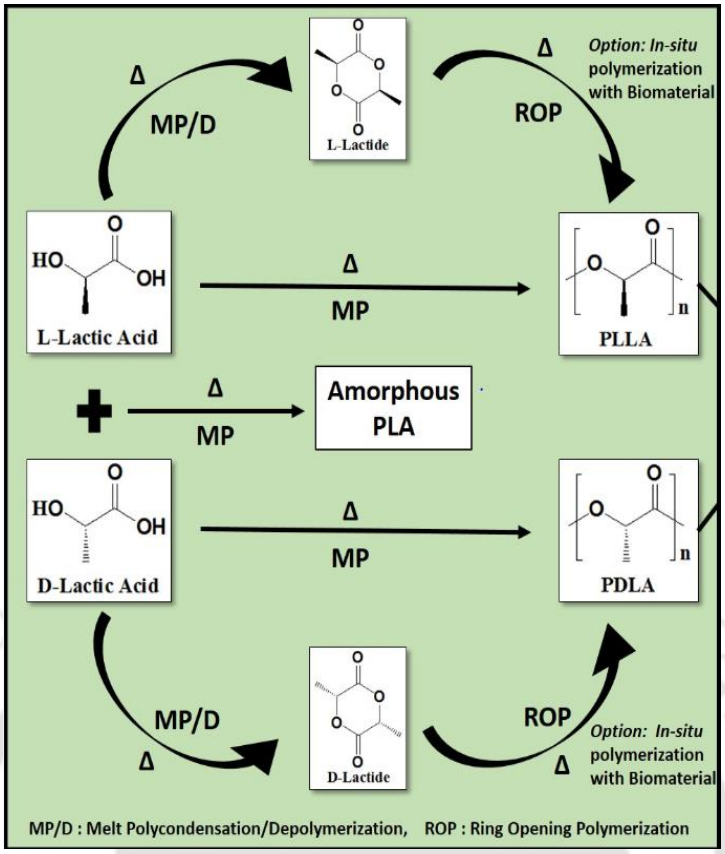

Figure 2.6: Different routes for the production of PLA for potential applications in various sectors.

2.4 Stereocomplex poly(lactic acid)

As defined by Slager and co-workers [60] "A polymer stereocomplex is a stereoselective interaction between two complementing stereoregular polymers that interlock and form a new composite, demonstrating altered physical properties in comparison to the parent polymers." Tsuji [37], has given the definition of stereocomplex as "When the interaction between polymers having different tacticity or configurations prevails over that one between polymers with the same tacticity or configuration, a stereoselective association of the former polymer pair takes place. Such association is described as stereocomplexation

or stereocomplex formation." Stereocomplex can form between isotactic and syndiotactic or optically active or opposite enantiomeric polymers.

Stereocomplex can be made by solution or melt mixing of the two enantiomers poly(L-lactide) (PLLA) and poly (D-lactide) (PDLA). As discussed previously, scientists are using these materials directly or by modifying [61] it into PLA matrix to enhance the properties of the parent material [62]. Stereocomplexation in PLA is a well-defined lattice arrangement of two different enantiomeric PLA chains. The main limitation in the synthesis of stereocomplex PLA (sPLA) is the formation of homocrystal with stereocomplex crystallites. Also the stereocomplex may form only with relatively low molecular weight (<100 KDa) PLA which affects the mechanical properties of final product. With an aim to improve the properties, different techniques are being developed by the researchers. Ikada and co-workers [57] have first reported the synthesis of stereocomplex PLA (sPLA) by solution mixing of PLLA and PDLA. They have dissolved PLLA or PLDA separately into methylene chloride and then mixed each other and subsequently upon precipitation into methanol, stereocomplex PLA was formed. The melting point of synthesized sPLA was enhanced by 50 °C to that of normal PLA. The different crystalline structure also proved sPLA formation. They suggested that the stereocomplex was formed through Van der Waals forces such as dipole-dipole interactions between the two different helical chains in solution where the molecular motion is sufficiently great. Several methods have been developed by different scientific groups for the formation of stereocomplexation in PLA. Methods such as solution casting [63], melt blending [64], precipitation [65], stereoblock [66, 67] etc. are used to develop the stereocomplexation in PLA.

Due to the interaction between enantiomeric PLA i.e. PLLA and PDLA, a different crystalline structure is formed as compared to enantiomeric pure PLA. So, for the formation of stereocomplex, molecular interaction between PLLA and PDLA is the major prequisite.

This interaction could be done by mixing low molecular weight PLLA and PDLA by solution cast or melt blending but it leads to inadequate mechanical properties of the end product. It is very important to have high molecular weight stereocomplex PLA for engineering applications. Yui and co-workers [68] reported the formation of stereocomplex crystallites in case of block copolymers of L and D-lactide. It was assumed that the degree of stereocomplex formation could be tailored by the composition of the block copolymers. They synthesized the block copolymer by solution polymerization of L-lactide in toluene and subsequently the addition of D-lactide and found that the melting point increased to 205 °C, which is a significant rise.

Characterization of the stereocomplex PLA is quite complicated. It can be examined by several methods such as Nuclear magnetic resonance (NMR), Differential scanning calorimetry (DSC), X-ray diffraction (XRD) etc. It is also found that the complex of PLLA and PDLA is not soluble in solvents which can dissolve the enantiomeric PLA. HFIP can be used to dissolve sPLA. So, this is also an approach to confirm the formation of stereocomplex PLA. Due to the different crystallite formation in stereocomplex PLA, it is easy to analyse using XRD technique. The enantiomeric pure PLA exists in several polymorphs such as α, β, γ form etc. Among these, alpha form is found to be the most stable form of PLA which crystallizes in the pseudo orthorhombic unit cell with dimensions a = 1.07 nm, b = 0.595 nm and c = 2.78 nm formed by two 10_3 helices whereas, the stereocomplex PLA takes 3_1 helical confirmation by parallel packing of L and D-lactide segment of chains in a triclinic unit cell of dimensions a = b = 0.916 nm, c = 0.870 nm, α = β = γ = 109.2°. The x-ray diffraction pattern for the stereocomplex PLA is found to have the peaks at 2θ values of 11.9°, 20.9° and 23.9° corresponds to the (110), (300/030) and (220) plane of stereocomplex crystals as shown in **Figure 2.7** [69]. The peaks at 16.7° and 19° corresponds to (110/200) and (203) plane of α form of homocrystals of PLA.

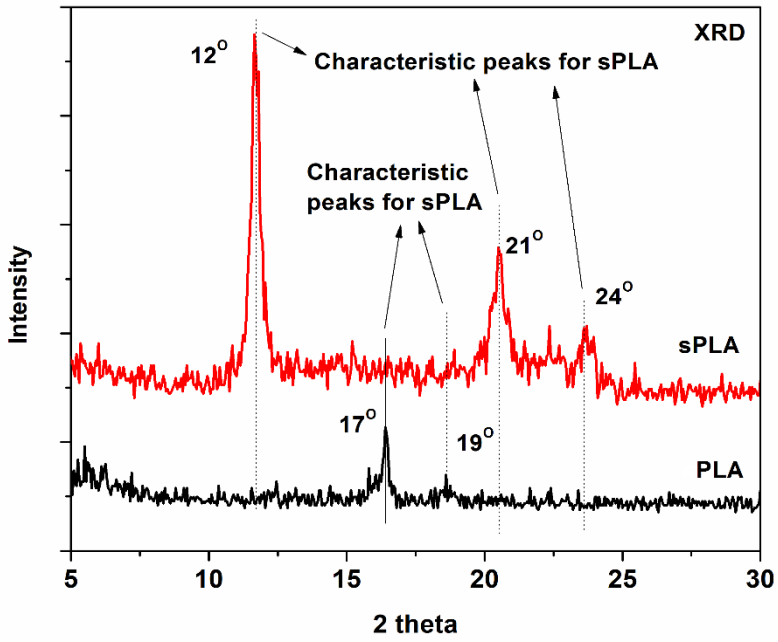

Figure 2.7: XRD patterns of enantiomeric PLA and stereocomplex PLA.

Similarly, using DSC as shown in **Figure 2.8**, the content of stereocomplex crystallite can be analysed easily because the stereocomplex PLA always has higher melting temperature than pure PLA.

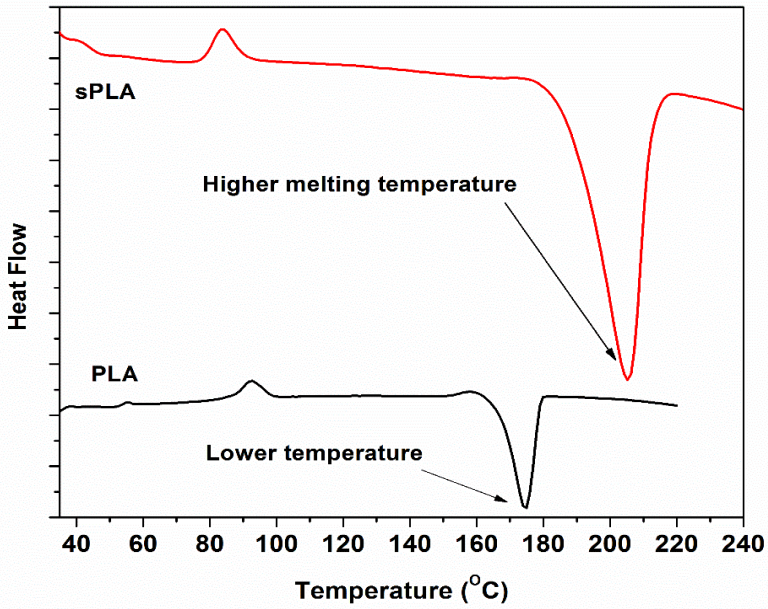

Figure 2.8: DSC thermogram of PLA and stereocomplex PLA.

In terms of production and marketing of the PLA, several industries have established units for its commercialization. Sulzer technology, Corbian Purac, Nature works LLC as Ingeo trade name are the big companies in the field of production of PLA which are also working to develop the technology for stereocomplex PLA.

2.4.1. Utilization of third component to improve the stereocomplexation in PLA

Several researchers are trying to improve the content of stereocomplex crystallites in PLA by addition of the third component apart from PLLA and PDLA. Li and co-workers [70] found that the addition of poly(4-vinyl phenol) (PVPh) in the PLLA/PDLA blend, accelerates the crystallization and reduces the size of spherulites of the stereocomplex. Addition of low content of PVPh in the blend of PLLA/PDLA also accelerates the ability of stereocomplex crystallization at nonisothermal crystallization of blend. Cheng and co-workers, 2011 [71] have studied the effect of poly(3-hydroxybutyrate) (PHB) on the crystallization behaviour of stereocomplex PLA. They found the negative effect of addition of PHB in sPLA. Sun and co-workers 2012 [72] studied the crystallization of stereocomplex PLA and graphene oxide (GO). They grafted GO with PDLA and blended with PLLA to form the stereocomplex. They found that incorporation of GO nanofiller enhanced the crystallinity and increased the fraction of stereocomplex crystallites content in the composite. It is also found that the increased amount of GO can act as blocking site and hinder the polymer chain mobility which leads to the hindrance to the growth of crystallites. Quan and co-workers 2012 [73] added the carbon nanotubes in sPLA matrix using direct melt mixing process and found that the crystallinity of the composite increased to 62% from 43% with 1% carbon nanotubes due to nucleation effect of CNT and also observed the improvement in electrical property. Bao and co-workers 2014 [74] have studied the effect of Poly(ethylene glycol) (PEG) on the formation of stereocomplexation

in PLA. They found increase in stereocomplex crystallites with increase in PEG content. The glass transition temperature of the material decreased from 62°C to 37°C due to the plasticizing effect of PEG. They also found that the low molecular weight PEG was an effective additive for the formation of stereocomplex crystallites. The low molecular weight PEG increases the segmental motion of the polymeric chains which leads to the formation of sPLA crystallites. With the similar aim to improve the properties of PLA, Purnama and co-workers 2014 [75] have synthesized the stereocomplex poly(lactide) containing cellulose nano-whiskers by supercritical fluid technology. They found 100% stereocomplex crystallite formation using this process and they have reported the melting point of sPLA more than 200°C. Han and co-workers [76] have used the zinc phenylphosphonate (PPZn) as nucleation agent in the formation of stereocomplex PLA. They found that the presence of PPZn enhances the crystallization rate as well as selectively promote the formation of stereocomplex crystallites.

Stereocomplex PLA can be a potential candidate for the packaging of the hot food and cups for beverages or any liquid food as well as other engineering application. Bor and co-workers [77, 78] studied the effect of different food stimulants on sPLA and found that the release of oligomeric chains and cyclic lactic acid is somewhat smaller than the enantiomeric pure PLA. They also have studied the effect of stereocomplexation on the stability migration resistance of PLA in microwave heating with different food stimulants such as ethanol, water etc. They found that due to the less amorphous phase present in the stereocomplex PLA, the amount of migrant including linear oligomeric chain or cyclic lactic acid found lesser amount than PLLA in 10% ethanol. The mass loss during microwave heating in water or 10% ethanol was less in case of stereocomplex than normal PLLA. This makes sPLA a potential candidate for the food packaging application. From the above discussion, it is evident that PLA may be the possible future of the plastic

industries and enhancement in the properties of PLA through stereocomplexation may be the tool for the development of polymers for heat stable packaging and other engineering applications.

From the literature, it is found that the addition of fillers into the polymer matrix not only improves the polymer properties, but is also important in the economic aspect. It is found that the inuniform distribution of reinforced material into polymer matrix adversely affects the properties of polymer. Poor distribution of filler into the matrix may be the result of non-compatibility of filler with polymer molecules. Grafting of polymeric chains on the filler surface may increase the distribution/dispersion of filler into the matrix which ultimately affects several properties of polymer. Keeping these observations into account, we have used three different fillers i.e. chitosan, cellulose microcrystals (CMC) and hydroxyapatite (HAP). Every filler has its own specificity and property in different application. In the current work, these fillers have been used for the exploration of different aspects of stereocomplexation in PLA properties.

2.5 Cellulose microcrystals (CMC)

Cellulose is the most abundant, naturally occurring, biobased, low cost material and has relatively excellent chemical and physical properties [79]. It is a polysaccharide which contains linear chains of beta one to four linkage of D-glucose units. Cellulose is the integral part of the primary cell wall of the plants. It is produced from the cotton, wood, bacteria (at times) etc. It is known that cellulose has large number of hydroxyl functional group present on its surface as shown in **Figure 2.9** and it can easily be modified [80].

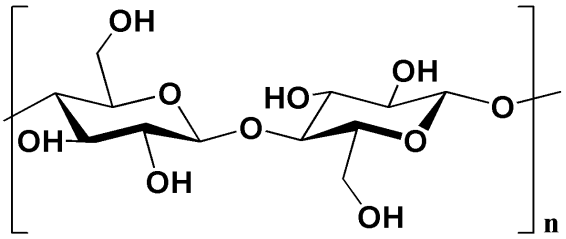

Figure 2.9: Molecular structure of cellulose.

Cellulose is semicrystalline in nature and has crystalline along with amorphous domains. The removal of amorphous domains by the act of acid hydrolysis produces the cellulose microcrystal as shown in **Figure 2.10**.

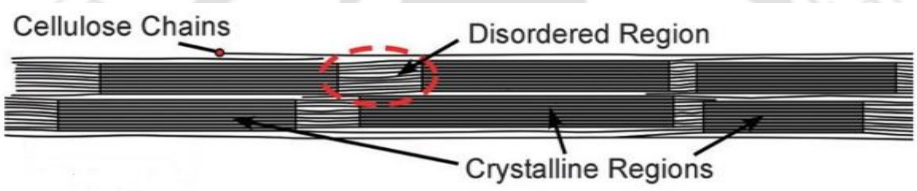

Figure 2.10: Crystalline and amorphous regions in cellulose bundle.

It is often observed that the reinforcing efficiency of fillers in polymer matrices is deeply affected by its uneven mixing and agglomeration [81-83]. So, modification of the CMC can be done in order to form uniform dispersion.

2.6 Chitosan

Chitosan is a polysaccharide containing random distribution of beta one to four linkage with acetylated and deacetylated D-glucosamine units as shown in **Figure 2.11**. It is one of the promising materials, which has relatively good gas barrier properties, biodegradable and nontoxic nature along with biocompatibility and antibacterial activity. It a completely compostable polymeric material. It is a naturally occurring polysaccharide and can be obtained by deacetylation of chitin harvested/found from the biological materials [84].

Chitosan is soluble in acidic media due to the presence of free amino groups which gets protonated in acidic environment [85].

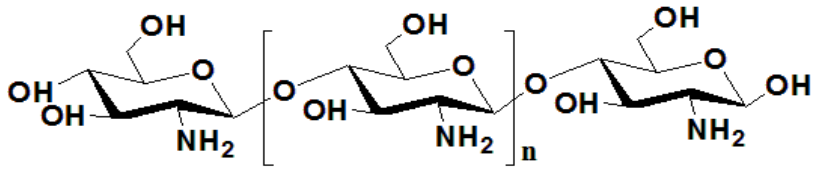

Figure 2.11: Molecular structure of chitosan.

From the last few decades, researchers and scientists have used chitosan in many applications such as biomedical [86], food industry [87], pulp and paper industry [88], wastewater treatment [89], agriculture etc. [90]. Due to its solubility in water, it could not be used in the packaging and engineering application. Chitosan can be processed in injection moulding instrument however, the shrinkage property hinders the industrial processing [91]. It is possible to transform the hydrophilic chitosan to hydrophobic in nature by chemical modification which may end up with uniform dispersion in hydrophobic medium. The uniform dispersion may lead to the improved properties of the substrate materials.

2.7 Hydroxyapatite (HAP)

Hydroxyapatite (HAP) is a bioactive nontoxic complex form of calcium phosphate which is 60-70% content of mammalian bones. Molecular structure of HAP is written as $Ca_5(PO_4)_3(OH)$. It can be a substitute for the broken tooth and bones in the living species such as humans. It is known that HAP with 1.67 molar ratio of Ca/P are biologically quite stable which results to slow biodegradability. It can be produced by several biological or synthetic methods such as precipitation [92, 93], hydrothermal [94, 95] and sol-gel method [96], hydrolysis [97, 98], solid state synthesis [99], from bio-resources such as eggshells

[100], seashells [101], plants [102], animal bones etc. [103]. Due to its similarity with mammalian hard tissues, HAP is one of the most investigated synthetic biomaterial. As limitation, the HAP cannot be used for the load bearing applications due to its brittle nature. Being a ceramic, HAP can be used for the biomedical application due to its properties such as biocompatibility and bioactivity. It has slow bioresorbable nature which allows it to be used for long term clinical applications. It can also be used in different applications such as gas sensing instrument [104], chromatography [105], catalyst [106, 107] etc. It is known that the material size affects the properties such as relative mechanical strength of the final products [108]. It can be found from the literature that the nano sized particles of HAP have more mechanical strength and bioactivity than bigger size particles [109, 110]. The HAP can also be used as filler in the formation of polymer biocomposite in order to improve the properties.

The details about the above mentioned fillers will be discussed in the respective chapters. The particulars of methodology are also discussed in the respective chapters. The material development cannot be complete without the characterization techniques. So, in subsequent section characterization techniques have been discussed.

2.8 Characterization of biopolymers and its composites

From the synthesis, to production and application followed by degradation; biodegradable polymers need to be characterized in several aspects. There are a number of characterization techniques which are utilized in this study. It is very important to understand the working principle along with basic information of the utilized techniques for polymers which have been listed as follows.

2.8.1 Morphological studies

Different microscopic techniques are employed to carry out the morphological studies of prepared samples. The effect of different fillers, additives, on the polymer surface or fractured surface can be seen by the morphological study. Mainly, FESEM, TEM, AFM and POM are basic required techniques.

2.8.1.1 Polarizing optical microscopy (POM)

POM is the type of microscope used for crystallographic study of small individual crystals of polymers and to obtain the data for spherulite growth and spherulite density. It uses the polarized light to investigate the optical properties of polymers which during the crystallization process, rotate the polarized light in particular direction and develop birefringence due to difference in refractive indices. With the help of polarizer and analyser installed in POM, spherulite growth and density can be measured. POM can be employed in either transmission or reflective mode.

2.8.1.2 Field emission scanning electron microscopy (FESEM)

FESEM is used for the visualization of small structures of any solid surface as small as 10 nanometre. FESEM is a technique which uses electron beam instead of light beam. Electrons generated from field emission source are accelerated in a high electric field gradient and develop a narrow scan beam by electronic lenses. This primary electron beam is bombarded on the samples and emits secondary electron which can be detected by detector and electric signals can be generated. The angle and velocity of the secondary electron generated from the samples determine the shape and size of the specimen. The generated electric signals are again amplified and transformed into images. To observe the samples in FESEM, the samples need to be thin coated with conductive metals such as gold

or gold-palladium. Formation of thin film of gold can be done using plasma sputtering method. FESEM analyses the surface morphology and elemental composition on the surface of materials.

2.8.1.3 Transmission electron microscopy (TEM)

TEM is a highly powerful microscopic technique for the analysis of nanoscale specimen in relatively less time. It uses the narrow and intense electron beam focused by magnetic lenses which interacts with specimen and transmits through it. Unlike FESEM, TEM is based on the image formation by transmitted electrons through specimen. It can provide the information about the internal characteristics of the samples such as morphology, crystallization etc. In comparison to FESEM, it has higher resolution and provides two dimensional images. Sample for TEM analysis should be very thin which allows the sufficient amount of electrons pass through it and form the image with minimum energy loss.

2.8.1.4 Atomic force microscopy (AFM)

AFM is the microscopic technique which can develop three dimensional image of the samples at nanoscale. In this technique, the mechanical probe scans the desired sample by traveling near the surface. Due to the forces between probe and surface, the probe deflects as per Hooke's law. The generated deflection changes the reflection of the laser beam bombarded on the top of the probe, and recorded with the help of piezoelectric element and detector. Unlike, TEM and FESEM, it does not require either vacuum or the treatment of samples. Other than imaging, AFM can measure the force generated by surface to probe and also can manipulate the sample texture.

2.8.2 Spectroscopic study

Study of molecular interaction behaviour of matter and its quantification using electromagnetic radiation i.e. visible, ultraviolet, x-ray, infrared etc. is called spectroscopy. Different characteristic properties i.e. crystal structure, molecular function group, molecular structure etc. of the matter can be known by using spectroscopic techniques such as FTIR, NMR, XRD etc.

2.8.2.1 Fourier transform infrared (FTIR)

FTIR is a relatively very fast characteristic technique which is based on the Michelson Interferometer. It uses infrared radiation to acquire an infrared spectrum of emission or absorption of solid, liquid or gases. The infrared radiation is incident on the surface of sample and it either reflects or absorbs the radiation. That absorption or reflection is the function of time converted to frequency domain by Fourier transform method which is plotted as a spectrum against the wave number. FTIR can be used for the identification of the molecules of polymers, biocomposites etc. by detecting its functional groups. For FTIR study, samples can be prepared in the form of thin film (in reflection mode) or in the form of pellet (in transmission mode) with potassium bromide (KBr) (1:100 ratio).

2.8.2.2 X-ray diffraction spectroscopy (XRD)

This analytical technique can be used for the identification of different phases of semi-crystalline polymer and gives information about the dimensions of unit cell. XRD uses the x-rays, generated by cathode ray tube, which interacts with crystalline sample. The generated constructive interference due to the interaction of monochromatic x-ray to crystalline polymer, which satisfies the Bragg's law, is detected, processed and calculated by the instrumentation. All possible diffraction directions are detected by scanning the sample through a range of 2θ angle which generates the x-ray pattern count and plot against angle.

2.8.2.3 Nuclear magnetic resonance spectroscopy (NMR)

NMR is an analytical technique used for the determination of atomic arrangement of molecules, purity of substance, content of element etc. It is based on the fact that when the population of nuclei is forced in an external magnetic field, the nuclei turn out to be aligned either with the magnetic field (alpha orientation) or against the field (beta orientation). In this technique, electromagnetic radiation is used to orient the nuclei from alpha to beta state and after removal of energy they get back to the relaxed alpha state. This process of nuclei generates the fluctuation in the magnetic field which is called resonance. This resonance is detected and converted into peaks by detectors with results in the NMR spectrum. Information of different elements such as proton, carbon, nitrogen etc. can be collected by ^{1}H-NMR, ^{13}C-NMR, ^{15}N-NMR analysis, respectively. For NMR analysis, sample can be analysed in solution form by dissolving the sample in deuterated solvent such as $CDCl_3$.

2.8.3 Thermal analysis

Knowing the effect of temperature on the polymer is very critical and important. Understanding the behaviour of polymers such as different transitions, thermal degradation etc. at higher temperature is crucial that can be measured by using different techniques such as DSC, TGA etc.

2.8.3.1 Differential scanning calorimetry (DSC)

In this technique, the amount of energy absorbed or released by sample is measured when it is heated or cooled in comparison to reference. DSC can be used to determine the different transition states of the polymers such as glass transition temperature, heat of fusion, heat capacity and crystallization temperature of polymers. Indirectly, the degree of crystallinity can also be calculated based on the melting and crystallization enthalpy. It measures the

qualitative and quantitative statistics on endothermic and exothermic processes. Using DSC data, one can study the kinetics of crystallization in polymers and do the theoretical analysis by using different available models for the crystallization in polymers.

2.8.3.2 Thermogravimetric analyser (TGA)

TGA provides information about physical transformation taking place in the material due to the gradual increase in the temperature. It measures the change in the mass/weight change (loss or gain) and rate of change due to the gradual increase in temperature or time in controlled environment due to absorption/desorption of volatile components, oxidation/reduction or decomposition of the sample. Using TGA, we can predict thermal or oxidative stability of the material and also determine the composition of material. The weight loss data can be plotted against the temperature or time to demonstrate the thermal transition in the sample. TGA can be coupled with other instrument such as FTIR, mass spectroscopy (MS) etc. to determine the content of generated vapour. Data generated using TGA can be used to study the thermal degradation kinetics of the material.

2.8.4 Mechanical and thermomechanical properties

In case of polymers, it is very important to understand the behaviour of material when it is subjected to load and heat. Mechanical properties such as fracture strength, tensile strength, elongation at break, storage modulus, loss modulus etc. need to be calculated in order to understand the material behaviour. UTM and DMA are the most common analysis methods to determine the mechanical properties of polymers.

2.8.4.1 Universal testing machine (UTM)

It is used for the study of tensile and compression strength of the polymer film or other shapes. In this technique, samples are prepared as per ASTM standard for the analysis. Other than tensile strength, elongation at break, and Young's modulus can also be measured. The mechanical properties of the polymer are highly dependent on the molecular weight of the polymer, amount of the filler or additive present in the biocomposite.

2.8.4.2 Dynamic mechanical analyser (DMA)

In DMA, the sample is subjected to the dynamic force or sinusoidal deformation with progressive increase in temperature to measure the viscoelastic behaviour i.e. loss and storage modulus of the polymer with known geometry either in tensile mode or compressive mode. Using DMA, one can measure the glass transition, amount of crosslinking as well as heat deflection temperature of the polymers etc. Samples are made as per ASTM standard. Several parameters such as specimen geometry, type of load, frequency, tightening torque, clamps, temperature program etc. affect the final data of the analysis.

2.8.5 Barrier properties

After the development of the polymer or polymer biocomposite, it needs to be tested for the barrier properties in order to be considered for packaging application. Oxygen and water vapour in air have a major impact on the quality of packaged material. Therefore, the study of permeability of oxygen and water vapour is very important.

2.8.5.1 *Oxygen transmission rate analyser (OTR)*

OTR tester is the instrument used to measure the amount of oxygen gas passing through polymer film in given period of time at particular temperature and humidity. Oxygen

permeability is highly influenced by the temperature and humidity in the test environment. Sample in the form of film with fixed area of exposure can be analysed using OTR tester. The tester involves a chamber having slot for the polymer film. Upper half consists of flow of oxygen gas and the lower one consists of inert gas flow connected to oxygen gas sensor. Inert gas takes permeated oxygen to the sensor for the measurement and calculation of amount. Using this, one can also measure the energy required for the permeation, diffusion of oxygen.

2.8.5.2 Water vapour transmission rate analyser (WVTR)

WVTR analysis is the measure of water molecules in vapour phase passing through polymer film. For some applications such as encapsulated electronics, breathable cloth, medicine, food etc. it is very important to measure the WVTR of the polymer films. WVTR is dependent on the interaction of water molecules and polymer film, wettability etc. It is possible to identify the effect of different fillers, additives, layer formation etc. on the water permeability of the polymer film.

2.8.6 Some other properties

2.8.6.1 Contact angle measurement (CA)

The angle between solid surface and tangent of the droplet is called contact angle. Contact angle is used for the estimation of surface properties i.e. hydrophilic or hydrophobic. It is also used to measure the interfacial tension between solid and liquid.

2.8.6.2 Optical polarimeter (OP)

This instrument is used to calculate the angle of rotation of plane polarized light passing through the optically active material in the solution. Optical activity of the substance highly affects the properties of the final products. Using optical polarimeter, we can measure the

optical rotation as well as specific rotation of the sample with known concentration. The concentration of two enantiomers can be measured. Sample for analysis can be prepared by dissolving calculated amount into the specific amount of solvent. OP can also be used for other applications such as calculation of concentration, purity measurement, determination of sugar or fructose etc.

2.8.6.3 Gel permeation chromatography (GPC)

Size exclusion chromatography is as type of high performance liquid chromatography (HPLC) where large polymer molecules can be separated on the basis of size or hydrodynamic volume of polymer chain. GPC is used for the determination relative molecular weight as well as the molecular weight distribution of the polymers. Normally, polystyrene is used as a standard for GPC. The instrument consists of pump, column or stationary phase, eluent or mobile phase, reservoir etc.

2.9 Research gap

From the literature it is found that the stereocomplexation in PLA could be a promising process which can improve its thermal, mechanical and barrier properties. So far, it has been noticed that the improvement in stereocomplexation in high molecular weight PLA is still a challenging task for the scientific community which is responsible for improving its thermo-mechanical properties. To summarize, significant attempts have been made successfully to develop stereocomplex PLA but most of the investigations have been conducted using low molecular weight PLLA/PDLA which inherently undergoes stereocomplexation due to the low polymer viscosity and higher segmental motion of polymer chains whereas adequate thermo-mechanical properties cannot be achieved for its end applications. Therefore, it is important to develop the new processes to produce high molecular weight (MW) heat stable stereocomplex poly(lactic acid) with adequate properties having high thermal and mechanical stability along with comparable barrier

properties. Therefore, this research attempts to modify different biomaterials by *in situ* ROP of lactide and utilize them as fillers with PLA in order to develop the heat stable stereocomplex PLA biocomposite along with the evaluation of its characteristic properties.

2.10 Objectives

As per stated gaps, the objectives of the thesis are as follows:

1. Development of process to synthesize and purify L and D-lactide and its polymerization
    a. Synthesis and purification of L-lactide, D-lactide and D, L-lactide
    b. Synthesis of poly(L-lactic acid) and poly(D-lactic acid) with desired MW
2. Development of compatible bio-fillers using cellulose, chitosan and using hydroxyapatite as a biomaterial based filler for its application in the formation of stereocomplex poly(lactic acid) based composites.
3. Synthesis and processing strategies for production of stereocomplex poly(lactic acid) with high heat stable, higher gas barrier and improved mechanical properties
4. Evaluation of the properties of developed materials
    - Effect of biofillers on thermal, mechanical and barrier properties
    - Comparative studies on degradation behavior of sPLA and its composites
    - Comparative studies on crystallization behavior of sPLA and its composites

CHAPTER: 3

Development of Precursors and Synthesis of Enantiomeric PLA

Abstract

The motivation behind this chapter is to produce high molecular weight poly(lactic acid) (PLA) and develop the method for the production and purification of L- or D-lactide. The purity of lactide directly affects the molecular weight of PLA. Microwave heating can reduce the production time for oligomerization while retaining the quality. The different lactide purification methods such as direct washing, direct crystallization and combined washing and crystallization are compared in order to produce high purity lactide. The purified lactide is used to produce high molecular weight PLA. The purity of lactide and PLA are also confirmed by acid value, optical polarity and NMR methods.

Graphical abstract

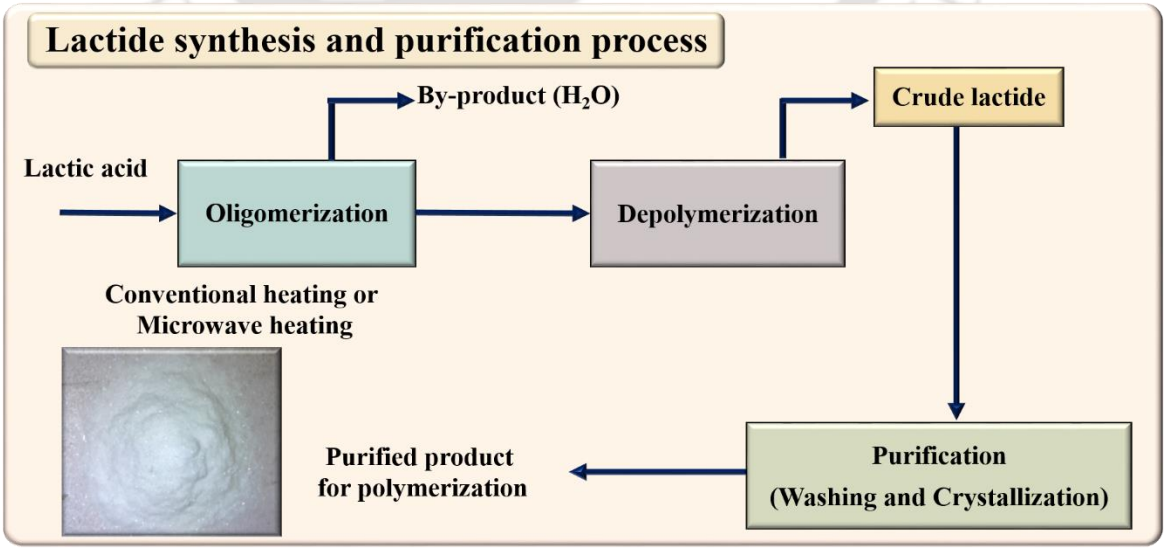

Filed Indian Patent Application Number: 201631022079

3.1 Introduction

Scarcity of fossil resources and pollution generated by petroleum based polymers are the significant driving forces for the exploration of biobased and renewable polymers. The development in the production growth of biobased materials in last few decades, as discussed in previous chapter indicates the potential of biobased material as useful products in various applications. Among these biobased materials, the production of lactic acid and PLA have encountered the exponential rise. Lactic acid is mainly used for food industry however, it is a building block for the synthesis of PLA which has the potential to replace the fossil based polymers and can be used for different applications.

Due to the hydroxyl and carboxylic groups, lactic acid can initiate the polycondensation reaction to end up with the production of PLA [111]. The polycondensation reaction results in the production of water as by-product which needs to be separated from the polymerization system to obtain PLA which is a reversible reaction and can lead to simultaneous depolymerization during the polymerization process. This process requires continuous removal of generated water molecules either by the flow of inert gas or under reduced pressure. It is very difficult to remove generated moisture in trace amounts from the viscous polymer melt which leads to the production of relatively low molecular weight PLA. The side reaction during polymerization is another drawback leading to the racemization of PLA i.e. transformation of L-lactic acid to D-lactic acid which may lead to the production of amorphous PLA. It is known that the molecular weight of the polymer significantly affects the properties of end product. Relatively high molecular weight PLA would have relatively good mechanical properties [112]. Few researchers have developed the process called solid state polymerization (SSP) in order to produce high molecular weight PLA by polycondensation reaction [113]. In SSP, the low molecular weight PLA

granules produced by polycondensation reaction are taken in either inert gas flow or vacuum at a temperature less than the melting temperature of the polymer. The main drawback of SSP process is that it has slow reaction rate. Another process to synthesize high molecular weight PLA is the ring opening polymerization (ROP) of lactide [114].

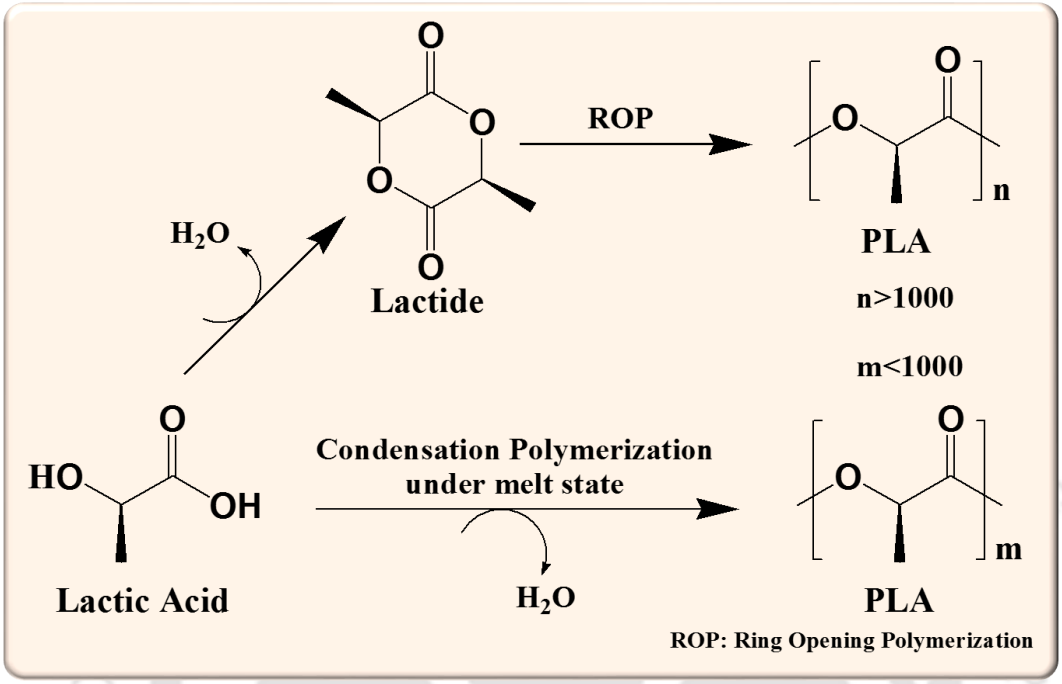

Figure 3.1: Production of PLA synthesized from lactic acid [114].

The main advantage of the process of ring opening polymerization is that it takes relatively less time to produce PLA. ROP leads to high molecular weight PLA which is required to produce products for different applications (**Figure 3.1**). The precursor for the ROP is lactide which is a dimer of the lactic acid. The synthesis of PLA through ROP can be done either in solution or bulk. Solution polymerization has lower rate of reaction whereas the bulk polymerization has higher rate of reaction. It is believed that the solution free process is an industrially viable process and gives high yield. To obtain the relatively good quality PLA (high molecular weight PLA), it is very important to use purified lactide. Lactide can

be produced by depolymerization of low molecular weight PLA followed by purification and low molecular weight PLA produced by polycondensation of lactic acid.

Various processes used for the production of PLA are shown in **Figure 3.2**. Synthesis of PLA via ROP of lactide is a three step process in which lactic acid is converted to oligomeric PLA which is further depolymerized in the presence of catalyst to produce lactide followed by purification. The purification step is very important to get high molecular weight PLA. Different research groups and industries have contributed in order to produce lactide. Very few research papers have been published however, several patents have been filled in this area.

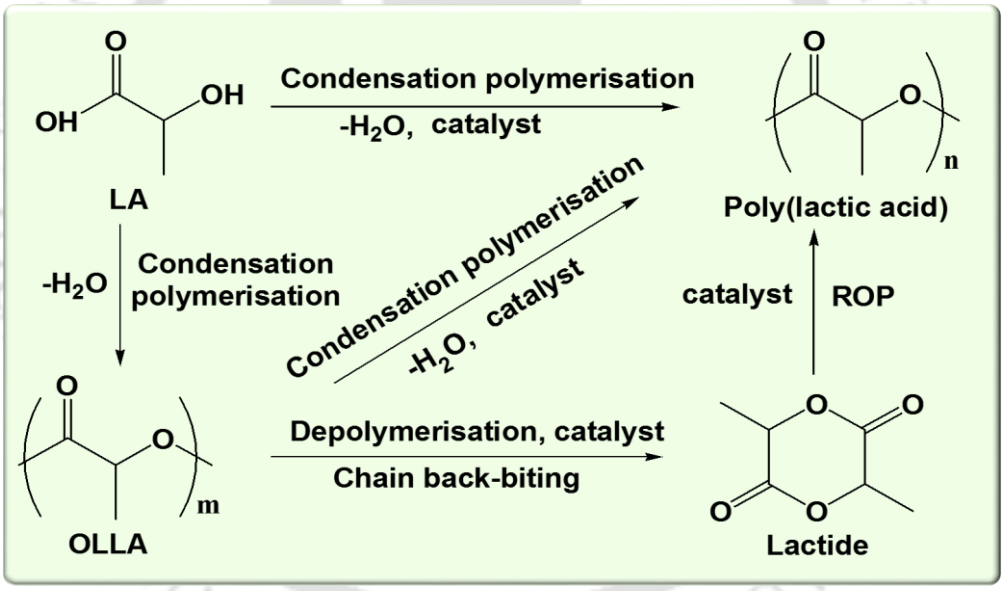

Figure 3.2: Routes for synthesis of poly(lactic acid) [18].

The crude lactide produced from the depolymerization of oligomeric lactic acid needs to be purified. As we know that lactic acid is a chiral compound and it can end up with four type of lactide as described in previous chapters i.e. L-lactide, D-lactide, D,L-lactide and meso-lactide. The D,L-lactide is the equal molar mixture of L-lactide and D-lactide whereas meso-lactide is the cyclic dimer of lactic acid which is having both L and D-lactic acid content in same molecule [18]. The crude lactide may contain several impurities such

as lactic acid, water, cyclic oligomer, catalyst, oligomeric PLA, meso-lactide etc. As the crude lactide may contain lactic acid monomer, lactic acid dimer which are acid components and hinder the polymerization of lactide lead to low molecular weight PLA. Also, other impurities like water lead to the undesirable hydrolysis of lactide or PLA. For the production of high molecular weight PLA with high optical purity, it is essential to develop the process which can generate optically pure lactide. The purification can be done by several processes such as crystallization, distillation, extraction etc. Each process has its own advantages and limitations. The distillation process involves the difficult operation and needs large number of equipments, the thermal polymerization may happen during distillation at high temperature of the crude lactide. To remove the impurities in trace amount, crystallization is an efficient process but may lead to low yield and for higher amount of impurities, the crystallization happens in low amount. It is also known that high molecular weight oligomeric PLA has higher viscosity which is undesirable however, low molecular weight oligomeric PLA produce higher amount of lactic acid monomer during depolymerization. So, it is also required to optimize the molecular weight of oligomeric PLA for the production of lactide. Thayer et al. [115] filed a patent in which they have reported the synthesis of L-lactide using lactic acid oligomer. They used tin or tin compound; yttrium or rare earth metal compounds; or antimony compounds as catalyst. They produced the oligomeric lactic acid with the degree of polymerization of approximately twenty monomer units by dehydration of lactic acid. They have used 1 to 8 weight percent of catalyst for depolymerization at 180°C-280°C which leads to production of lactide by distillation. Idage et al. [116] have patented the process for the preparation of L-lactide of high chemical yield and optical purity. They have used zinc and tin metal compound of 150-micron size as a catalyst. In this process, lactic acid is melt polymerized at 150°C-160°C for 2-3 hours under N_2 flow followed by polymerization at reduced

pressure for ~6 hours. 0.1-0.5 wt% of catalyst is used for depolymerization of oligomers for ~12 hours at 160°C-200°C in order to obtain crude lactide. The obtained crude lactide is refluxed in toluene followed by washing with water or ethyl acetate at low temperature.

A process for the purification of lactide was patented by Yamaguchi et al. [117] wherein the crude lactide was obtained by distilling the vapour of lactide from prepolymer under reduced pressure at 180°C-230°C. Tin, zinc, lead, iron, antimony, magnesium and titanium in powder form and organic acid salts, inorganic acid salts, metals or metal oxides etc. are used as catalysts. The prepolymer was obtained by dehydration and condensation of lactic acid (average molecular weight between 400 Da to 3000 Da) at 160°C-180°C under reduced pressure. Further, the crude lactide was purified by removing the meso-lactide by washing with water so as to acquire purified D, L-lactide (equal molar mixture of L and D-lactide). It is known that meso-lactide solubilizes in water faster than L or D-lactide. So, the meso-lactide present in crude lactide was dissolved in water at 30°C and filtered out. The remaining lactide was dissolved in organic solvent such as acetone or methyl isobutyl ketone and recrystallized in order to receive the crystal of L-lactide of high purity and optical purity.

Another method for the production of lactide was patented by Mariage et al. [118] wherein the purification was done by precipitating lactide using diisopropyl ether at 60°C after melting it at 85°C. After filtration in hot condition, the filtrate was dried in vacuum at room temperature. Ohara et al. [119] have used ethanol to purify the lactide. In this method, they produced low molecular weight PLA (~2000 Da) by heating at 130°C for 2 hours under normal pressure and gradually reduced the pressure and maintained the temperature between 130°C to 160°C for 4 hours. The oligomeric PLA was depolymerized under reduced pressure at 160°C to 200°C in order to produce lactide. The crude lactide in ethyl

alcohol at 25°C was then filtered through glass filter and the solid was dried by rotary evaporator at 40°C and 1 torr for 1 hour which yielded purified lactide.

Benecke et al. [120] have patented a process for the production of the lactide directly from the lactic acid. They explained the production of lactide via back-biting reaction which is the result of catalytic trans-esterification of oligomeric PLA. They have used alumina silica combination and zeolites as catalyst (optionally), acidic catalyst such as silica gel, phosphoric acid/ ion exchange resin (catalyst particle size 2-6 mm), lactic acid was fed into bed of preheated silica catalyst which converted lactic acid to lactide under inert gas flow at reaction temperature of 150-225°C. Bhatia et al. [121] have patented and disclosed the process for the production of lactide. In presence of tin octoate, they synthesized the oligomer of lactide acid at 167°C for 2 hours by removing the moisture in the stream of N_2. The oligomer was mixed with acetone to make the process easy to move the lactide by pump to other equipment at room temperature. They used five plate reactor and maintained the strong flow of N_2 preheated at 185°C and fed the acetone crude lactide mixture. The lactide product was recovered at the top of the reactor from N_2 stream by scrubbing with acetone. The excess acetone was evaporated and water at low temperature was used to precipitate the solid lactide. After filtration, the cake was washed with isopropyl alcohol and excess solvent was evaporated.

The discussed patents and literature suggest the different approaches to produce the high purity lactide in order to yield high molecular weight PLA. The motivation for the present work is to develop the cost effective and novel approach for the production of PLA. In the current study, the process for the production and purification of lactide is developed. The oligomeric lactic acid is produced by dehydration and condensation of lactic acid in different heating environment i.e. conventional heating and microwave heating which is depolymerized by heating in presence of catalyst. Purification is carried out with different

solvent washing and recrystallization and the purity is examined by acid value and the molecular weight of synthesized PLA using purified lactide.

3.2 Experimental Section

3.2.1 Materials

L-lactic acid (90 wt %) was procured from Purac India, D-lactic acid (90 wt %) purchased from Musashino Chemical Laboratory, Ltd (China), Tin oxide (SnO), Tin(II) 2-ethylhexanoate, were purchased from Sigma Aldrich India. Methanol (MeOH), and Ethanol (EtOH) were purchased from Merck India and Ethyl Acetate (EA) was supplied by Fisher Scientific India. De-ionized water was produced using Elix-3, Milli-Q, Millipore (~18.2 MΩ.cm at 25°C) USA.

3.2.2 Oligomer synthesis

The oligomeric PLA is synthesized by dehydration and condensation of lactic acid. Two heating modes are used i.e. conventional heating and microwave heating. The known amount of lactic acid is taken into a three necked round bottom flask equipped with stirrer, nitrogen flow and condenser. N_2 flow is continued and temperature is set to 110°C for two hours to remove the excess amount of water in lactic acid. Thereafter, the temperature is increased to 150°C and oligomerization continued for 6 hours. In case of microwave heating, oligomerization is done in a domestic microwave machine (Make: Samsung, Model: MC-8091HLQ) equipped with inert gas in out flow and condenser. Reaction is done at 20% power of microwave for 2-4 hours.

3.2.3 Lactide synthesis and purification

Lactide is synthesized in the polymerization reaction setup shown in the **Figure 3.3**. The oligomer synthesized in microwave is taken in the reaction system and temperature of the

system is increased to 220°C-250ºC and fixed amount of SnO catalyst is added in inert condition. The pressure is gradually reduced and reaction continued for the determined time to synthesize the lactide via depolymerisation of the oligomer. The lactide was collected into the receiver and stored for further purification process.

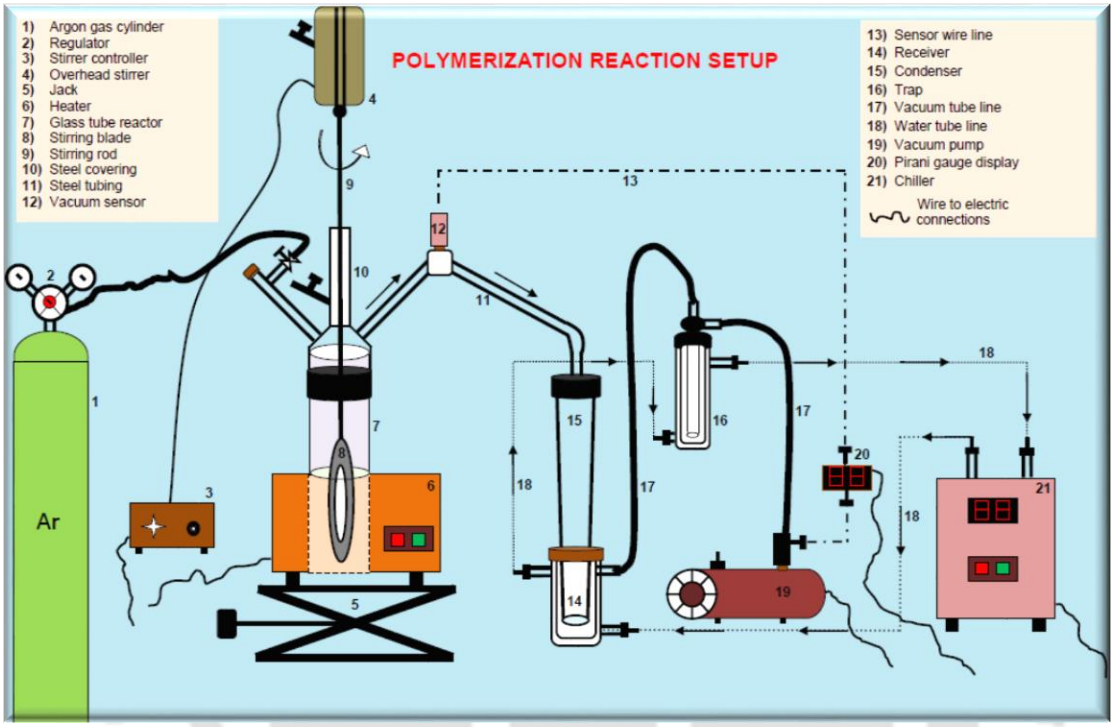

Figure 3.3: Reaction setup for lactide synthesis.

The purification of lactide is done by washing and crystallization. The comparison of three methods is done i.e. only washing, only recrystallization and combined washing and crystallization. For washing of lactide, five solvents are selected and the performance of these is checked by the yield and the molecular weight of synthesised PLA. 200 gm of crude lactide is crushed to powder using mortar and pestle and mixed with deionized water (5 times of crude lactide weight) to form the slurry. The slurry is transferred to the vacuum filtration unit equipped with Buchner funnel the excess water is filtered. Either of listed solvents (methanol, ethanol, acetone, ethyl acetate or acetonitrile, amount equal to the formed cake) is added to the cake and soaked followed by filtration in reduced pressure and

drying in vacuum oven. Same process is repeated for number of times to get washed lactide ready for polymerization. The crystallization of the lactide is done using three different solvents such as ethyl acetate, methanol and ethanol (**Table 3.1**). For recrystallization, dried washed lactide is dissolved in fixed amount (0.5 times of wt. of dried washed lactide) of either of solvents (ethyl acetate, methanol, ethanol) at elevated temperature 55-60°C. The dissolved solution is filtered using vacuum filtration unit set at temperature 55-60°C in order to remove the undissolved content in the solution. Obtained filtered solution is kept in the shallow container and the temperature is reduced to ~5°C gradually which resulted in the crystalline form of lactide which is separated using vacuum filtration unit. The solid purified lactide is dried in the vacuum oven for 6 hours at room temperature and 6 hours at 50°C to remove the excess solvent present.

Table 3.1: Specification of different solvents.

Solvent	**(a)**	**(b)**	**(c)**	**(d)**	**(e)**	**(f)**	**(g)**
Water	48.0	99.9	2.333	18.02	15.74	1.333	1.000
Methanol	29.7	64.7	13.02	32.04	15.5	1.331	0.792
Ethyl acetate	18.2	77.1	9.733	88.11	25	1.372	0.897
Lactic acid	--	122.0	0.001	90.08	3.87	1.427	1.206
Lactide	--	255.0	--	144.13	--	1.448	1.340

a) Solubility parameter ($MPa^{1/2}$), **b)** Boiling point (°C), **c)** Vapor pressure (kPa@20°C), **d)** Molecular weight (g/mole), **e)** Acidity**, f)** Refractive index, **g)** Density (g/cm^3)

3.2.4 Ring opening polymerization of lactide

Synthesis of PLA from purified lactide is done by ROP method. 2 gm of lactide is taken into the ampoule followed by the addition of tin octoate catalyst solution in toluene. Lactide and catalyst are subsequently heated to 60ºC for the removal of excess amount of toluene and moisture or oxygen for 2 hours under reduced pressure. Then, the ampoule is sealed using heating torch under vacuum and kept in hot air oven at 160°C for two hours for ROP. When the reaction is completed, the ampoule is cooled using ice water to stop the reaction. The material obtained is stored in inert environment for further characterization.

3.2.5 Characterization

Gel permeation chromatography (GPC) (Shimazdu, Japan) is used for the measurement of molecular weight of prepared biocomposite at 40°C. HPLC grade chloroform is used as an eluent with a flow rate of 1.0 mL.min^{-1}. Columns are calibrated with polystyrene standard in the range of 144 Da to 500 kDa. The samples are prepared by the addition of 5-10 mg of samples in 1 mL of chloroform and filtered using 0.45 µm syringe filters before analysis. The thermal transitions of the prepared specimen are estimated using Netzsch DSC 204 F1 Phoenix Differential Scanning Calorimeter. 5 to 10 mg of specimen are heated from 25°C to 190°C with scan rate of 10°C.min^{-1}.

The ^{1}H-NMR spectra of the specimen are recorded using Bruker 600 MHz NMR spectrometer. The samples are prepared by dissolving specimens in deuterated chloroform ($CDCl_3$).

Acid value of the samples is measured as per given **Equation 3.1**

$$Acid\ value = \frac{ml\ of\ sample \times Normality\ (NaOH) \times 40}{gm\ of\ lactide} \qquad 3.1$$

The samples are prepared by dissolving the pre-measured amount of lactide in methanol and titrated with alcohol solution of sodium hydroxide in presence of phenolphthalein as indicator.

Specific rotation of the samples is measured using automatic polarizing optical microscopy from Rudolph research analytical, USA. The length of the cell utilized for optical polarimetry is 100 mm. The system is calibrated with quartz automatic calibration using methanol as a reference. Samples are prepared by dissolving lactide into methanol with 1 gm per 100 mL concentration.

3.3 Results and Discussion

3.3.1 Oligomerization of lactic acid

Oligomerization is conducted using two different heating modes i.e. conventional heating and microwave heating (**Figure 3.4**). Microwave power and time is optimized after running set of reactions with different conditions. It is found that 2 hours of microwave (20% power of 800 watt) exposure is sufficient to polymerize 500 gm of lactic acid and temperature is reached to ~190°C as shown in **Figure 3.5**. As we know that the microwave works at molecular level and the heat is generated by the friction of molecules in dipole rotation due to microwave energy, the heating is very fast in comparison to the conventional heating and took less time.

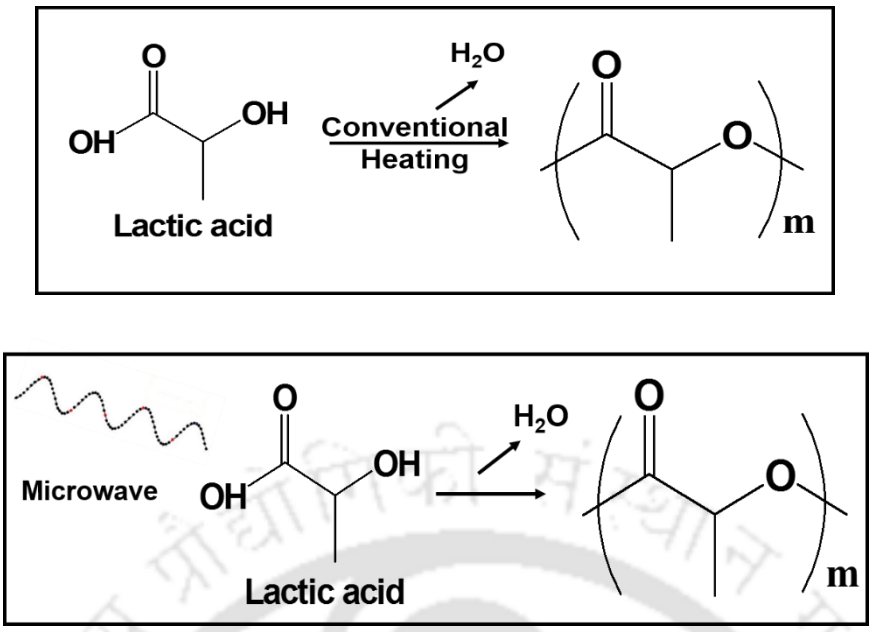

Figure 3.4: Oligolactic acid synthesis using conventional and microwave heating.

In the commercial microwave oven, the microwave power can be set in the multiples of 20% of total power (800 watt) where 20% is the lowest power. The oligomerization is done at 20% microwave power and oligomer is synthesized for different time duration in microwave. The molecular weight of oligomer obtained from 500 gm batch of lactic acid and its specific rotation is shown in **Figure 3.6**. It can be seen that the molecular weight of the oligomer is increased as the microwave time increased. Within 2 hours, it reached more than 1500 Da. In case of lactic acid, it is very important to monitor the specific rotation of the molecules in order to get high quality lactide and PLA. Specific rotation of the oligomer increased as the chain length of PLA molecules increased. The initial specific rotation of the lactic acid is found to be ~12° which is increased with increase in the molecular weight of the oligomer. It reached to ~104° in two hours of microwave and found to be reduced beyond two hours. This may be attributed to the inversion of the lactic acid or the formation of lactide as by-product during oligomerization.

The oligomer prepared by dehydration of lactic acid via conventional heating needed 8-10 hours to remove excess water from the bulk lactic acid in inert gas flow. Due to the increase in concentration of lactic acid, it began to polymerize which generated molecules of water as by-product. Removal of these molecules is not possible only by the flow of inert gas. Vacuum is applied gradually and stable to ~0.1 mbar for 7 hours which enhanced the process to remove the water and accelerated the polymerization process. Oligomer obtained by the process had the molecular weight of Mw <1000 Da, and PDI = 1.1.

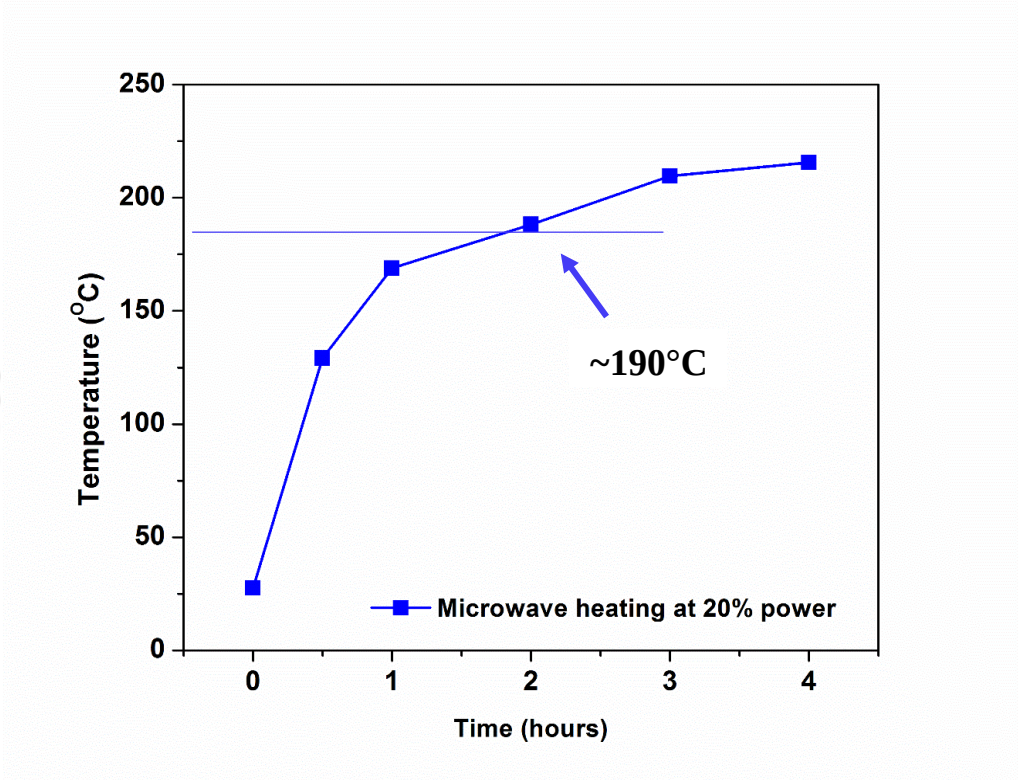

Figure 3.5: Microwave heating temperature vs time required for the oligomerization of 500 gm batch of lactic acid.

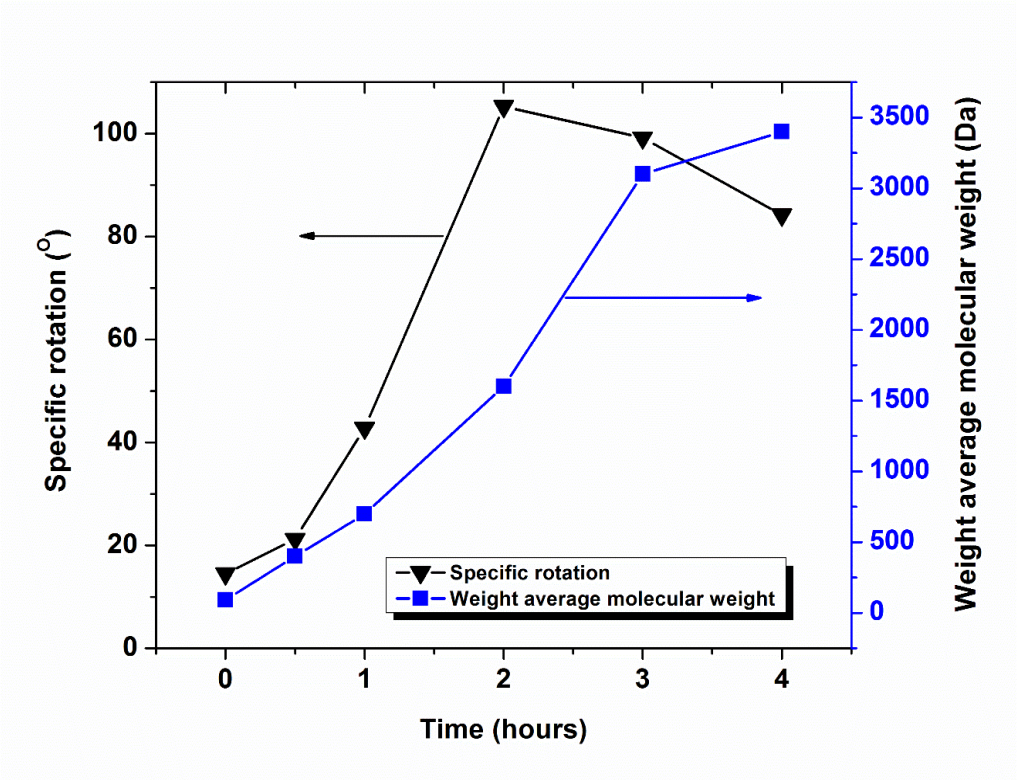

Figure 3.6: Track of molecular weight and specific rotation of oligomer vs microwave heating time.

3.3.2 Lactide synthesis and purification

Further, the oligomer is heated to 220°C-250°C and gradually the pressure is decreased to ~0.01 mbar after addition of 0.1-10 wt% Tin Oxide (SnO) as catalyst. As the temperature reached the set temperature, the oligomer began to depolymerize into lactide. This process is carried out for 12-25 hours to convert the entire 1000 gm of oligomer to lactide. Crude lactide received from the reactor may contain impurities in the form of lactic acid, oligomer, trimer, cyclic oligomer etc. The purification is done to remove the unwanted entity from lactide. Purification of crude product is a crucial step for the PLA synthesis. The molecular weight of polymer depends on the impurities present in the lactide. In this study, the effective solvents for purification are sorted and three different purification techniques are compared: simple washing with solvent, direct recrystallization and washing followed by recrystallization.

The impurities in the form of lactic acid or dimer, trimer of lactic acid or cyclic oligomer which are soluble in water can be removed by washing with water. Further, the alcohol soluble content of moisture can be removed through washing with other solvent such as methanol, ethanol, ethyl acetate, acetonitrile. To select the best solvent, 20 gm of crude lactide is first crushed to powder and washed with chilled water at 5°C followed by washing with other solvents in the vacuum filtration unit. From **Figure 3.7**, it can be concluded that water and acetonitrile combination is effective in washing process which gave molecular weight in the range of 100 kDa however, the yield of 4.5% is relatively very low in comparison to other solvents. Water and methanol combination showed the highest yield 26.1% and molecular weight is found to be ~61,000 Da which is a relatively better yield.

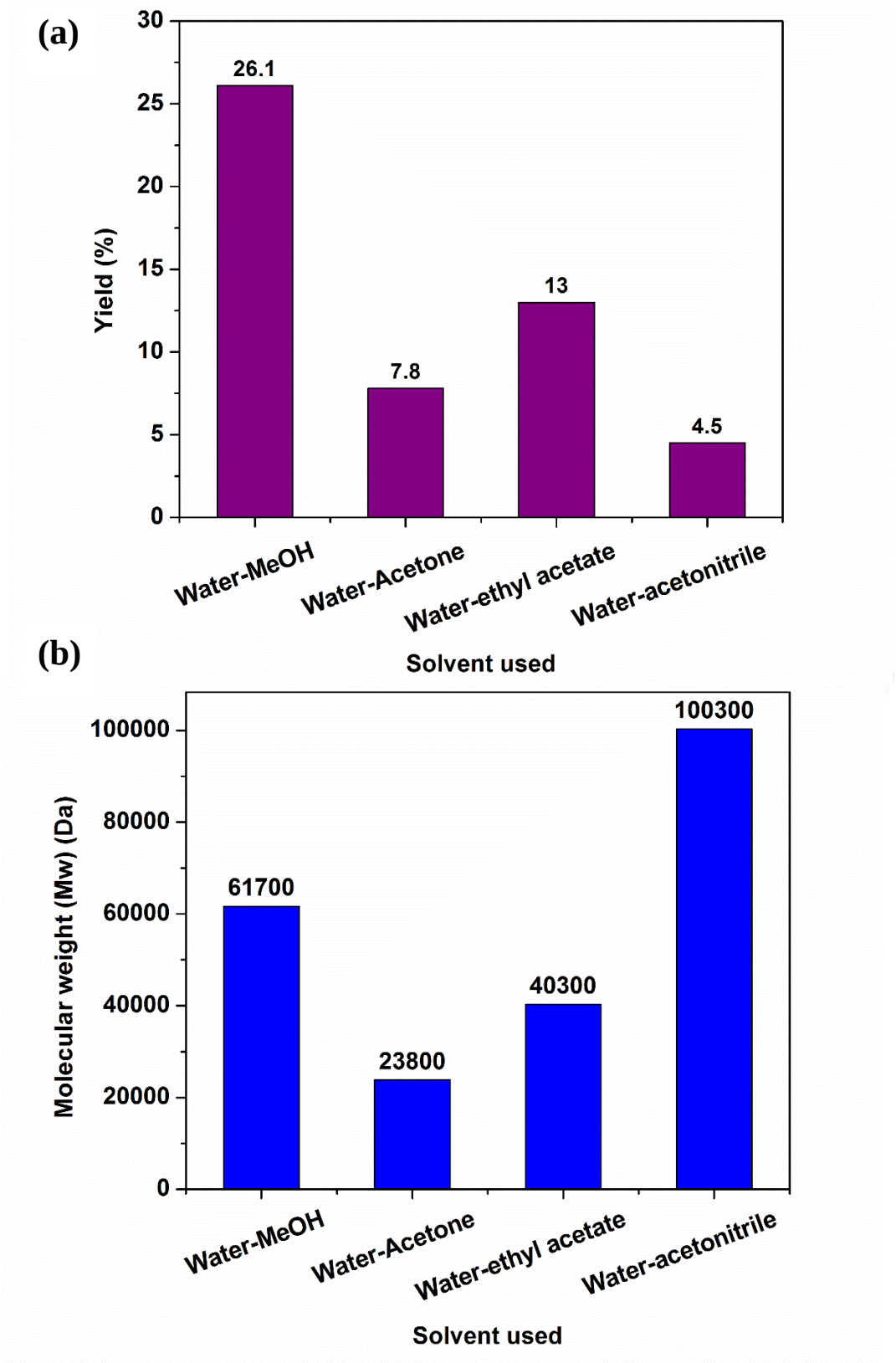

Figure 3.7: (a) Solvent versus %yield & (b) molecular weight for solvent screening.

The yield for water and methanol combination is observed high because lactide is not soluble in water at lower temperature (5°C) and washing the crude lactide with cold water removes impurities such as lactic acid, low molecular weight oligomers, cyclic oligomers etc. Subsequently washing the lactide with methanol removes the remaining water and other oligomeric contents present in the lactide. In the case of other solvents, water is very less soluble in ethyl acetate which is responsible for non-removal of water after wash with cold water which leads to low molecular weight PLA as well as yield. So, water and methanol combination is chosen for the further washing analysis of crude lactide.

From the commercialization point of view, it is very important to avoid the process which involves high energy requirement. In this regard, the washing process is extended by increasing the cycles of washing by selected water-methanol combination. It is found from **Table 3.2** that the molecular weight of PLA is increased from ~8 kDa to 104 kDa with increase in the cycles of washing which shows that the purification is enhanced due to the washing process. It is found that the acid value reduced from ~63 to ~12 which is responsible for the enhancement of the PLA molecular weight. Washing beyond four times is not effective as it can be concluded that the washing process has the limitation to reach to acid value of 12 and subsequently the yield reduced drastically. However, for the production of low molecular weight PLA (<100 kDa), the lactide obtained only from washing process can be used.

Table 3.2: Effect of washing cycles on acid value of lactide and molecular weight of PLA.

Sl. No.	No. of washing	Amount of water used (mL)	Amount of MeOH used (mL)	Wt. of crude after washing	Acid Value	PLA Molecular weight	
						Mw	PDI
01	One	1000	177	154	62.8	7,900	2.5
02	Two	308	154	103	34.4	51,500	2.08
03	Three	103	50	97	27.3	92,500	2.11
04	Four	--	48	72	11.6	115,000	2.22
05	Five	--	36	66	12.1	104,500	2.35

In direct crystallization process, the crude lactide is directly dissolved in the selected solvent at elevated temperature and recrystallized by cooling the solution followed by filtration. Three solvents such as ethanol, methanol and ethyl acetate are tested for direct crystallization. The criteria for the selection of solvent is the molecular weight of final synthesized PLA. Screening of solvent for the direct crystallization is done by dissolving 100 gm of crude lactide in 100 mL of different solvents at 55°C. Solution is cooled down slowly and set to -5°C for 3 hours. Recrystallized lactide is filtered out from the solution using vacuum filtration and dried in vacuum at 60°C for 12 hours. The dried lactide is polymerized and characterized. It is concluded from **Table 3.3** that the molecular weight of PLA synthesized using ethyl acetate and methanol crystallized lactide is approximately equal (~92 kDa) and higher than ethanol crystallized lactide (~56 kDa). However, the percentage yield of lactide recrystallized using ethyl acetate is highest (~68%). In case of ethyl acetate and methanol, the acid value is found to be lower (~13) than ethanol (~36).

So, using these results, it can be concluded that ethyl acetate is found to have good results for recrystallization of lactide. Ethyl acetate is further used for the purification of lactide.

Table 3.3: %Yield and acid value of purified lactide and molecular weight of synthesized PLA.

Sl. No.	Solvent used	Yield (%)	Acid value	PLA Molecular weight	
				Mw (Da)	PDI
01	Ethyl acetate	68	13.4	94,700	2.1
02	Ethanol	50	35.6	56,200	2.2
03	Methanol	53	12.6	92,900	1.6

In the purification of crude by combination of washing and recrystallization processes, the crude lactide is first washed with water-methanol mixture and dried under vacuum. Then obtained material is dissolved in ethyl acetate followed by its crystallization as explained in direct crystallization. The crystallization is repeated for the second time in order to get higher purity. From **Table 3.4**, it is found that the acid value significsntly reduced to 1.7 after second recrystallization. For washing process, acid value is found to be ~63 and for first recrystallization process it is ~15. The reduction in the acid value directly affected the molecular weight of the synthesized PLA. After second recrystallization, molecular is weight found to be more than 300 kDa.

Table 3.4: Results for combined washing and crystallization process.

Sl No.	Steps	Solvent used	wt. of crude after step	Acid value	PLA Molecular weight	
					Mw	PDI
01	Washing	Water followed by methanol (5 times of crude weight)	392 gm	62.8	7,600	1.8
02	First crystallization	Ethyl acetate (0.5 times wt. of washed crude)	272 gm	14.6	81,700	2.8
03	Second crystallization	Ethyl acetate (0.5 times wt. of first crystallized lactide)	245 gm	1.7	356,100	1.7

Further, the purity of the lactide after purification process is analysed by DSC and NMR study. DSC analysis of the lactide and PLA is shown in the **Figure 3.8**. It is found that the onset melting temperature of the lactide purified by single washing is ~80°C which increased to 97.5C in case of recrystallization. The results suggest that the washing cum recrystallization process is an effective process which gave high purity lactide. The melting temperature of synthesized PLA using different lactide is also found to increase from 150°C to 168°C which suggested high purity of lactide.

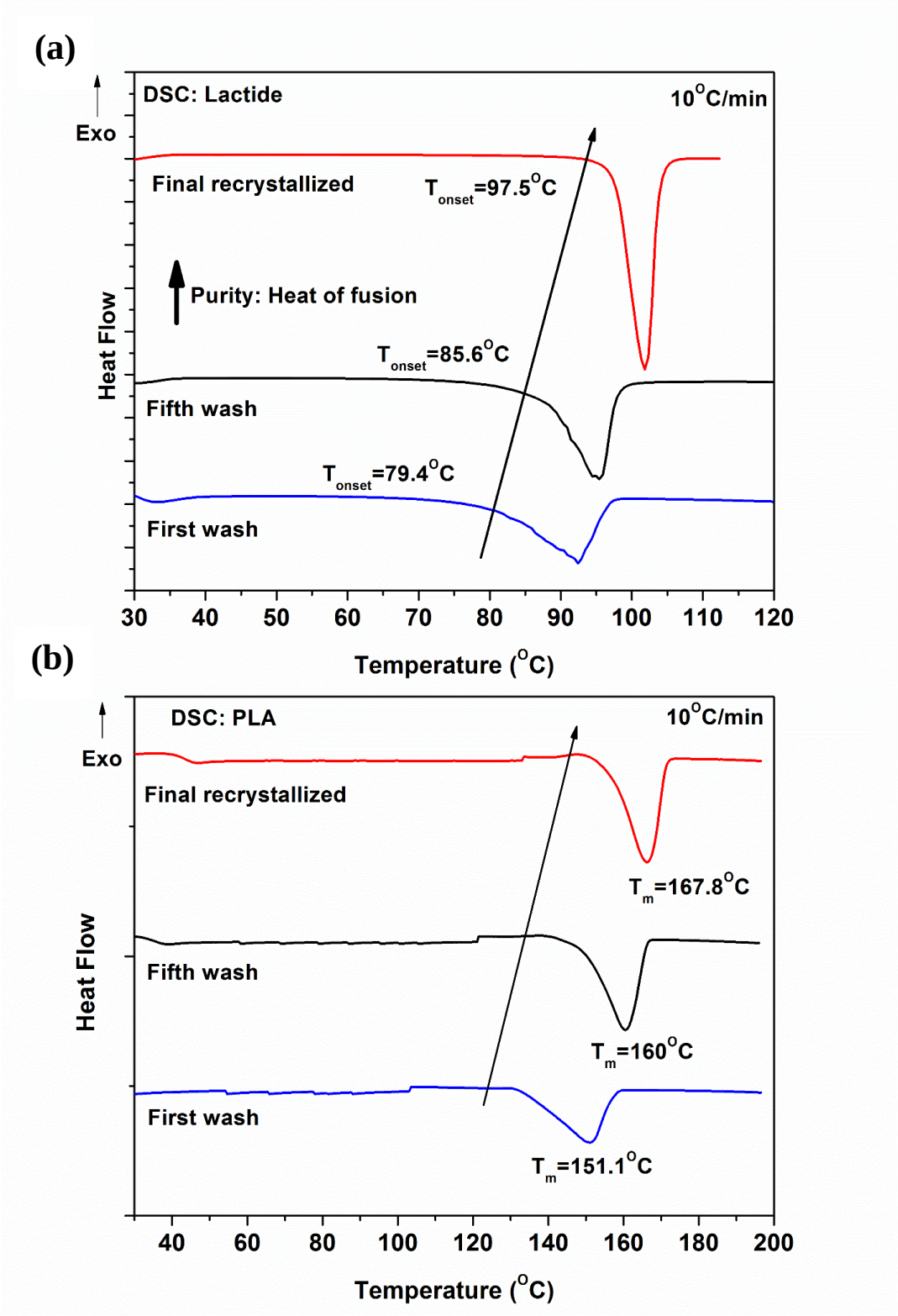

Figure 3.8: DSC thermogram of different purity (a) lactide & (b) PLA.

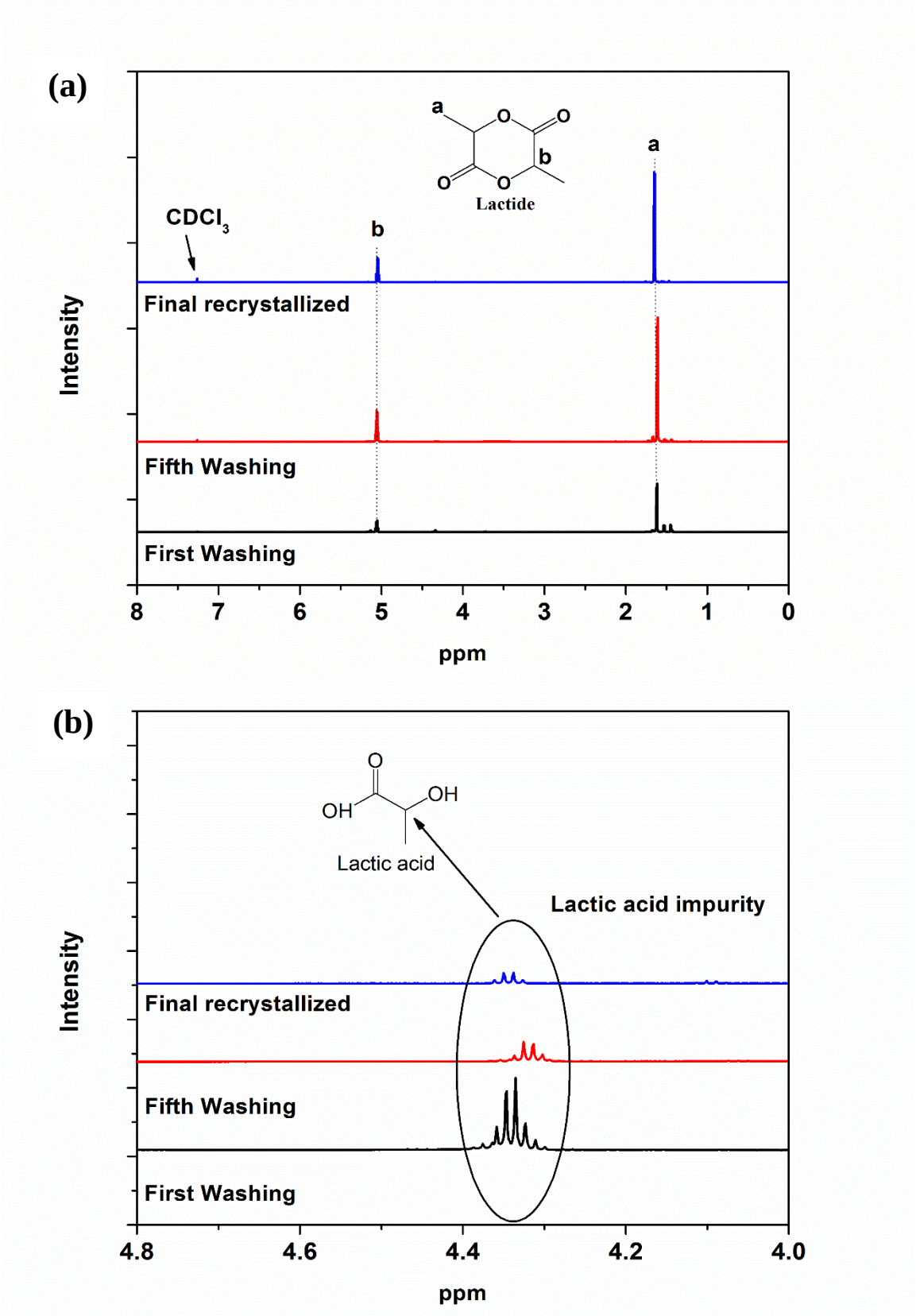

Figure 3.9: ^{1}H-NMR of different purity lactide (a) & (b).

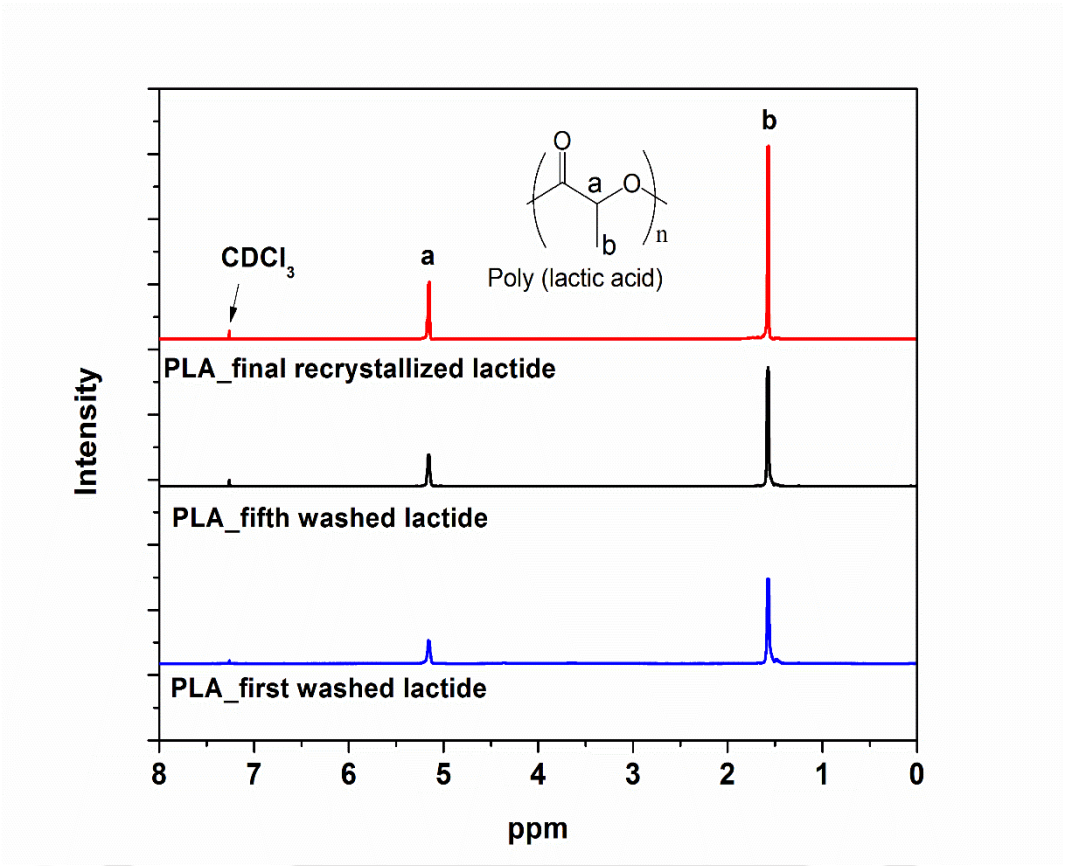

Figure 3.10: ^{1}H-NMR of PLA from lactide.

The proton NMR is a powerful tool to analyse the impurity present in the system. The ^{1}H-NMR spectra of purified lactide is shown in the **Figure 3.9**. The resonance peak at 5.16 ppm and 1.57 ppm represents methylene and methyl groups present at lactide molecules. After magnifying the spectra, it is found that peak between 4.3 to 4.4 ppm belonged to the impurity of terminal hydroxyl group of lactic acid or oligomer. The intensity and the area under the curve is reduced as the lactide is more purified recrystallization method. Similarly, the ^{1}H-NMR spectra of PLA synthesized using different purity lactide is shown in **Figure 3.10** and found similar behaviour as lactide. The terminal methylene group is presented by spectra between 4.3 to 4.4 ppm and the intensity and area under the curve is significantly reduced for PLA from lactide purified by recrystallization process. The terminal methyl group present in PLA chains is shown by peak at 1.47 ppm which is diminished as the purity of lactide is improved.

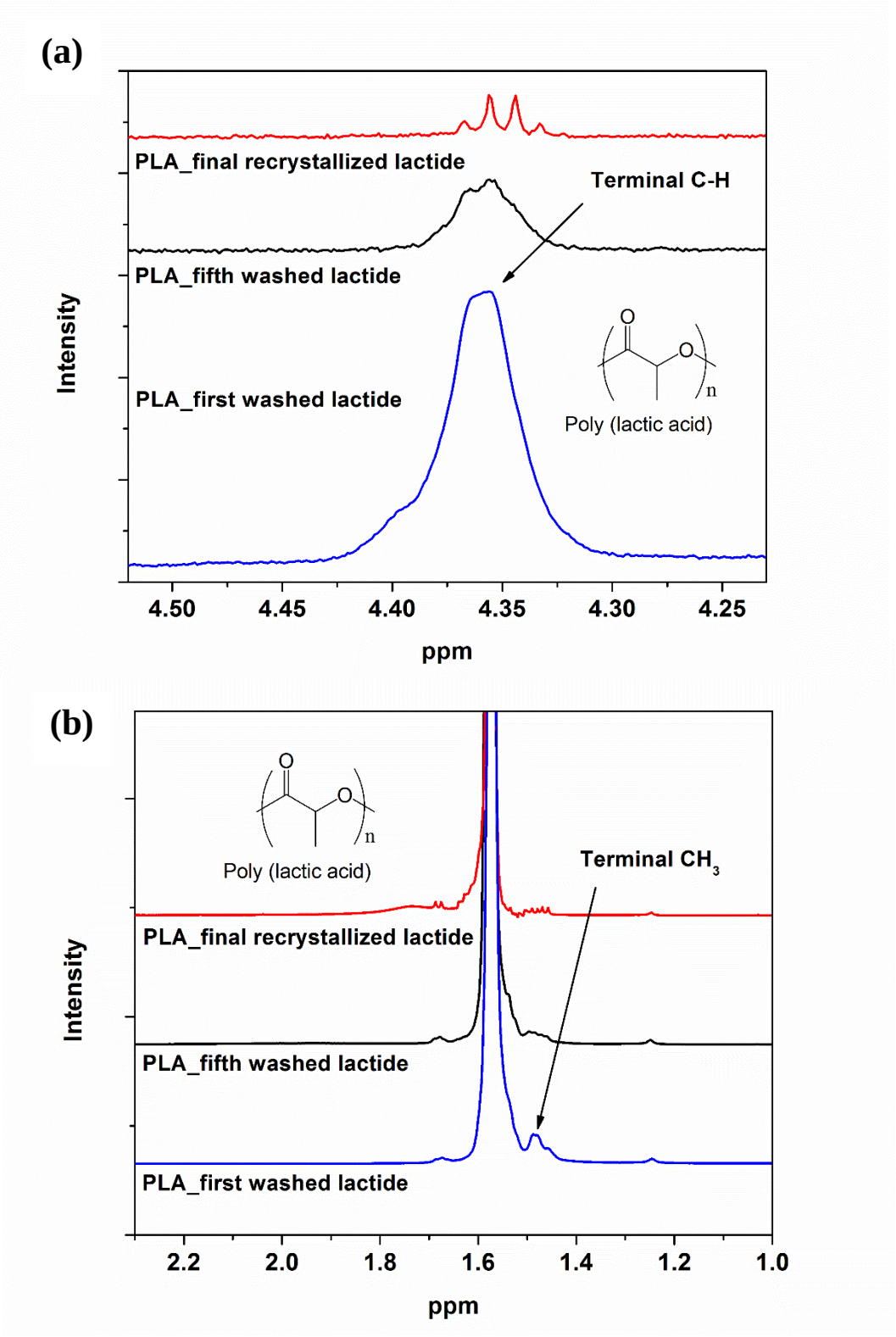

Figure 3.11: Magnified ^{1}H-NMR of PLA from different purity lactide.

3.4 Conclusions

Overall, it is found that microwave heating approach is relatively faster where 500 gm of L-lactic acid can be oligomerized with M_w 1500 Da in 2 hours at 20% power of microwave. For washing, water and methanol combination is found suitable and ethyl acetate showed good results for the recrystallization of lactide. In case of only washing, the molecular weight of synthesized polymer is observed very low to be ~8 kDa which rose to ~100 kDa after 5 times washing with a significant reduction in the yield. Whereas in case of direct crystallization, the molecular weight reached to the desired amount (100 kDa) but the yield is relatively low. Combined washing and recrystallization is found effective to remove the impurities present and for higher product yield, relative to other processes. The acid value for the purified lactide using washing cum recrystallization is found to be ~1.7 which subsequently gives PLA with higher molecular weight i.e. 300 kDa.

CHAPTER: 4

Synthesis and Characterization of Stereocomplex PLA-Cellulose Microcrystal based Biocomposite

Graphical abstract

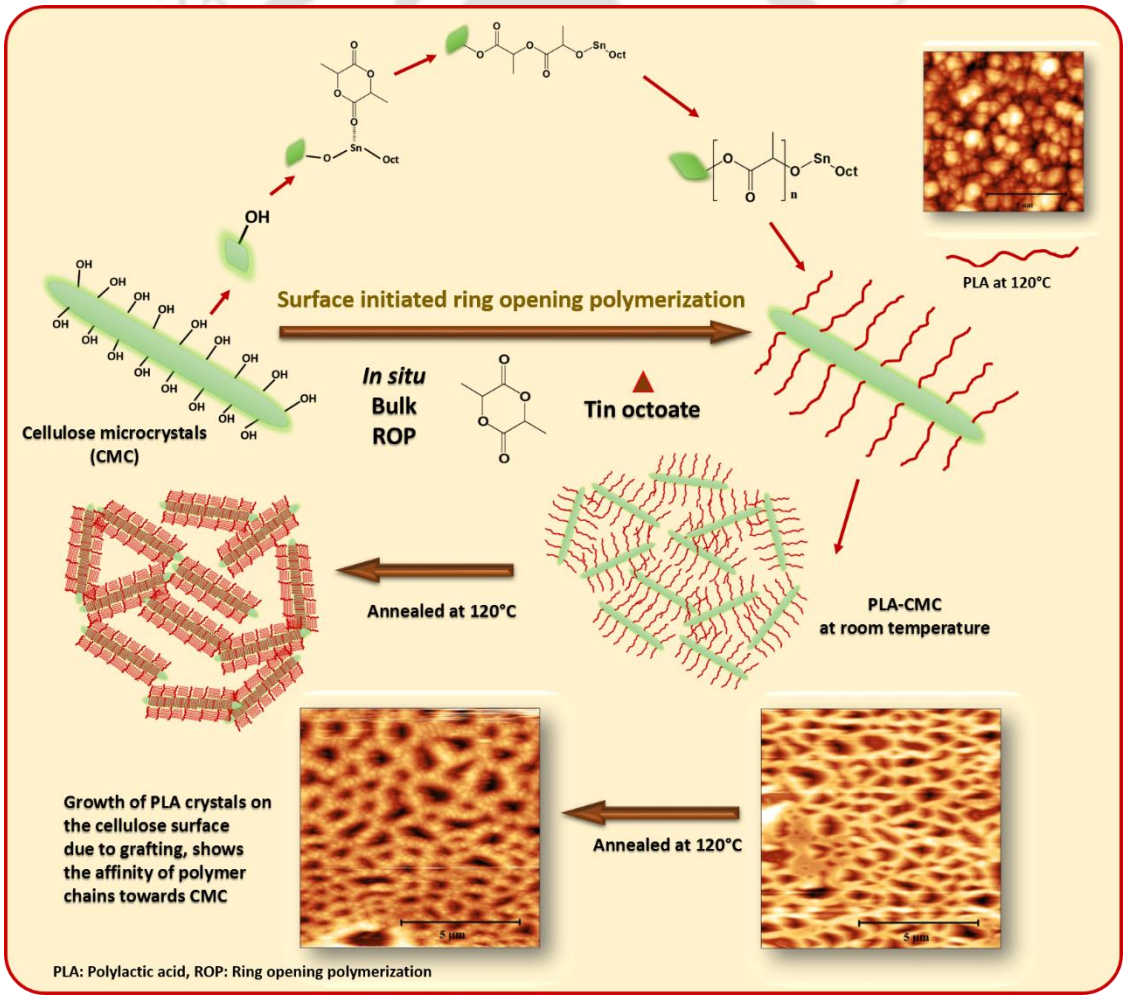

ACS Sustainable Chemistry & Engineering 2017, 5 (8), 6835-6844

Abstract

This work presents a facile, solvent-free approach for the fabrication of PLA biocomposites, followed by melt extrusion process to prepare stereocomplex PLA films with excellent thermomechanical and gas barrier properties. Presence of stereocomplex crystallites improves the thermal properties of PLA; however in case of high molecular weight poly(L-lactic acid) and poly(D-lactic acid) blends, the formation of stereocomplex crystallites is predominantly lesser compared to homocrystallites. Grafting of biofillers with polymer matrix chains may help in uniform dispersion of CMC enhancing the formation of stereocomplex crystallites. Henceforth, stereocomplex PLA is fabricated with chemically modified cellulose microcrystals (CMC) as filler, which is prepared by in-situ ring opening polymerization of D-lactide. The stereocomplexation in the blend system is found to be enhanced by the extended molecular surface area provided by grafted CMC. As confirmed by morphological analysis, the modification of CMC drives the uniform dispersion into the matrix and reduction in the size of CMC in the range of ~200 nm diameter. Increased melting temperature (~209°C) with no evidence of homocrystallites confirms the role of grafted CMC in the formation of stereocomplex crystallites by suppressing the development of homocrystals. The fraction of stereocomplex crystallites is found to be 100%, which is confirmed by the X-ray analysis. The enhanced stereocomplexation in the composites resulted in ~50% improvement in the tensile strength in comparison to pristine PLLA/PDLA blend. Interestingly, the oxygen permeability and water vapour permeability are reduced by ~25% and ~35%, respectively. The improved thermomechanical properties of the biocomposites through enhanced stereocomplexation may comply with the requirement for high temperature engineering and packaging applications.

4.1 Introduction

The increasing concern about the environmental and human health issues [122] encourages the research and scientific community to develop biobased material for different applications. Among the list of biodegradable polymers, PLA (PLA) has comparable gas barrier, thermal and mechanical properties, which make it a promising candidate in order to replace the petroleum based polymers [123]. PLA is a kind of biobased aliphatic polyester derived from lactic acid, which is a fermented product of renewable resources such as corn, potato or other glucose rich materials [13]. In adverse, due to carrying some shortcomings over existing biomass derived plastics, such as low glass transition temperature, low melting temperature, poor melt strength, low crystallization rate, relatively poor gas barrier properties etc., reduces its extensive use in several engineering applications. In this regards, the properties of PLA are trying to improve through various routes and enormous researches are going worldwide and attention has been given to stereocomplexation and fabrication of biocomposite [124] of PLA.

Stereocomplexation of PLA was first introduced by Ikada and coworker [57]. They have reported increased melting temperature of the stereocomplex PLA by ~50°C in comparison to enantiomeric pure PLA. Stereocomplexation is a special type of crystalline arrangement of PLA chains that can be fabricated by solution or melt mixing of the two enantiomers i.e. poly(L-lactic acid) (PLLA) and poly(D-lactic acid) (PDLA). Formation of stereocomplex crystallites increase the chain packing, which ultimately leads to increase in the crystalline density of the PLA. Subsequently, the physical properties of the material such as thermal, barrier, mechanical properties also get enhanced. It is also reported that, in case of molar mass more than 100 kDa, homocrystals evolve along with stereocomplex crystallites, which gives negative impact to the properties of end product such as decreasing

the melting temperature of the PLA with relatively poor mechanical and gas barrier properties.

On other hand, producing biocomposite using natural fillers such as clays [123, 125], cellulose [30], cellulose nanocrystals [44], silk [126, 127], chitosan [42, 128], gums [129], sucrose palmitate [130], etc. also enhances the thermal, barrier and mechanical properties of PLA. Researchers are using these materials directly or after modification [61, 131] with polymer matrices to enhance the polymer properties to act as proper packaging materials [62]. Among these materials, cellulose is the most abundant, naturally occurring, biobased, low cost material and has relatively excellent chemical and physical properties [79]. It is often observed that the reinforcing efficiency of fillers in polymer matrices is deeply affected by its uneven mixing and agglomeration [81-83]. It is know that the cellulose have large number of hydroxyl functional group present on its surface and it can easily be modified [80]. *In situ* polymerization of monomer in presence of fillers is found to be effective in order to make uniform mixture, which leads to the improved properties of the materials [125, 132-139]. In the case of PLA, hydroxyl functional group present on the surface of cellulose molecules can initiate the polymerization of lactide and propagates on the surface of cellulose. Researchers have adopted the dual strategy i.e. stereocomplexation and formation of biocomposite, to form the stereocomplex PLA cellulose based biocomposite. Jiang et al. [140] have directly used cellulose nanocrystals as nucleating agent in the PLLA/PDLA blend matrix and they found improved crystallizability of the blend. Habibi et al. [141] have studied the effect of stereocomplexation on cellulose PLA biocomposite. They synthesized the surface modified cellulose nanocrystal by ring opening polymerization of D-lactide in solution and melt blended with PLLA in order to form stereocomplex. Similar process of modification of cellulose has been utilize by Wu et al. and Miao et al. [137, 142] and stereocomplex are been reported either by solution or by

melt blending method. Purnama and Kim [143] have prepared the biocomposite of stereocomplex polylactide and cellulose nanowhisker using supercritical fluid technology. They grafted the cellulose nanowhisker with PLLA or PDLA and mixed with each other in the ratio of 1:1, and treated the same in supercritical condition in presence of carbon dioxide and dichloromethane. Other methods such as use of comb-shaped cellulose-g-poly(lactide) nanohydrids [144] or cellulose acetate-g-poly(lactic acid)s with comblike topology [145] was also been employed by the researchers to fabricate the stereocomplex PLA cellulose biocomposite. It is common in most of the research articles that grafting or modification of cellulose involves toxic organic solvents and same is also used in the fabrication of stereocomplex PLA cellulose biocomposite. Several report is available which deals with the crystallization kinetics of stereocomplexation in PLA cellulose biocomposite. However, to the best of our knowledge, no literature has yet been reported emphasizing its real-time application oriented properties like packaging and high temperature engineering field.

In this work, a simple and versatile method for chemical modification of cellulose microcrystals (CMC) and its subsequent use in the fabrication of stereocomplex PLA cellulose biocomposite has been presented. PDLA grafted CMC has been produced by *in situ* ring opening bulk polymerization of D-lactide in presence of CMC and the same is used as filler into the PLLA matrix. It is assumed that, due to grafting of PDLA on the surface of CMC, modified CMC will be dispersed uniformly and the PDLA chains will provide the extended molecular surface area, which may enhance the stereocomplexation in matrix. The mechanism of stereocomplexation in presence of PDLA-*g*-CMC and its effect on various properties of the fabricated biocomposites including mechanical, barrier and thermal properties are discussed.

4.2 Experimental section

4.2.1 Materials

L-lactic acid and D-lactic acid are procured from Purac, India and Musashino Japan, respectively. Tin oxide (SnO), cellulose microcrystals (CMC) and stannous octoate are supplied from the Sigma Aldrich. Toluene and chloroform are provided by Merck India. L-lactide and D-lactide are synthesized by two-step polymerization and depolymerization procedure. L-lactic acid or D-lactic acid was dehydrated at 110°C to get the oligomeric PLLA or PDLA and it is depolymerized in presence of tin oxide to obtain the L-lactide or D-lactide after purification. All chemicals are used as received without further purification.

4.2.2 Preparation of PDLA grafted CMC

PDLA grafted CMC with different CMC composition are synthesized through *in situ* ring opening polymerization. *In situ* polymerization is conducted in a glass ampoule with magnetic stirring bar dipped in oil bath. D-lactide and required amount of CMC and catalyst tin octoate toluene solution are added to the ampoule with monomer and catalyst molar ratio of 2000:1. The ampoule is purged with argon gas for one hour to make it free of moisture and dissolved oxygen. The vacuum is applied to the ampoule for two hours to eliminate the excess amount of toluene. Ampoule is sealed under the vacuum condition and oil temperature is raised to 105°C. After mixing of monomer, CMC and catalyst is for two hours, the temperature is increased to 160°C and ampoule is left for two more hours for ring opening polymerization. The obtained PDLA grafted CMC is removed by breaking the ampoule and named as PDLA-CMC. PLLA and PDLA blends are also synthesized in the same fashion. The granulated form of PLLA, PDLA and composite are kept in vacuum oven at 40°C for 12 hours to remove the residue monomer.

4.2.3 Preparation of stereocomplex PLA-CMC based biocomposite

In this procedure, PDLA-CMC and PLLA (both lab synthesized) with 1:1 weight ratio are mixed and extruded into the twin screw miniextruder (HAAKE^{TM} MiniLab II from Thermo Scientific). Miniextruder is first heated to 210°C for 30 min and the screw speed is maintained at 30 rpm. Initially, the neat PLLA is extruded to get the uniform temperature into the equipment. The mixture of PLLA and PDLA-CMC is introduced into the closed loop for melt mixing of materials. After two minutes, the loop is opened to receive the mixed melt into the injection moulding cylinder maintained at 210°C (HAAKE^{TM} MiniJet Pro from Thermo Scientific) for formation of dumbbell shape articles. The mold temperature is kept constant at 90°C. The stereocomplex PLA biocomposite with 0.5%, 2.5% and 5% CMC content denoted as sPLA-0.5%CMC, sPLA-2.5%CMC and sPLA-5%CMC, while neat stereocomplex PLA is denoted as sPLA.

4.2.4 Characterization

The FTIR spectra of the samples is measured by attenuated total reflection (ATR) mode in Frontier FT-IR spectrometer (Perkin Elmer, USA) at room temperature. Spectra is recorded after 16 scan from wave number 4000 cm^{-1} to 650 cm^{-1}. The purification of grafted CMC is done by dissolution followed by centrifugation process. Grafted CMC is dissolved into the chloroform (10 mg/mL) and centrifuged at 5000 rpm and again dissolved the solid residue into chloroform to remove the excess PLA or oligomeric chains and centrifuged it. This process is repeated four times and complete removal of ungrafted PLA chains is confirmed by FTIR. The prepared biocomposite directly analysed and spectra are recorded.

The molecular weight of prepared materials is measured using the gel permeation chromatography (GPC) (Shimazdu, Japan) at 40°C. HPLC grade chloroform is used as eluent with flow rate of 1.0 $mL.min^{-1}$. The system is calibrated using the mono-dispersed

polystyrene standard. Prepared biocomposite dissolved into the chloroform with 5% HFIP content and filtered through 0.45µm PTFE syringe filters before analysis. The molecular weight and specific rotation of the PLLA and PDLA-CMC is tabulated in **Table 4.1**.

The surface topography and morphology of CMC and other PLA composites are assessed using Atomic force microscopy (AFM) (Agilent, Model 5500 series) with silicon cantilever having a spring constant of 42 N/m at a resonance frequency of 320 kHz. The samples are prepared by drop casting followed by drying at room temperature for 48 hours. AFM images is analysed with the Gwyddion software (version 2.41).

Field Emission Scanning Electron Microscope (FESEM) is used to examine the topography of the fractured surface of different samples placed on carbon tape. The samples are further coated in gold sputtering unit for 30s and characterized using FESEM (Sigma, Zeiss, GmbH) at accelerating voltage of 3-4 kV.

The thermal behaviour of the biocomposite is measured using the differential scanning calorimeter (DSC) (Phoenix DSC 204 F1 NETZSCH, GmbH) under nitrogen atmosphere. 5 to 10 mg of sample is heated from 20°C to 250°C and kept isothermal at 250°C for 2 minute to get rid of thermal history. Material is cooled to 20°C with 10°C.min^{-1} cooling rate and then heated to 250°C with same heating rate.

X-ray diffraction (XRD) spectra are taken using Model-D8 Advance system diffractometer (Bruker, Germany) equipped with Cu-Kα radiation (λ= 0.1541 nm) as X-ray source operating (40 kV, 40 mA) at a scan rate of 3° per min in the 2θ range 5–40°. The degree of crystallinity and fraction of stereocomplex crystallites (f_{sc}) are determined using following equation

$$X_{c,sc}(\%) = \frac{A_{c,sc}}{\left(A_{c,sc} + A_a\right)} \times 100 \qquad (4.1)$$

$$X_{c,hc}(\%) = \frac{A_{c,hc}}{\left(A_{c,hc} + A_a\right)} \times 100 \quad (4.2)$$

$$f_{sc}(\%) = \frac{X_{c,sc}}{\left(X_{c,hc} + X_{c,sc}\right)} \times 100 \quad (4.3)$$

Where, $X_{c,sc}$ and $X_{c,hc}$ is the degree of crystallinity of stereocomplex and homo crystallites, respectively. $A_{c,sc}$ and $A_{c,hc}$ is the area for the stereocomplex, homo crystallites and A_a is the area of amorphous phase.

The oxygen gas transmission rate (OTR) for the biocomposites with various loading of CMC is determined using OX2/231 oxygen permeability tester (Labthink, China). Measurements are carried out at 23°C using oxygen gas of high purity (99.999%) on a film having an area of 50 cm^2 following the ASTM D3985 standard. Pure oxygen (99.9%) at pressure of 0.5 bar and a flow rate of 20 mL/min is maintained into the upper half of the sample chamber during analysis while nitrogen gas is continued into the lower half of the chamber. The chambers are purged for at least 6 hours before measurement. The test is performed for at least 6 hours so as to reach steady state.

Water vapor transmission rate (WVTR) are recorded using a PERMATRAN-W® Model 1/50 (Mocon, USA) following ASTM standard E398-03. The relative humidity (RH) is fixed to 100% in the wet chamber and 10% in the dry chamber, yielding a driving force of 90% RH. The film of 50 cm^2 area is analyzed at atmospheric pressure and at temperature of 37.8±0.1°C.

The tensile strength and percentage elongation of prepared samples (5 mm width, 2 mm thickness and 50 mm gauge length) are measured using universal testing machine (KIC-2-050-C, Kalpak instruments and controls, India) equipped with 500 N load cell at

constant cross-head speed of 5 mm.min^{-1} in tensile mode. Three replicates of each sample are tested and the average results are reported with standard deviation.

Mechanical stability of the prepared biocomposites at higher temperatures with dynamic force application are measured using DMA (DMA 242 E model, NETZSCH GmbH) in the temperature range 25–160 °C at 2 °C.min^{-1} heating rate, 1 Hz frequency and 10 µm displacement amplitude.

4.3 Results and Discussion

4.3.1 Synthesis of PDLA Graft CMC

FTIR is a powerful tool to examine the conformation of molecular functional groups and is employed to analyze the grafting of CMC with PLA molecule. **Figure 4.1**, shows the spectra of PLA, CMC and grafted CMC. It can be seen that the characteristic peaks for PLA are located at 1754 cm^{-1}, 1453 cm^{-1}, 1382 cm^{-1}, 1362 cm^{-1}, 1127 cm^{-1} and 868 cm^{-1}, which corresponds to the carbonyl stretching, methyl bending, symmetric and asymmetric bending of –CH-, stretching of –C-O- and –C-C- backbone of PLA [13], respectively. Peaks corresponding to stretching vibration of hydrogen bonded hydroxyl group and C-H symmetrical stretching in CMC are located at 3384 cm^{-1} and 2898 cm^{-1}, respectively. The –CH_2, –CH and OH deformation is assigned to 1427 cm^{-1}, 1373 cm^{-1} and 1317 cm^{-1}, respectively. Wavenumber 1210-920 cm^{-1} is attributed to the C-O stretching of C-OH and C-O-C bond. Peak at 894 cm^{-1} corresponds to stretching and deformation of C-O-C, C-C-H, C-C-O in CMC [146]. Spectra of grafted CMC is recorded after purification. It is observed that the spectrum of grafted CMC has one additional peak at 1754 cm^{-1} along with all the characteristic peaks of CMC. The presence of characteristic peak for carbonyl group i.e. C=O of PLA at 1754 cm^{-1} in spectra of grafted CMC shows the grafting of PLA chains on the surface of CMC. Peaks related to methyl bending, bending of C-H and stretching of

C=O in PLA chains found to be merged with peaks related to CMC. The broadness of the spectra at 3384 cm^{-1} is reduced as CMC is grafted with PLA chains. Further, it is also seen that the suspension of the grafted CMC is more stable than pristine CMC as shown in **Figure 4.2**.

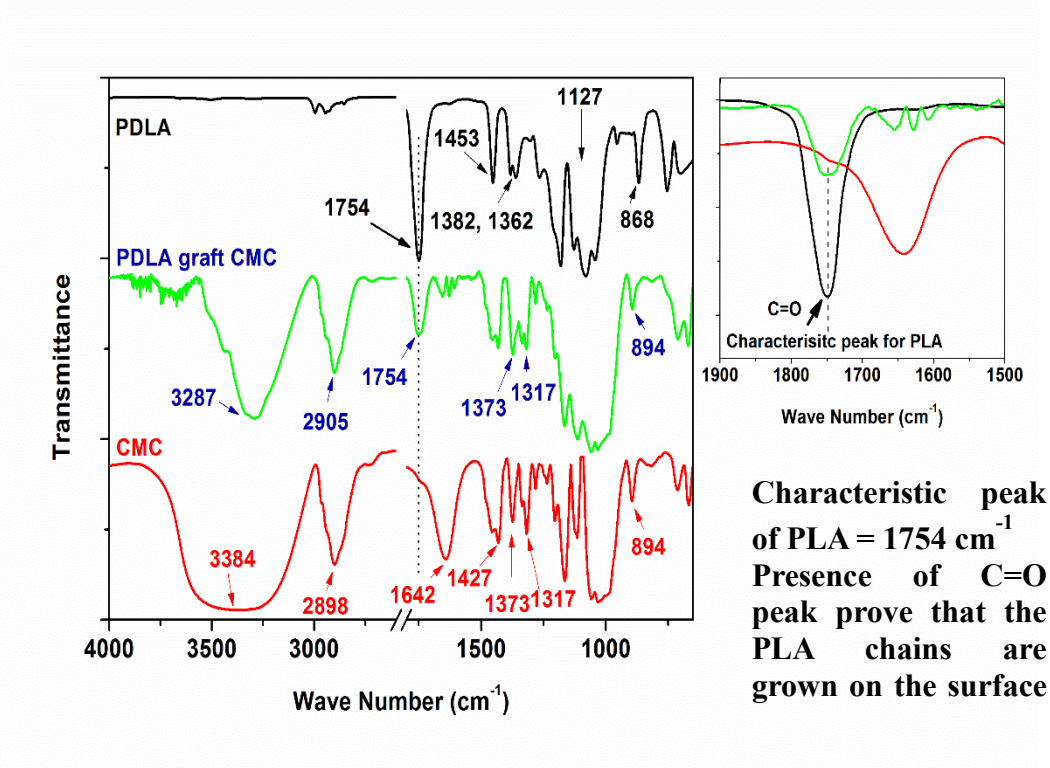

Figure 4.1: FTIR spectra of CMC, Graft CMC and PDLA.

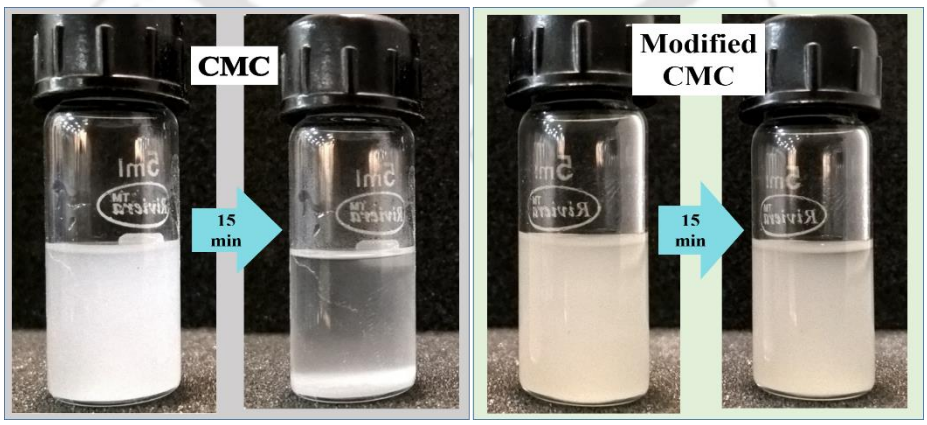

Figure 4.2: Dispersion of CMC and grafted CMC.

Table 4.1: Molecular weight and specific rotation of the synthesized PLA.

Sample Name	M_w (kDa)	PDI	$[\alpha]^{25}_{589}$
PLLA	239	1.5	-157
PDLA	182	1.5	156
PDLA-1%CMC	192	2.1	--
PDLA-5%CMC	222	1.9	--
PDLA-10%CMC	217	2.1	--

M_w: Weight average molecular weight, PDI: Polydispersity index, $[\alpha]^{25}_{589}$: Specific rotation measured in Chloroform **(**1 gm/100 mL)

The AFM images of several samples are shown in the **Figure 4.3-1 and 4.3-2**. Specimens are prepared by solution-drop cast method followed by drying. In the case of pristine CMC, the particles of CMC have formed the percolated self-structure as shown in **Figure 4.3-1a**. Sample of PDLA-1%CMC are also cast on the cover slip same as pristine CMC, same percolated structure is formed due to presence of CMC shown in **Figure 4.3-1b**. To understand the crystallization and spherulite formation by PDLA, the same sample is annealed at 120°C for one hour and AFM images shown in **Figure 4.3-1c**. It is found that the PDLA chains are crystallized on the surface of the CMC due to grafting which helps to the PDLA chains for epitaxial growth on CMC as compared to pristine PDLA (**Figure 4.3-1d**). With increasing CMC concentration, the void space between the CMC particles reduced as shown in **Figure 4.3-2e**. The growth of spherulite on the surface of CMC confirms that PDLA chains have the affinity towards CMC which may be happening due to the grafting.

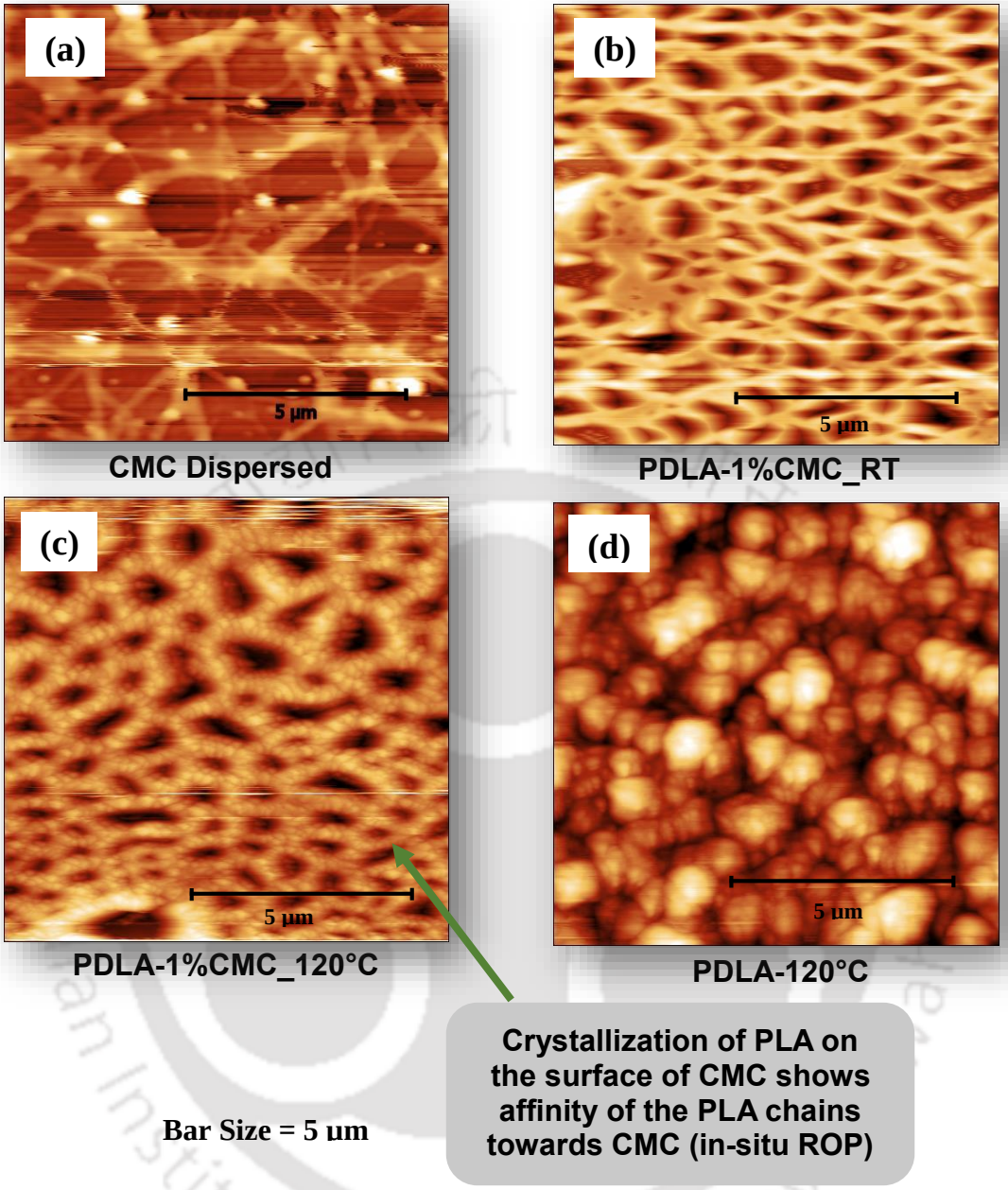

Figure 4.3-1: AFM images of the (a) dispersed CMC, (b) PDLA-1%CMC (room temperature) (c), PDLA-1%CMC (annealed at 120°C) (d), pristine PDLA (annealed at 120°C).

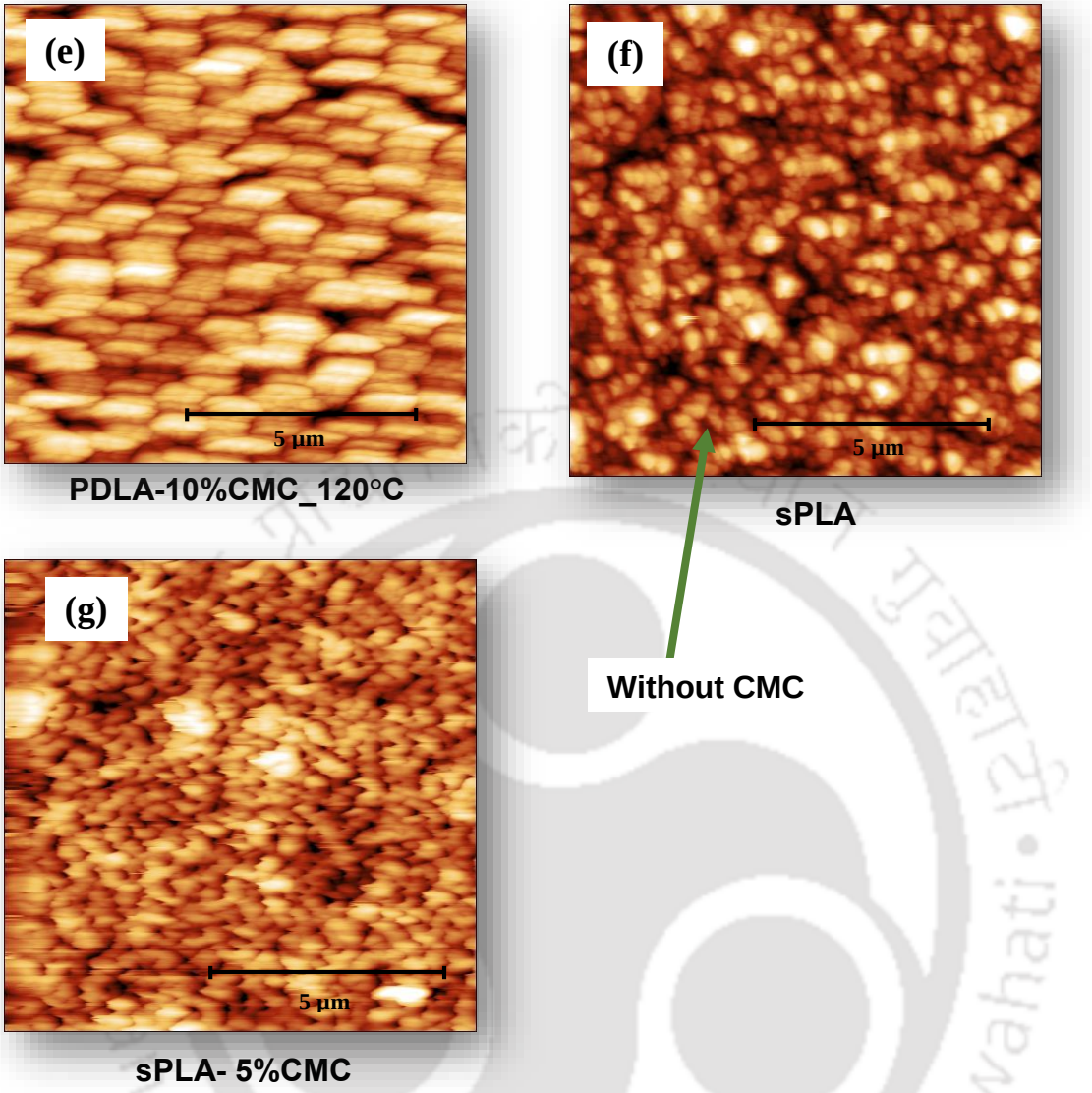

Figure 4.3-2: AFM images of the (e) pristine PDLA-10%CMC (annealed at 120°C), (f) sPLA (annealed at 120°C), (g) sPLA-5%CMC (annealed at 120°C).

From the above discussion, the grafting and its effect has been summarized in the **Figure 4.4,** which shows that the *in situ* synthesis of PDLA in presence of CMC leads to the development of grafted CMC. These grafting helps to enhance the dispersion of the CMC into PLA polymeric matrix which ultimately affect properties of the final product.

4.3.2 Stereocomplex formation

Prepared grafted CMC is used as filler into the PLA matrix to examine its effect on the formation of stereocomplex crystallites. Calorimetry is the best suited analytical technique for the determination of stereocomplex crystallites in PLA. It is known that the homocrystals of PLA is having melting temperature less than ~180°C whereas, stereocomplex crystallites are having melting temperature above 200°C [147].

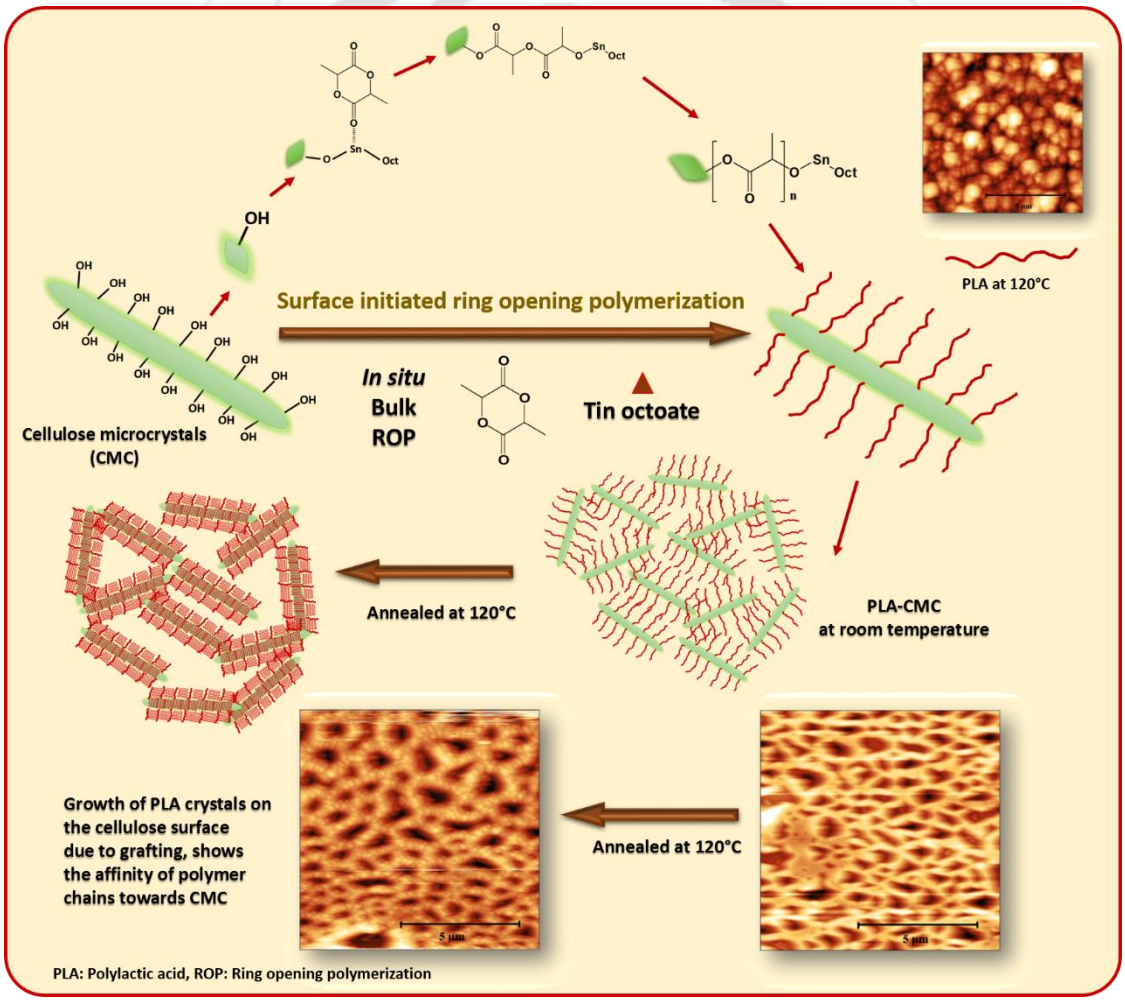

Figure 4.4: Schematic diagram for the modification of CMC and its demonstration by AFM images.

DSC analysis of the biocomposites has been shown in **Figure 4.5a**. It can be seen that the thermogram of sPLA have three distinct types of endothermic peaks two at 151.8°C and 179.3°C, which are related to the homocrystals of PLLA and PDLA; whereas, the third peak at 211.1°C is related to the stereocomplex crystallites. However, the peaks related to the homocrystallites are disappeared with the addition of the grafted CMC into PLA matrix. It may so happen that the CMC helped in the formation of stereocomplex crystallites while developing some hindrance in homocrystallization. To dig down more into this phenomenon, detailed study is performed through XRD and FTIR analyses of the samples and discussed in the subsequent sections. The DSC exotherm of samples in cooling cycle are shown in **Figure 4.5b**. From the figure, it is found that the crystallization peak shifted towards the higher temperature range from 116.2°C to 144.1°C. Increase in the crystallization temperature gives the evidence about the restriction of polymer chains due to presence of grafted CMC, which requires more chain folding to form crystallites. At higher temperature, polymer chains have higher energy to diffuse easily from entangled chain to lamella which subsequently yield to grow spherulites.

Formation of stereocomplex crystallites are further analysed by X-ray diffraction analysis, and the diffraction spectra are shown in **Figure 4.6**. It is known that the PLA homocrystals crystalizes (alpha form) in a pseudo-orthorhombic unit cell of dimensions a=1.07 nm, b=0.595, c= 2.78 nm containing 10_3 helical structure (10Å rise per 3 monomeric units). The diffraction peaks for PLA situated at 14.7°, 16.6° and 19° are corresponds to the (010), (200/110) and (203) crystal planes, respectively. Whereas, the stereocomplex crystallites of PLA crystallized in a triclinic unit cell with dimensions a=0.916 nm, b=0.916 nm, c=0.870 nm, α=β=109.2° and γ =109.8° having 3_1 helical structure (3 Å rise per monomeric units) [69]. The diffraction pattern at 11.8°, 20.6° and 23.9° are related to stereocomplex crystallites and corresponds to the (110), (300)/(030) and (220) lattice planes, respectively.

It has been found that the intensity of diffraction pattern for the homocrystals is reduced as the content of grafted CMC increased to 2.5% and vanished in case of 5% grafted CMC content. Similarly, the intensity of the peaks related to the stereocomplex crystallites enhanced drastically with increase in the grafted CMC content (**Figure 4.6a**). It shows that the presence of grafted CMC in the matrix promotes the formation of stereocomplex crystallites and suppress the development of the homocrystals. In term of crystallinity, it has been seen that the overall crystallinity is more or less remain same at about ~55% and only the content of homocrystals is reduced from 19.6% for sPLA to 0% for sPLA-5%CMC and crystallinity for stereocomplex crystallites increased from 32.4% to 54.6%. The fraction of stereocomplex crystallites in the matrix increased from 62.3% to 100%, shown in **Figure 4.6b**, confirms that the presence of grafted CMC provides the extended enantiomeric molecular surface area for the interaction with opposite enantiomeric PLA chains.

Formation of the stereocomplex crystallites in the PLA matrix is also confirmed by the FTIR as shown in **Figure 4.7**. It is well-known that the FTIR spectra is sensitive to the crystalline form of PLA; further spectra of PLA and grafted CMC is compared to understand the effect of grafted CMC in PLA formation of stereocomplex crystallites. Full spectra of all samples are shown in **Figure 4.7a**, the characteristic peaks correspond to PLA is already mentioned in the previous section. The characteristic peak for the stereocomplex 3_1 helical structure is located at 908 cm^{-1} [148], increased intensity of the peak at 908 cm^{-1} in comparison to sPLA suggest the enhancement in the content of stereocomplex crystallites, qualitatively, as shown in **Figure 4.7b**.

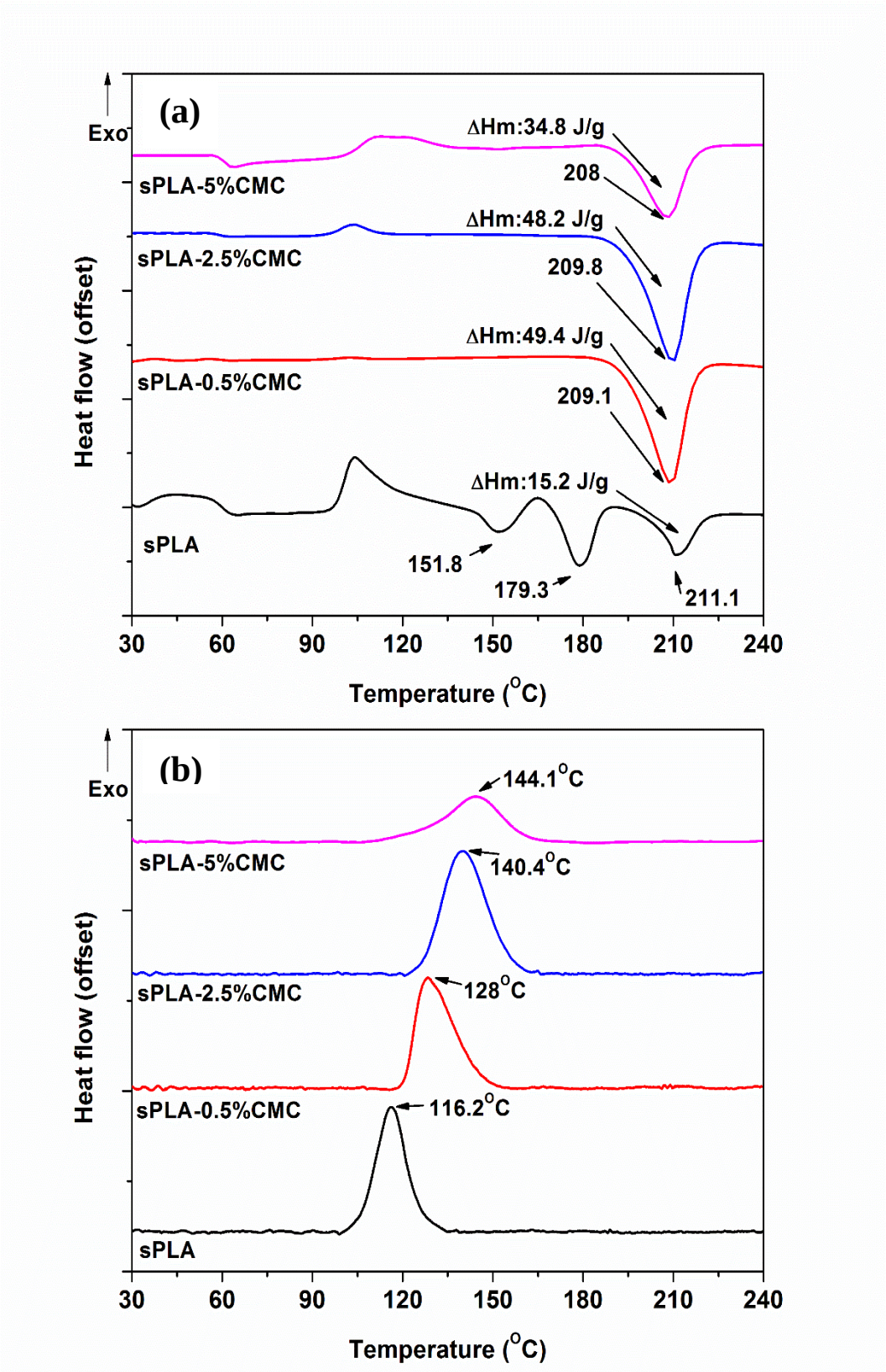

Figure 4.5: DSC thermogram of sPLA and sPLA-CMC biocomposite: (a) heating cycle and (b) cooling cycle.

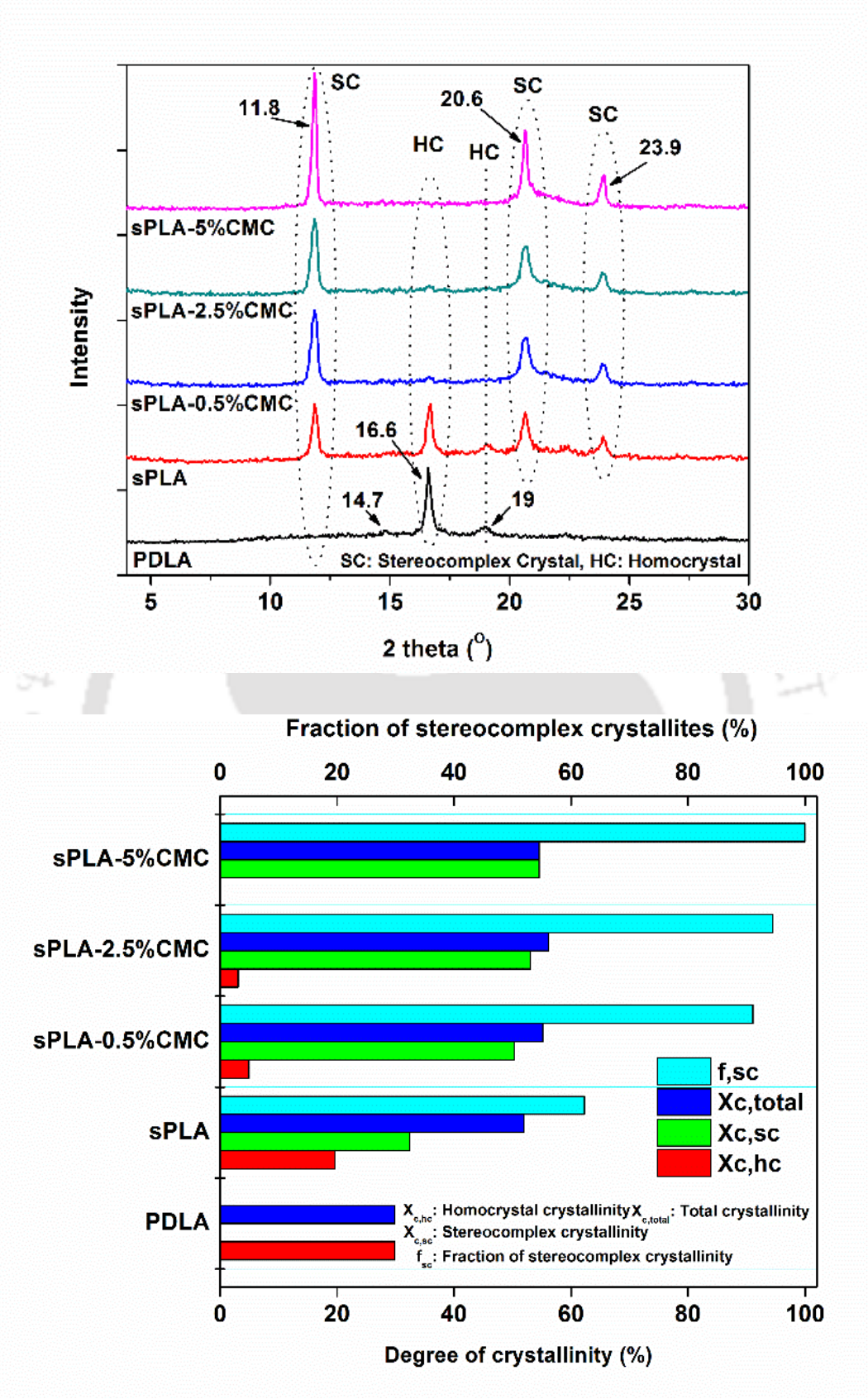

Figure 4.6: X-ray diffraction of (a) sPLA and sPLA-CMC biocomposite and (b) its degree of crystallinity.

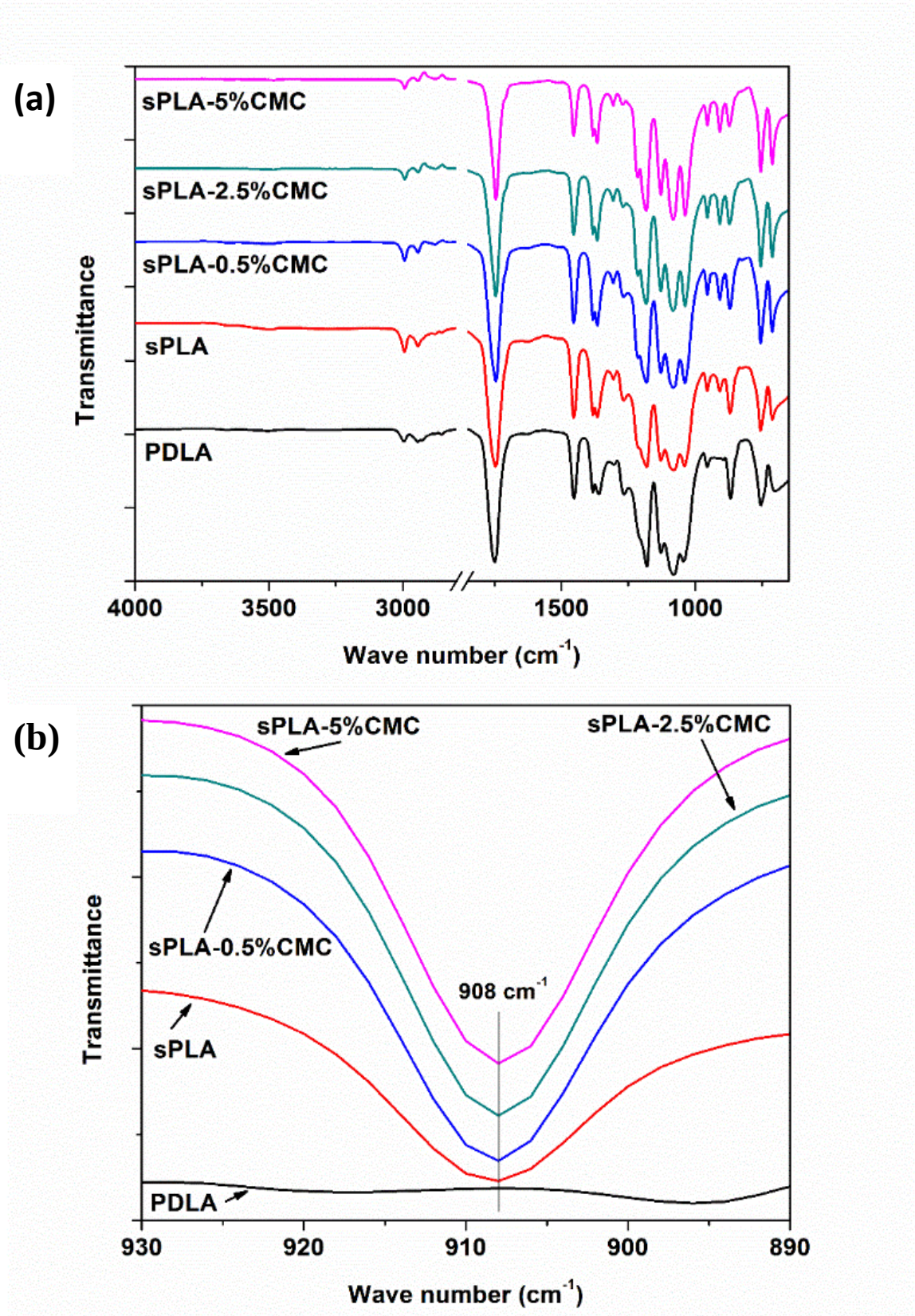

Figure 4.7 a-b: FTIR spectra of sPLA and sPLA-CMC biocomposites magnified peak at 908 cm^{-1}.

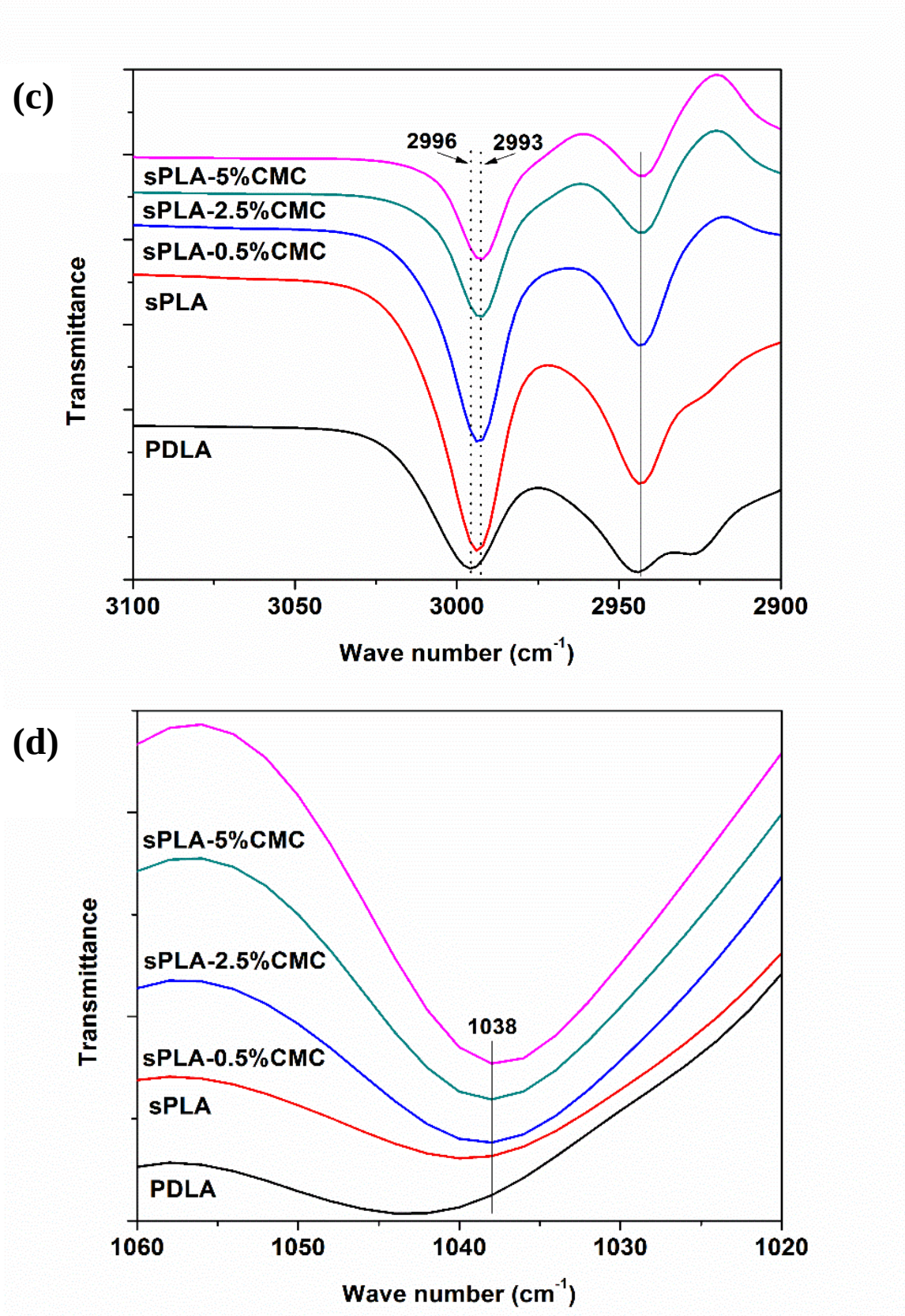

Figure 4.7 c-d: FTIR spectra of sPLA and sPLA-CMC biocomposites.

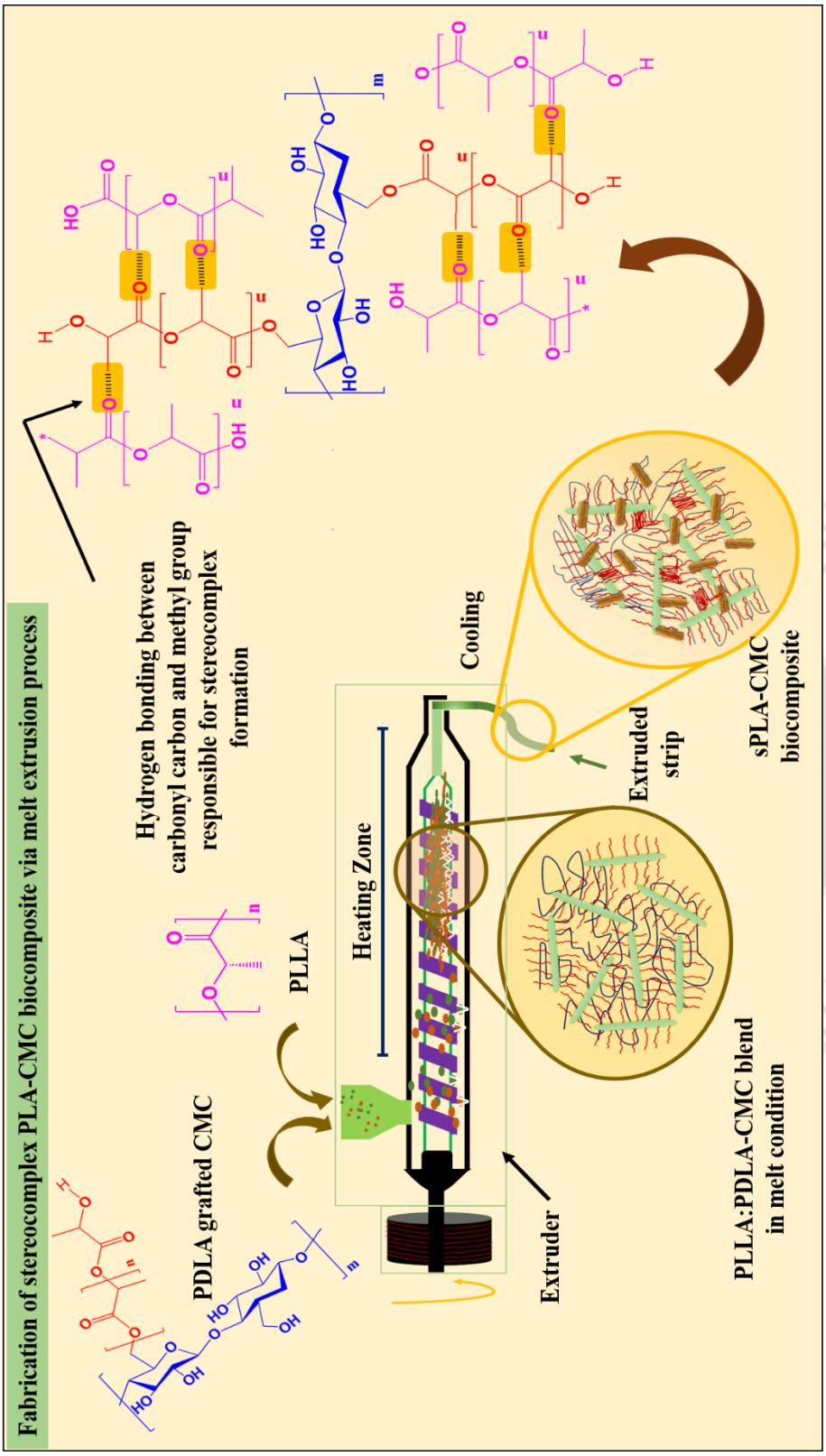

Figure 4.8: Schematic diagram for the formation of sPLA-CMC biocomposite and its stereocomplex.

The stereocomplex crystal formation is the ultimate result of interaction between opposite enantiomeric PLA chains or molecules. The establishment of hydrogen bond between carbonyl carbon of one enantiomeric PLA molecule and methyl hydrogen of opposite enantiomeric PLA molecule is responsible for the stereocomplexation in PLA, which come in the existence due to the presence of opposite helical structure of PLLA and PDLA [149]. This hydrogen bonding is also confirmed by the red shift of crystalline sensitive peak of PLA from 1040 cm^{-1} to 1038 cm^{-1} (**Figure 4.7d**) and shift of methyl stretching vibration spectra from 2996 cm^{-1} to 2993 cm^{-1} (**Figure 4.7c**).

From the above discussion, it can be concluded that the grafted CMC complement the formation of stereocomplex crystallites, while suppressing the development of the homocrystallization. The schematic diagram in **Figure 4.8** can be made on the basis of above discussion, which shows the melt mixing of PDLA-CMC and PLLA and its cooling. During cooling, the melt crystallized and form the stereocomplex crystallites depending on the content of grafted CMC.

4.3.3 Gas barrier properties

Effect of grafted CMC on stereocomplexation in PLA matrix and ultimate effect on the gas barrier properties is estimated. It has already been discussed in the previous section that the homocrystals form pseudo orthorhombic unit cell with 10_3 helical (10 Å rise per 3 monomeric unit) structure and stereocomplex crystallites form triclinic unit cell with 3_1 helical (3 Å rise per monomeric unit) structure. Lower length rise per unit of monomeric units for the stereocomplex crystallites suggest the compact nature of crystals, which may prevents the diffusion of gaseous molecules through it. Development of the biocomposite proven to be able to enhance the barrier properties such as oxygen transmission rate (OTR) and water vapour transmission rate (WVTR) of the PLA [42, 129, 150]. Due to compact

crystalline nature of stereocomplex crystallites, the surface of PLA sheet or film gets modified and it reduces the solubility of water molecules and prevent subsequent permeation. Similarly, dense structure of stereocomplex crystallites reduce the diffusion of the oxygen molecules, which reduces the oxygen permeability of PLA. The present work refers inclusion of fillers into the PLLA/PDLA blend system that are not only efficient in improving the degree of stereocomplexation but also increases the inherent oxygen and water barrier property through entailing tortuous path for the molecules. [54]. The water vapour permeability of different samples are shown in **Figure 4.9**. WVTR for sPLA is found to be 8.91 gm.mm.m^{-2}.day^{-1} and is reduced to 5.81 gm.mm.m^{-2}.day^{-1} after addition of 2.5% grafted CMC. So there is found that approximately 34.8% WVTR is reduced due to addition of grafted CMC. This reduction can be attributed to the film surface modification by the formation of stereocomplex crystallites. WVTR is highly dependent on the surface energy, which may be enhanced by the formation of stereocomplex crystallites and the dense packing of PLA chains also hinders the diffusion of water molecules. However, for sPLA-5%CMC, WVTR again increased to 7.07 gm.mm.m^{-2}.day^{-1}, which may be due to the presence of high amount of grafted CMC. CMC, without modification, is recognized as hydrophilic substance and it may become hydrophobic after modification [151]. However, increased content of grafted CMC may develop the diffusion pathway for the water molecules to permeate through it and may be accountable for increased WVTR. Enhanced stereocomplexation and content of grafted CMC also have the effect on the oxygen permeability. The OTR of samples are shown in **Figure 4.10** and found that the enhanced stereocomplexation and fillers in the matrix influences the oxygen permeability. The OTR for sPLA found to be 8.1×10^{-2} cm^3.mm.m^{-2}.day^{-1}.kPa^{-1} is reduced to 6.1×10^{-2} cm^3.mm.m^{-2}.day^{-1}.kPa^{-1} when 5% grafted CMC added to the matrix, where approximately 25% OTR is reduced. Increased crystalline domain in the matrix prevents

the diffusion of oxygen molecules and the presence of filler increases the tortuous path for the oxygen molecules.

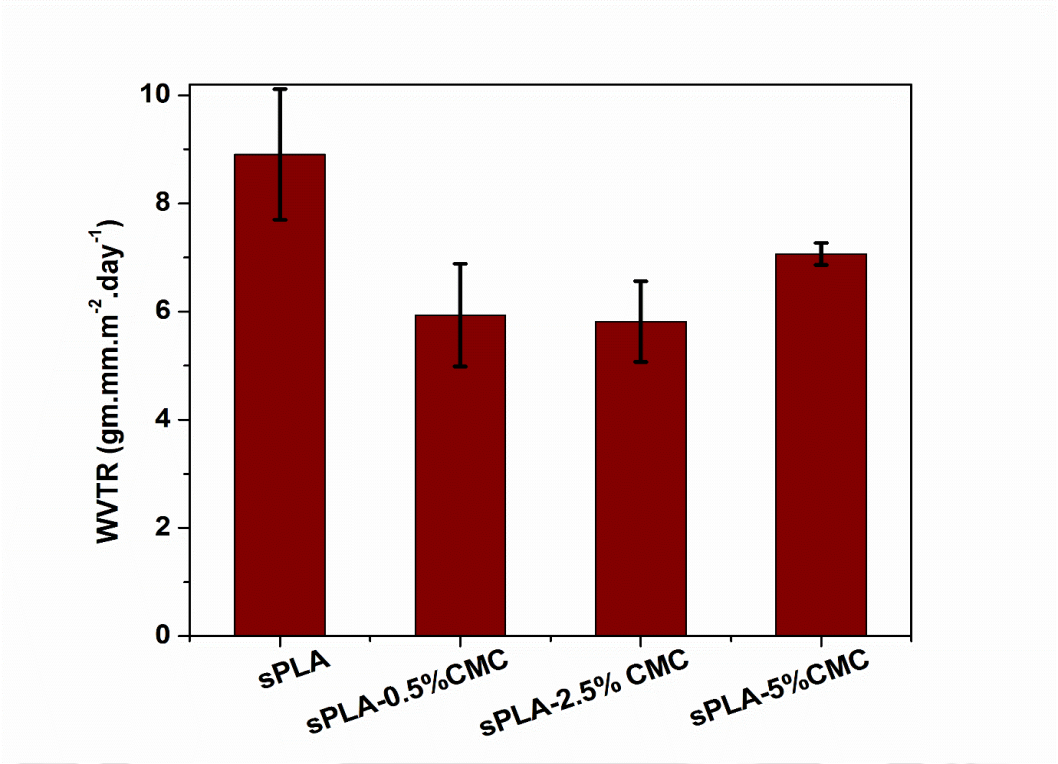

Figure 4.9: Normalized water vapour transmission rate of sPLA and sPLA-CMC biocomposite.

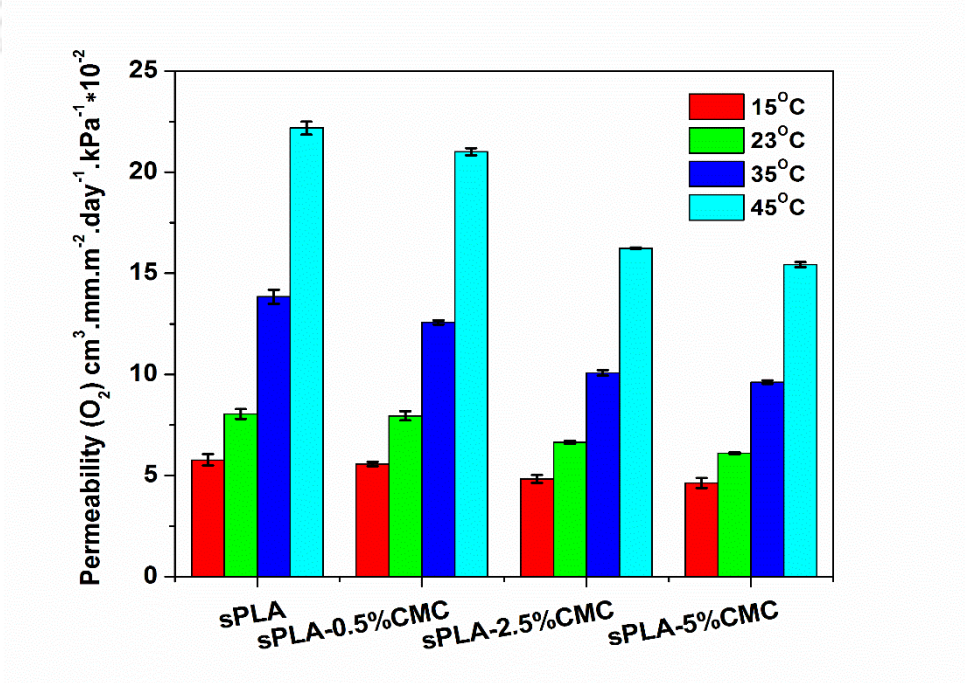

Figure 4.10: Oxygen permeability of sPLA and sPLA-CMC biocomposite.

4.3.4 Mechanical properties

Effect of stereocomplexation and presence of filler into PLA matrix on mechanical properties are also examined. The ultimate tensile strength (UTS) and percentage elongation of the samples are shown in the **Figure 4.11**. The UTS of sPLA without filler is found to be 28.6 MPa and appreciable enhancement of ~50% is noticed in case of sPLA-5%CMC. Increment in the tensile strength can be ascribed to the interaction of PLLA chains with the grafted CMC, which provides extended arms of PDLA. The PLLA and PDLA chains forms the stereocomplex crystallites and the CMC hinders the segmental motion of the chains, which ultimately increases the resistance to mechanical pull. As reported, the modification of the CMC and its use as filler in the PLA matrix improves the tensile properties at the cost of the percentage elongation break [152, 153]. However, in this study, the percentage elongation at break first increased from ~1.8% for sPLA to ~38% for sPLA-0.5%CMC and this increase can be the result of stretching of stereocomplex crystallites, which is induced by the grafted CMC. Elongation at break is further reduced to ~24% in case of sPLA-5%CMC. The reduction in the elongation can caused by induced rigidity of the polymer chains by CMC, which is a direct reflection of reinforcement. The increased content of CMC segregates the polymer chains and reduce the mobility, which ultimately affect the tensile strength and elongation. This enhancement in the tensile strength and percentage elongation is also result of uniform dispersion of CMC into the polymer matrix. The FESEM of the fractured surface of sPLA and sPLA-CMC biocomposites along with neat CMC are shown in the **Figure 4.12**, which shows uniform dispersion of CMC. It can clearly be perceived that the size of the CMC is subsequently reduced during melt processing of polymer composites. Average diameter of the CMC is found to be ~8 µm, which is reduced to ~220 nm during melt processing which promote the dispersion of the filler and results in the improvement of mechanical properties.

The adhesion of polymer with filler is also a significant parameter which has significant impact on tensile strength and percentage elongation. The AFM study of the composite can give indirect information regarding adhesion of polymer to fillers. As discussed in previous section, comparison of AFM images of sPLA and sPLA-5%CMC is shown in **Figure 4.3-2**. In the **Figure 4.3-2f**, the grains of grown spherulite of sPLA can be seen easily which is seen as percolated structure in case of sPLA-5%CMC (**Figure 4.3-2g**). This percolated and channelled growth of the spherulite on the surface of CMC, confirms the adhesion and affinity towards the filler.

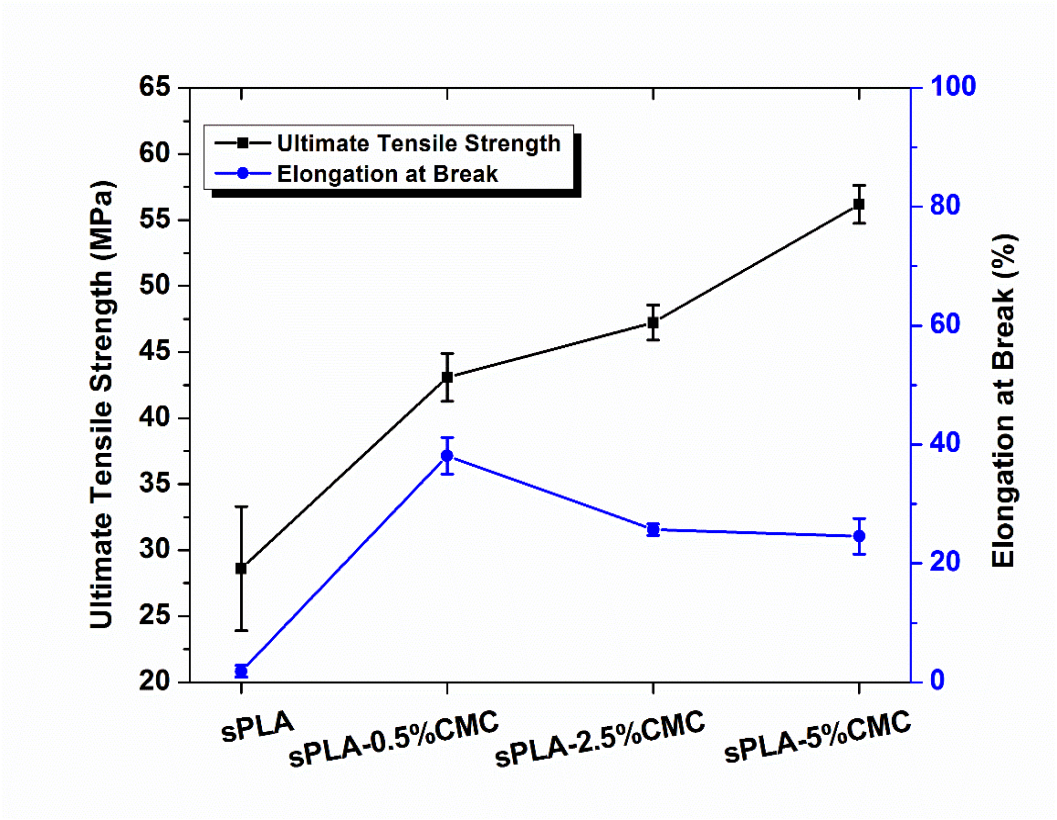

Figure 4.11: Ultimate tensile strength and percentage elongation of sPLA and sPLA-CMC biocomposite.

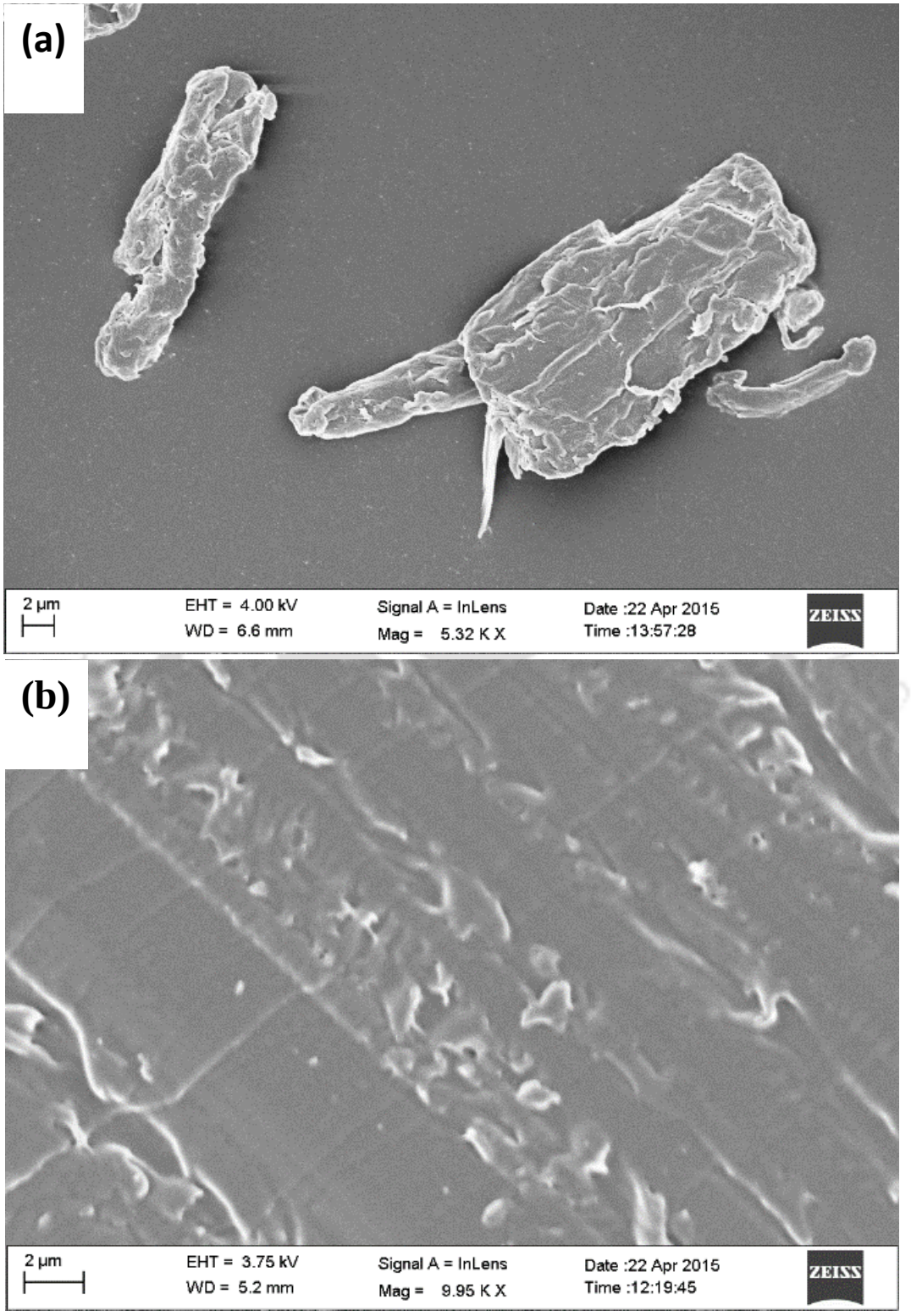

Figure 4.12 a-b: FESEM images of (a) CMC, (b) sPLA.

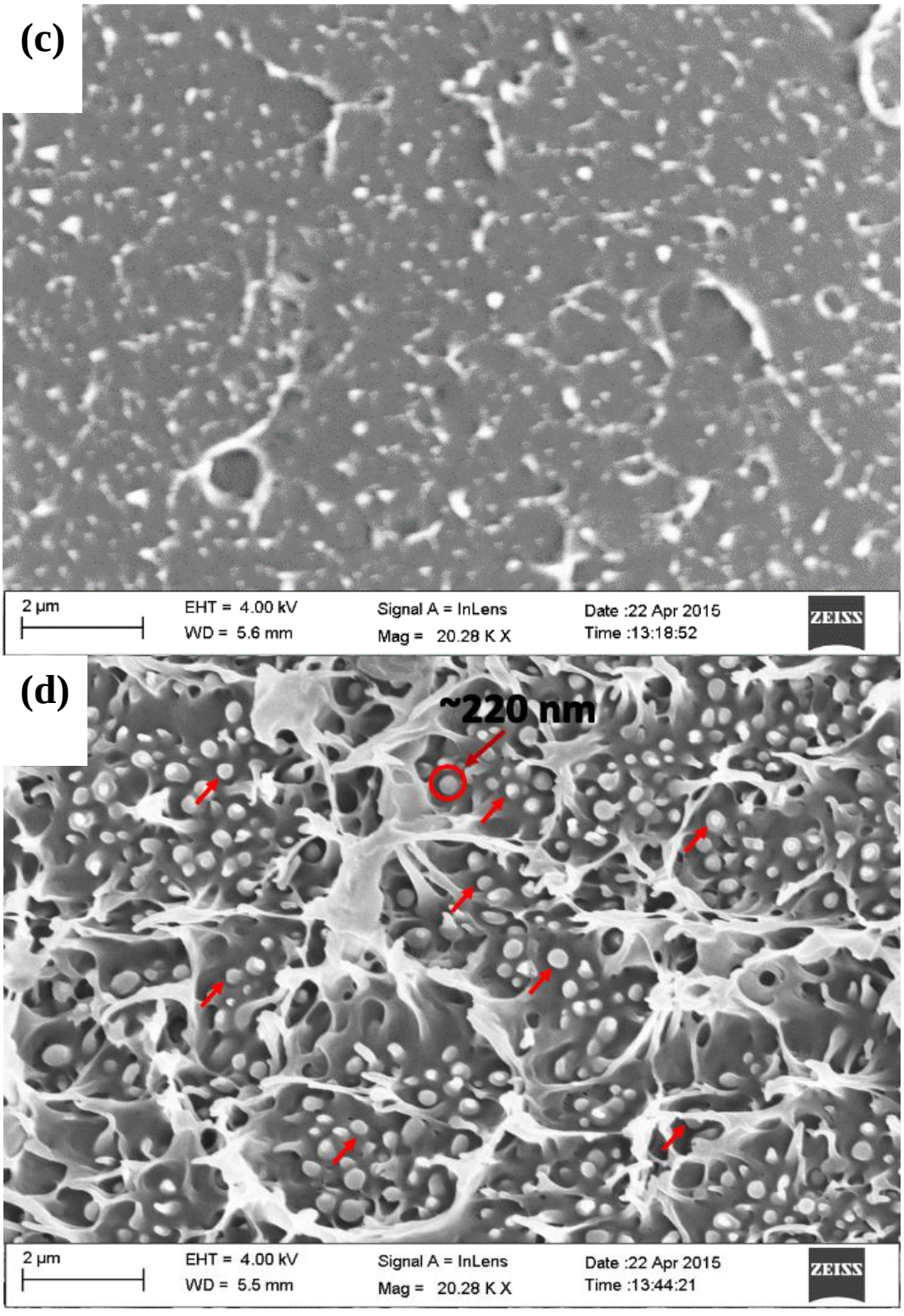

Figure 4.12 c-d: FESEM images of (c) sPLA-2.5%CMC and (d) sPLA-5%CMC biocomposite.

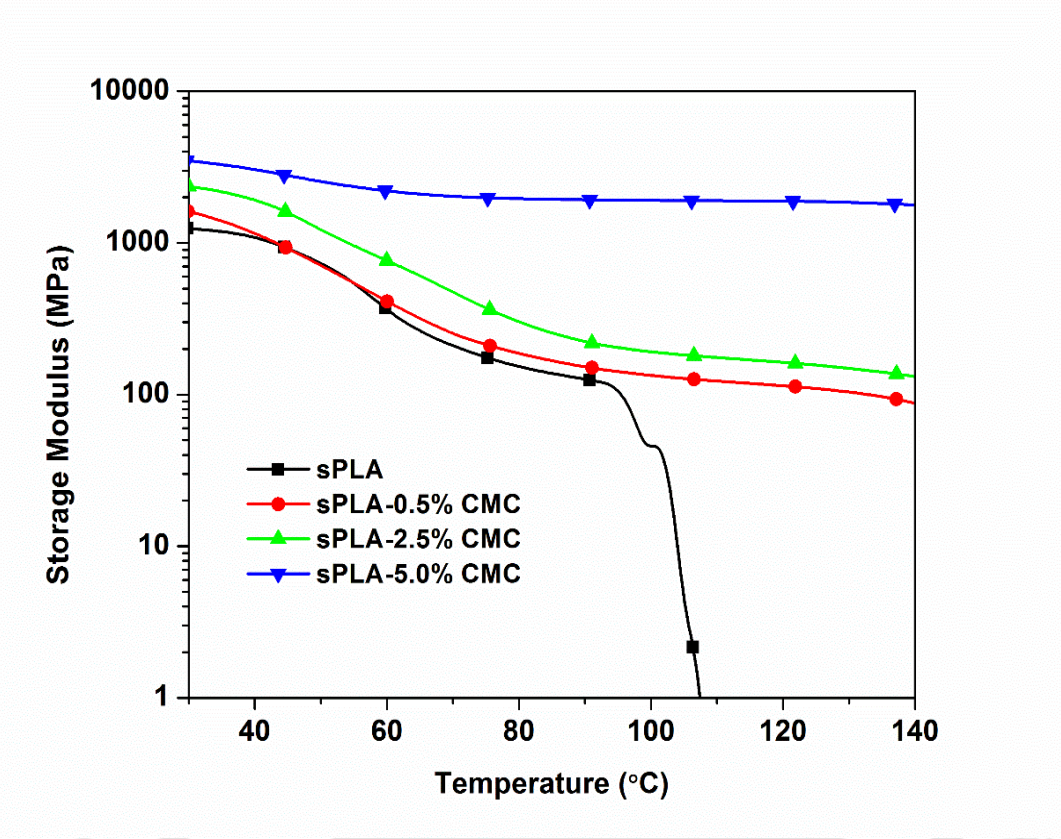

Figure 4.13: Storage modulus of sPLA and sPLA-CMC biocomposite.

Stereocomplexation and presence of filler exert a substantial effect on thermomechanical properties of sPLA. The dynamic mechanical analysis (DMA) of biocomposites suggest the enhancement in the thermomechanical properties. The plot for storage modulus against temperature is shown in the **Figure 4.13**. It is observed that the storage modulus of the composite is improved to more than 3500 MPa before glass transition in case of sPLA-5%CMC compared to sPLA. It is also confirmed that composite is thermomechanically stable till 140°C in comparison to ~100°C of pristine sPLA. It is observed that the reduction in storage modulus after glass transition become significantly lesser for sPLA-5%CMC, which can be attributed due to the enhanced stereocomplexation and the reinforcing action of the grafted CMC that reduced the mobility of the polymer chains significantly.

4.4 Conclusions

A facile solvent-free approach is adopted for the fabrication of stereocomplex PLA/CMC biocomposites which shows outstanding thermal, mechanical and gas barrier properties. The *in situ* modification of CMC with PDLA is found to be highly effective in enhancing the dispersion of CMC into the polymer matrix, as suggested by FESEM micrograph. The uniformly dispersed, grafted CMC provided extended molecular surface area for the formation of stereocomplex crystallites, hindering the homocrystallization phenomenon. While AFM analysis also indicated good degree of interaction between polymer matrix and the grafted CMC, thereby leading to improved state of filler dispersion within the polymer matrix, which directly influenced the development of stereocomplex crystallites in the resulting biocomposites. By the combined effect of enhanced stereocomplexation and the CMC fillers, the oxygen permeability and water vapour permeability are reduced by ~25% and ~35%, respectively. The improved storage modulus (~3500 MPa) and tensile strength (50%) over neat sPLA are the results of effective reinforcement of PLA as well as grafted CMC fillers, which are highly effective in enhancing stereocomplexation over homocrystallization in the biocomposite. Hence, the involved solvent-free bulk polymerization technique for the modification of CMC and the versatile method of stereocomplex PLA biocomposite fabrication may turn out to be an efficient way to enhance properties that can be related to applications both in high temperature engineering and packaging applications.

CHAPTER: 5

Effect of Modified Chitosan on the Properties of Stereocomplex PLA

Graphical abstract

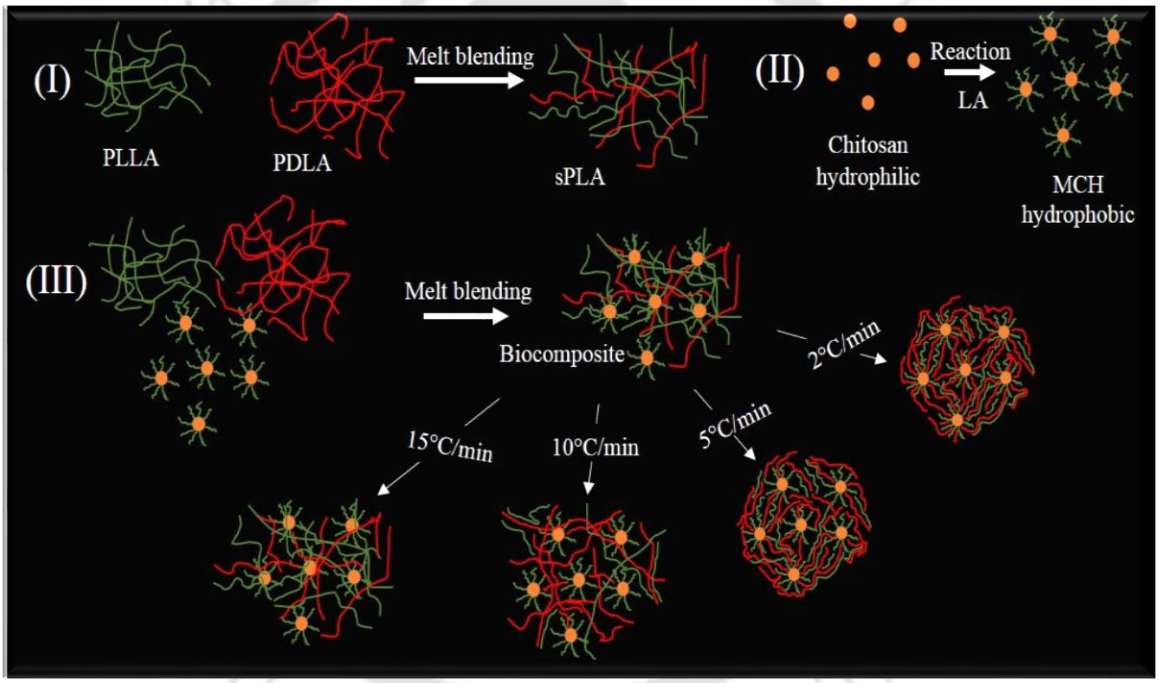

Article communicated

Abstract

High molecular weight stereocomplex poly(lactic acid) (PLA) is essential for the development of its biocomposites using melt processing technique which could be a promising solution to use for high temperature engineering applications. Herein, we have explored the potential of chitosan for improvement of stereocomplexation in PLA. Chitosan is chemically modified with oligomeric PLA by simple condensation polymerization reaction. Preparation of biocomposite of PLLA/PDLA and modified chitosan (MCH) is performed using melt processing technique. Grafting of oligomeric PLA on the chitosan surface could increase the molecular surface area which leads to the enhancement in the formation of stereocomplex crystallites. The effect of MCH content on the structural, morphological, thermal and mechanical properties of PLLA/PDLA are investigated with various techniques. The modification of chitosan and formation of stereocomplexation in PLA is confirmed by FTIR and XRD techniques, respectively. It is also found that the heat treatment on sPLA and its composites is having significant effect on the stereocomplexation. The degree of crystallinity, measured using XRD, of stereocomplex crystallites is increased to ~70% for 1.5 wt % MCH content without presence of homocrystals. The heat deflection temperature of the biocomposite is increased to ~145°C for 1.5% MCH in comparison to ~70°C for sPLA. From the tensile test of biocomposites, improvement in UTS and Young's modulus are observed. Oxygen barrier property analysis of prepared biocomposite film have been done to access their probable application in the packaging industry. Improved stereo-complexity enhanced the oxygen permeability and reduction found to be 56% for 3 wt% MCH loading.

5.1 Introduction

In recent decades, the disposal of petroleum based polymer and plastic iste has become a threat to our environment [154]. Development of biodegradable polymers such as poly(lactic acid) (PLA), poly(hydroxybutyrate) (PHB) etc. is one of strategy to overcome this problem. PLA is a biodegradable and biocompatible polymer produced from monomer lactic acid which can be produced by renewable resources such as wheat [155], corn [156] etc. Due to its good mechanical strength and easy processability over other biodegradable polymers [157], it is used in the packaging [158, 159], biomedical application [160] and some engineering application etc. The stereocomplex PLA (sPLA) [57] which is a special crystalline arrangement other than enantiomeric PLAs [161], has been the attraction for the researchers and studied extensively. Due to its special crystalline arrangement, it has superior thermal, mechanical and gas barrier properties than the enantiomeric pure PLA [63]. Due to the Van der Waals interaction between PLLA and PDLA chains, the melting point of sPLA is ~50°C higher than the PLA [57].

Stereocomplex PLA can be prepared by either solution [162] or melt blending [163] of enantiomeric PLA in 1:1 ratio. In the solution processing, sPLA can be prepared by precipitation or solution cast method. Several other methods such as thin layer formation [161], hydrolytic degradation etc. have been developed to form sPLA. Due to involvement of solvent, these methods are not industry viable. In the melt mixing process, two enantiomer of PLA mixed by melting it and cooled to form sPLA. In this process, with stereocomplex crystallites, homocrystals also forms. It has been seen that the formation of stereocomplex crystallites is the result of relatively low molecular weight PLA chains. Another technique is developed by Purnama et al. [164] to synthesize sPLA using super critical fluid. Synthesis of stereoblock PLA or use of fillers [165] or biofillers such as

cellulose nano/micro crystals [75], clays [166] into sPLA matrix can be the methods to prevent formation of homocrystals.

Chitosan is a biodegradable, nontoxic, biocompatible polymer with antibacterial activity [167]. It is a naturally occurring polysaccharide and can be obtained by deacetylation of the chitin harvested/found from biological materials. Chitosan is water soluble in acidic environment due to the presence of free amino groups which gets protonated in acidic environment. Chitosan has been used in many applications such as food industry, pulp and paper industry, wastewater treatment, agriculture etc. [168]. Due to its solubility in the water, it could not be used in the packaging and engineering application.

Fortunati et al. [169] have prepared biocomposite of PLA and chitosan by extrusion method and studied its properties. They found that the chitosan and PLA are not compatible and do not form uniformly disperse of PLA-chitosan matrix. They also found that addition of chitosan led to significant decrease in mechanical properties which proved that chitosan does not have the reinforcement effect after adding in to PLA matrix and it even made PLA more fragile. Gartner et al. [170] have coated the PLA film with the PLA/chitosan solution blend and tested the adhesion of PLA/chitosan blend on PLA film. Improvement in adhesion properties is achieved due to the use of methyldiphenyl diisocyanate (MDI). They found that without MDI chitosan has no contact with PLA film, which suggest the non-compatibility of chitosan with PLA. Spiridon et al. [171] studied the effect of keratin on PLA/chitosan composite prepared in brabender. They found that thermal degradation of PLA is faster in presence of chitosan and decrease in the mechanical properties which suggest the further improvement is required in interfacial adhesion of chitosan and PLA. Torres-Huerta et al. [172] prepared PET/PLA/chitosan biocomposite using extrusion method. They concluded that the presence of chitosan in the poly(ethylene terephthalate) (PET) matrix favours the degradation rate.

Using grafted material with enantiomeric PLA in the formation of stereocomplex PLA is a unique approach which enhances the molecular surface area for the interaction with the other enantiomer PLA. Due to the increased molecular surface area the content of stereocomplex crystallites can be easily enhanced which leads to enhancement in the properties of end product. In this direction, we have chemically grafted the chitosan with low molecular weight PLA which can be dispersed easily in the PLA matrix and prepared the biocomposite by blending the modified chitosan (MCH) with PLLA and PDLA mixture.

In this work, we have chemically modified chitosan while *in situ* lactic acid polymerization. After modification with low molecular weight oligomeric PLA, the modified chitosan (MCH) is dissolved and dispersed in organic solvent and PLA polymer matrix which indicate the improved miscibility of chitosan in polymer matrix. We have prepared the biocomposite of PLLA, PDLA and modified chitosan (MCH) using melt blending process to form the stereocomplex PLA and studied the effect of modified chitosan on the structural, morphological, thermal, gas barrier and thermomechanical properties of stereocomplex PLA.

5.2 Experimental section

5.2.1 Materials

Poly(L-lactic acid) (2003D grade) was supplied by NatureWorks®. PDLA was synthesized via ring opening polymerization (ROP) of bulk D-lactide in the presence of tin octoate (Sigma Aldrich) as catalyst. The ROP is done in vacuum at 160°C for 2 hours. Unreacted lactide in the synthesis process is removed by volatilization process for 2 hours at 110°C. D-lactide is synthesized by two step process. D-lactic acid supplied by Musashino Chemicals, China is oligomerized by removing the water content in the system at 150°C

followed by vaporization of produced D-lactide via depolymerization of oligomer at 250°C in presence of tin oxide (Sigma Aldrich) as catalyst. Produced D-lactide was purified by washing and recrystallization process followed by drying in vacuum at 60°C. L-lactic acid was procured from Pioma Chemicals as brand name Purac PF-90. Chitosan (medium molecular weight) was purchased from Sigma Aldrich. All materials are used as received. Properties of PLLA and PDLA is listed in **Table 5.1**.

Table 5.1: Properties of PLA used in the experiment.

Material Name	**T_g (°C)**	**T_m (°C)**	**M_w (kDa)**	**M_n (kDa)**	**PDI**	**Specific rotation [α]**
PLLA (2003D)	57	157	183	100	1.8	-154°
Lab synthesized PDLA	57	178	224	122	1.8	156°
Oligomer (MCH)	--	--	4.3	3.3	1.3	--

T_g and T_m are calculated using DSC, the M_w, M_n and PDI are calculated using GPC compared with standard polystyrene standard, the specific rotation [α] of the sample are measured using polarimeter at 25°C with 1.0 gm/100 mL concentration

5.2.2 Preparation of Modified Chitosan

Preparation method is adopted from elsewhere [42]. Lactic acid and chitosan are taken in the ratio of 3.33:1 (wt/wt%) and mixed properly in round bottom flask (RBF). The mixture is left idle for 12 hours for complete soaking of Lactic acid into chitosan. The prepared soaked mixture is kept in microwave and inert atmosphere is generated by purging nitrogen gas through RBF. Condensation polymerization reaction is performed for lactic acid-grafted-chitosan or modified chitosan (MCH) preparation in microwave. The

microwave is operated at 110°C for 30 minutes. The moisture and other byproducts are removed during reaction. After completion of the reaction, microwave is stopped and inert atmosphere is removed. A highly viscous product of dark black colour is obtained which is collected for further analysis and use for other applications.

5.2.3 Preparation of biocomposite of PLLA/PDLA and MCH

The biocomposite of PLLA, PDLA and modified chitosan (MCH) is prepared by melt blending using twin screw extruder HAAKE Minilab II and moulded using injection moulding machine HAAKE Minijet Pro from Thermo Scientific Germany. Firstly, all materials are dried in hot air oven at 60°C for 24 hours. PLLA and PDLA is mixed in 1:1 ratio and desired percentage (0, 0.5, 1.0, 1.5, 2, 3 and 4 %) of the MCH is added into the mixture. The mixture is extruded in twin screw extruder at 210°C with screw speed 50 rpm. The produced blend is taken for injection moulding with cylinder temperature 220°C and mould temperature at 90°C. The melt is injected with injection pressure of 700 bar and held for 5 second. The dumbbells (shown in **Figure 5.1**) are removed from the mould after 10 second.

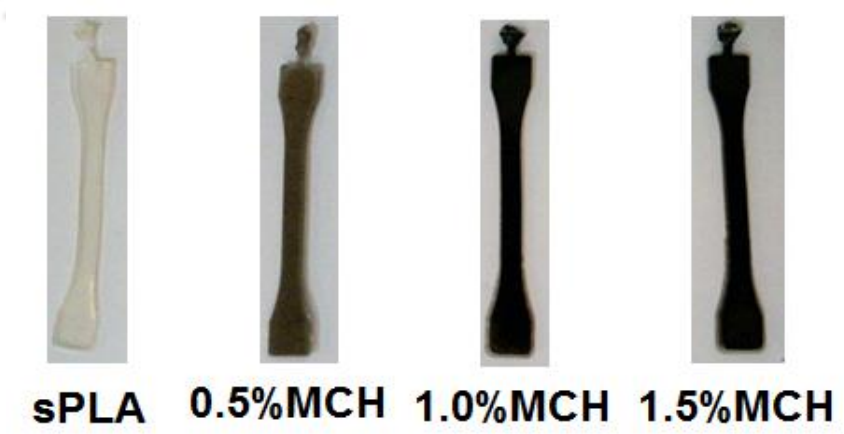

Figure 5.1: Processed dumbbells of sPLA with various amount of MCH.

5.2.4 Characterization

FTIR (Nicolet Magna-560) is used to identify possible intramolecular interaction between PLLA and PDLA and modified chitosan. The analysis is done by scanning the sample from 4500 cm^{-1} to 400 cm^{-1} with resolution of 4 cm^{-1} with accumulation of 64 scans. The samples are prepared as thin film by hot press.

The ^{1}H and ^{13}C NMR spectra of the specimen are recorded using Bruker 600 MHz NMR spectrometer. The sample are prepared by dissolving specimens in deuterated chloroform ($CDCl_3$).

Thermal properties of the biocomposite are measured by differential scanning calorimeter DSC 204F1 Phoenix from Netzsch (Germany) (pre-calibrated using Indium standards) equipped with CC300 N_2 cooling system, under nitrogen flow of 20 mL/min. The specimens are melted at 240°C with heating rate of 50°C/min and kept at 240°C for 5 min to remove the thermal history of the processing. After thermal history removal specimen are cooled to 30°C with cooling rates of the 2, 5, 10 and 15°C/min and then heated to 240°C with same heating rate as cooling.

Thermal degradation analysis of the biocomposite is done on TGA 4000 thermogravimetric analyser from Perkin Elmer. The samples (7-10 mg) are heated from 30°C to 700°C with scan rate of 20°C/min in 20 mL/min flow of nitrogen.

Shimadzu XRD-6000 X-ray diffractometer with copper Kα radiation (at 30 kV and 40 mA) and a monochromatized wavelength of 1.542 Å (0.154 nm) is used to characterize the crystal structure of samples. The scanning 2θ angles are ranging from 5° to 30° with a scanning rate of 2° per minute.

The degree of crystallinity of the specimen are calculated using **Equations 5.1** and **5.2**

$$X_{c,sc}(\%) = \frac{A_{c,sc}}{(A_{c,sc} + A_a)} \times 100 \quad (5.1)$$

$$X_{c,hc}(\%) = \frac{A_{c,hc}}{(A_{c,hc} + A_a)} \times 100 \quad (5.2)$$

Where, $X_{c,sc}$ and $X_{c,hc}$ is the degree of crystallinity of stereocomplex and homo crystallites, respectively. $A_{c,sc}$ and $A_{c,hc}$ is the area for the stereocomplex, homo crystallites and A_a is the area of amorphous phase. The program for the heat treatment of sample is given in **Figure 5.2**.

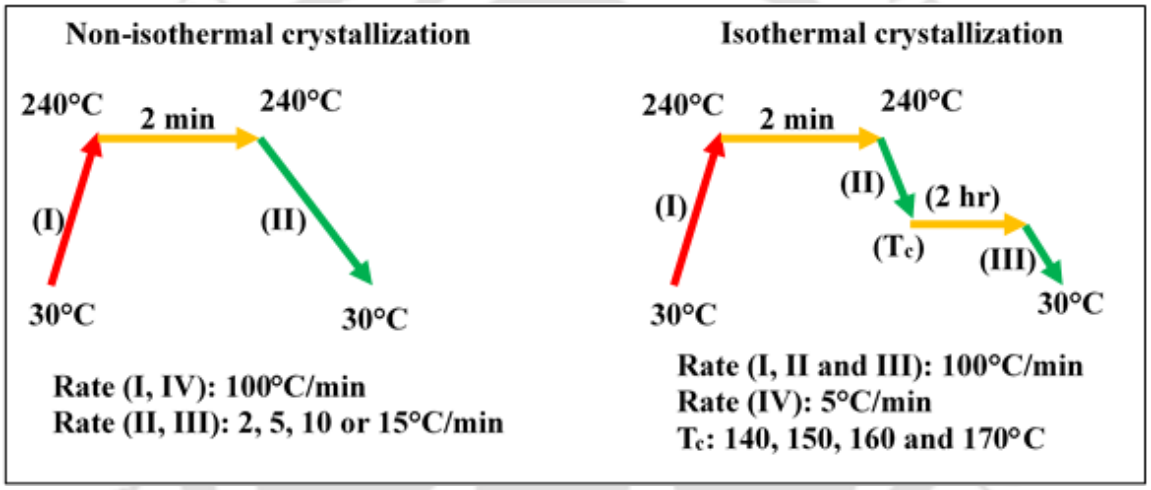

Figure 5.2: Thermal treatment program for X-ray diffraction analysis.

The Heat deflection temperature **(**HDT) of the specimen is estimated using the dynamic mechanical analyzer (DMA). The sample dimension is kept 10 mm × 5 mm × 2 mm [Length (L) × Width (W) × Height (H)]. The HDT is measured using three-point bending module. The force required for the analysis are calculated using the **Equation 5.3** mentioned in the ASTM- 648-07 standard as

$$F = \frac{2}{3}\left[\frac{\sigma(H^2 \times W)}{L}\right] \quad (5.3)$$

Where, σ is the stress on the specimen (0.455 MPa). The calculated force is 0.6067 N. The sample strain (Ɛ) are calculated using the **Equation 5.4**

$$\varepsilon = 6 \times \frac{(Deflection)_{ASTM} \times (Thickness)_{ASTM}}{(Length)^2_{ASTM}} \quad (5.4)$$

Where, deflection (ASTM), thickness (ASTM), and length (ASTM) mentioned in ASTM 648-07 standard are taken as 0.25 mm, 13 mm and 127 mm. The estimated strain i.e. 0.121% is used to calculate the deflection length (D) using the **Equation 5.5**

$$D = \varepsilon \times \frac{(length)^2_{sample}}{6 \times (thickness)_{sample}} \quad (5.5)$$

The calculated length of deflection is 10.08 µm. It means that the HDT estimated using DMA will be the temperature at which the sample deflects 10.08 µm with applied force of 0.6067 N at heating rate 2°C/min.

DMA analysis are carried out with a Dynamic mechanical analyser DMA 242E Artemis from Netzsch GmbH. A three-point bending clamp is used at a frequency of 1 Hz and oscillating amplitude of 40 µm. The sample are heated from 30°C to 100°C at a heating rate of 3°C/min in 100 mL/min nitrogen flow.

Tensile properties of injection moulded samples are measured using universal testing machine UTM from Kalpak, India. Three dumbbell shape specimens are characterized for each composite. The test is performed at a crosshead speed of 5 mm/min using gauge length of 50 mm.

TEM analysis is done to determine the shape and size of modified chitosan and its distribution into the PLA matrix. TEM samples are prepared by placing the small drop of biocomposite solution on carbon coated TEM grid. The grid is kept at room temperature to

evaporate and drain out the chloroform which leave a thin layer of the biocomposite on grid. The TEM analysis is performed on the JEM 2100 from JEOL. The morphology of the fractured surface of sPLA and MCH biocomposite is characterized using Sigma FESEM from Zeiss USA operating at acceleration voltage of 3-5 kV. Samples are obtained by fracturing the dumbbell in small pieces and stick on the stub using carbon adhesive tape and gold coated in sputtering unit before analysis.

The oxygen transmission rate (OTR) of sPLA and prepared stereocomplex biocomposite is calculated using OX2/231 oxygen permeability tester supplied from Labthink China. The measurement is done with carrier gas Argon (99.99%) at cylinder pressure of 0.5 bar and flow rate of 10 mL/min and 20 mL/min in lower chamber and upper chamber of diffusion cell, respectively. The test gas O_2 (99.9%) flow rate is set to 20 $mL.min^{-1}$ with cylinder pressure 0.5 bar. The exposed area of specimens is 50 cm^2 and the analyses are done at temperatures 15°C, 23°C, 35°C and 45°C for 6 hours. Before analysis, the specimen is conditioned with argon gas for 2 hours at 0%RH relative humidity at required temperature. The OTR values at 50% of the steady state value are taken as halftime ($t_{1/2}$) and used for the calculation of diffusion coefficient (D). The correlation between diffusion coefficient and halftime is derived by normalizing the Fick's second law **Equation 5.6** [173].

$$J(t) = \frac{Pp}{l}\left[1 + 2\sum_{n=1}^{\infty}(-1)^n \exp\left(-\frac{D\pi^2 n^2 t}{l^2}\right)\right] \quad (5.6)$$

The oxygen flux (J (t)) which is normalized by film thickness (l) and oxygen pressure (p) defines Permeability (P) as P = Jl/p. Number of sheets used for the film preparation is denoted as n and in the present work n=1. A't half'time, the J (t) = J/2 and D can be calculated by **Equation 5.7**

$$D = \frac{l^2}{7.119 t_{\frac{1}{2}}} \quad (5.7)$$

The solubility coefficient (S) of the material is calculated from the following **Equation 5.8**

$$P = D \times S \quad (5.8)$$

5.3 Results and discussion

5.3.1 Chemical characterization of modified chitosan by NMR and FTIR spectroscopy

The grafting of the oligomeric PLA on chitosan is analyzed using ^{1}H-NMR, ^{13}C-NMR and FTIR spectroscopy. The main purpose of oligomer grafting onto chitosan molecule is to increase the hydrophobicity of the chitosan and increase the solubility in organic solvents. The solution of modified chitosan in chloroform shows that, after modification, the chitosan is soluble in organic solvents such as chloroform and the presence of brown colour of the MCH solution is probably due to the formation of amide linkages. The ^{1}H and ^{13}C-NMR spectra of the PLA and modified chitosan is shown in the **Figure 5.3**. In ^{1}H-NMR spectra (**Figure 5.3a**), chemical shift of the characteristic peaks at 1.57 ppm for methyl group and 5.16 ppm for methenyl group, corresponds to the PLA. In case of MCH, the additional broad peak is found at 5.67 ppm which is for the proton connected to nitrogen of chitosan molecule, suggesting the presence of chitosan in the sample. The proton in methenyl group connected to the amide group indicated by the chemical shift at 1.66 ppm. The protons present on chitosan backbone connected to methenyl and methylene group could be found between 3.53 to 3.87 ppm.

Similarly, the ^{13}C-NMR spectra of PLA and MCH is shown in the **Figure 5.3b**. The chemical shift for the carbon of the PLA backbone are found at 169.9, 69.1 and 17.1 ppm for carbonyl carbon, methenyl carbon and methyl carbon, respectively. For MCH, an

additional peak is found at 179.3 ppm which is related to the carbonyl carbon connected to the amide group of chitosan. The carbon related to the chitosan skeleton is overlapped with methenyl carbon peak between 66 to 70 ppm. This analysis suggest that the chitosan molecules is modified by the oligomeric PLA and forms the amide linkage.

5.3.2 Grafting analysis and stereocomplexation in biocomposite using IR spectroscopy

Analysis for grafting of lactic acid with chitosan is done by using FTIR analysis and the spectra is shown in the **Figure 5.4**. The regular peaks at 1541 cm^{-1} and 1655 cm^{-1} corresponding to strong N-H bending vibration of the secondary amides and strong -C=O stretching vibration of the primary amides respectively are observed for chitosan as well as for LA-g-CH (MCH) master batch sample. A well-known peak at 1720 cm^{-1} is observed in lactic acid spectra which attributed to the presence of ester carbonyl group (-C=O) stretching vibrations. This peak shifted towards higher wave number and located at 1742 cm^{-1} in the case of LA-g-CH. It supports the grafting of lactic acid on chitosan backbone. The other regular peaks at 1454 cm^{-1}, 1375 cm^{-1}, 1121 cm^{-1}, 1041 cm^{-1} and 870 cm^{-1} are detected in lactic acid spectra which corresponds to $-CH_3$ bending, -CH- bending, -C-O- stretching, -OH bending and -C-C- stretching respectively. These peaks are also observed in LA-g-CH sample but some of the peaks such as 1121 cm^{-1} and 1041 cm^{-1} are shifted towards higher wavenumber and located at 1131 cm^{-1} and 1045 cm^{-1}.

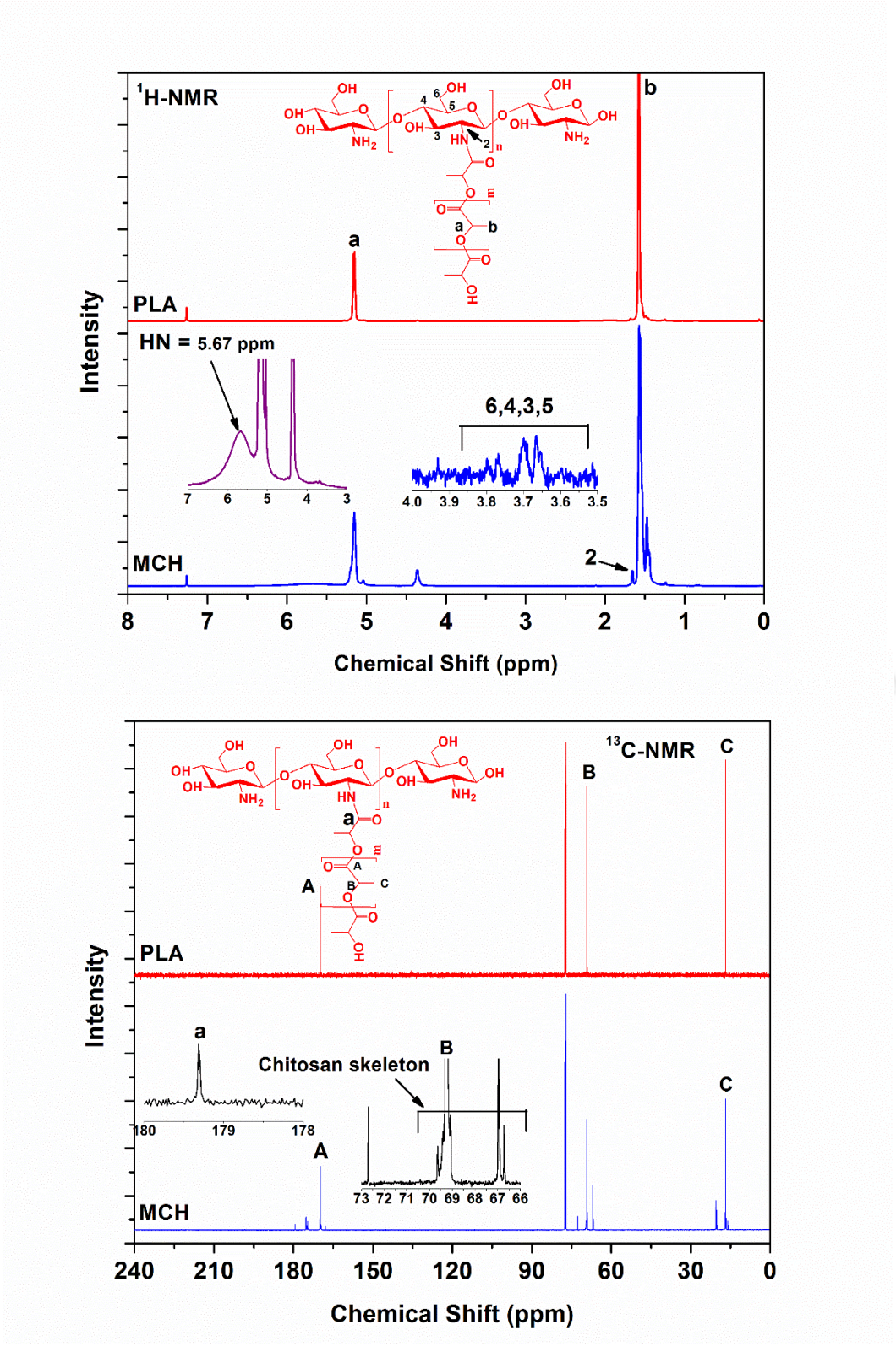

Figure 5.3: (a) ^{1}H-NMR and (b) ^{13}C-NMR spectra of PLA and modified chitosan (MCH).

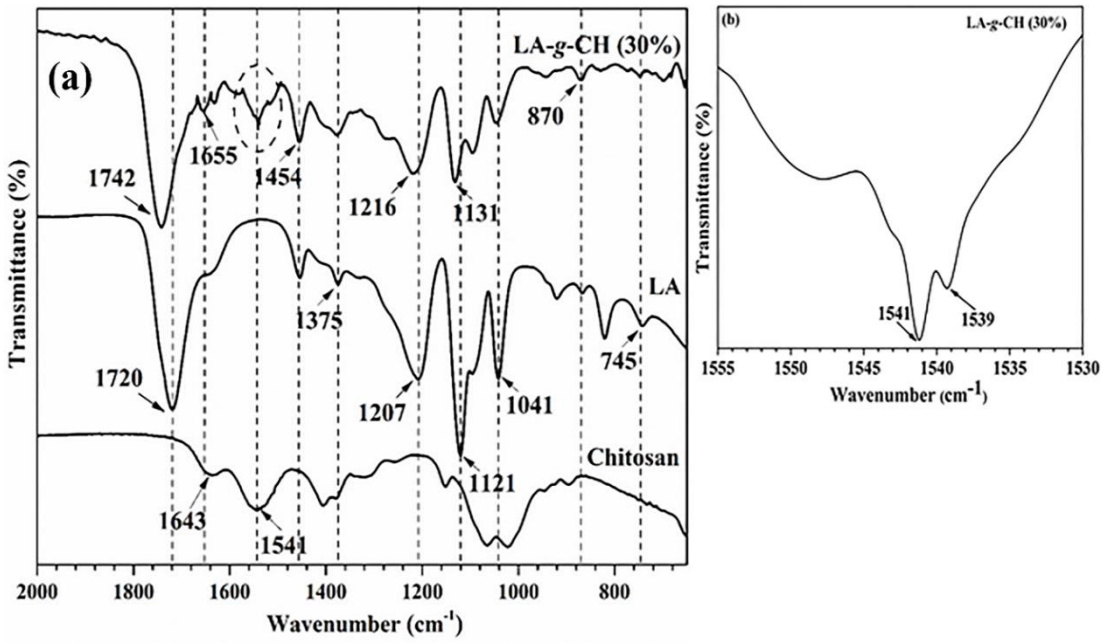

Figure 5.4: (a) FTIR spectra of chitosan, lactic acid and LA-g-CH in the range of 650 cm^{-1} to 2000 cm^{-1} and (b) FTIR spectra of LA-g-CH in the range of 1530 cm^{-1} to 1555 cm^{-1}.

A new additional peak is observed in LA-g-CH sample at 1539 cm^{-1} which corresponding to amide ester linkage (-OCONH-) of chitosan with lactic acid. This peak is absent from chitosan and lactic acid spectra which clearly indicates that the repeat units of lactic acid is grafted on chitosan backbone.

We compared the FTIR spectra of PLLA, PDLA and its MCH biocomposites to confirm the formation of stereocomplex crystallites and the effect of MCH. The principle peaks, related to stereocomplex crystallites formation, are summarized in the **Table 5.2**. The IR band for biocomposites is shown in the **Figure 5.5**. In the case of PLLA and PDLA, the band 2995 cm^{-1}, 2945 cm^{-1} are assigned to asymmetrical and symmetrical stretching of methyl group. The stretching region of –CH is observed as band at 2881 cm^{-1}. The characteristic vibration of helical backbone of the chain with CH_3 rocking mode is observed at 955 cm^{-1}. The peak at 870 cm^{-1} is attributed to C-COO stretching. The band at 756 cm^{-1}

is the band related to the crystalline phase of PLA and stretching and deformation of methylene group.

Table 5.2: FTIR spectra assignment for sPLA-MCH biocomposite.

Sr. No.	Assignment	Wave number (cm^{-1})
01	Asymmetrical stretching of CH_3	2995→2993
02	Symmetrical stretching of CH_3	2945→2941
03	Stretching of CH	2881→2877
04	Coupling of rocking of CH_3 and stretch of C-COO	955
05	Coupling of rocking of CH_3 and stretch of C-COO and characteristic peak for the stereocomplex crystallite with 3_1 helix confirmation	908
06	Stretch of C-COO	874←870
07	Deformation of C-H, assigned to crystalline phase	756
08	Bending of C-H	715

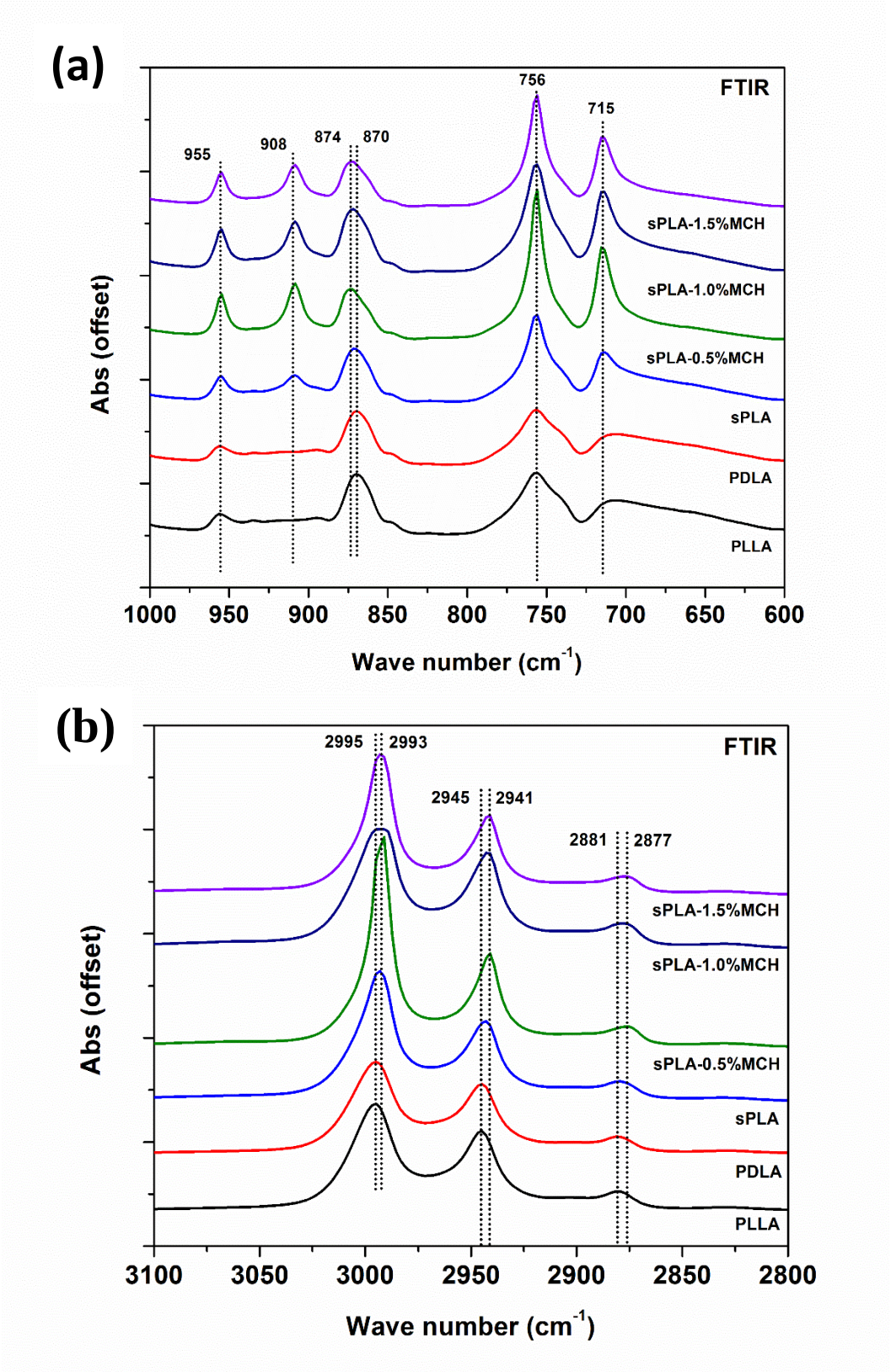

Figure 5.5: FTIR spectra of PLLA, PDLA, sPLA and MCH biocomposite in the range of (a) 2000 cm^{-1} and in the range of (b) 600 cm^{-1} to 1000 cm^{-1}.

It is known that the stereocomplex crystallites of PLA exhibit different FTIR spectra than homo crystallites. In the **Figure 5.5a,** a new peak can be seen at 908 cm^{-1} is evolved in the case of stereocomplex and its MCH biocomposite. The new peak at 908 cm^{-1}, is characteristic band for the stereocomplex crystallites with 3_1 helical confirmation. Its intensity increased as MCH is added to the blend which suggest that the crystal packing is more compact and dense. In the **Figure 5.5b**, compare to the FTIR spectra of homo crystallites, the stereocomplex spectra shown peak shift for symmetrical (4 cm^{-1}), and asymmetrical (2 cm^{-1}) stretching of CH_3 group and stretching of –CH group. Low frequency shift in the case of stereocomplex crystallites, suggest the interaction of the C=O and -CH which form weak hydrogen bond between the PLLA and PDLA chain in the crystal. High frequency shift in the band for stretching of C-COO from 870 to 874 cm^{-1}, suggest the formation of the stereocomplex crystallites. The peak at 920 cm^{-1} which is related to the homocrystals of PLA is not observed in the spectra.

5.3.3 Melting behaviour of biocomposite

The specimens are melted at 240°C and then cooled with several cooling rates 2, 5, 10, 15C°/min. and then heating with different heating rate. The **Figure 5.6a and 5.6b** shows the DSC thermograph of sPLA and its MCH biocomposite. It can be seen that the heating/cooling rate is having significant effect on the stereocomplexation in PLA and it helps to suppress the formation of the homocrystals. From the **Table 5.3**, it is found that the enthalpy of the homocrystals decreased with decrease in the heating rate. Increase in the melting temperature of the biocomposite compared to neat sPLA is evident that addition of the MCH into PLLA/PDLA matrix significantly affect the formation of stereocomplex crystallites. When the heating rate reduced from 15°C/min to 2°C/min, the exothermic peak area related to homo PLA disappeared.

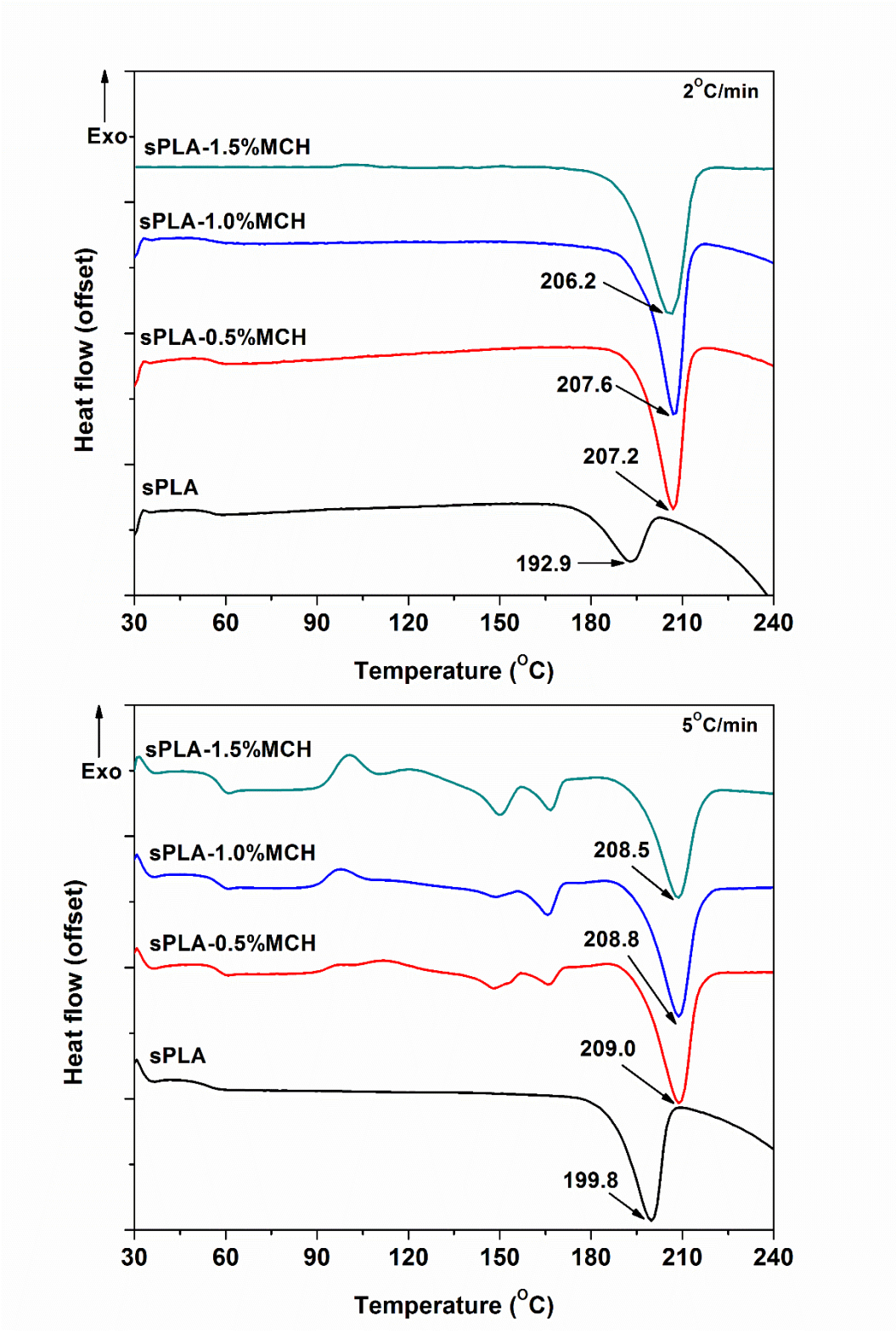

Figure 5.6a: Thermograph of sPLA and its MCH biocomposite with different scanning rate 2°C.min^{-1} and 5°C.min^{-1}.

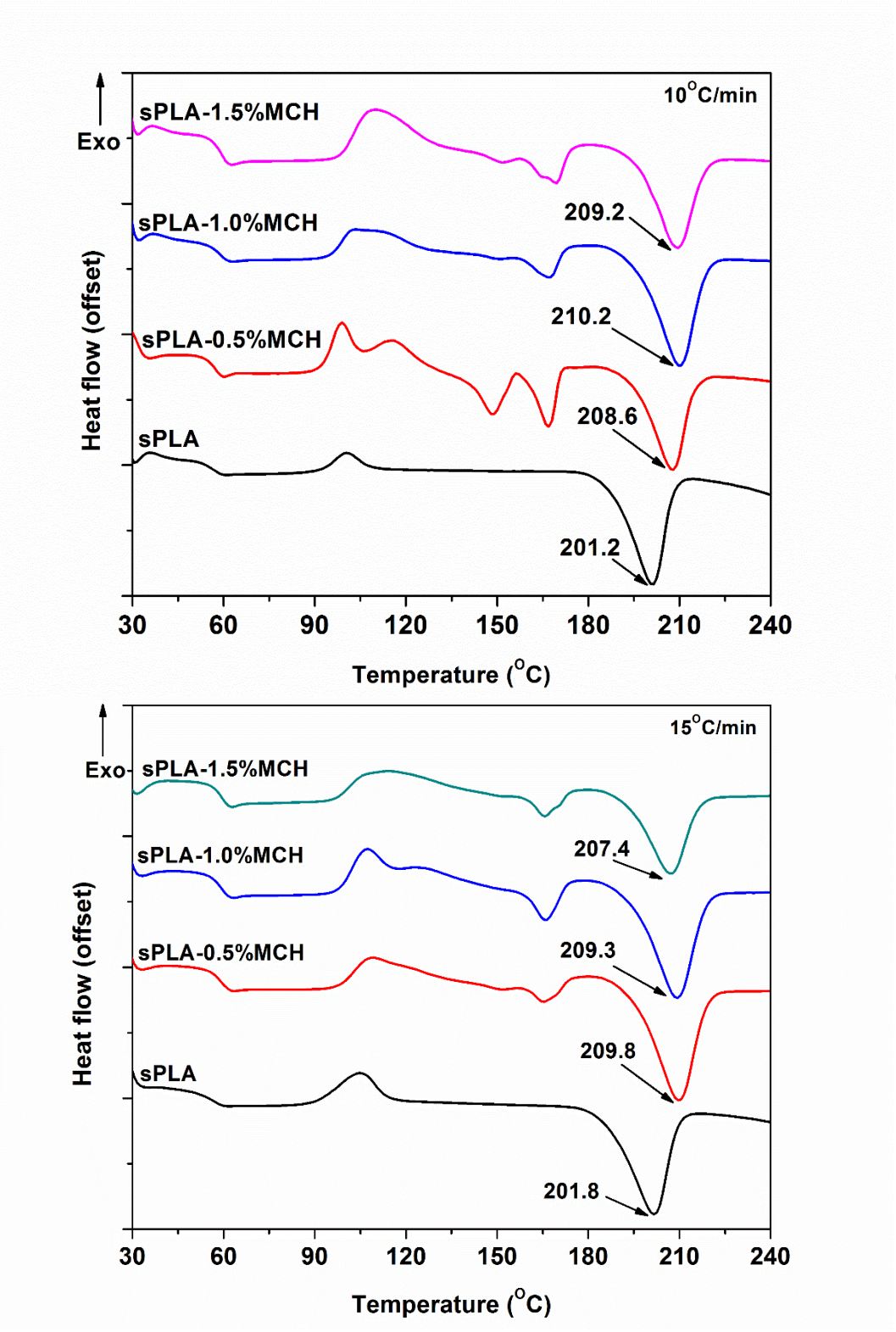

Figure 5.6b: Thermograph of sPLA and its MCH biocomposite with different scanning rate 10°C.min^{-1} and 15°C.min^{-1}.

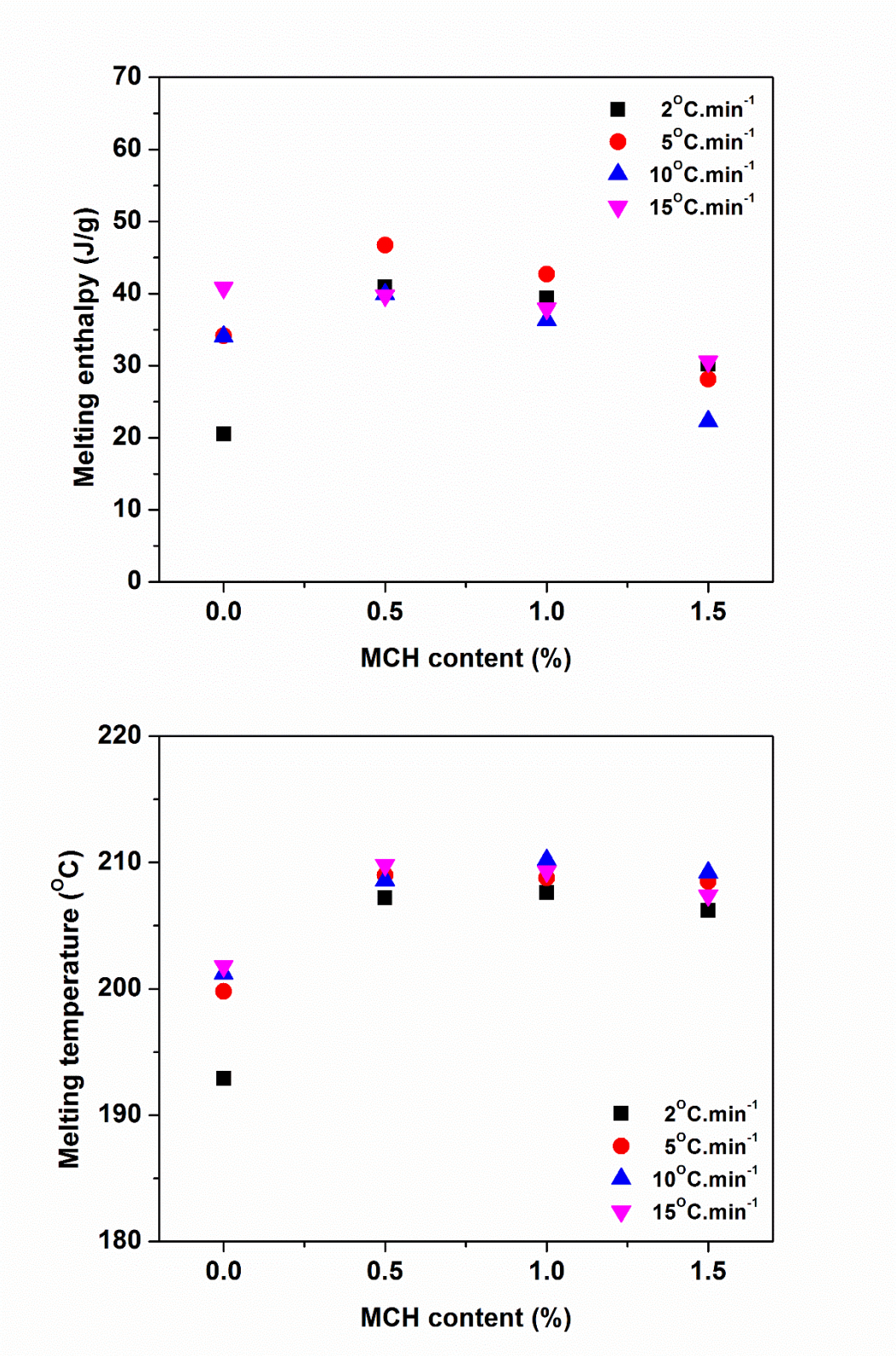

Figure 5.7: Comparison of (a) melting temperature and (b) melting enthalpy with respect to MCH content at different heating rate.

Table 5.3: Thermal properties of sPLA and it MCH biocomposite obtained from DSC.

Sample Name	β (°C.min^{-1})	T_g (°C)	$T_{m,hc}$ (°C)	$\Delta H_{m,hc}$ (J.g^{-1})	$T_{m,sc}$ (°C)	$\Delta H_{m,sc}$ (J.g^{-1})
sPLA	02	53.8	--	--	192.9	20.6
sPLA-0.5%MCH		55.9	--	--	207.2	40.9
sPLA-1.0%MCH		55	--	--	207.6	39.4
sPLA-1.5%MCH		56.9	--	--	206.2	30.2
sPLA	05	53.5	--	--	199.8	34.2
sPLA-0.5%MCH		57.7	148.2, 166.1	3.67, 2.4	209.0	46.7
sPLA-1.0%MCH		57.2	166	2.32	208.8	42.7
sPLA-1.5%MCH		57.6	150.3, 166.5	4.55, 2.87	208.5	28.1
sPLA	10	54.5	--	--	201.2	34.0
sPLA-0.5%MCH		58.5	149.3, 167.7	9.6, 8.4	208.6	39.9
sPLA-1.0%MCH		58.6	167.2	5.42	210.2	36.3
sPLA-1.5%MCH		58.6	169.3	5.11	209.2	22.3
sPLA	15	54.1	--	--	201.8	40.8
sPLA-0.5%MCH		58.3	165.4	3.85	209.8	39.7
sPLA-1.0%MCH		58.4	165.9	7.29	209.3	37.9
sPLA-1.5%MCH		58.7	165.5	5.57	207.4	30.6

T_g: Glass transition temperature, $T_{m,hc}$: Melting temperature for homocrystals, $T_{m,sc}$: Melting temperature for stereocomplex crystals, $\Delta H_{m,hc}$: Enthalpy of fusion for homocrystals, $\Delta H_{m,sc}$: Enthalpy of fusion for stereocomplex crystals, β: Heating rate

In the **Figure 5.6a**, PLLA/PDLA (sPLA) with heating rate 2°C/min, no homocrystals endotherm is observed but the melting temperature is increased from 192.9°C to 207.6°C with the addition of 1% MCH. It could be result of formation of homocrystals and its endotherm is merged with the endotherm of stereocomplex crystallites which lead to the lowering of the overall melting temperature of sPLA. Improvement in the melting temperature, due to the addition of MCH, may be the result of presence of more oriented

chain. Low molecular weight oligomeric PLA chains which are grafted on the surface of the chitosan may be helping in the formation of the stereocomplex crystallites. The enthalpy of the melting of stereocomplex crystals is also increased from 20.6 J/g to 39.4 J/g (**Figure 5.7**) with the addition of 1% MCH.

5.3.4 Effect of heat treatment on stereocomplexation

All melt crystallized specimen of sPLA and its MCH biocomposite are characterized by WAXD. The specimens are melt crystallized isothermally and non-isothermally at different crystallization temperatures (140, 150, 160 and 170°C for 2 hour) and at different cooling rates (2, 5, 10 and 15°C/min). It is already know that the stereocomplex crystallites exist in the 3_1-helical confirmation and formed by parallel packing of the L-lactide and D-lactide segments [161]. Homocrystals of PLLA or PDLA holds 10_3 helical form. The diffraction peaks appeared at 17° and 19° are the characteristic peaks for the alpha form of the PLLA or PDLA which crystalized in a pseudo-orthorhombic unit cell with dimensions a = 1.07 nm, b = 0.595 nm and c = 2.78 nm [161]. The peaks in diffraction pattern for stereocomplex crystallites appeared at 11°, 21° and 24°. Stereocomplex crystallites crystallized in a pseudo-trigonal unit cell with dimensions a = b = 0.916 nm, c = 0.870 nm, $\alpha = \beta = 109.2°$, $\gamma = 109.8°$ [174].

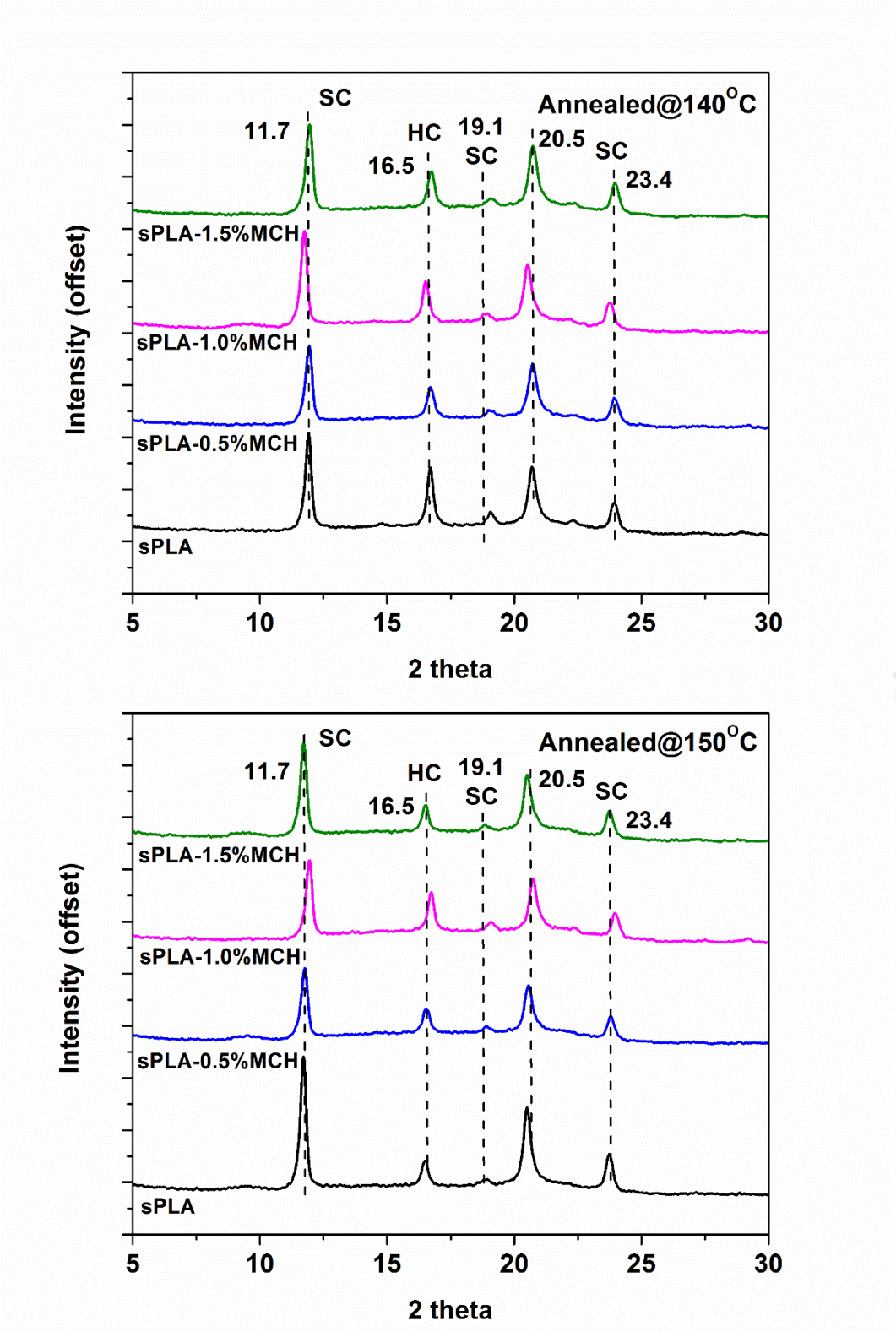

Figure 5.8a: X-ray spectra of sPLA and its MCH biocomposite melt annealed at temperature 140°C and 150°C.

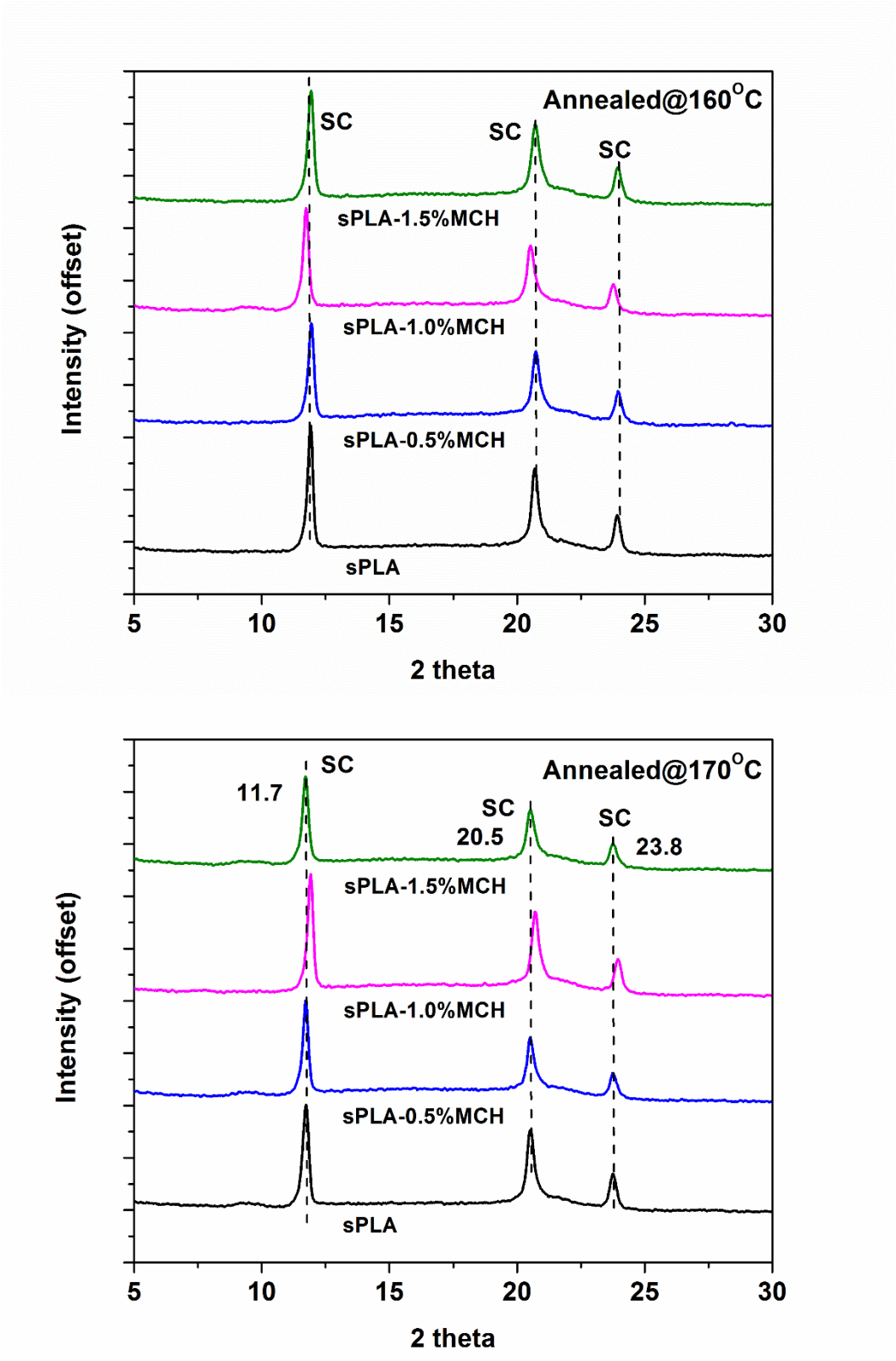

Figure 5.8b: X-ray spectra of sPLA and its MCH biocomposite melt annealed at temperature 160°C and 170°C.

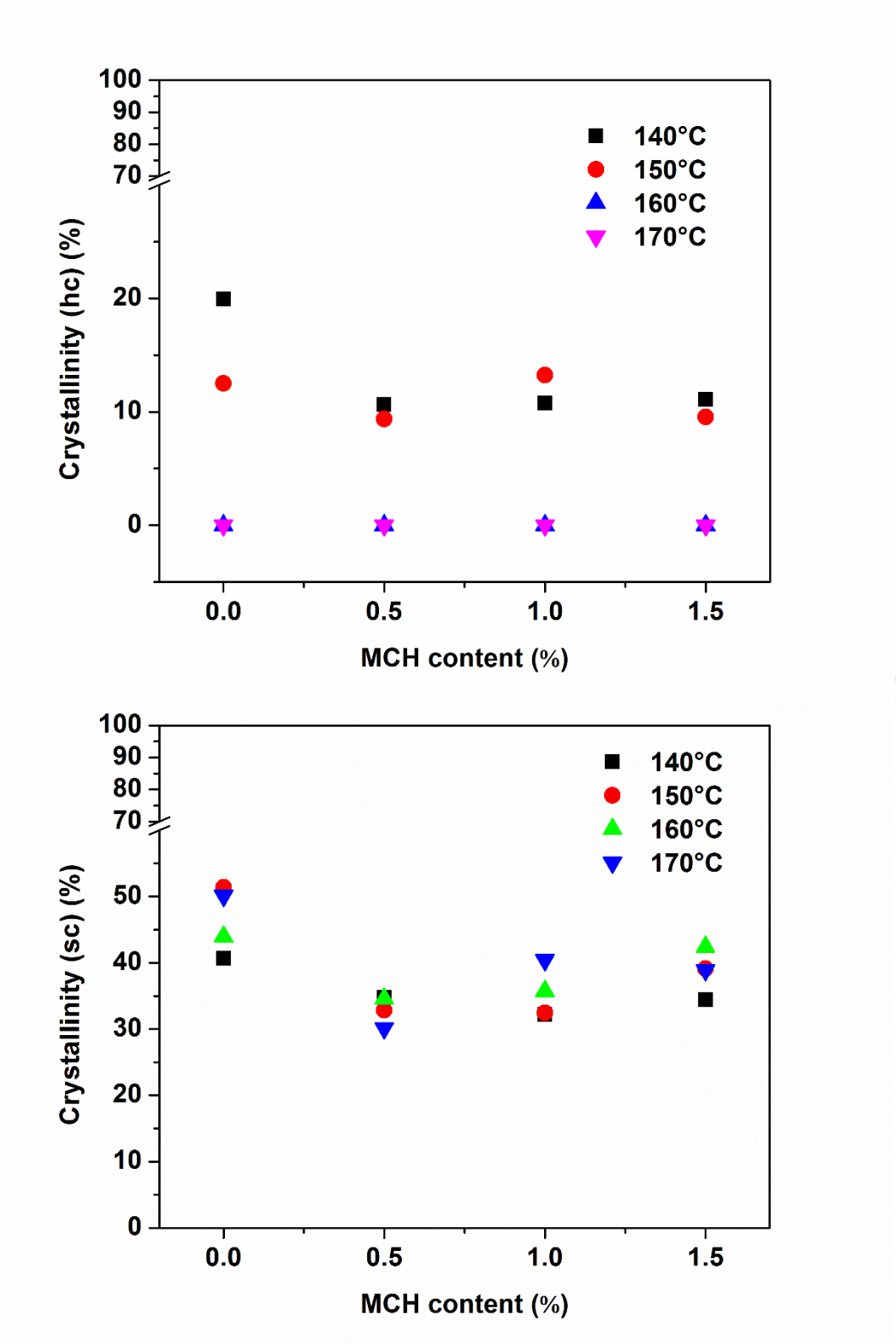

Figure 5.9: Degree of crystallinity of sPLA and its MCH biocomposite (a) after isothermal crystallization for homocrystals and (b) stereocomplex.

Table 5.4: Degree of crystallinity of homo and stereocomplex PLA and its MCH biocomposite.

MCH content (%)	Degree of crystallinity (%)							
	Isothermally crystallized							
	140°C		150°C		160°C		170°C	
	SC	HC	SC	HC	SC	HC	SC	HC
0	40.6	19.9	51.4	12.5	43.9	0.0	50.1	0.0
0.5	34.8	10.6	32.9	9.4	34.6	0.0	30.1	0.0
1.0	32.2	10.8	32.4	13.2	35.7	0.0	40.4	0.0
1.5	34.4	11.1	39.1	9.5	42.7	0.0	38.9	0.0
MCH content (%)	**Non-isothermally crystallized**							
	2°C.min^{-1}		**5°C.min^{-1}**		**10°C.min^{-1}**		**15°C.min^{-1}**	
	SC	HC	SC	HC	SC	HC	SC	HC
0	49.7	14.4	52.0	14.6	33.5	26.3	27.2	20.6
0.5	56.8	7.0	38.8	23.6	28.9	29.3	20.1	17.9
1.0	66.4	0.0	51.9	10.7	21.9	20.5	15.2	13.1
1.5	69.1	0.0	48.8	10.4	28.6	17.5	24.2	13.7

HC: Homocrystal, SC: Stereocomplex

The diffraction pattern for isothermally crystallized specimens are shown in the **Figure 5.8a and 5.8b**. In the case of isothermally crystallized specimen, it is found that the crystallization of samples at T_c of 150°C or less than that gives peaks at ~17° and ~19° (**Figure 5.8a**), which are the characteristic peaks for homo crystallites of PLA, as well as ~12°, ~21° and ~24°, which are the characteristic peaks for the stereocomplex crystallites of PLA. In the case of specimens which have been crystallized at 160°C or more than that, gives only peaks at ~12°, 21°, and 24° (**Figure 5.8b**) [175]. The result shows that the stereocomplex crystallites are formed at all T_c but no homo crystal is formed at temperature 160°C or higher. The diffraction pattern in the **Figure 5.8** shows that if the specimens are annealed at 150°C or lower temperature it forms stereocomplex crystallites with homo

crystals. However, if the specimens are annealed at 160°C or more, it is forming only stereocomplex crystallites and there is no evidence of homo crystals.

The calculated degree of crystallinity for stereocomplex and homo crystallites is shown in the **Figure 5.9** and data are listed in the **Table 5.4**. It could be seen that homocrystals is found for specimen annealed at temperature 140°C and 150°C. However, in the case of annealing temperature 160°C and 170°C, there are no peaks corresponding to homo crystallites. It is also confirmed that the degree of crystallinity for stereocomplex crystals is not changing significantly with T_c. Only the peaks corresponding to homo crystallites are disappeared with increase in annealing temperature. However, in the case of sPLA, the melting temperature confirmed by DSC are relatively less which could be the result of the formation of imperfect stereocomplex crystallites.

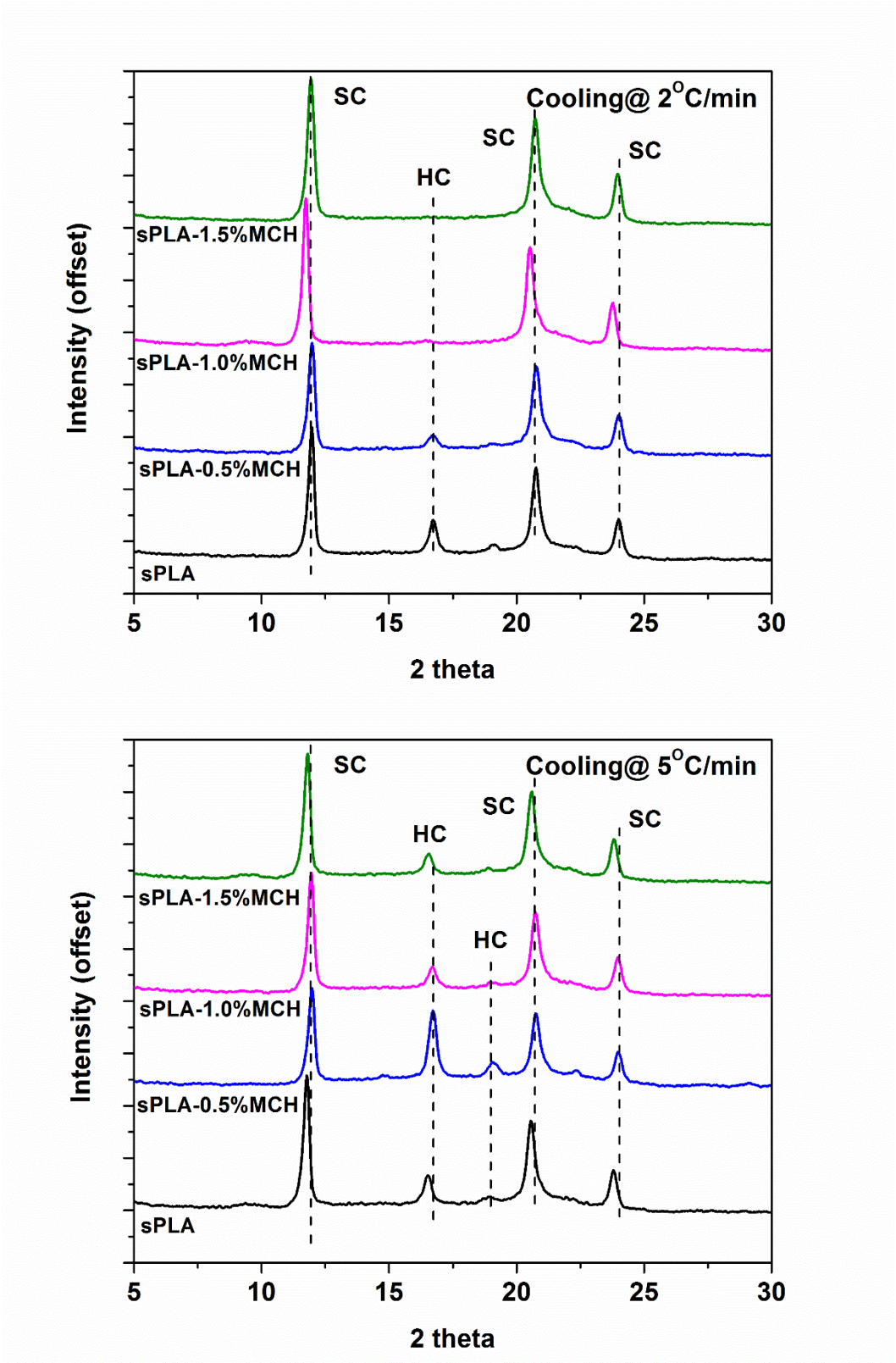

Figure 5.10a: X-ray spectra of sPLA and its MCH biocomposite cooled at cooling rate of 2°C.min^{-1} and 5°C.min^{-1}.

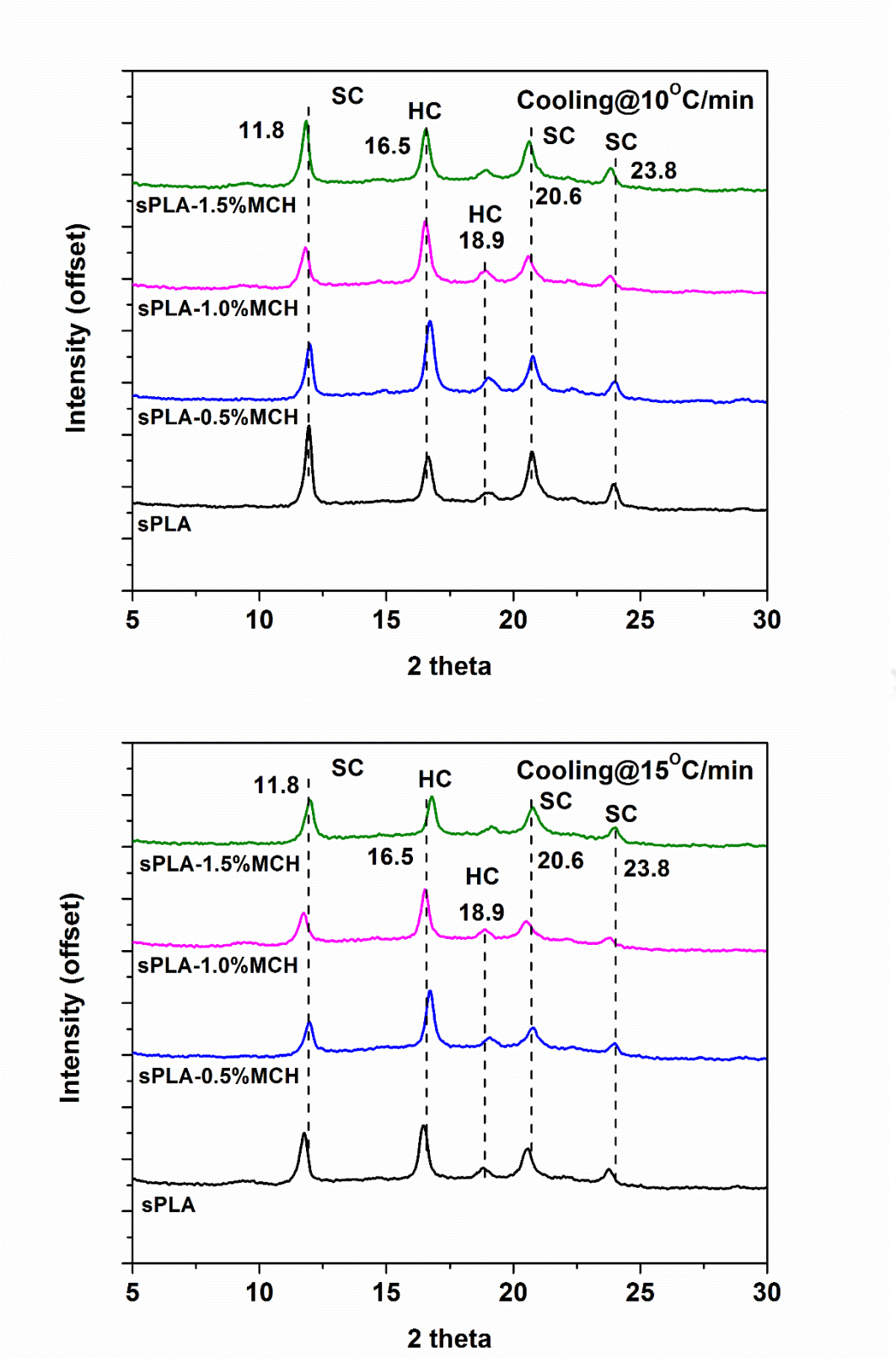

Figure 5.10b: X-ray spectra of sPLA and its MCH biocomposite cooled at cooling rate of 10°C.min^{-1} and 15°C.min^{-1}.

In the case of specimens crystallized non-isothermally, it is found that MCH content and cooling rate have a significant role in the formation of stereocomplex crystals. As the cooling rate is decreased the intensity of peaks related to homo crystallites decreased. From the **Figure 5.10a and 5.10b**, it is found that the content of MCH helps in the formation of stereocomplex crystals. At cooling rate 2°C/min, the peaks related to homocrystals disappeared and only peaks correspond to stereocomplex crystals appeared. The degree of crystallinity for non-isothermally crystallized specimens are shown in the **Figure 5.11**. As the content of MCH increases the total crystallinity also increases. The degree of crystallinity for stereocomplex crystallites is increased to ~70% for 1.5% MCH content and no evidence is found for the homocrystals. With increase in the cooling rate the total crystallinity decreased.

In the pure sPLA, stereocomplex crystallites are forming but crystals of pure enantiomeric PLA are also appeared which may lead to the decrease in the properties. Addition of MCH into the matrix, helps to form only stereocomplex crystallites when melt cooled with low cooling rate. Melt cooling of the specimen with low rate may give enough time to the chain to be in ordered structure, this may be explained by **Figure 5.12**. In the picture, it is shown that at low cooling rate the chains are able to arrange themselves and form ordered structure. The percentage of stereocomplex crystals increased with increase in the content of MCH. It occurred as MCH is providing the extra molecular surface area in the form of small chain length PLLA which gives large interfacial area. It is already evidenced that the stereocomplex crystallites forms easily with low molecular weight chains [162].

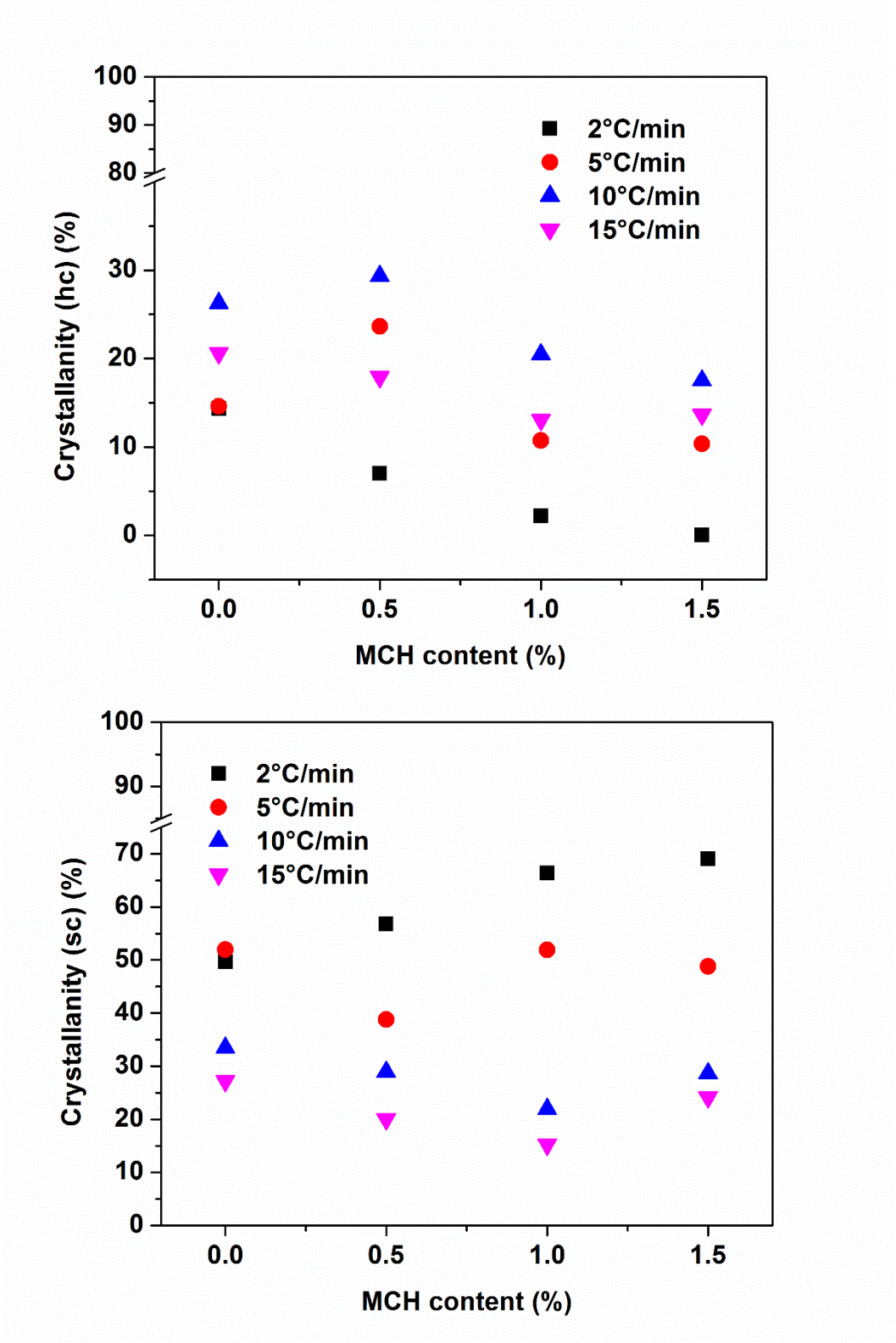

Figure 5.11: Crystallinity of sPLA and its MCH biocomposite (a) after non-isothermal crystallization for homocrystals and (b) stereocomplex.

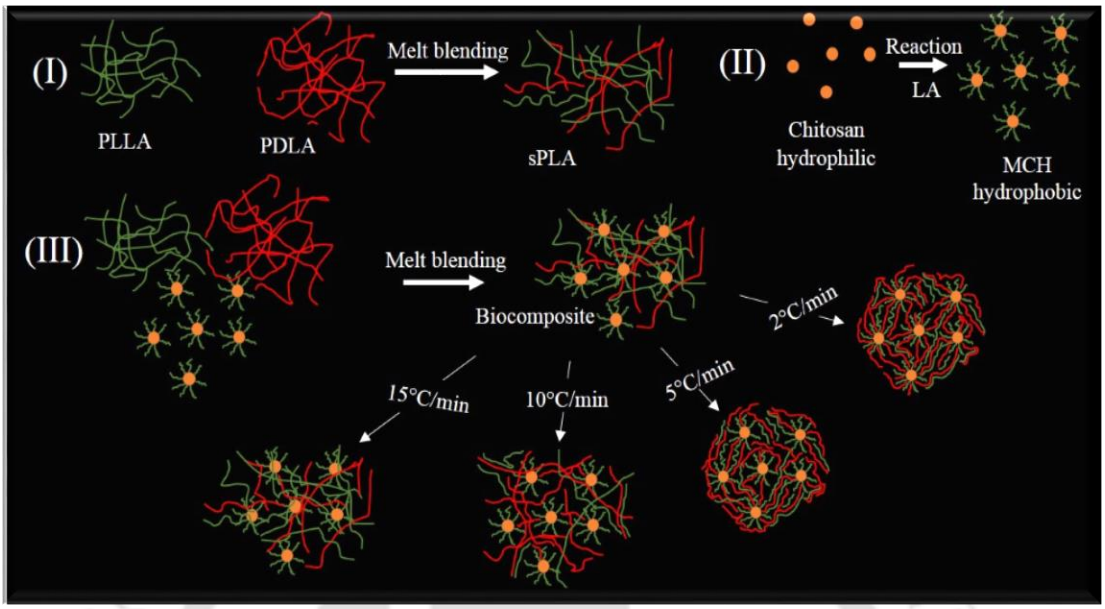

Figure 5.12: Schematic for (I) melt blending of PLLA/PDLA, (II) chitosan modification and (III) heat treatment of sPLA-MCH biocomposite.

5.3.5 Gel formation due to the stereocomplexation

It is known that the stereocomplex crystallites of PLA does not dissolve in the chloroform and forms the gel. Gel content (gel %) are measured as per literature [152] given as

Equation 5.9

$$gel\% = \frac{W_{gel}}{W_i} \times 100 \qquad (5.9)$$

Where, W_i and W_{gel} are the initial mass of biocomposite and mass of dried gel after washing with chloroform followed by vacuum drying, respectively.

Figure 5.13 shows the gel fraction of the PLA MCH biocomposite with respect to the content of the MCH. It is confirmed that the annealing and melt cooling has significant effect on the formation of stereocomplex crystallites. In the case of as prepared specimen, the gel fraction of sPLA is ~3% which increased to more than 15%. It confirms the influence of MCH on stereocomplexation of PLA. The gel fraction is increased after

annealing the specimen at 160°C. The fraction is approximately 40% for all the composites. A significant enhancement is noted in the case of melt cooling with cooling rate of 2°C/min the gel fraction increased to more than 70%. Cooling at 2°C/min provides enough time to the molecules to be arranged. Presence of the MCH increased the molecular surface area for the formation of the stereocomplex crystallites.

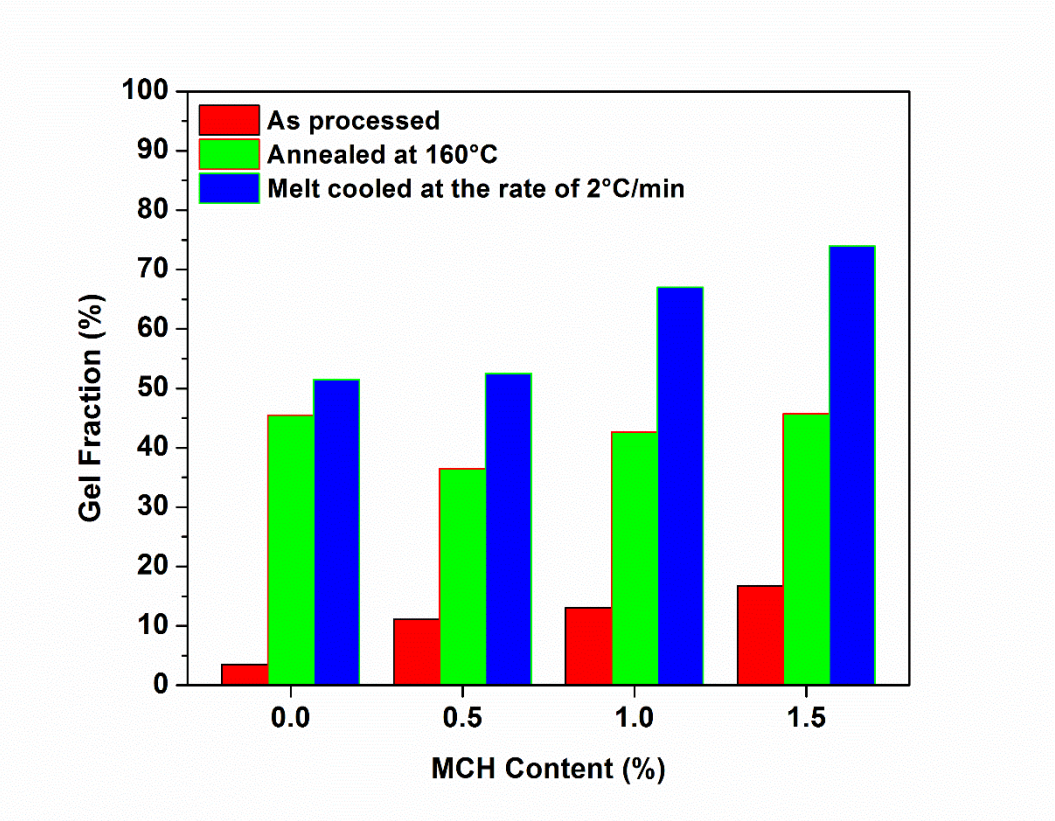

Figure 5.13: Gel fraction of sPLA and MCH biocomposite after washing with chloroform.

5.3.6 Viscoelastic property and heat deflection temperature analysis

We studied the viscoelastic properties of sPLA with MCH biocomposite before and after annealing using DMA. **Figure 5.14a and 5.14b** showed the storage modulus and tan delta of sPLA with various content of the MCH before annealing and after annealing at 160°C, respectively. The storage modulus of sPLA found to be 2295 MPa which increased to 3580 MPa after addition of the MCH to sPLA matrix. Below glass transition temperature, the biocomposite is in glassy state and no change is found in shape of the molecular chains

due to the frozen micro-Brownian motion. The storage modulus of the biocomposite is drastically deceased after the temperature of 57°C which is the glassy region or glass transition of the biocomposite. At glass transition, the region called glass-rubber transition or softening region, the micro-Brownian motion of the polymer chains starts due to the presence of free volume beside the chains which permits the chain segments to rotate. The sudden drop of the storage modulus in the glass transition region is due to the initiation of the micro Brownian motion in the molecular chain. As the temperature increased, the average distance between neighboring molecules also increased which leads to enhanced free volume. After the glass-rubber transition, the entangled chains continuously travel. After annealing the sample at 160°C, decrease in the storage modulus is highly reduced after 57°C which suggest that the material became crystalline and stiff and does not show the glass transition. A crystallized chain segment can absorb or store much more energy for the given condition than free chain segments. At this point, the micro-Brownian motion of the chain segment restricted due to the decreased free volume. The increase in the degree of crystallinity, due to annealing, reduce the free volume of the matrix and freeze the molecular motion. The tan delta, which is the measure of the internal friction of the material at particular condition, found for the biocomposite more than 1 without annealing. It confirms that the loss modulus is higher than the storage modulus of the biocomposite. It suggests that the viscous behavior of the biocomposite dominated over the elastic behavior. After annealing the samples at 160°C, the tan delta reduced drastically and it is less than one. It suggests that the biocomposite is elastic, crystalline and stiff in nature. Presence of these crystalline nature and chitosan into the matrix may also be responsible for the improved heat deflection temperature.

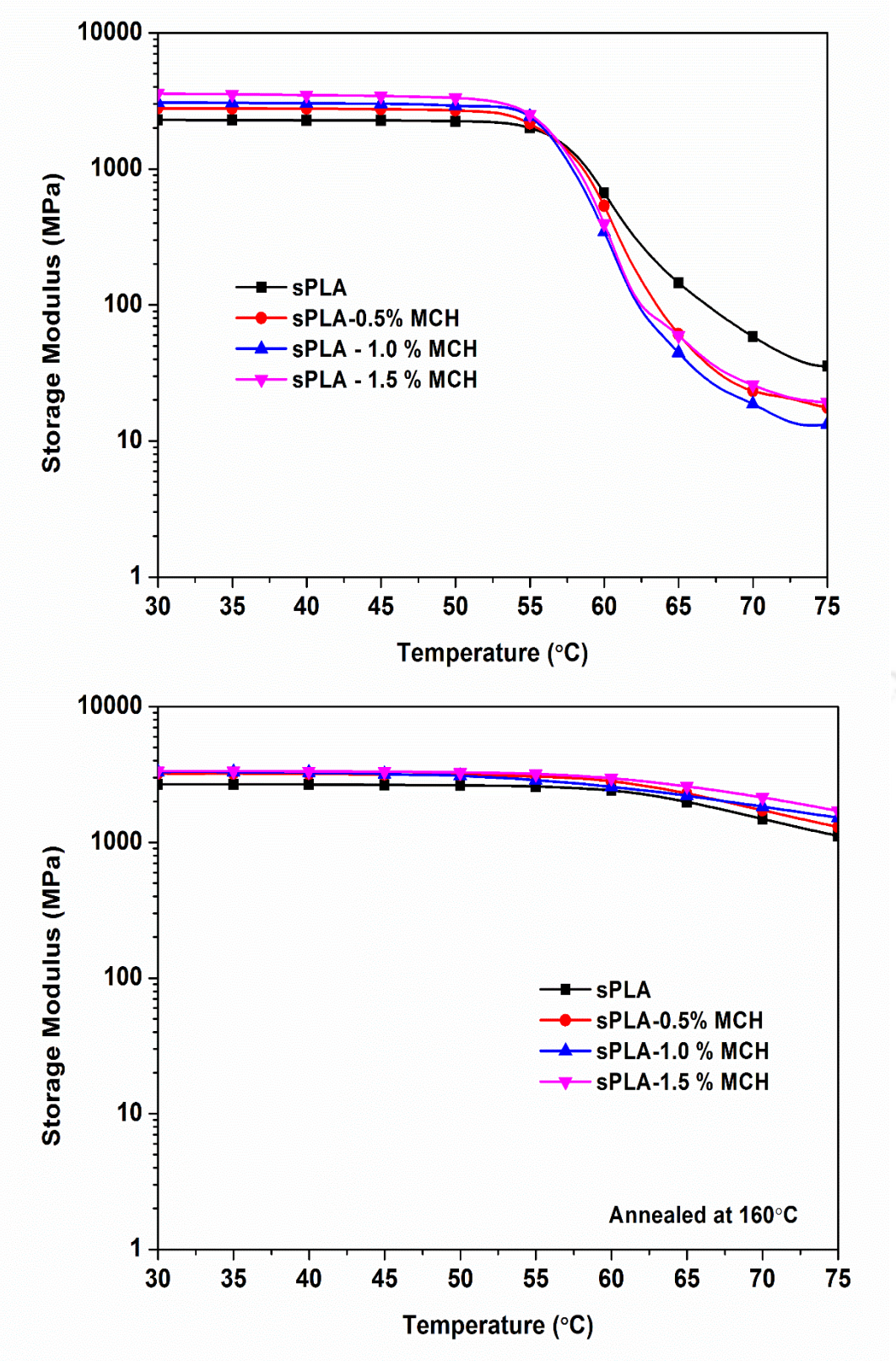

Figure 5.14a: Storage modulus (a) before and (b) after annealing at 160°C of sPLA with various content of MCH.

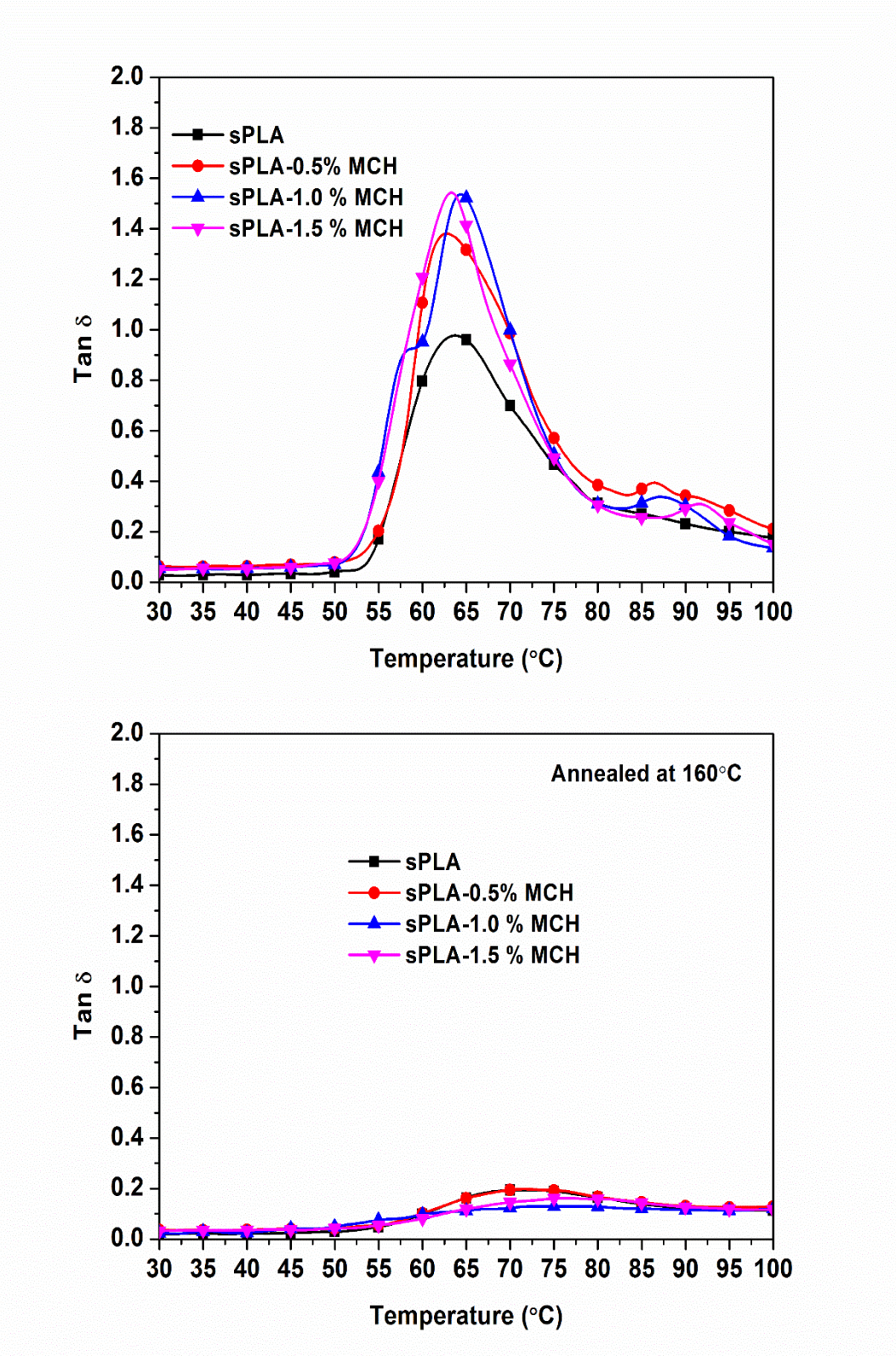

Figure 5.14b: Tan delta (c) before and (d) after annealing at 160°C of sPLA with different contents of MCH.

Heat deflection temperature are estimated by observing the temperature at which the polymer deflects under controlled stress using dynamic mechanical analyzer. The **Figure 5.15** show the deflection length with respect to the temperature for sPLA with various amount of MCH before (**Figure 5.15a)** and after (**Figure 5.15b)** annealing at 160°C. A significant improvement is noticed in the HDT when MCH are added to sPLA. The HDT of sPLA, as prepared, is estimated as ~58°C which further improved to ~80°C after addition of the 1.5% MCH. After annealing at 160°C for 2 hours, HDT of sPLA enhanced to ~68°C and improved to 145°C in the case of 1.5% MCH. The reinforcement of the modified chitosan in the PLLA/PDLA matrix leads to enhancement in the HDT. The network formation between PLA matrix and modified chitosan increased the HDT of biocomposite. The picture of lab made sPLA and its comparison with commercial PLA at elevated temperature is shown in **Figure 5.16**. It is known that the addition of the fibrous component into the polymer matrix enhances the HDT [27]. The chitosan microspheres reinforced into sPLA interact with the PPLA and PDLA chains and restrict the movement of polymer chains by reducing the segmental freedom of movement. The low molecular weight chains grafted on the surface of the chitosan interact with the other PLA species in the matrix and formed the stereocomplex crystallites. Presence of chitosan and formation of the stereocomplex crystallites reduced the chain slippage which ultimately leads to the improvement in the HDT of the biocomposite. Which could also be confirmed by the lower value of tan delta in DMA analysis.

Ultimate tensile strength and young's modulus of sPLA and MCH biocomposite is also measured and shown in the **Figure 5.17**. It can be seen that the UTS is improved from ~29 MPa for sPLA to ~63 MPa for sPLA with 1.5% MCH content. In the case of young's modulus, it increases from ~1.9 GPa for sPLA to 2.8 GPa for 1.0% MCH content. This

improvement in the biocomposite may be found due to the formation of stereocomplex crystallites which is formed due to the presence of MCH.

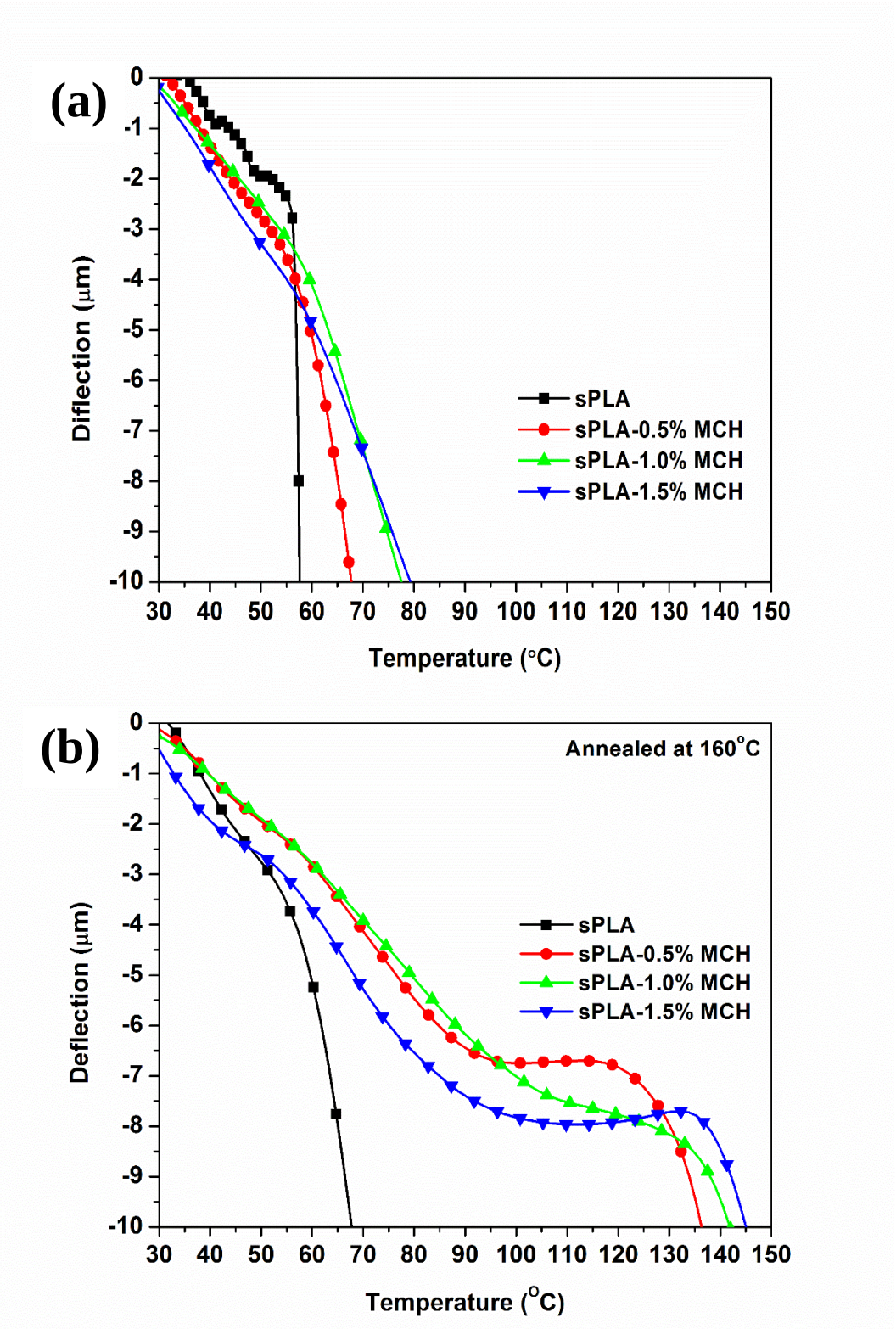

Figure 5.15: Heat deflection of sPLA with different amount of MCH with change in (a) temperature before annealing and (b) after annealing at 160°C.

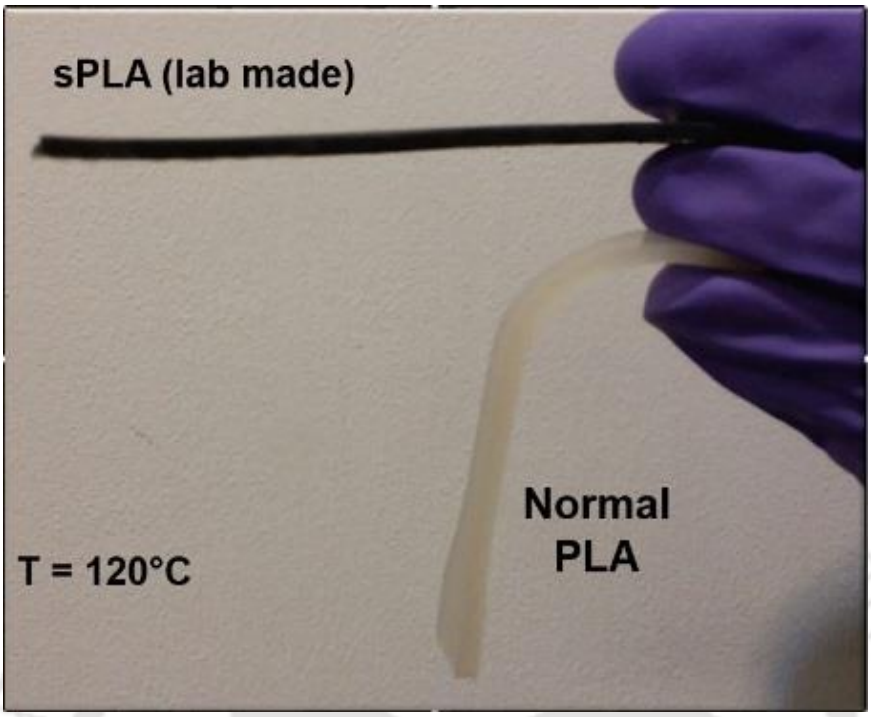

Figure 5.16: Physical examination of HDT of sPLA.

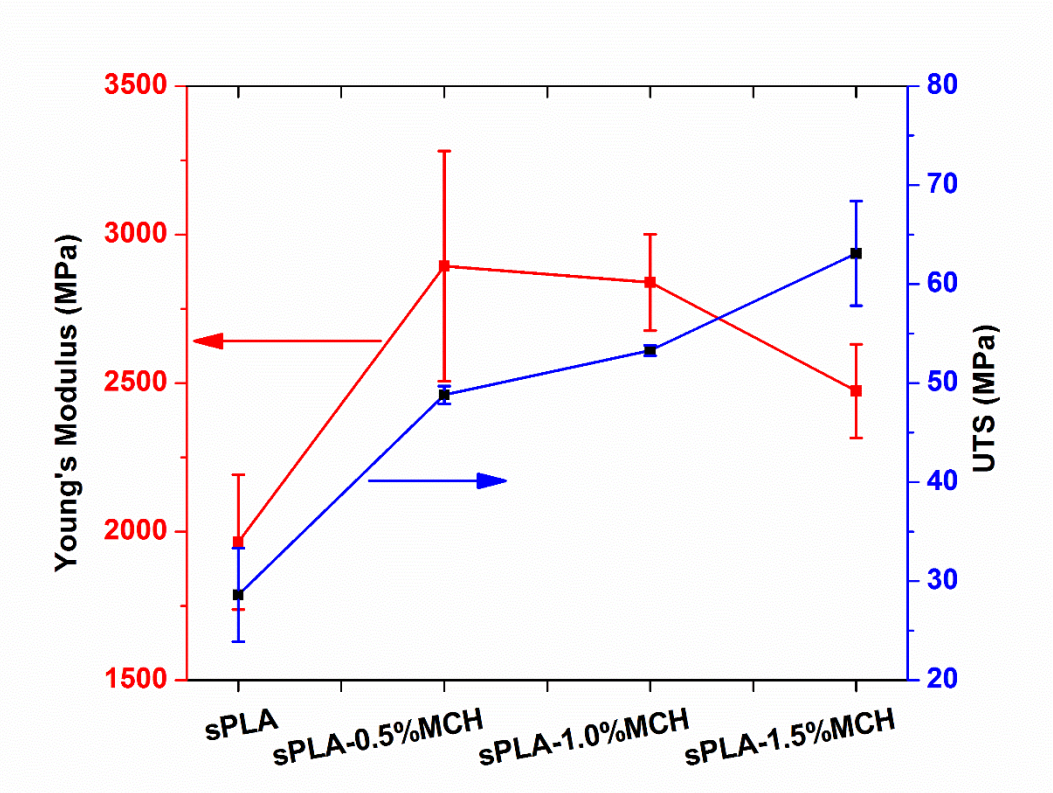

Figure 5.17: Ultimate tensile strength (UTS) and Young's modulus of sPLA and MCH biocomposite.

5.3.7 Distribution of MCH and morphology of biocomposite

The dispersion of MCH is analyzed using TEM which showed that MCH particles are three dimensional, spherical and nicely dispersed in PLA matrix as shown in **Figure 5.18**. The surface morphology of biocomposite films showed two phases; one is continuous polymer matrix and other is discontinuous MCH phase in the form of spherical particles which showed a core-shell like structure. The shell of spheres is hydrophobic and core is hydrophilic in nature. The dispersion of PLA and MCH is based on hydrophobic-hydrophilic interaction which creates only the spherical shape because it is the most favorable shape due to the lowest surface energy when repulsion forces act from all sides on the MCH particles.

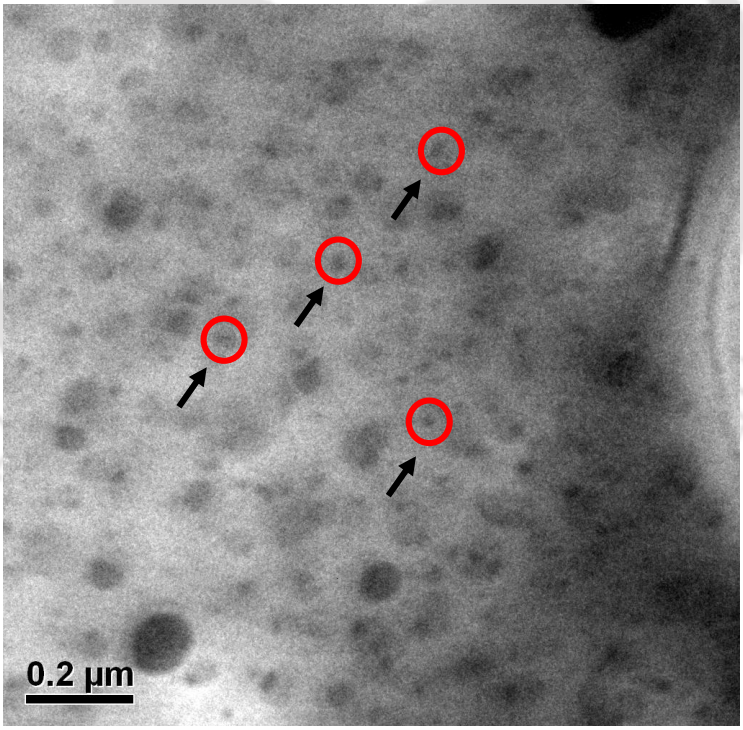

Figure 5.18: TEM image of the modified chitosan hanging in the matrix of PLA.

The morphology of the fractured surface of PLA matrix and MCH biocomposite is studied by FESEM and shown in the **Figure 5.19**. It can be clearly seen that the smoothness of the polymer is disturbed due to the presence of MCH and it became rougher surface compared to the neat polymer. Nano/micron sized bumps of MCH are distributed all over the surface which increased the molecular surface area responsible for the formation of stereocomplex crystallites.

Table 5.5: Oxygen permeability and permeability parameter measured at 23°C and 0%RH humidity for sPLA with various MCH loading.

Sample Name	(a)	(b)	(P)	(D)	(S)
sPLA	13.4	--	6.67	2.17	3.56
sPLA-1%MCH	8.3	38.1	4.17	1.83	2.63
sPLA-2%MCH	6.0	55.2	2.99	1.27	2.72
sPLA-3%MCH	5.9	56.0	2.95	1.40	2.43

a) OTR ($cm^3.mm/m^2.day$), b) % reduction respect to sPLA, P) Permeability [$(cm^3.mm/m^2.day.kPa)\times10^{-2}$], D) Diffusivity [$(cm^2/s)$ $\times10^{-8}$], S) Solubility [$(cm^3/cm^3.Pa)$ $\times10^{-3}$]

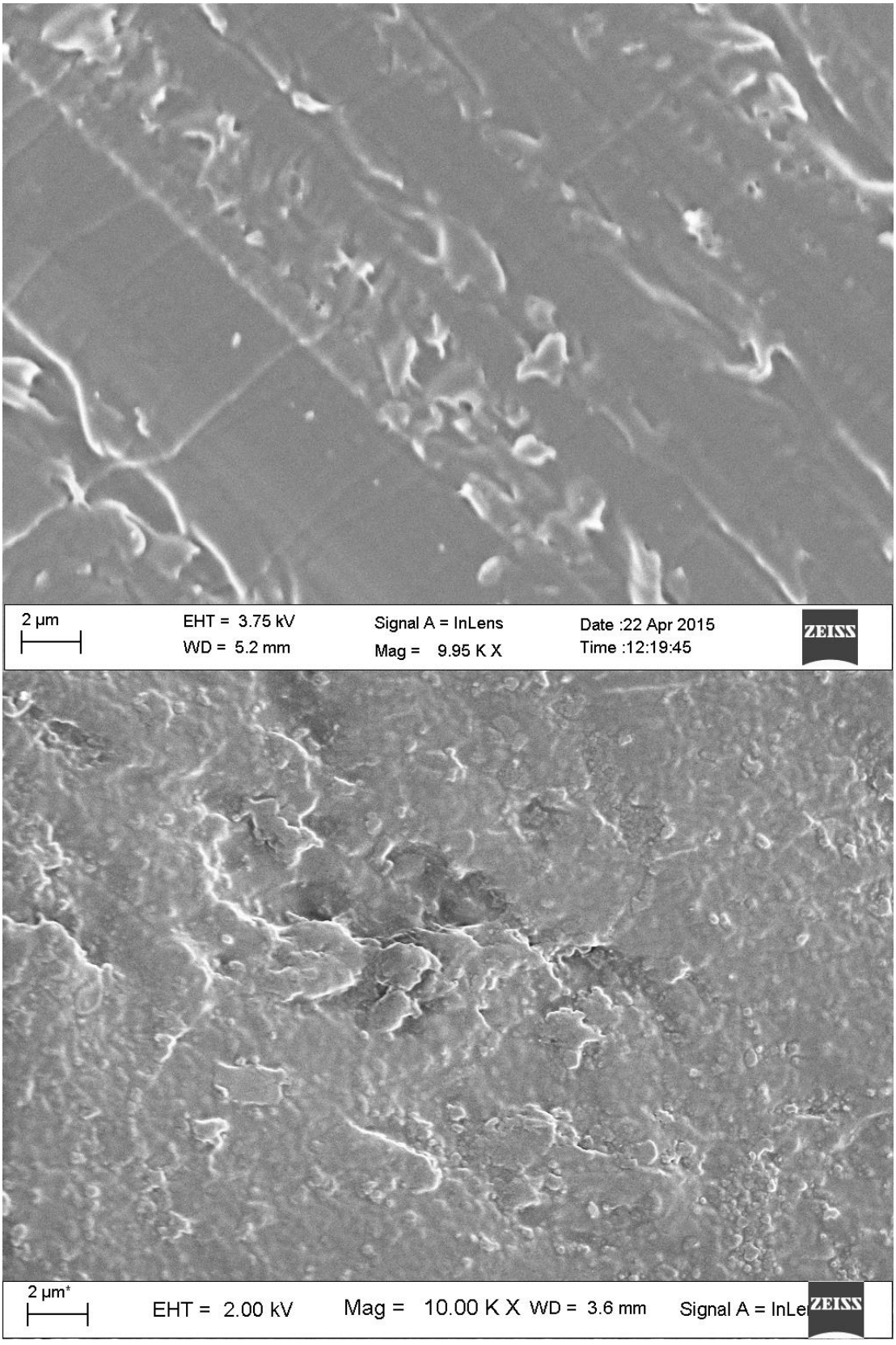

Figure 5.19: FESEM images of fractured surface of (a) sPLA and (b) sPLA-MCH biocomposite.

5.3.8 Oxygen barrier properties

The result of OTR and oxygen permeability parameters provide the insight into the mechanism of oxygen transport through the PLA-MCH biocomposite film. The oxygen transmission rate and permeability parameters such as diffusion coefficient, solubility coefficient and permeability of the film of sPLA with different amount of MCH content are summarized in the **Table 5.5**. The biocomposite showed a drastic reduction in OTR value upon incorporation of the MCH into sPLA (PLLA/PDLA) matrix. At 23°C and 0 %RH humidity, bare sPLA showed an oxygen permeability of 6.67 ($cm^3.mm.m^{-2}.day^{-1}.kPa^{-1}\times10^{-2}$). The permeability of sPLA containing 3 wt% MCH, is decreased to 2.95 ($cm^3.mm.m^{-2}.day^{-1}.kPa^{-1}\times10^{-2}$). This corresponds to a reduction of 56% compared to the bare sPLA. In comparison with the OTR of neat PLA as 19 ($cm^3.mm.m^{-2}.day^{-1}.kPa^{-1}\times10^{-2}$) reported by Dhar at el. [44], the percentage reduction in the oxygen permeability is found to be 84.5%. The chitosan content and improvement in the stereocomplexation in the biocomposite are may be the main cause of enhancement in the oxygen barrier properties. We have understood in the previous section that the addition of the MCH improves the stereocomplexation. Stereocomplex crystallites are relatively highly packed crystalline section in the matrix which may prevent the oxygen transport through the film [58]. Presence of the chitosan produces the tortuous path, which also prevents the oxygen molecules to permeate through the film [49]. Diffusion and solubility parameters predicted from the half time value are decreased by 35.5% and 31.7%, respectively, observed at 23°C and 0% RH. The chitosan content in the matrix may be responsible for the decrease in the diffusivity by increasing the tortuous path and the improved packed crystalline phase may reduce the solubility of the oxygen molecule into the matrix.

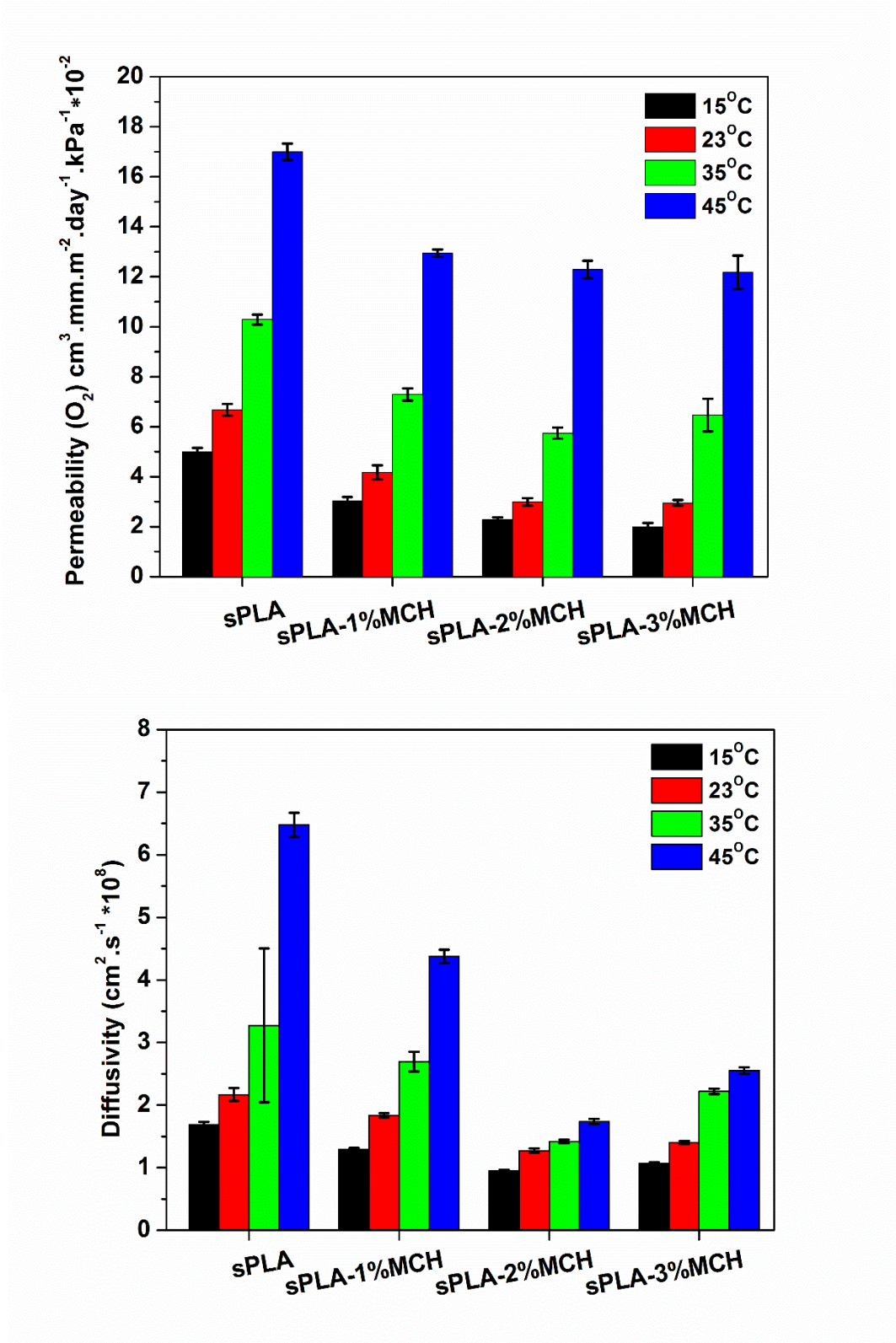

Figure 5.20a: Variation of (a) oxygen permeability and (b) diffusivity of sPLA with different amount of MCH with respect to temperature.

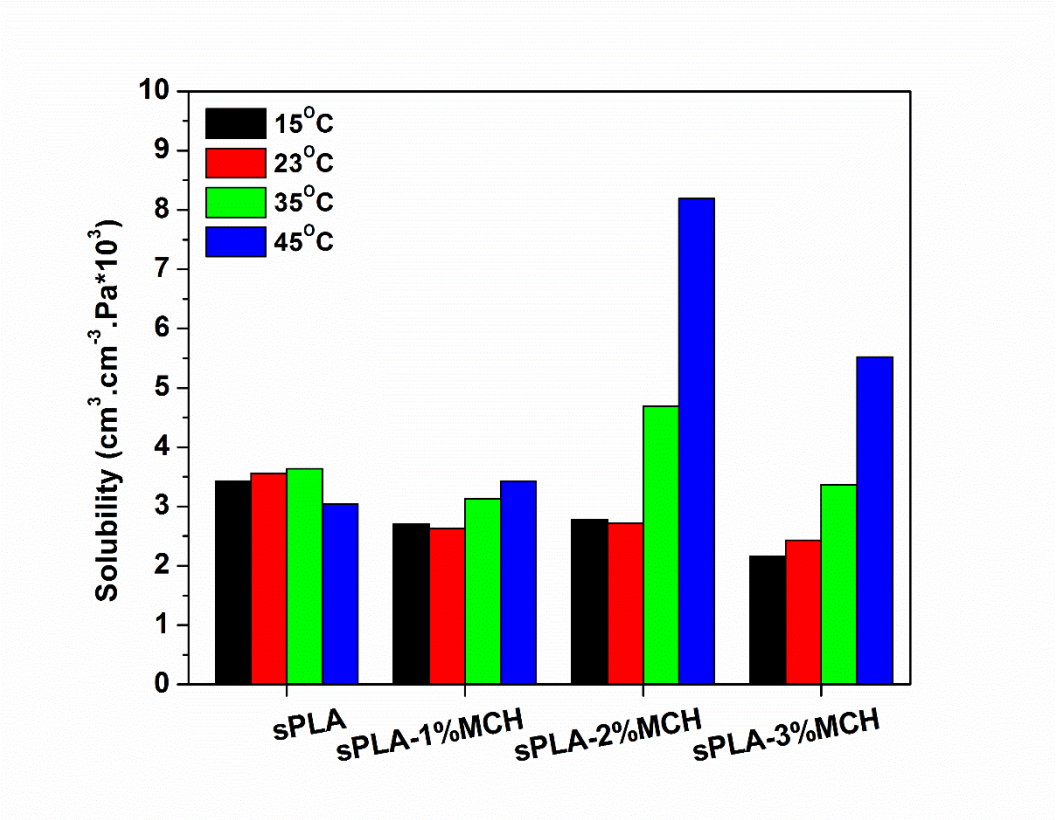

Figure 5.20b: Variation of solubility of sPLA with different amount of MCH with respect to temperature.

It has already been theorized that the gas permeation depends on the size and amount of the pores in the polymer matrix which is called as static free volume and the frequency of the channel formation is called dynamic free volume [173]. The presence of chitosan in the matrix may help to decrease the static free volume. Formation of the stereocomplex crystallites, due to the presence of MCH, hindered the segmental motion of the polymer chains which leads to the reduction in the dynamic free volume.

The oxygen permeability variation is studied over the temperature range to understand the effect of MCH loading on polymer matrix. **Figure 5.20a and 5.20b** shows the change in oxygen permeability, diffusivity and solubility of sPLA with various MCH loading in range of 15°C to 45°C. It is found that the oxygen permeability (**Figure 5.20a)** with respect to the temperature increased, is in line with the behaviour observed in the conventional polymer. Increment in the temperature resulted in the rise of oxygen permeability. At higher

temperatures, molecules contain higher energy and they move much more easily through the film. With increase in the content of MCH the permeability decreased and similar trend is obtained for the diffusivity also. In case of oxygen solubility (**Figure 5.20b**), there is less variation with change in MCH content. To understand the temperature dependency of permeability and diffusivity of sPLA with MCH variation, an attempt is made to fit the Van't Hoff- Arrhenius equation with permeability (**Equation 5.10**) and diffusivity (**Equation 5.11**) data

$$P(T) = P_o \exp\left(\frac{-E_P}{RT}\right) \tag{5.10}$$

$$D(T) = D_o exp\left(\frac{-E_D}{RT}\right) \tag{5.11}$$

where, P_o and D_o are the pre-exponential factors for the permeability ($cm^3.mm.m^{-2}.day^{-1}.kPa^{-1}$) and diffusivity ($cm^2.s^{-1}$), respectively, E_P and E_D are the activation energies ($J.mol^{-1}$) for permeation and diffusion, respectively, R (8.314 $J.K^{-1}.mol^{-1}$) is the universal gas constant and T is the absolute temperature (K). The E_P and E_D may be calculated by linear fitting of ln P(T) or ln D(T) vs T^{-1} plot.

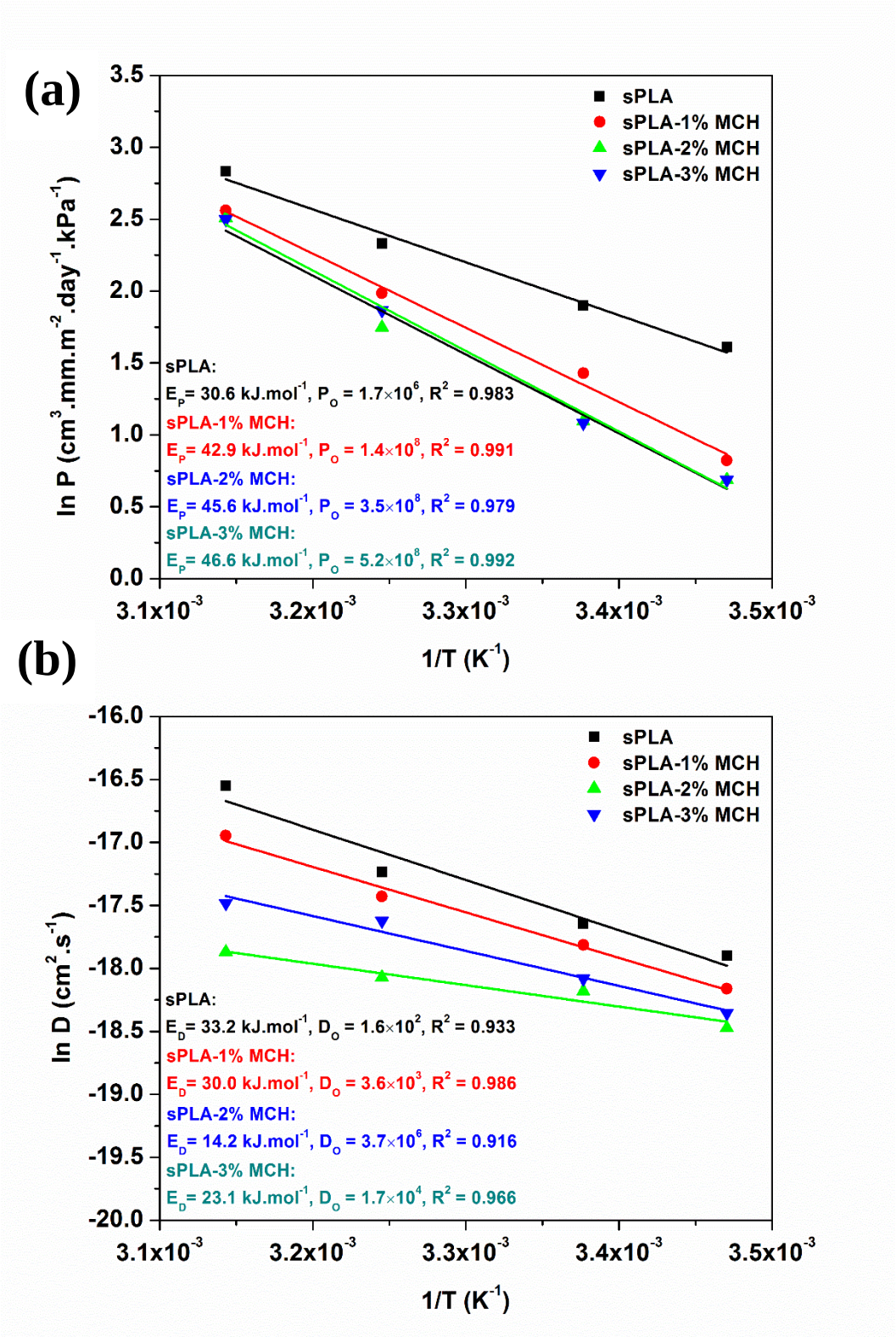

Figure 5.21: Temperature dependence of (a) permeability and (b) diffusivity fitted with Van't Hoff-Arrhenius equation for sPLA with various MCH loading

Figure 5.21 shows the linear fit of the permeation and diffusion data with Van't Hoff- Arrhenius equation. The calculated value of the activation energy of permeation (**Figure 5.21a**) are 30.6, 42.9, 45.6 and 46.6 $J.mol^{-1}$ for sPLA, sPLA-1%MCH, sPLA-2%MCH and sPLA-3%MCH, respectively. The calculated activation energies are the indicator of the energies required for oxygen molecule to overcome the barrier formed in the presence of MCH. Increase in the activation energy for the permeation is evidence of the formation of stable barrier by stereocomplexation and chitosan which offer tortuous pathway for the oxygen molecule to diffuse through the film. This results in lower gas permeation and improved gas barrier properties. The activation energy of diffusion (**Figure 5.21b**) are found to be 33.2, 30, 14.2 and 23.1 $kJ.mol^{-1}$ for sPLA-1%MCH, sPLA-2%MCH and sPLA-3%MCH, respectively. It has been shown that the diffusivity of the oxygen reduced with incorporation of the MCH, but it is also found that the temperature dependency of the biocomposite is reduced. It leads to the reduction in the activation energy of diffusion for the biocomposite.

5.4 Conclusions

Chemical modification of the chitosan is done successfully and the biocomposite of the high molecular weight PLLA/PDLA and MCH is prepared using melt extrusion process. The prepared biocomposite is having melting temperature more than 207°C with ~40 J/g enthalpy in the case of 1% MCH content. Formation of stereocomplex crystallites is proven by using FTIR and XRD analysis. It is found that the heat treatment has significant effect on the formation of stereocomplex crystallites. When annealed at or more than 160°C, no homocrystals is formed however the degree of crystallinity is ~40%. In the case of nonisothermal cooling of biocomposite with the rate of 2°C/min, the degree of crystallinity increased to ~70% for 1.5% MCH content and no homocrystallites is found. The gel fraction of the biocomposite after and before annealing also confirmed the formation of

stereocomplex crystallites. Due to the presence of MCH, which is responsible for the enhancement in the formation of stereocomplex crystallites into PLA matrix, heat deflection temperature is improved from ~70°C for sPLA to 145°C for sPLA at 1.5%MCH. It is also confirmed by DMA analysis before and after annealing. Due to the formation of stereocomplex crystallites and presence of chitosan, the ultimate tensile strength enhanced from ~29 to ~63 MPa and ~1.9 to ~2.8 GPa. Oxygen barrier of the biocomposite films is improved significantly and a reduction of 56% is observed with respect to sPLA blend. Due to introduction of MCH in sPLA, the diffusivity and solubility of oxygen molecules in the biocomposite film reduce by ~36% and ~32%, respectively and increase in the activation energy from 30.6 to 46.6 kJ.mol^{-1} for permeation of oxygen is observed.

CHAPTER: 6

Fabrication and Characterization of Stereocomplex PLA-Hydroxyapatite Biocomposite

Graphical abstract

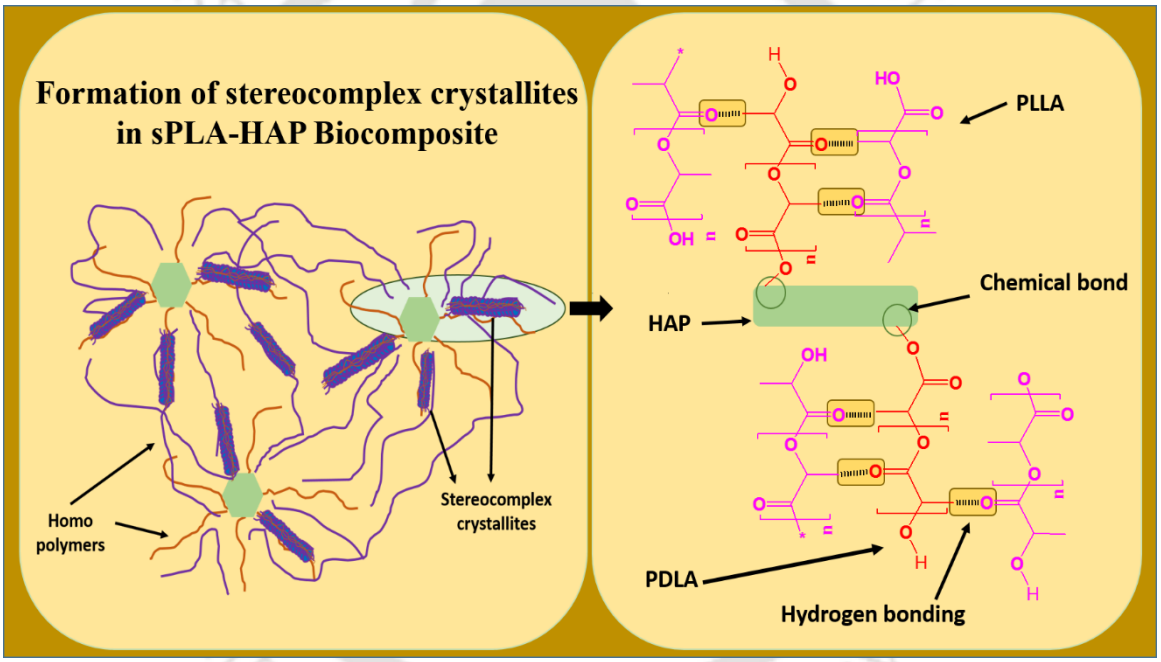

ACS Omega 2017, 2 (7), 4039-4052

Abstract

Development of high molecular weight stereocomplex poly(lactic acid) (PLA) with no trace of homocrystallites is highly desirable. In this study, nano hydroxyapatite (HAP) which is fabricated from fish scale bio-waste is used as grafting agent with poly (D-lactic acid) during in situ ring opening polymerization of D-lactide. This grafted PDLA is used in the development of the stereocomplex PLA biocomposite. It is demonstrated that the use of grafted HAP resulted in the formation of stereocomplex PLA with 100% stereocomplex crystallites fraction with melting temperature of ~227°C without homocrystals. Grafting of HAP ensures the uniform dispersion confirmed by microscopic analysis in ~60 nm range which leads to significant improvement in mechanical, thermomechanical and barrier properties of biocomposites. The biocomposite tensile strength, elongation at break and storage modulus are found to improve as high as ~16%, ~130% and ~47% respectively with reduction of ~48% and ~34% in oxygen permeability and water vapor transmission rate. Improvement in the stereocomplexation leads to enhancement of properties due to the improvement in interfacial interaction and uniform dispersion resulted by grafting of HAP with PDLA. It is believed that grafted HAP played dual role viz. acting as bridge between uncoiling chains in tensile direction by providing the extended molecular surface area in the form of PDLA chains and develop the restriction to the chain mobility.

6.1 Introduction

In recent past, poly(lactic acid) (PLA) has been considered as a potential candidate to replace the traditional petroleum based thermoplastics for several applications such as textile, agriculture, biomedical, packaging etc. [27]. PLA can be produced using lactic acid as monomer which is a chiral molecule and has been derived from renewable agriculture resources [13]. Due to the chiral properties of lactic acid, PLA has two semi-crystalline stereoisomers such as poly(L-lactic acid) (PLLA) and poly(D-lactic acid) (PDLA). It has been known that the PLLA and PDLA can be crystallized in several polymorphs such as alpha, beta and gamma form at different processing conditions [176]. In 1987, Ikada et al. have reported the formation of special type of polymorphs in PLA by mixing PLLA and PDLA called stereocomplex, made by combining right and left handed helical polymer chains, and found its melting temperature 50°C higher than normal enantiomeric pure PLA [57]. Similar phenomenon was also seen by Miyamoto et al. in stereospecific poly(methyl methacrylate) (PMMA) [177]. Due to the intermolecular hydrogen bond between PLLA and PDLA, stereocomplex crystallites take compact polymer chain packing compared to homocrystals [178]. Stereocomplexation in PLA promises superior thermal [179], mechanical [180], thermomechanical [163] and barrier properties [181] than enantiomeric pure PLA which makes it an interesting polymorph to study.

The formation of stereocomplex crystallites is highly dependent on the mannered arrangement of PLLA and PDLA chains in the blend and it becomes complicated due to the similar temperature range for crystallization of homo and stereocomplex crystallites. It has been confirmed that the stereo complex crystallites with a trace amount of homocrystals can be formed by mixing PLLA and PDLA in 1:1 ratio [63]. Furthermore, it is limited to the low molecular weight polymers such as less than 100 kDa, and amount of homocrystals

found excessively higher in case of high molecular weight polymers (higher than 100 kDa) [182]. Therefore, development of PLA with higher content of stereocomplex crystallites is the prevailing issue among polymer scientists in order to get PLA with improved thermal, mechanical and barrier properties.

In this context, several research groups are trying to develop different techniques such as solid state polymerization [183], development of stereo diblock copolymer [184], supercritical fluid technology [164, 185], layer by layer assembly [186] etc. in order to prepare relatively high molecular weight PLLA/PDLA blend with high content of stereocomplex crystallites. Some of the researchers have used the modified or unmodified fillers such as nano-crystalline cellulose [140], nano-graphite [187], graphene oxide [58, 72], carbon nanotube [188, 189], lignin [190] and other polymers [191-193]. In the present work, hydroxyapatite has been used as a filler into the PLA matrix. Hydroxyapatite (HAP) is bioactive nontoxic complex form of calcium phosphate which is the 60-70% content of mammalian bones. It can be produced by several biological or synthetic methods such as precipitation, hydrothermal and sol-gel method, hydrolysis, solid state synthesis [99], from bio-resources such as eggshells, seashells, plants, animal bones etc. [103]. Due to its similarity with mammalian hard tissues, HAP is one of the most investigated synthetic biomaterial. Ample amount of research has been done on the fabrication of PLA-HAP biocomposite for different applications [194-197]. Due to the poor interfacial adhesion with PLA and poor mechanical properties, HAP needs to be modified [198]. To avoid the agglomeration of HAP particles, researchers have grafted HAP to PLA via *in situ* ring opening polymerization. Du and Zen developed poly(D,L-lactic acid) (PDLLA) grafted HAP via solution ring opening polymerization in toluene and used it for the shape memory application [199]. Qiu and his group modified the HAP surface with lactic acid in toluene

before grafting with PLLA at 130°C for 80 hours and blended with PLLA at 170°C. The prepared composite showed good mechanical properties and uniform microstructure [200]. In the same direction, Hong et.al. have found good dispersion of HAP in polymer matrix after grafting with PLA in xylene solution which lead to the improvement in mechanical properties [201]. Similarly, Wang and his group have modified the surface of HAP with lactic acid oligomer and found the improved dispersion which lead to the enhancement in the properties of end product [202]. A large number of researchers have grafted HAP involving toxic solvents which are not industrially viable techniques. As per our knowledge, so far, no literature is available which address the modification of HAP in bulk and its application in the development of stereocomplex PLA.

Therefore, the current work is dedicated to develop a facile process to graft HAP via *in situ* bulk ring opening polymerization (ROP) of lactide. It promises better compatibility with PLA molecules which is confirmed by morphological studies. Stereocomplex PLA-HAP biocomposite is developed with different HAP content. The molecular structure, mechanical, thermal, thermomechanical and barrier properties of prepared biocomposite are investigated which evidently demonstrates the usability of grafted HAP in the enhancement of stereocomplexation of PLA and its ultimate application.

6.2 Experimental section

6.2.1 Materials

L-lactide and D-lactide were produced from L-lactic acid (Purac, India) and D-lactic acid (Musashino Japan), respectively, by two step polymerization and depolymerization procedure. L-lactic acid or D-lactic acid is dehydrated to get the oligomeric PLLA or PDLA and it is depolymerized in presence tin oxide to obtain the L-lactide or D-lactide and used

after purification. Tin oxide (SnO) and stannous octoate (Tin octoate) was procured from Sigma Aldrich. Hydroxyapatite (HAP) was provided by Mr. Arbind Prasad (Department of Mechanical Engineering, IIT Guwahati). Catalyst solution was prepared by dissolving 1 gm of Tin octoate in 10 mL of Toluene (Merck India). HPLC grade chloroform and Hydrochloric acid (HCl) were purchased from Merck India. Sodium hydroxide (NaOH) was obtained from HiMedia, India. All chemicals were used as received.

6.2.2 Preparation of PDLA grafted HAP

HAP is grafted with PDLA via bulk ring opening polymerization of D-lactide. Dried ampoule equipped with magnetic stirrer is filled with required amount of purified D-lactide, HAP and tin octoate. Lactide and catalyst molar ratio ([L]/[C]) is maintained to 2000:1. The ampoule is purged with argon gas for one hour to make ampoule free of moisture and oxygen content. The vacuum is applied to the ampoule for two hours to eliminate the excess amount of toluene. Ampoule is sealed using heating torch under the vacuum condition and oil temperature is raised to 105°C. Mixing of monomer, HAP and catalyst is done for two hours, after that temperature is increased to 160°C and ampoule is left for two more hours for ROP. The obtained PDLA grafted HAP is recovered by breaking the ampoule and named as PDLA-HAP. As same fashion, PLLA and PDLA is also synthesized. The granulated form of PLLA, PDLA and PDLA-HAP are kept in vacuum oven at 40°C for 12 hours to remove the residue monomer.

6.2.3 Preparation of stereocomplex PLA HAP biocomposite

To prepare the stereocomplex PLA, HAP biocomposite, PDLA-HAP and PLLA with 1:1 weight (1 gm each) ratio are dissolved in 70 mL of chloroform (5% hexafluoroisopropanol (HFIP) solution) in a single neck round bottom flask (RBF) at room temperature for

48 hours. The obtained solution is cast on a polytetrafluoroethylene (PTFE, 150 mm diameter) petri-dish kept at room temperature. Petri-dish is covered with perforated aluminium foil in order to reduce the rate of evaporation of solvent. After drying for 24 hours, the obtained film is kept in vacuum oven at 60°C for 48 hours to remove the residual content of solvent. The stereocomplex PLA biocomposite with 0.5%, 1% and 2.5% HAP content denoted as sPLA-0.5%HAP, sPLA-1%HAP and sPLA-2.5%HAP whereas blend of pristine PLLA and PDLA indicated as sPLA. The prepared biocomposite films are used for its characterization.

6.2.4 Characterization

Gel permeation chromatography (GPC) (Shimazdu, Japan) is used to determine the molecular weight of prepared biocomposite at 40°C. HPLC grade chloroform is used as eluent with flow rate of 1.0 $mL.min^{-1}$. The system is calibrated using the mono-dispersed polystyrene standard. Prepared biocomposite is dissolved into the chloroform and filtered through 0.45µm PTFE syringe filters before analysis. The molecular weight and specific rotation of the PLLA, PDLA and PDLA-HAP biocomposites is tabulated in T**able 6.1**.

Table 6.1. Molecular weight of produced biocomposite.

Sample Name	Weight average molecular weight (Mw)	Polydispersity index (PDI)	Specific rotation $[\alpha]_{589}^{25}$
PLLA	197	1.9	-157
PDLA	255	1.8	156
PDLA-1.0%HAP	299	1.7	--
PDLA-2.0%HAP	299	1.6	--
PDLA-5.0%HAP	275	1.7	--

The chemical structure of PDLA and PDLA grafted HAP are studied using 600 MHz nuclear magnetic resonance (NMR) spectroscopy (Bruker, Germany). ^{13}C-NMR spectra of samples are recorded after dissolving the samples in deuterated chloroform ($CDCl_3$) for 48 hours.

Calculation of the amount of PDLA grafted on HAP is made by thermo-gravimetric analysis (TGA, Perkin Elmer). Weight loss of sample (6-8 mg) is recorded by heated in the temperature range from 30°C to 700°C at a heating rate of 10°C.min^{-1} under an inert environment of nitrogen gas. PDLA grafted HAP is purified by removing the unreacted PDLA chains from the system via dissolution and centrifugation followed by drying process before analysis.

The FTIR spectra of the biocomposites are measured by attenuated total reflection (ATR) mode in Frontier FT-IR spectrometer (Perkin Elmer, USA) at room temperature. Spectra is recorded after 16 scans from wave number 4000 cm^{-1} to 650 cm^{-1}. The prepared biocomposite is directly analyzed and spectra are recorded.

Field Emission Scanning Electron Microscope (FESEM) is used to examine the topography of the fractured surface of different samples placed on carbon tape. The samples are further coated in gold sputtering unit for 30s and characterized using FESEM (Sigma, Zeiss, GmbH) at accelerating voltage of 2-4 kV.

The thermal behaviour of the biocomposite is measured using the differential scanning calorimeter (DSC) (Phoenix DSC 204 F1 NETZSCH, GmbH) under nitrogen atmosphere. Thermograph is recorded by heating the sample from 20°C to 250°C with 10°C.min^{-1} heating rate. The percentage crystallinity of sPLA and biocomposite is calculated as per following equation

$$X_{c,sc}(\%) = \frac{\Delta_{m,sc} - \Delta H_c}{\Delta H_{mp,sc}} \times 100 \quad (6.1)$$

$$X_{c,hc}(\%) = \frac{\Delta H_{m,hc} - \Delta H_c}{\Delta H_{mp,hc}} \times 100 \quad (6.2)$$

$$f_{sc}(\%) = \frac{X_{c,sc}}{(X_{c,hc} + X_{c,sc})} \times 100 \quad (6.3)$$

Where, $X_{c,sc}$ and $X_{c,hc}$ is the degree of crystallinity of stereocomplex and homo crystallites respectively. $\Delta H_{m,sc}$ and $\Delta H_{m,hc}$ is the enthalpy of fusion at melting for stereocomplex crystallites and homocrystals, $\Delta H_{mp,sc}$ and $\Delta H_{mp,hc}$ is the heat of fusion of a perfect crystal (93.6 $J.g^{-1}$ for homocrystals and 142 $J.g^{-1}$ for stereocomplex crystal) [69] and ΔH_c enthalpy of cold crystallization, f_{sc} (%) is the percentage of faction of stereocomplex crystallites into the system.

X-ray diffraction (XRD) spectra are determined using Model-D8 Advance system diffractometer (Bruker, Germany) equipped with Cu-Kα radiation (λ= 0.1541 nm) as X-ray source operating (40 kV, 40 mA) at a scan rate of 3° per min in the 2θ range of 5–40°.

The tensile strength and percentage elongation of prepared samples (7 mm width, ~0.2 mm thickness and 15 mm gauge length) are measured using tensile stress testing stage (TST 350, Linkam) equipped with 20 N load cell at constant cross speed of 1 $mm.min^{-1}$ in tensile mode. Stage is controlled by system controller PE95/T95 with system software Linksys 32. Three replicates of each sample are tested and the average results are reported with standard deviation.

Thermo-mechanical stability of the prepared biocomposites at higher temperatures with dynamic force application are measured using DMA (DMA 242 E model, NETZSCH

GmbH) in the temperature range 25–190 °C at 2°C.min^{-1} heating rate, 1 Hz frequency and 10 µm displacement amplitude.

The oxygen gas transmission rate (OTR) for the biocomposites with different loading of HAP is determined using OX2/231 oxygen permeability tester (Labthink, China). Measurements are carried out at 23°C using oxygen gas of high purity (99.999%) on a film having an area of 50 cm^2 following the ASTM D3985 standard. Pure oxygen (99.9%) at a pressure of 0.5 bar and a flow rate of 20 mL/min is maintained into the upper half of the sample chamber during analysis while nitrogen gas is continued into the lower half of the chamber. The chambers are purged for at least 6 hours before measurement. The test is performed for at least 6 hours so as to reach steady state.

Water vapour transmission rate (WVTR) is recorded using a PERMATRAN-W® Model 1/50 (Mocon, USA) following ASTM standard E398-03. The relative humidity (RH) is fixed to 100% in the wet chamber and 10% in the dry chamber, yielding a driving force of 90% RH. The film of 50 cm^2 area is analyzed at atmospheric pressure and at temperature of 37.8±0.1°C.

6.3 Results and discussion

6.3.1 Characterization of fabricated nano hydroxyapatite

The nanohydroxyapatite is characterized by electron microscopy to check the morphology and size of the particles which is shown in **Figure 6.1**. At 20 kX magnification it is difficult to clearly identify separate HAP particles (**Figure 6.1a**). Images at higher magnification (50 kX) showed the particles and agglomeration of HAP. The particle size is found in the range of 30-60 nm. Some of the particles are found agglomerated, where nano size powder form clusters which is in the range of 2-3 microns. The ratio Ca/P is found to be 1.68 which confirms the fabrication of HAP [203].

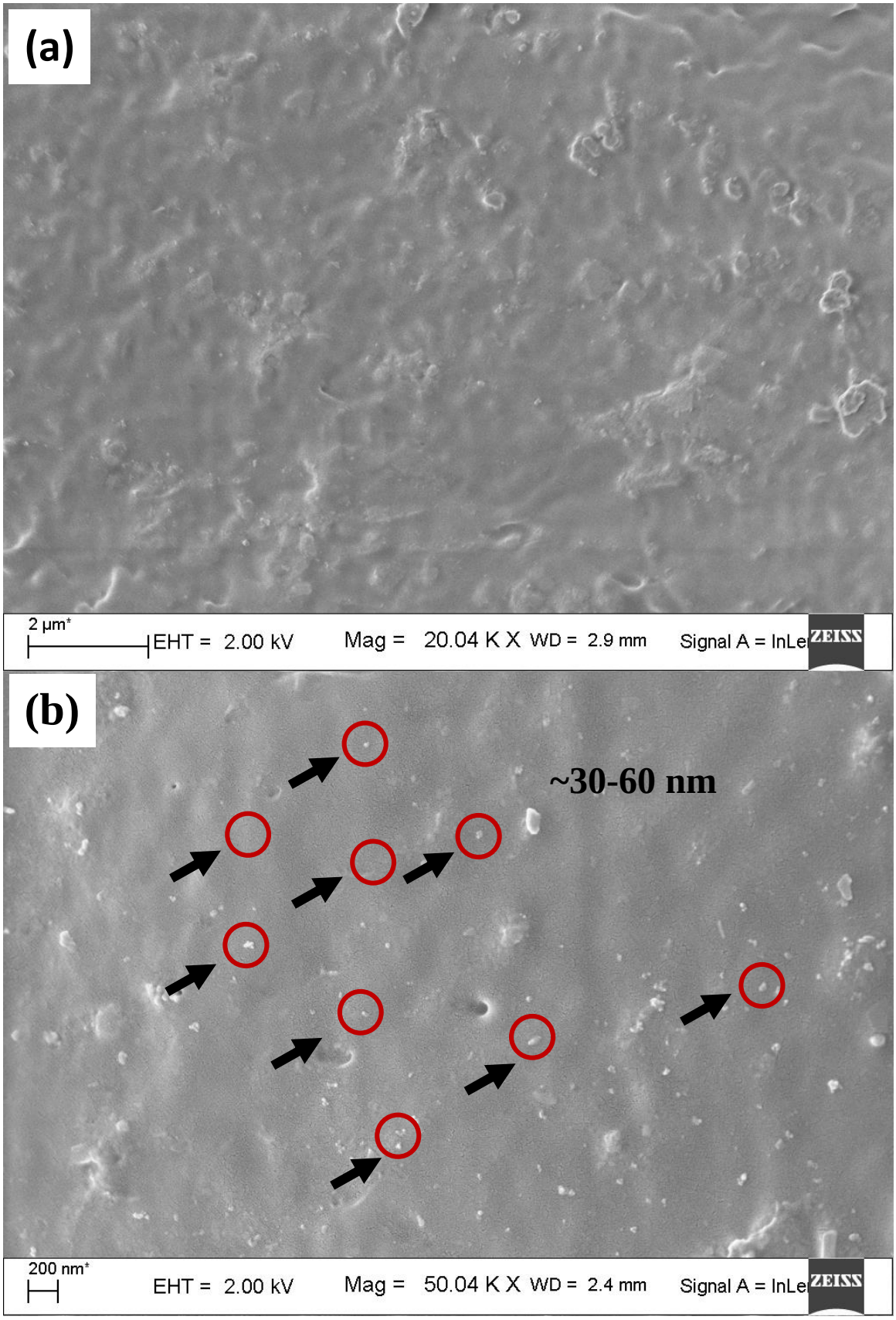

Figure 6.1: FESEM images of nano hydroxyapatite particles at (a) 20 kX and (b) 50 kX.

6.3.2 Chemical modification of HAP

In order to improve the dispersion and homogeneity into polymer matrix, HAP is modified by *in situ* grafting with PDLA via bulk ROP of D-lactide. It is assumed that the hydroxyl group present in HAP molecule would contribute as co-initiator for the ROP of lactide by coordination insertion mechanism along with catalyst tin octoate [18]. It is clearly known that HAP is not soluble in the solvents like chloroform, however, it is partially soluble and formed stable suspension when grafted with PDLA (**Figure 6.2**). ^{13}C-NMR is a precise and powerful tool for the molecular structure analysis of molecules. This method may also be useful for the determination of grafting of molecules with other molecules. The ^{13}C-NMR study of PDLA and PDLA grafted HAP is done and presented in F**igure 6.3**. It is found that the peak present at chemical shift 16.6 ppm, 69.1 ppm and 169.4 ppm corresponds to the methyl, methine and carbonyl carbon of the PLA chain. In comparison to the spectra of PLA-HAP, one additional chemical shift is found at 175.3 ppm which corresponds to the terminal carbonyl carbon connected with oxygen-calcium element of HAP. Similar mechanism of grafting of PLA with starch has been described elsewhere [204]. The schematic representation of the grafting of HAP with PDLA is shown in F**igure 6.4**.

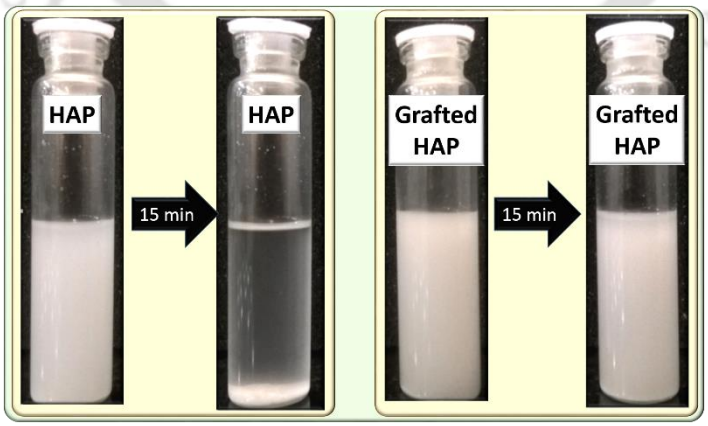

Figure 6.2: Dispersion of grafted HAP in comparison with pristine HAP in chloroform.

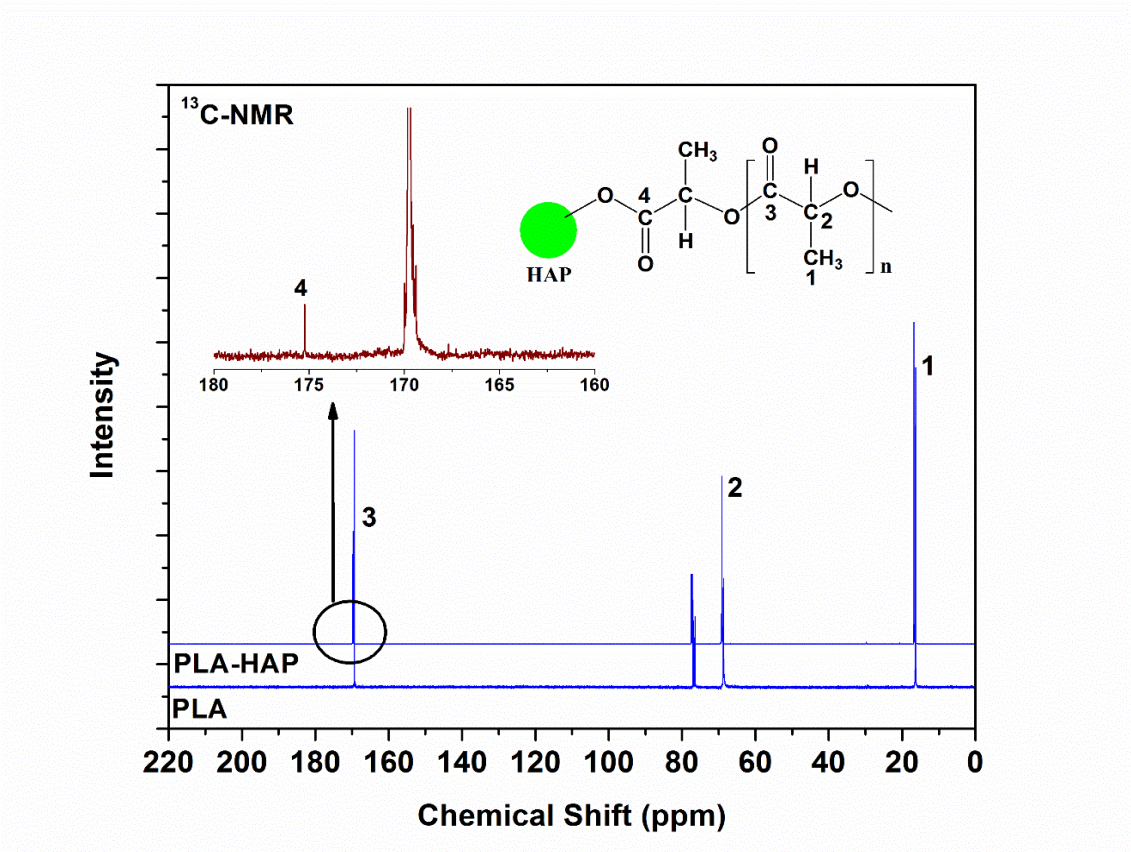

Figure 6.3: Comparison of ^{13}C-NMR spectra of PLA and PLA-HAP.

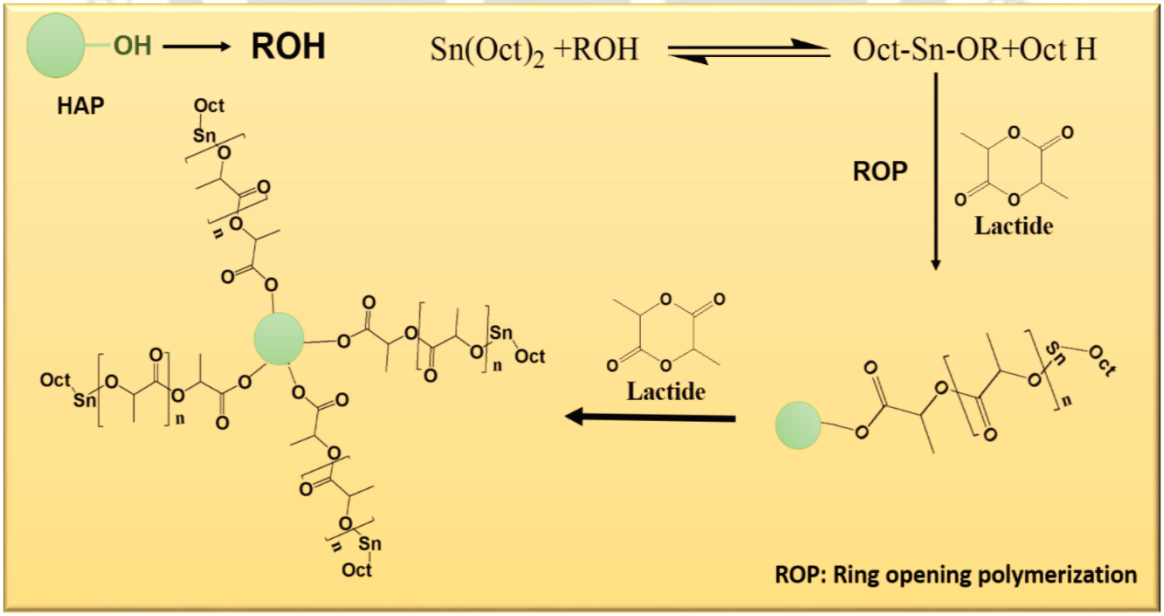

Figure 6.4: Schematic representation of grafting of HAP with PDLA.

Further, it is known that HAP is an inorganic material which is thermally stable below 900°C and no loss in its molecular structure is observed at higher temperature [205]. In this case, TGA can be an effective method to calculate the amount of PDLA chain connected with HAP. Comparison of TGA graph of HAP and PDLA-HAP is shown in **Figure 6.8**. Approximately 2.2% reduction in weight loss found in case of PDLA-HAP in comparison to pristine HAP which suggests that ~2.2% of PDLA is chemically bound to HAP molecules and degraded against rise in temperature.

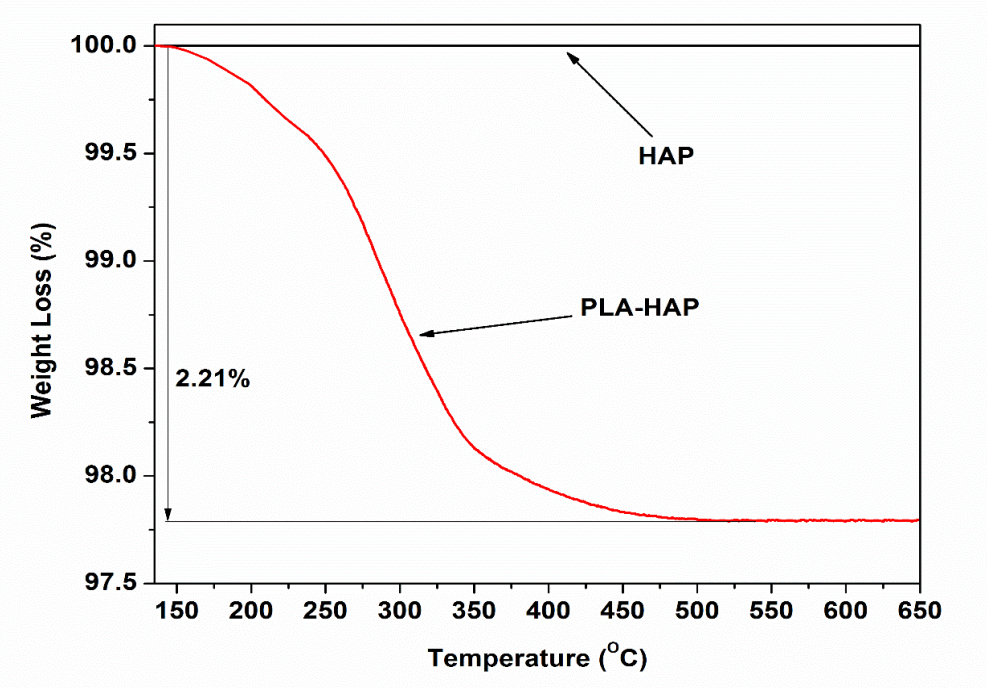

Figure 6.5: Weight loss of PLA-HAP in comparison with HAP against temperature.

6.3.3 Stereocomplex PLA-HAP biocomposite

The FTIR spectra of sPLA and sPLA-HAP biocomposites is presented in the **Figure 6.6a.** All samples have shown similar spectra as sPLA. The peaks at 2923 cm^{-1} and 2847 cm^{-1} are assigned to the stretching vibration of –C-H of PLA. The band at 1747 cm^{-1} corresponds to the carbonyl (C=O) stretching of PLA. Spectra at 1452 cm^{-1} corresponds to the bending

of methyl group and 863 cm^{-1} assigned to the –C-C- stretching of the backbone of PLA molecule. FTIR is the instrument which is highly sensitive to the arrangement of the chains in crystalline segment. The peak at 908 cm^{-1} in **Figure 6.6b** is related to the 3_1 beta helical structure of stereocomplex PLA chains [179]. The intensity of the peak is increased as the content of HAP enhanced which qualitatively suggests the increase in the content of stereocomplex crystallites in the matrix. The interaction between carbonyl carbon of one enantiomeric PLA and methyl group of the other enantiomeric PLA which form the hydrogen bond, leads to the formation of stereocomplex crystallites. This hydrogen bonding affects the vibration peak at 1038 cm^{-1} assigned to C-CH_3 group of PLA which red shifted to 1035 cm^{-1} corresponds to the C=O···CH_3 stretching mode (**Figure 6.6c**) which confirms the formation the formation of stereocomplex crystallites [148].

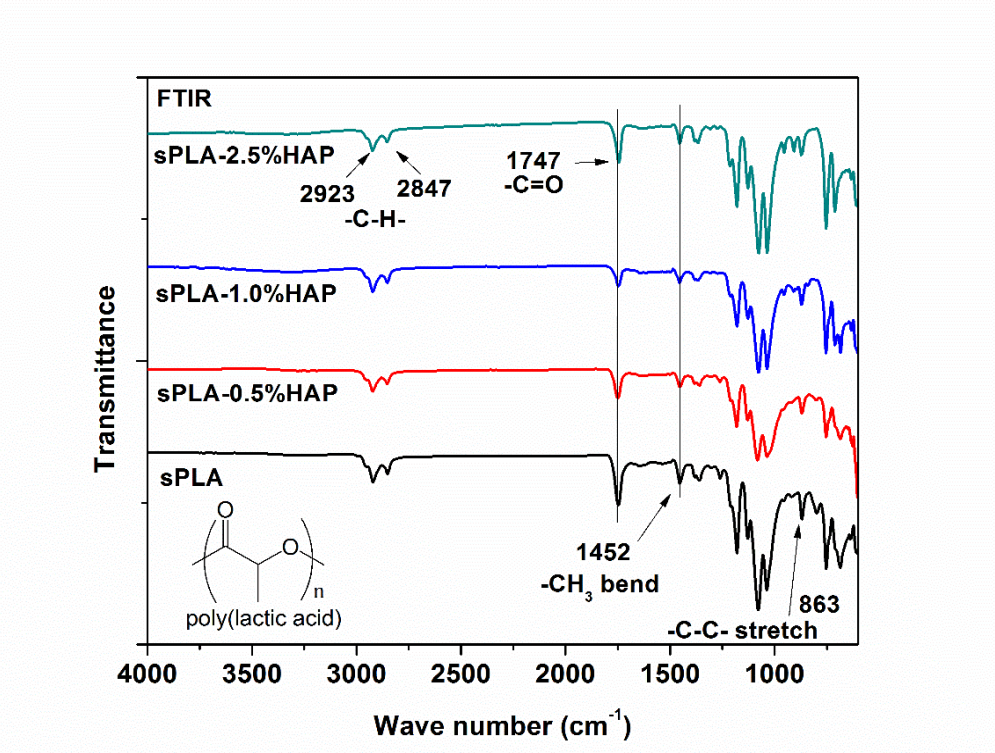

Figure 6.6a: FTIR spectra of sPLA and sPLA-HAP biocomposite.

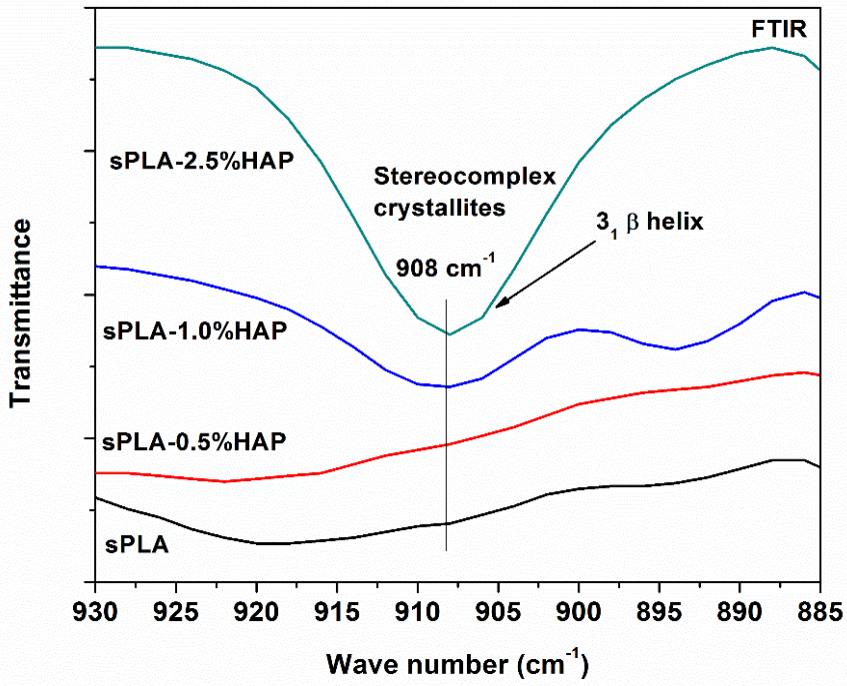

Figure 6.6b: Magnified FTIR spectra (930 cm^{-1} to 885 cm^{-1}) of sPLA and sPLA-HAP biocomposites.

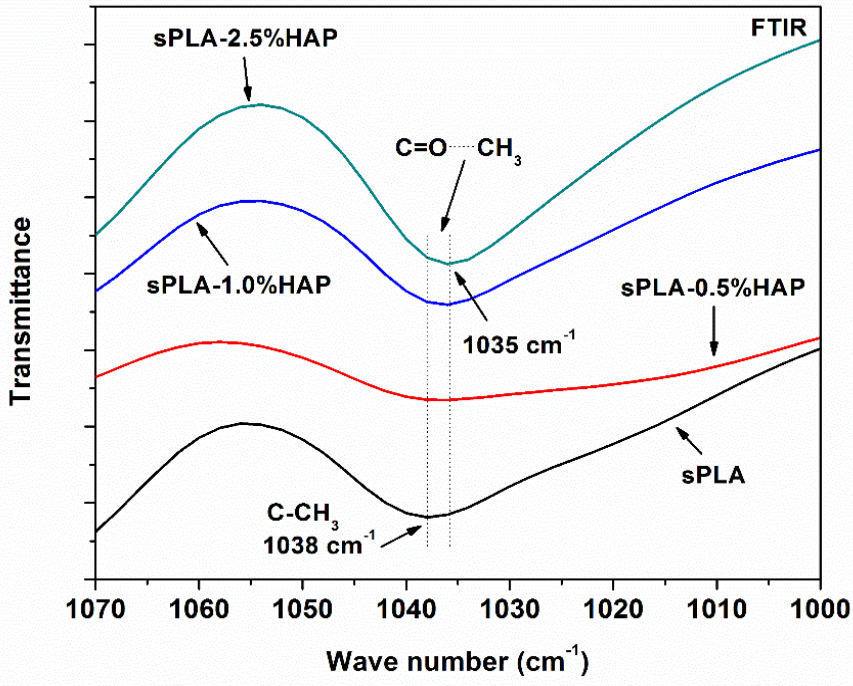

Figure 6.6c: Magnified FTIR spectra (1070 cm^{-1} to 1000 cm^{-1}) of sPLA and sPLA-HAP biocomposites.

It is well known that the stereocomplex crystallites in PLA have higher melting temperature than normal PLA homocrystals [57]. The DSC analysis of sPLA and other sPLA-HAP biocomposites is shown in the **Figure 6.7a**. The thermogram showed that sPLA had crystals of homopolymers with trace amount of stereocomplex crystallites. The melting peaks at 152°C and ~178°C are associated to the melting of homocrystals and melting peak at ~210°C corresponds to the stereocomplex crystallites. Increase in the content of grafted HAP in polymer matrix leads to increase in the melting enthalpy ($\Delta H_{m,sc}$) of the stereocomplex crystallites from ~17 $J.g^{-1}$ for sPLA to ~55 $J.g^{-1}$ for sPLA-2.5%HAP and helps in the reduction of melting enthalpy ($\Delta H_{m,hc}$) of homocrystals from ~28 $J.g^{-1}$ (sPLA) to 0 $J.g^{-1}$ (sPLA-5%HAP) (**Table 6.2**). Increase in melting temperature from ~210°C for sPLA to ~227°C for sPLA-2.5%HAP suggests the perfectness and increased amount of stereocomplex crystallites. Decline in degree of crystallization ($X_{c,hc}$) for homocrystals is found from ~30% for sPLA to 0 % for sPLA-2.5%HAP. The degree of crystallization ($X_{c,sc}$) for stereocomplex crystals is improved from ~12% for sPLA to ~39% in case of sPLA-2.5%HAP with no trace of melting enthalpy for homocrystals which reaches to 100% fraction of stereocomplex crystallites as shown in **Figure 6.7b**.

Table 6.2: Melting temperature and enthalpy of sPLA and sPLA-HAP biocomposites.

Sample Name	$\Delta H_{m,hc}$ ($J.g^{-1}$)	$\Delta H_{m,sc}$ ($J.g^{-1}$)	$T_{m,hc}$ (°C)	$T_{m,sc}$ (°C)
sPLA	27.6	17.1	152, 178.6	210.8
sPLA-0.5%HAP	29.5	17	178.8	219.6
sPLA-1.0%HAP	5.8	35.4	178	222.9
sPLA-2.5%HAP	0	55.1	--	227.4

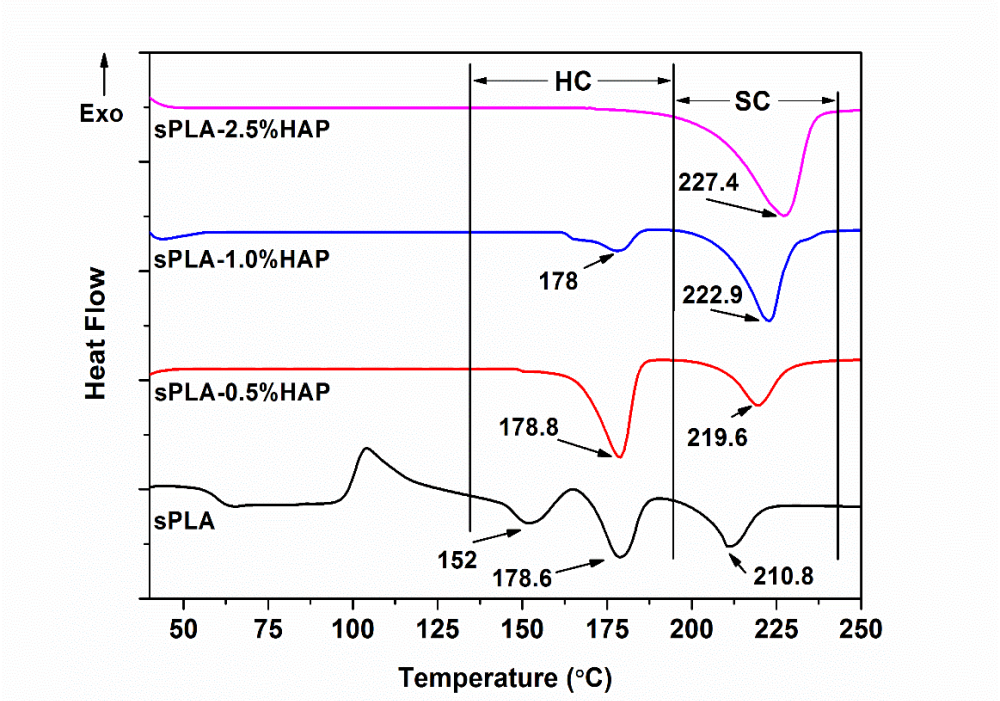

Figure 6.7a: DSC thermogram of sPLA and sPLA-HAP biocomposite.

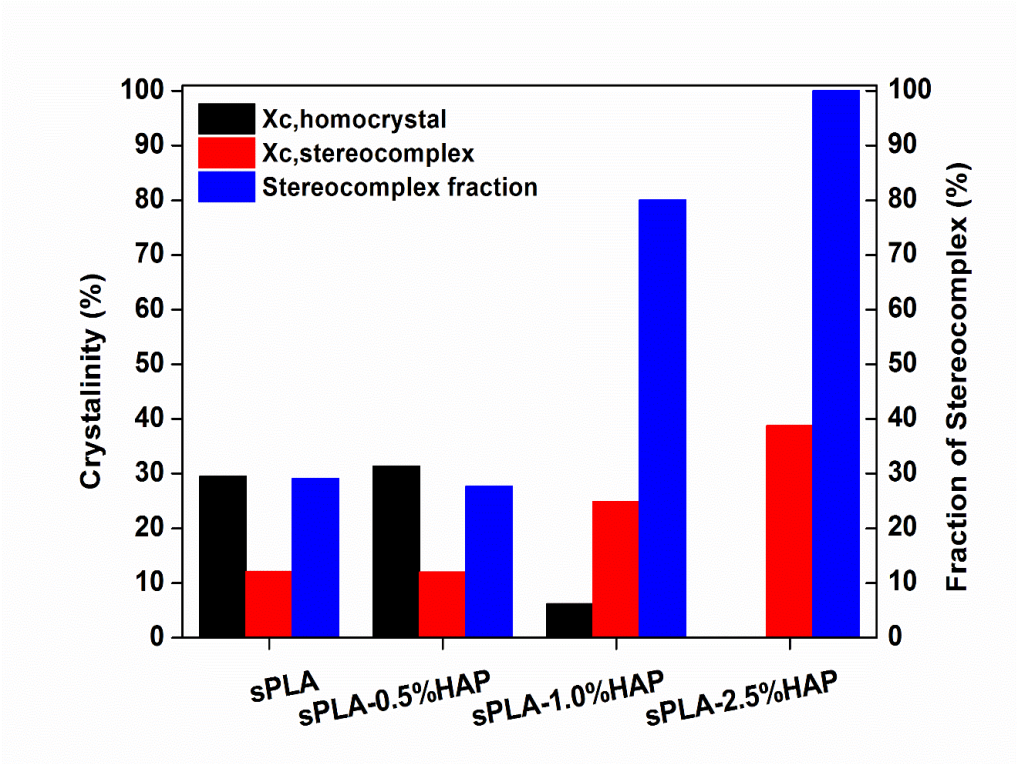

Figure 6.7b: Crystallinity (homocrystals stereocomplex) and fraction of stereocomplexation of sPLA and sPLA-HAP biocomposite.

Further, the effect of grafted HAP on stereocomplexation in PLA matrix is analyzed using X-ray diffraction. XRD is a powerful tool which can give information about the crystalline domain in the semicrystalline polymer system. The XRD pattern of sPLA and sPLA-HAP biocomposites are shown in the **Figure 6.8**. As per the known evidence, the stereocomplex PLA chains arrange themselves in a triclinic unit cell with dimensions of a= 0.916 nm, b= 0.916 nm, c= 0.870 nm, α=β=109.2° and γ =109.8° which is having 3_1 helical structure (3 Å rise per unit of monomer) [69]. The x-ray diffraction pattern at peaks 11.8°, 20.6° and 23.9° are related to stereocomplex crystallites and corresponds to the (110), (300)/(030) and (220) lattice planes, respectively whereas, homopolymer PLA crystalizes (alpha form) in a pseudo-orthorhombic unit cell of dimensions a=1.07 nm, b=0.595, c= 2.78 nm holding 10_3 helical structure (10Å rise per 3 unit of monomer). Peaks for PLA situated at 14.7°, 16.6° and 19° in x-ray diffraction corresponds to (010), (200/110) and (203) crystal planes, respectively. It is clear from the pattern that the peaks related to the stereocomplex evolved and peaks related to the homocrystals is diminished with increase in the grafted HAP content.

The above discussion suggests that the presence of grafted HAP in the polymer matrix helps in the development of stereocomplex crystallites and thus limiting the evolution of the homocrystallites. This improvement leads to the enhancement of other properties of biocomposites.

6.3.4 Effect of grafted HAP on mechanical and thermomechanical properties of sPLA

The presence of filler into the polymer matrix enhances the mechanical and thermomechanical properties; however, uniform dispersion of fillers is the most critical parameter. Effective ways to improve the dispersion is the modification of fillers while *in situ* diluting it grownup matrix. In this work, the filler i.e. HAP is grafted with PDLA which is miscible in the bulk PLLA matrix due to grafted PLA chains onto HAP which lead to the uniform dispersion of HAP. The FESEM analysis of fractured surface of sPLA and sPLA-HAP biocomposite is shown in **Figure 6.9**. The fractured surface of sPLA (**Figure 6.9a**) is smooth and free from presence of any foreign particles whereas in sPLA-HAP (**Figure 6.9b**) biocomposite HAP particles are found as uniformly dispersed particles. The size of the dispersed HAP is found to be ~60 nm.

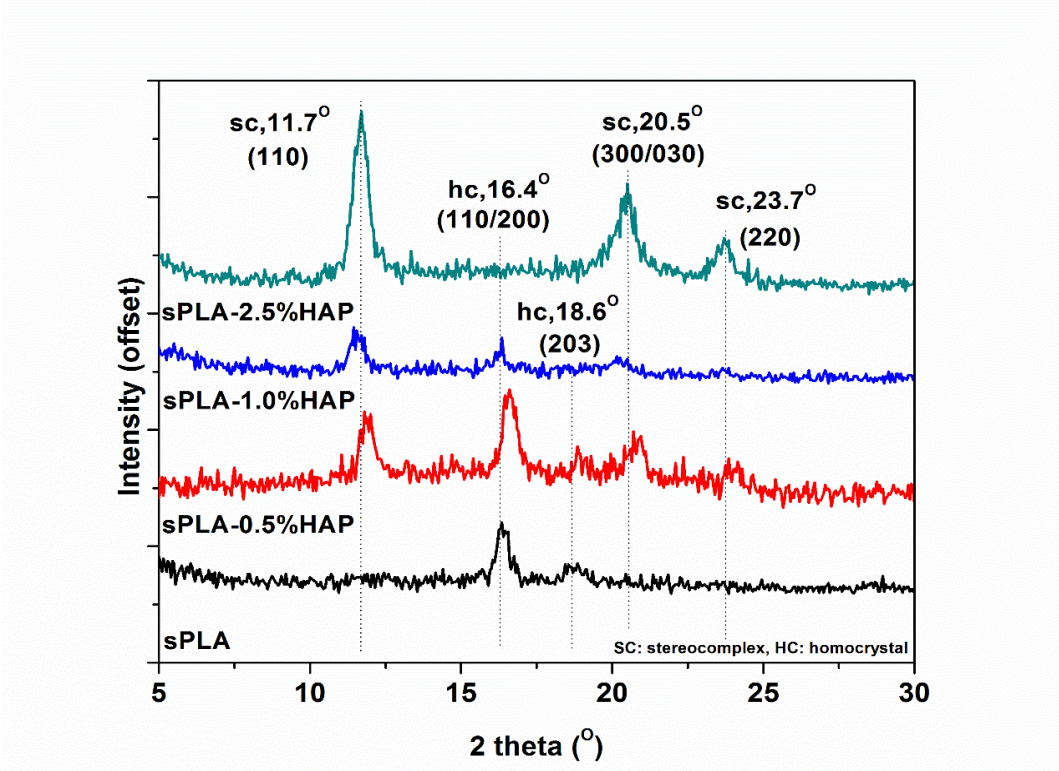

Figure 6.8: X-ray diffraction of sPLA and sPLA-HAP biocomposite.

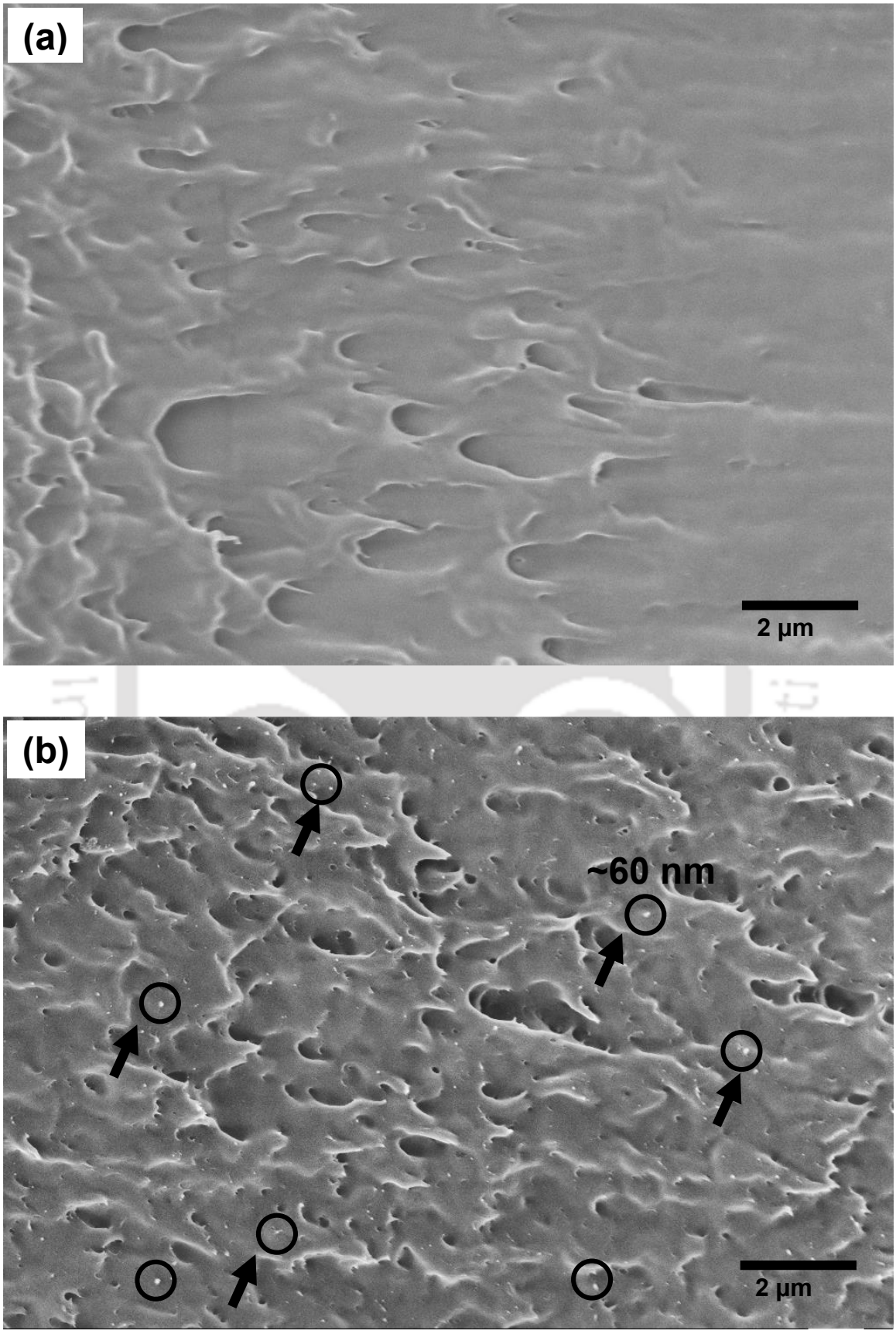

Figure 6.9: FESEM images of fractured surface of sPLA and sPLA-HAP biocomposite.

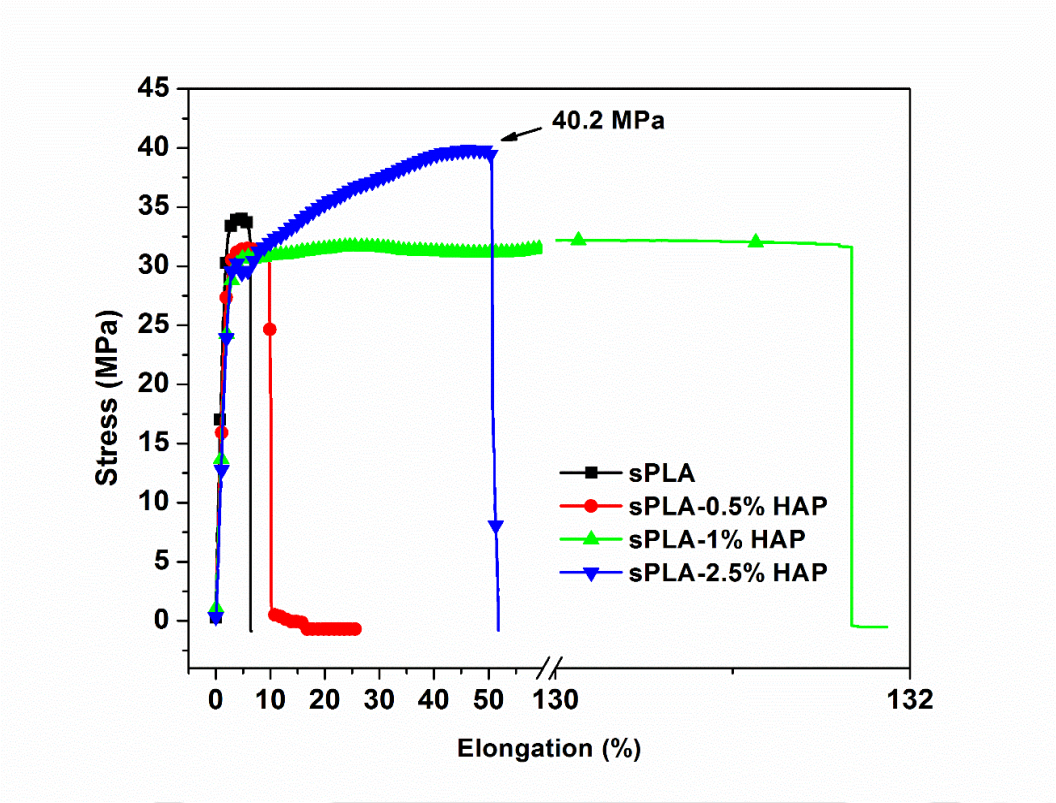

Figure 6.10a: Representative date for stress of sPLA and sPLA-HAP biocomposite against elongation percentage.

The presence of grafted HAP in PLA matrix is playing dual role, simultaneously i.e. uniformly reinforced filler into the matrix and provided the extended molecular surface area, in the form of PDLA chains, which efficiently interacts with PLLA chains and form the stereocomplex crystallites. Load-elongation curve for sPLA and sPLA-HAP biocomposites against elongation percentage (%) is presented in F**igure 6.10a**. The ultimate tensile strength (UTS) is found to be improved by ~16% i.e. 40.2 MPa for sPLA-2.5%HAP in comparison to sPLA i.e. 33.8 MPa. Improvement in the degree of crystallinity suggests significantly more intermolecular bonding and cross linking in the form of stereocomplexation which may be responsible for the increment in the tensile strength. It also suggests the strong interfacial bonding between HAP and polymer chains. The elongation at break is found to be 131.6% for sPLA-1%HAP in comparison to 6.3% for sPLA (**Figure 6.10b**) which implies that the ductility of sPLA is significantly improved

with incorporation of modified HAP. It is known that improvement in ductility ensures the delay in fracture which reduces the abrupt failure of the biocomposite. The integrated molecular surface area in the form of PDLA on modified HAP acts as a bridge between sliding and elongating polymeric chains and prolong the breakage process. It also suggest a strong interaction between matrix and filler and may be result of chain uncoiling or chain sliding in the biocomposite [14]. It is observed that the specimen is gradually elongated and propagated over the entire length and became narrow. The elongation at break is reduced to ~55% in case of sPLA-2.5%HAP. Increase in the content of HAP into the matrix ensures the upsurge in the tensile strength due to the confinement of polymer chains and formation of stereocomplex crystallites. However, HAP particles present in the matrix at higher amount may generate voids during the elongation process which ultimately induce the breakage and occurrence of rapture of bonds resulting into reduction in elongation at break in sPLA-2.5%HAP as compared to sPLA-1%HAP.

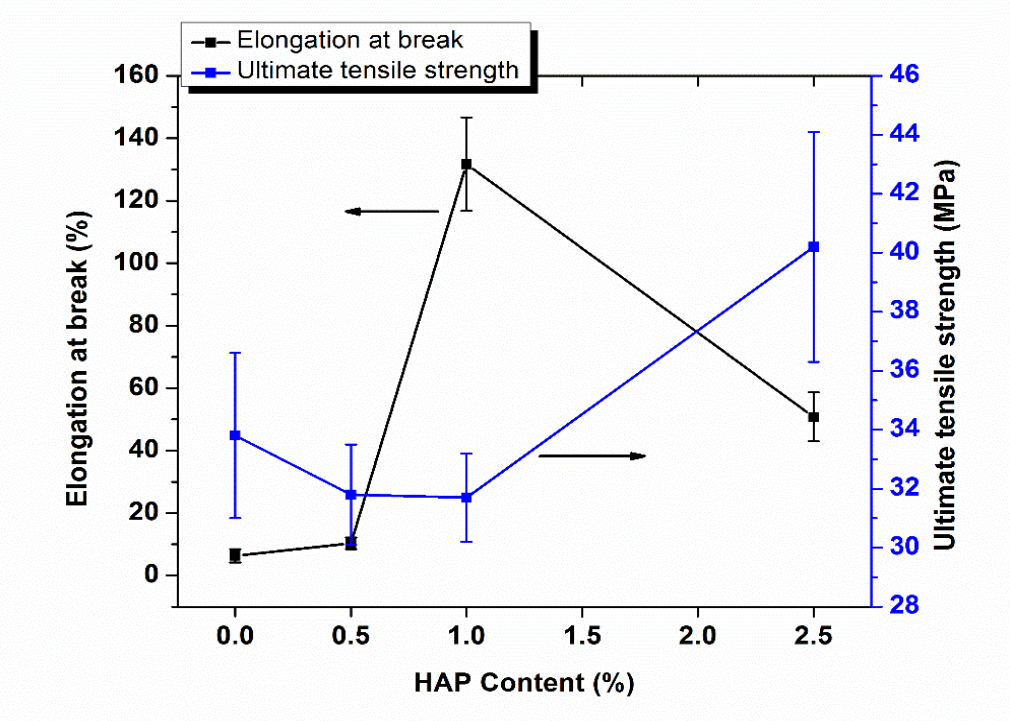

Figure 6.10b: UTS and elongation at break of sPLA and sPLA-HAP biocomposite.

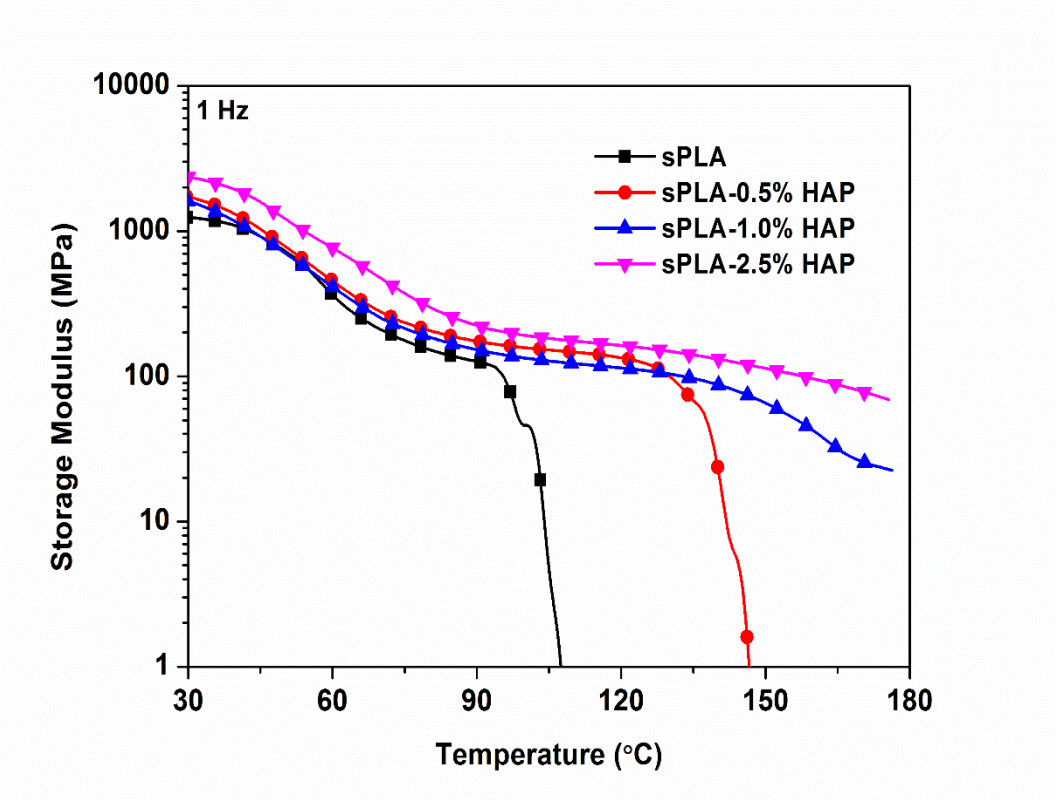

Figure 6.11a: Storage modulus of sPLA and sPLA-HAP biocomposite against temperature.

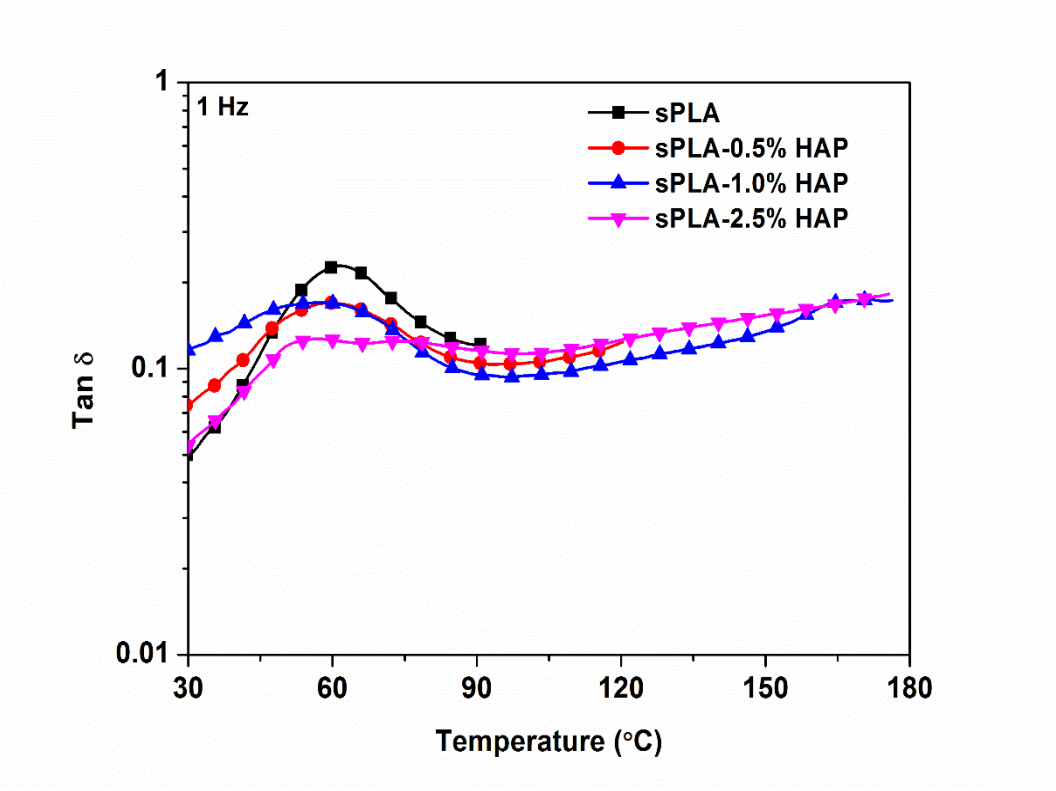

Figure 6.11b: Tan delta of sPLA and sPLA-HAP biocomposites against temperature.

The effect of grafted HAP on the thermal stability of sPLA-HAP biocomposite is analyzed by measuring the storage modulus and tan delta in the temperature range from 30°C to 180°C on applied dynamic force using DMA in tensile mode. The storage modulus of sPLA and sPLA-HAP biocomposite is shown in **Figure 6.11a**. The storage modulus at 30°C is found to be ~1243 MPa in case of sPLA which is enhanced to ~2350 MPa for sPLA-2.5% HAP and remained higher than sPLA or other sPLA-HAP biocomposites throughout the temperature range. This improvement in the storage modulus of biocomposites shows stiffness of viscoelastic polymer which resists the deformation on the act of applied force and is also attributed to the increased polymer chains rigidity. The loss tangent curve is shown in **Figure 6.11b** as function of temperature. The peaks are related to the glass transition of the polymers indicating the movement of amorphous polymeric chains which is the transition of material from hard glass state to soft rubbery state. Changes in the peak shape with increase in HAP content indicate the relation to polymer structure and internal molecular motion. The fillers present in the polymeric system affect the glass transition by developing the hindrance to the movement of polymer chains. The peak becomes flattened in the case of sPLA-2.5%HAP which may be the result of hindrance to polymer chains developed by HAP nanoparticles as well as increase in stereocomplex crystallites content. This increase in the stereocomplexation suppresses the intensity of tan delta peak for sPLA-2.5%HAP in comparison to sPLA. As discussed in the previous section that the stereocomplex crystallites are tightly packed compared to the homocrystals which induce the chain rigidity [206]. This analysis suggests that the prepared biocomposite is thermally more stable than pristine sPLA at elevated temperature.

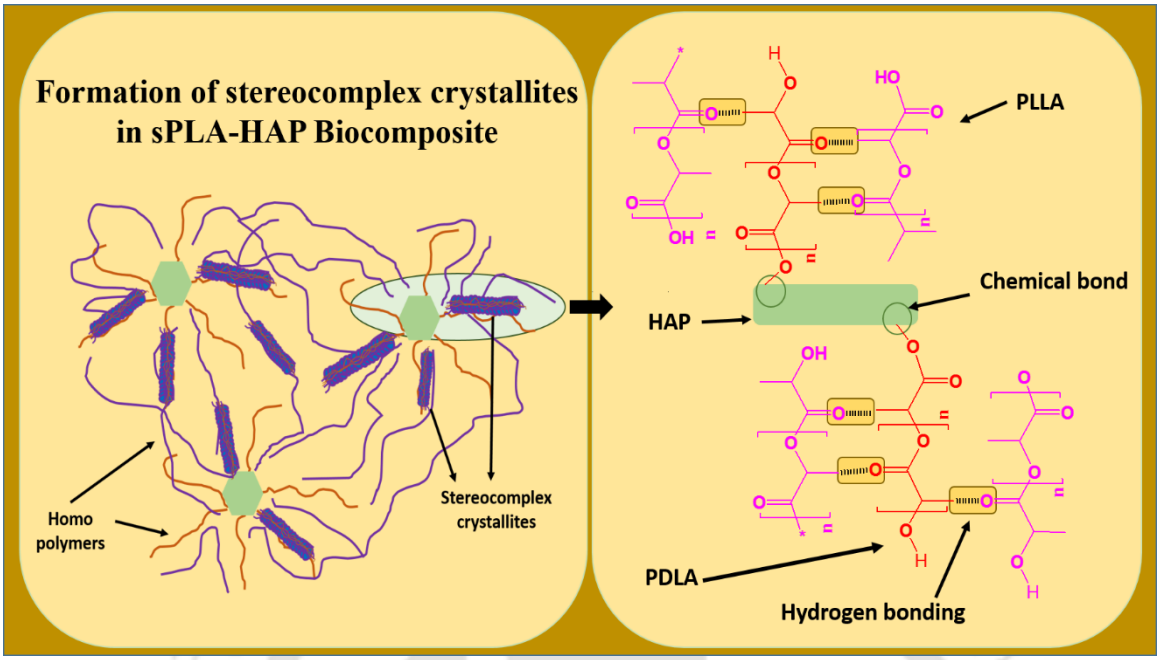

Figure 6.12: Representative sketch for the formation of stereocomplex crystallites in sPLA-HAP biocomposite.

From the above discussion, we could conclude that the grafted HAP plays dual role viz. developing the uniformly dispersed biocomposite and supporting in the formation of stereocomplex crystallites in sPLA-HAP biocomposite via providing the extended molecular surface area in the form of PDLA which interacts with PLLA and forms the stereocomplex crystallites. The formation of stereocomplex crystallites in presence of grafted HAP is delineated in the form of sketch in **Figure 6.12**.

6.3.5 Gas barrier properties

The barrier properties of the polymers are the crucial parameters for deciding the target applications. The prepared biocomposite films are analyzed for oxygen permeability and water vapour permeability. OP results are shown in **Figure 6.13** at different temperature range which shows the significant drop of nearly 48% in oxygen permeability at 23°C. The molecular compactness and degree of crystallinity are the parameters which highly affect

the gas permeability. The formation of stereocomplex crystallites due to the presence of grafted HAP increase the compactness of the polymer chains. Increase in the crystalline density directly affects the oxygen permeability as diffusion of oxygen molecules are hindered in crystalline domain [207]. The FESEM analysis of fractured surface as discussed in previous section, showed the uniform dispersion of HAP which indicates the interaction of polymer chains with HAP particles and responsible for the formation of stereocomplex crystallites. The HAP may also be contributing in the reduction in the oxygen permeability by developing the tortuous path for the oxygen molecules.

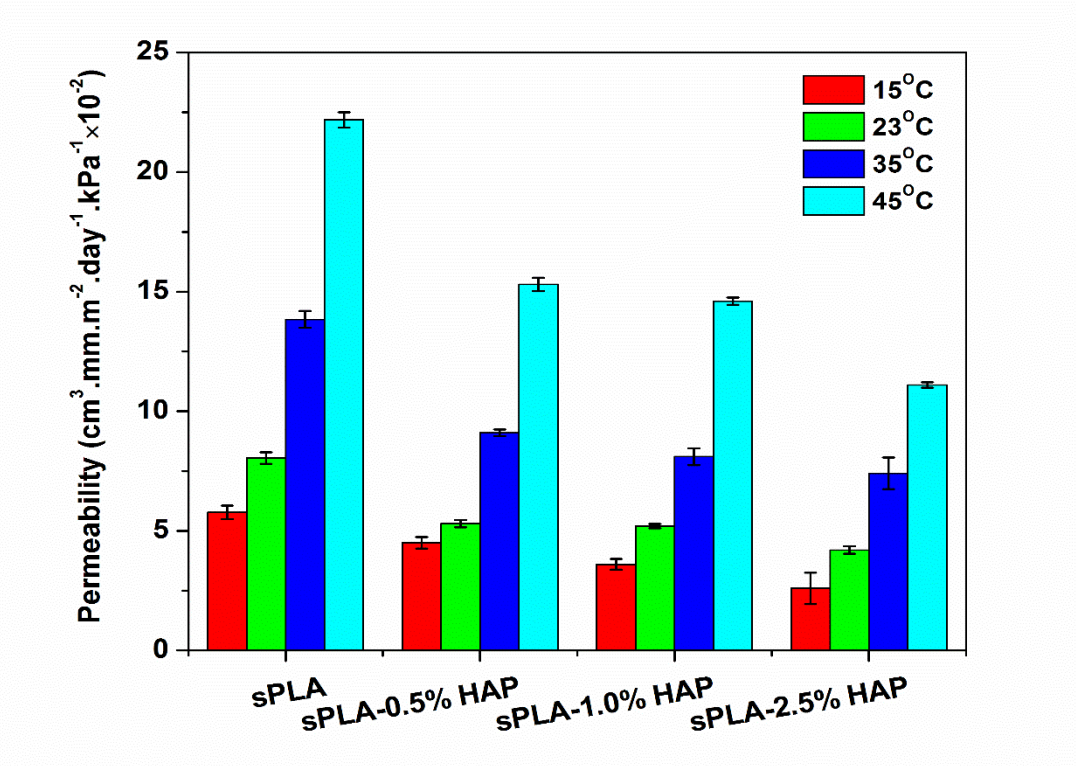

Figure 6.13: Oxygen permeability of sPLA and sPLA-HAP biocomposites at different temperatures.

Water vapor permeability of sPLA and sPLA-HAP biocomposites is shown in the **Figure 6.14**. 34% reduction is observed for sPLA-2.5%HAP in comparison to sPLA. The grafting of HAP with PDLA chains enhance the interaction of HAP with polymeric chains which increased the dispersion and resulted in the enhancement of stereocomplexation. Improvement in the degree of crystallinity affects the bulk surface property of sPLA and makes it resistant to moisture. Development of stereocomplex crystallites may be responsible for the hindrance to the diffusion of water molecules.

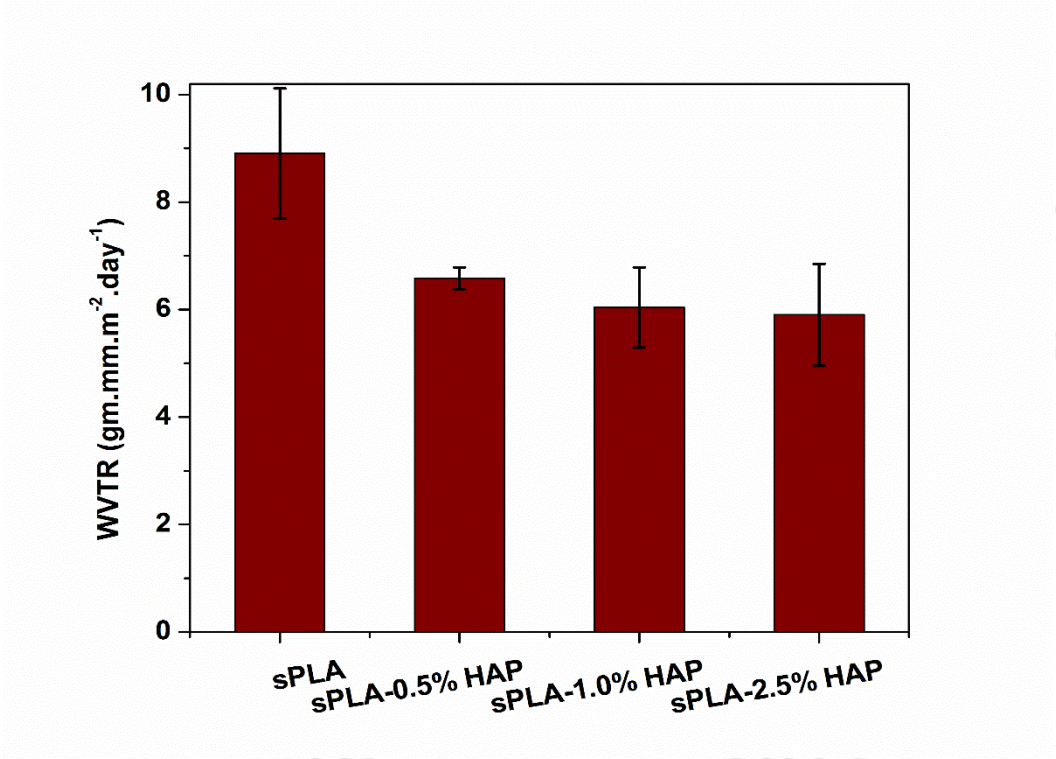

Figure 6.14: WVTR of sPLA and sPLA-HAP biocomposites.

6.4. Conclusions

We have successfully grafted the HAP with PDLA *in situ* bulk ring opening polymerization of D-lactide and the same is confirmed by ^{13}C-NMR and subsequently TGA and produced high molecular weight PDLA-HAP biocomposite. Stereocomplex PLA-HAP biocomposite is produced with 100% stereocomplex crystallite content and melting temperature is found to be ~227°C with no trace of homocrystals. It is concluded that the grafted HAP played dual role in the polymer matrix viz. developing uniform dispersion in polymer which is confirmed by morphological study and the formation of stereocomplex crystallites by providing the extended molecular surface area in the form of PDLA. Presence of peak at 908 cm^{-1} and redshift of bands at 1038 cm^{-1} in IR spectra confirmed the formation of stereocomplex crystallites which is further established by X-ray diffraction and calorimetry. Improved stereocomplexation ultimately affected the elongation at break (132%) and the tensile strength (40.2 MPa). Storage modulus estimated by dynamic mechanical analyzed is improved by ~47% at 30°C and showed the enhancement in the thermomechanical stability at elevated temperature which is also confirmed by the broadening of tangent loss curve of biocomposites. The enhancement in the stereocomplexation resulted 48% and 34% reduction in oxygen permeability and water vapor transmission, respectively.

CHAPTER: 7

Crystallization Kinetics of Stereocomplex PLA and Fabricated Biocomposites

Abstract

It is confirmed from the previous chapters that CMC, chitosan and HAP are facilitating the formation of stereocomplex crystallites. It is very important to study the crystallization behavior of the biocomposites which is essential in measuring the thermodynamic parameters. These parameters could be used for the development of instrumentation for the processing of the polymers. In this study, the isothermal crystallization of sPLA and other prepared biocomposites are carried out at different temperatures. Avrami equation is used for the calculation of the half time for crystallization in order to understand the nucleation and crystallization rate constant. It is predicted that nucleation is temperature dependent and activation energy is calculated using Arrhenius equation. Other parameters such as nucleation constant, product of lateral and fold surface free energy are measured using Lauritzen and Hoffmann equation and the nucleation free energy is measured.

7.1 Introduction

Most of the thermoplastic polymers are semi-crystalline in nature [208]. Although PLA is suitable for several applications, a number of limitations restrict its commercial usage. Forming the stereocomplexation in PLA can significantly improve the polymer properties which can be explored for various applications. On the other hand, development of homocrystallites along with the stereocomplex crystallites in the high molecular weight PLA matrix affects the characteristics of the final product [14]. This happens due to the low interaction of the opposite enantiomeric PLA chains which are responsible for the formation of stereocomplex crystallites. Hindrance to chain diffusion through matrix, limitation of proper mixing, higher affinity towards same enantiomeric chains etc. could be the possible reasons for the formation of homocrystals along with stereocomplex crystallites [183]. The current work describes the new technique which has been developed for enhancing the stereocomplexation in PLA which provides extended molecular surface areas which in turn increase the interaction of opposite enantiomeric chains (PLLA and PDLA) for the formation of stereocomplex crystallites. Results are confirmed from the studies in previous chapters indicating the role of organic or inorganic grafted fillers in the enhancement of stereocomplexation in PLA.

The degree of crystallinity, rate of crystallization, crystal structure etc. of the polymer affects its thermal, mechanical and barrier properties [207]. The use of fillers or modified/grafted fillers improves the crystallization rate of PLA which is favorable for various processes such as molding, film formation, and extrusion etc. of PLA. Therefore, the study of crystallization kinetics of the polymers is extremely important to understand the effect of different grafted fillers on the crystallization of stereocomplex PLA.

7.2 Thermodynamics of crystallization

From the thermodynamic point of view, melting or crystallization of solid material preferably high molecular weight polymers correspond to the Gibbs free energy (ΔG) [209]. In case of crystallization of polymers, the Gibbs free energy of crystallization must be lower as compared to that of melting (i.e. $\Delta G_c < \Delta G_m$). The crystallization of the polymers is different than that of non-polymeric substances. In non-polymeric materials, crystallization proceeds by mechanism of nucleation and growth. For the growth of crystals with significant barrier, the size of newly formed nuclei should be greater than a critical size. In contrast, the crystallization in polymers is quite complicated. In the process of growth, the free energy of polymer has several metastable states due to reorganization of the chain confirmations [210].

Crystallization in polymers begin with nucleation (formation of small amount of crystalline material) due to variation in density or order of the super-cooled melt (i.e.) cooling of melt below its freezing point without crystallization. Crystallization, in first step, is the formation of primary nuclei, called primary nucleation followed by the continuation of crystallization on the growth surface by induction of increasing polymer molecules which is known as secondary nucleation. If the nucleus formation takes place spontaneously due to super-cooling without any pre-existing second surface or nucleus, the phenomenon is termed as uniform nucleation. However, if nucleus is formed with the help of second phase such as existing nucleus or foreign particles, the nucleation is termed as heterogeneous nucleation. Primary nucleation can be either uniform or heterogeneous nucleation, whereas secondary nucleation can only be heterogeneous nucleation. Heterogeneous nucleation can be thermal and athermal nucleation. Thermal and athermal nucleation are time dependent processes. The nucleation process which occurs throughout the crystallization is called as

thermal nucleation and the process where all the crystals begin to grow at the same time is called athermal nucleation [210-213].

Generally, it is well understood that the polymers crystallize in conventional manner where polymer chains fold back and forth into stems to form lamellae. Normally, polymer chains encounter two preferred orientations: one being perpendicular to substrate surface (edge-on lamellae) and other being completely parallel (flat-on lamellae) to the substrate surface. The lamellar thickness is denoted as l and other two dimensions are denoted as x and y. The orientation of lamellae is the orientation of the normal of the basal planes. Planes parallel to the substrate surface in case of edge-on lamella and perpendicular to the substrate surface for flat-on lamella are called basal planes. The lamellae orientation is always parallel to the basal surface whereas the chain orientation is not always parallel to the basal plane. Polymer lamellae are circumscribed between two basal plans covered by several such lateral surfaces and chain folds. The formation of particular structure of crystallites are dependent on the orientation of chains such as edge-on or flat-on. Edge-on lamellae exhibit in fibrous form with nearly uniform width, which are further grouped into spherulites, axialites, and hedrites. However, flat-on lamellae form different and complicated patterns like dendrites, seaweeds and regular form like hexagons, squares and lozenges of faceted single crystals. It is found from the literature that the edge-on lamellae are found in the thin film whereas flat-on lamellae are preferred in ultrathin films and monolayers which suggest that, in general, polymers like PLA show edge-on lamellae formation and form the spherulites when cooled from melt [209].

After understanding the nucleation effect, the kinetic effect needs to be considered. When crystallized at temperature between glass transition and melting, the nucleation of edge-on and flat-on lamellae occur in comparable rates due to which both nucleation will compete with each other depending on the thickness of film as well as other factors such as

crystallization temperature, molecular weight, interaction between polymer and substrate etc. An increase in molecular weight or temperature gives enough energy to the chains going for edge-on orientation to overcome the interaction with substrate to move towards flat-on orientation. Therefore, edge-on orientation is kinetically preferred.

In the process of polymer solidification, formation of nearly spherical geometry of stacked crystal lamellar is called spherulite. When spherulites are examined in the polarizing optical microscope, they are seen to exist in colours due to their anisotropic nature. The colours are correlated with the retardation of material i.e. distance between the fast and slow light ray when they pass through the material, film thickness, birefringence and other parameters. The difference between the high and low refractive indices, which are related to the interaction between free electrons within the spherulite and light photon, is defined as birefringence [214].

7.3 Bulk crystallization kinetics

7.3.1 Avrami Model

Developed Avrami equation [215-217] is used to understand the isothermal crystallization kinetics. The quantitative relations between density of germ nuclei, growth nuclei and transformed volume are developed and expressed in terms of a characteristic time scale for given substance and process. The relation is shown in the following equation:

$$1 - X_t = \exp(-kt^n) \tag{7.1}$$

where, Avrami exponent ‘n’ depends on the type of nucleation (sporadic means random appearance of nucleus or instantaneous means occurrence of nucleus without delay) and number of growth dimension.

The value of 'n' can be any positive integer between 1 and 4. For example the value n = 3 represents the crystallization in three-dimension growth and instantaneous nucleation. 'X_t' is the fractional crystallinity at time 't' and 'k' is the crystallization rate parameter or composite rate constant function of both nucleation rates (N) and growth rate parameter (G). Avrami equation is based on the several assumptions. The growth takes place in constant radial direction, density and shape of nuclei are considered to be constant, no volume change is encountered during phase transformation of crystallization and no secondary crystallization is considered. These assumptions lead to the fractional value of 'n' which cannot be explained on any physical basis. The value of 'k' can be used to measure the activation energy (ΔE) through Arrhenius equation [218]

$$\frac{1}{n}(\ln k) = \ln k_{\circ} - \frac{\Delta E}{RT} \tag{7.2}$$

where, 'R' is the universal gas constant and 'k_o' is a temperature independent pre-exponential factor.

The different thermodynamic parameters related to the crystallization process can be evaluated using regime theory of crystal growth. The growth of the spherulites is dependent on the crystallization temperature. The relation between temperature and growth rate is given by Lauritzen and Hoffmann [212] which is expressed as:

$$G = G_o \exp\left[\frac{-U^*}{R(T_c - T_\infty)}\right] \exp\left[\frac{-K_g}{f T_c \Delta T}\right] \tag{7.3}$$

where, T_∞ is the hypothetical temperature below which viscous flow ceases ($T_\infty = T_g - 30$ K), U^* is the activation energy for the segmental diffusion to the crystallization site from melt ($U^* = 6300$ J.mol^{-1}), $f = 2T_c/(T_m^o + T_c)$ is the correction factor, K_g is the nucleation constant, G is the growth rate of spherulite, G_o is a

pre-exponential factor, T_c is the crystallization temperature, ΔT is the degree of super-cooling ($\Delta T = T_m^o - T_c$),

The nucleation constant (K_g) is related to the surface free energy and is expressed as: [219]

$$K_g = \frac{m b_o \sigma \sigma_e T_m^o}{k \Delta H_f^o} \tag{7.4}$$

where, b_o is the thickness of monomolecular layer in the crystal, σ and σ_e are the lateral and folding surface free energies, respectively, H_f^o is the heat of fusion per unit volume ($\Delta H_f^o = \Delta H_m^o \times \rho_c$), ΔH_m^o is equilibrium melting enthalpy, T_m^o is equilibrium melting temperature, ρ_c is the crystal density of polymer (stereocomplex PLA = 1.27 g.cm^{-3}) [220], k is the Boltzmann constant, m is the constant dependent on the regime of crystallization (m = 4 for regime I and III, m = 2 for regime II) and b_o is the distance between two adjacent fold planes.

Thomas-Staveley equation [221] is used for the determination of the lateral surface free energy

$$\sigma = \alpha \Delta H_f^o (a_o b_o)^{1/2} = \alpha \Delta H_f^o (A_o)^{1/2} \tag{7.5}$$

Where, a_o is the width of the molecular chains in the crystal or lattice constant α is an empirical constant usually ranging between 0.1 and 0.3, A_o is the cross sectional area of a chain in the crystal.

As, it can be seen from the images of spherulites, the size of spherulites is too small and measuring the growth rate is quite difficult, the half time ($t_{1/2}$) for the crystallization can replace the spherulite growth rate (G) [219]. It is believed that the nucleation rate is found to be maximum at $t_{1/2}$. Therefore, the equation can be written as:

$$\frac{1}{t_{1/2}} = G_o \exp\left[\frac{-U^*}{R(T_c - T_\infty)}\right] \exp\left[\frac{-K_g}{f T_c \Delta T}\right] \quad (7.6)$$

Equation can be arranged by taking natural logarithm as

$$\ln \frac{1}{t_{1/2}} + \frac{U^*}{R(T_c - T_\infty)} = \ln G_o - \frac{K_g}{T_c \Delta T f} \quad (7.7)$$

The plot between $\ln(1/t_{1/2}) + U^*/R(T_c - T_\infty)$ versus $1/T_c \Delta T f$ will give strength line and slope of the line is calculated as value of K_g for the polymer.

The crystallization regime for particular crystallization temperature range can be determined using Lauritzen Z test and Z can be defined as:

$$Z \approx 10^3 \left(\frac{L}{2a_o}\right)^2 exp\left(-\frac{X}{T_c \Delta T}\right) \quad (7.8)$$

where, L is the effective lamellar width.

The energy required for the formation of critical size of nucleus or the free energy of nucleation (ΔG^*) [222] can be calculated from the given equation:

$$\Delta G^* = \frac{4 b_o \sigma \sigma_e T_m^o}{\Delta H_f^o \Delta T} \quad (7.9)$$

7.4 Experimental section

The samples i.e. sPLA, sPLA-CMC, sPLA-MCH and sPLA-HAP prepared in the previous chapters are taken for the analysis. The isothermal crystallization study is done using differential scanning calorimetry (DSC). 5-7 mg of the sample is taken into the platinum crucible with lid and kept in the chamber with nitrogen flow of 20 mL.min^{-1}. The sample is heated to 250°C with the rate of 30°C.min^{-1} and kept at same temperature for 3 min and then cooled to desired crystallization temperature with the rate of 50°C.min^{-1}. The sample

is kept at crystallization temperature isothermally for sufficient time for complete crystallization.

The growth and density of spherulite is captured via polarizing optical microscopy (POM) equipped with hot stage. Same program as DSC is used for the POM study.

7.5 Results and discussion

Understanding of the thermal behavior of polymer composites either isothermally or non-isothermally can be helpful for the processing of polymers and designing of the equipment. Generally, polymer processing units uses the isothermal treatment of the polymers which is more reliable and design friendly. Study of variation in polymer structure either molecular or bulk at isothermal condition is important in order to process to the final valuable product. The melt processed polymer is molded into different shapes and sizes. The cooling temperature affects the crystalline property as well as other properties. The addition of additives or fillers significantly affect the crystallization kinetics of the melt blended polymers.

7.5.1 Effect of grafted CMC on crystallization of sPLA

Grafting of the cellulose microcrystals is done via ring opening polymerization of D-lactide which is discussed in the previous Chapter 3. Stereocomplex PLA biocomposite is prepared by melt blending of PDLA grafted CMC and PLLA with 0.5%, 2.5% and 5% CMC content. The isothermal kinetic data are recorded at 120°C, 140°C and 160°C for stipulated time range. It is known that crystallization in polymers normally occur in the temperature range from glass transition to melting temperature. Heat flow with respect to time during isothermal crystallization of sPLA and sPLA-CMC biocomposites at 120°C, 140°C and 160°C is given in the **Figure 7.1** and **Figure 7.2**. In case of sPLA, it is found that the width of the crystallization is reduced as the temperature lowered which reflected increment in

the crystallization rate. Addition of grafted CMC with sPLA significantly shifted the exotherm peaks and shortened the crystallization time which means improvement in the crystallizability of the polymer. The influence of crystallization temperature is similar to that of sPLA.

As crystallization is an exothermic process, the heat released during isothermal crystallization is assumed to be proportional to the macroscopic rate of crystallization. So, the relative crystallinity (X_t) of the sample at time t can be calculated using given equation

$$X_t = \frac{\int_0^t \frac{dH}{dt} dt}{\int_0^\infty \frac{dH}{dt} dt} = \frac{\Delta H_c}{\Delta H_\infty} \quad (7.10)$$

Where, dH/dt is the rate of heat evolution, ΔH_∞ is the total heat generated during crystallization and ΔH_c is the heat generated at time 't'.

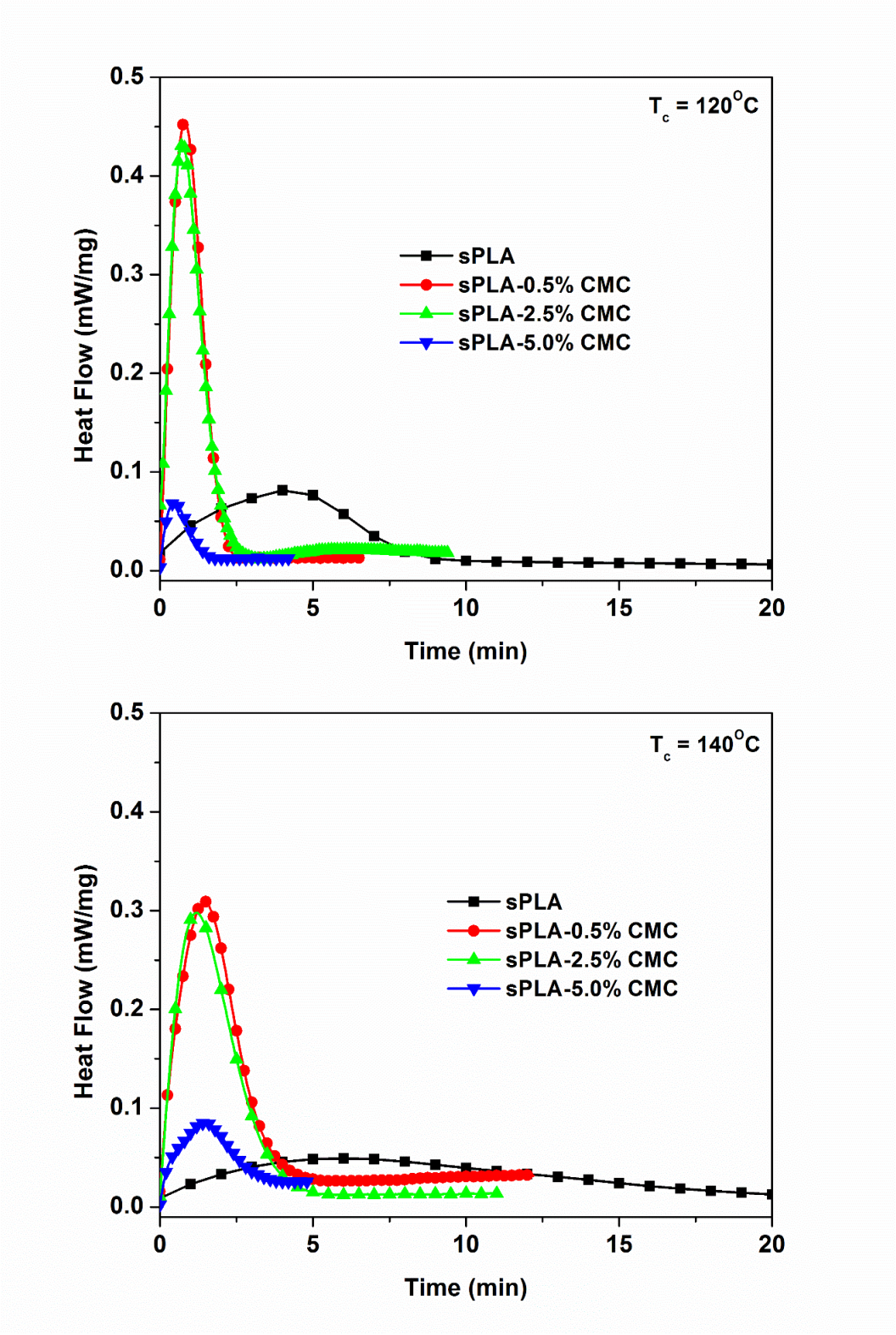

Figure 7.1: Heat flow versus time during isothermal crystallization of sPLA and sPLA-CMC biocomposites at 120°C and 140°C.

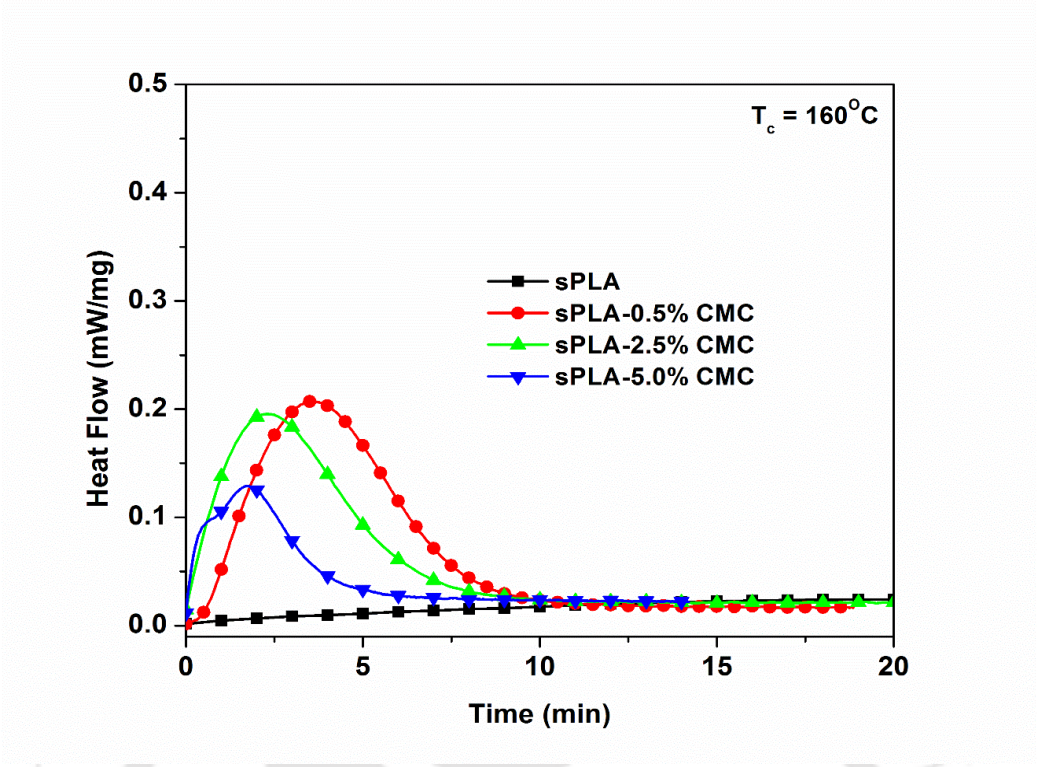

Figure 7.2: Heat flow versus time during isothermal crystallization of sPLA and sPLA-CMC biocomposites at 160°C.

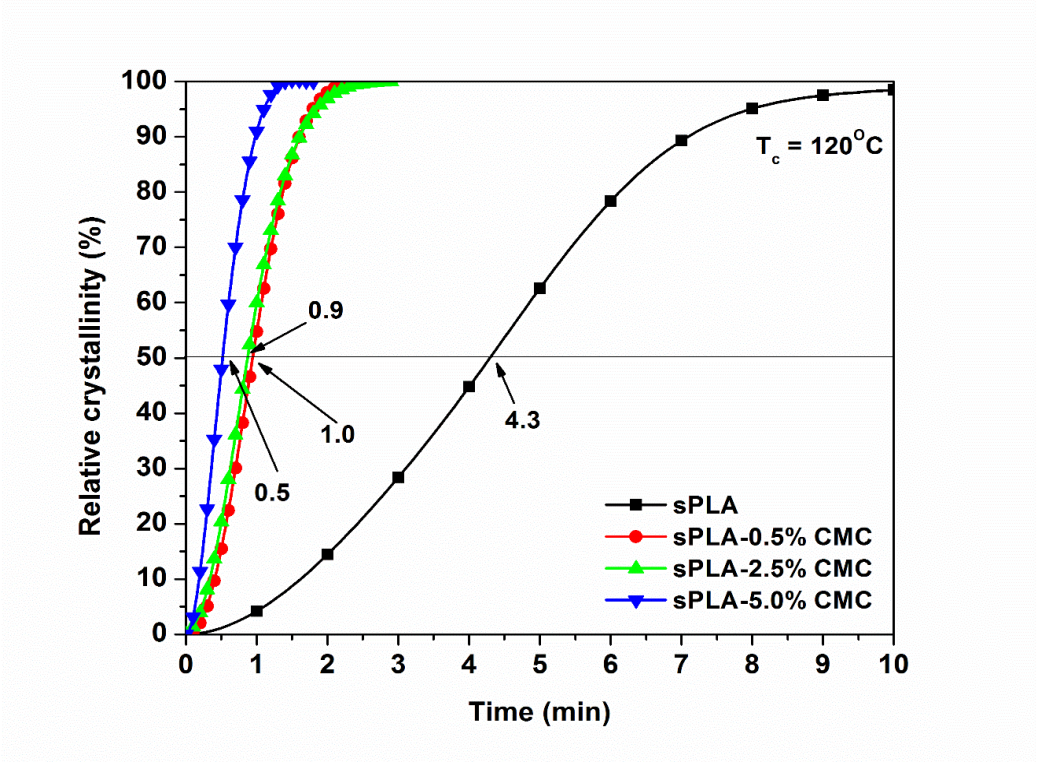

Figure 7.3: Relative crystallinity of sPLA and sPLA-CMC biocomposite at 120°C.

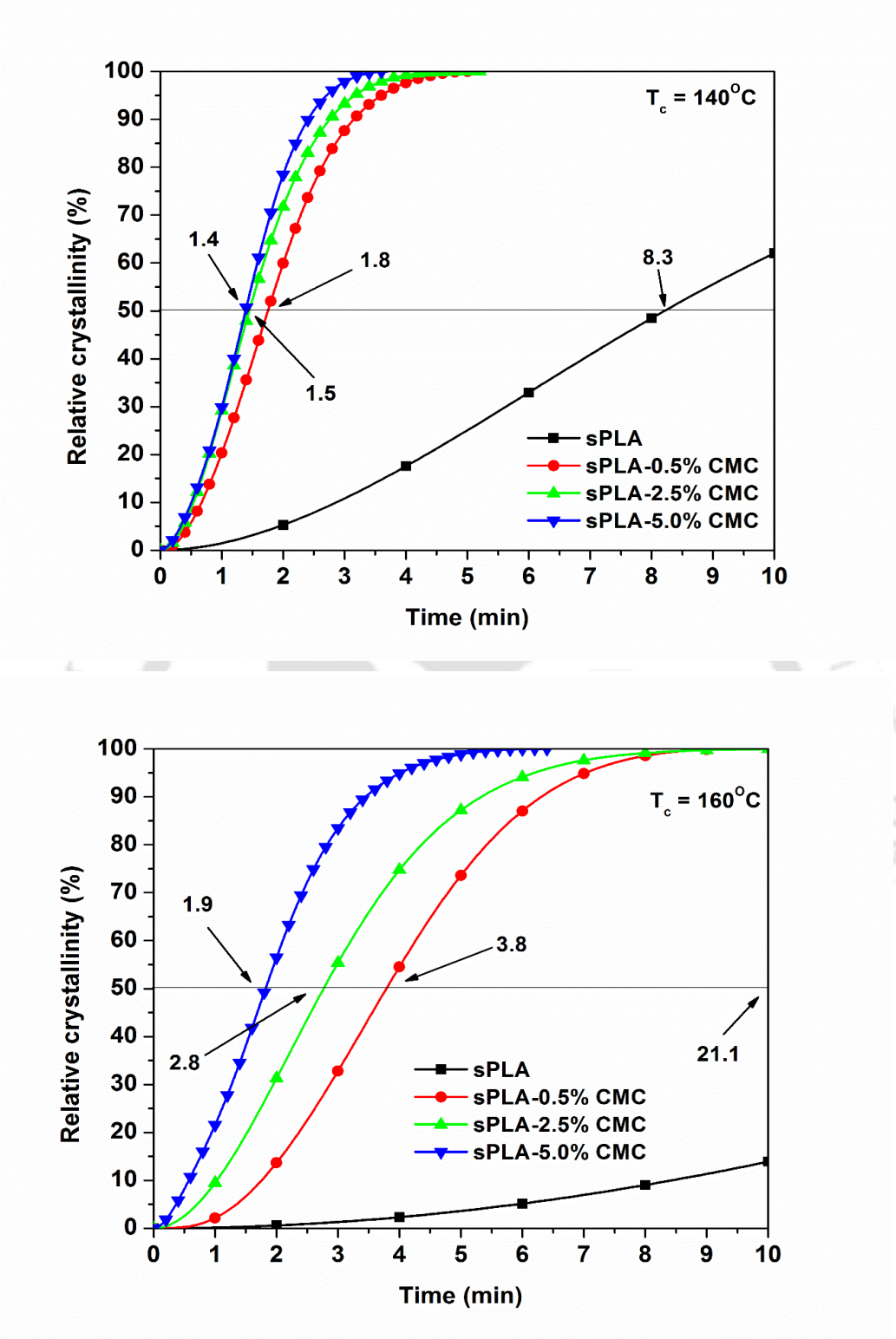

Figure 7.4: Relative crystallinity of sPLA and sPLA-CMC biocomposite at 140°C and 160°C.

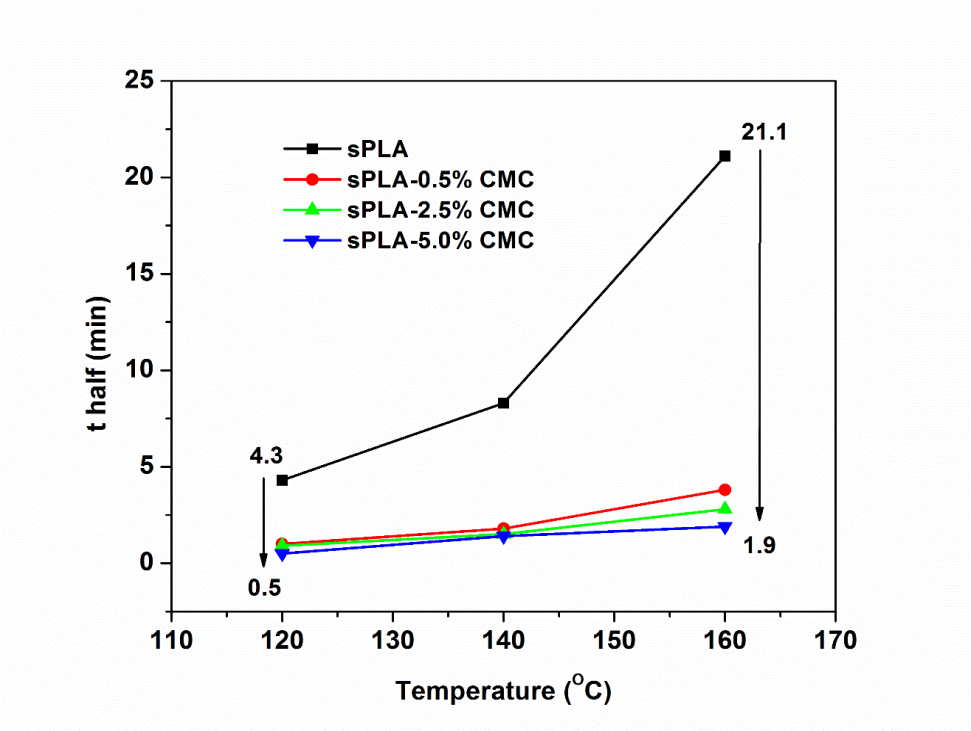

Figure 7.5: Half time of crystallization of sPLA and sPLA-CMC biocomposite at different temperatures.

The relative crystallinity of sPLA and sPLA-CMC biocomposite at different times is shown in the **Figure** 7.**3** and **Figure 7.4**. It can be seen that the characteristic S-shape isothermal data shifts towards higher time zone with increase in isothermal crystallization temperature which shows the reduction in the crystallization rate. The time at which the relative crystallinity reaches 50% is called ‘‘t half’’ ($t_{1/2}$) which is measured from the sigmoidal curve data. The data for ‘t half’ is shown in the **Figure** 7.**5** which suggests that ‘t half’ for sPLA is increased from 4.3 min to 21.1 min as the isothermal crystallization temperature increased to 160°C from 120°C. Similar effect is found in sPLA-CMC biocomposite. However, ‘t half’ time for sPLA-CMC biocomposite is reduced as compared to sPLA. It is reduced from 4.3 min to 0.9 min at 120°C and 21.1 min to 1.9 min at 160°C.

The rate of crystallization (G) can be estimated by $\tau_{1/2}$ which is related to the time necessary for 50% relative crystallinity and represents the bulk crystallization rate for each isothermal

crystallization temperature. G is the reciprocal of 't half' or $[(t_{1/2})^{-1}]$. A significant change in the crystallization rate is observed with increase in the isothermal crystallization temperature. In case of sPLA, the rate is reduced from 0.248 min^{-1} for 120°C to 0.048 min^{-1} for 160°C which is significantly increased to 1.98 min^{-1} for 120°C and 0.59 min^{-1} for 160°C. Increment in the growth rate shows the remarkable contribution of grafted CMC on the enhancement of nucleation in sPLA.

The nucleation and rate of crystallization in polymer has significant importance in the processing in polymer industries. The parameters ultimately affect the solid state properties of the polymers. Several methods have been developed to study the crystallization during processing. The most popular model for analyzing experimental crystallization data is Avrami equation. Generally, it is known and considered that the crystallization process is the composite of the two stage called primary crystallization and secondary crystallization. Avrami equation can be used to understand the crystallization process. The equation 7.1 can be rewritten as

$$\ln[-\ln(1 - X_t)] = \ln k + n \ln t \qquad (7.11)$$

The plot of Avrami equation is given described **Figure**s 7**.6** and **Figure** 7**.7** which is fitted as straight line. The linear regression of plotted lines yielded the Avrami exponents and rate constants. The spherulites can grow in more than one dimension leading to the Avrami exponent in the range of 1.8 to 4. The values of 'n' and 'k' are given in **Table 7.1**. The obtained values of 'n' are found to be ~2 in case of sPLA and increased to 2.6 for sPLA-0.5%CMC. Increase in the 'n' value indicates that the growth of the spherulites taking place in higher dimension compared to sPLA. Again, 'n' value reduced to ~2 for sPLA-2.5%CMC and sPLA-5.0%CMC shows that the spherulite growth may be resulting on the surface of CMC in two dimension.

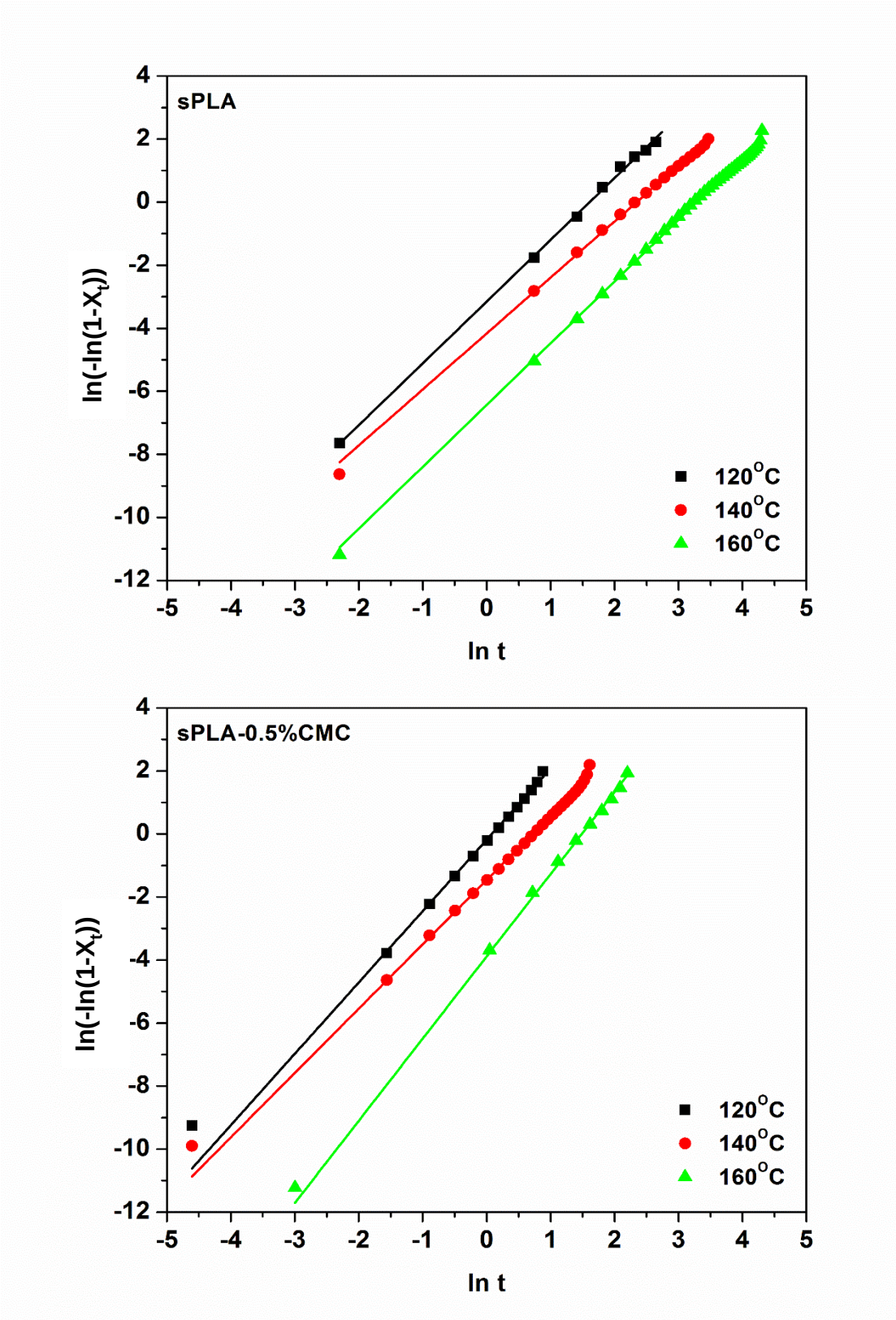

Figure 7.6: Plot of ln [-ln (1-X_t)] vs ln t for isothermal crystallization of sPLA and sPLA-0.5%CMC biocomposite at different temperatures.

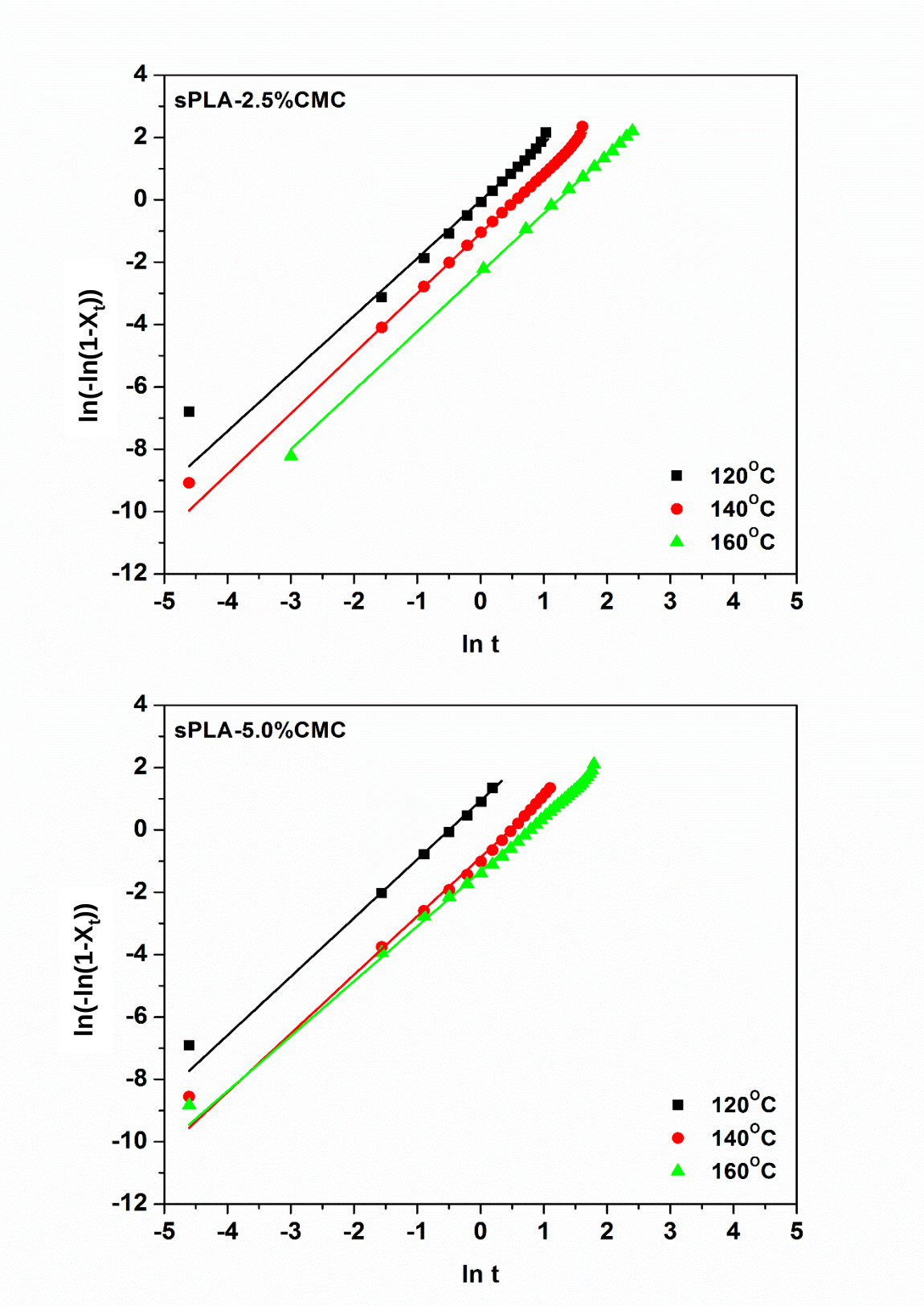

Figure 7.7: Plot of ln [-ln (1-X_t)] vs ln t for isothermal crystallization of sPLA-2.5%CMC and sPLA-5.0%CMC biocomposite at different temperature.

The lamellar crystals which aggregate for the formation of spherulites in polymers form the unsymmetrical structure due to presence of grafted CMC doesn't allow it to grow isotropically. The overall crystallization rate constant (k) of sPLA is found to be reduced with increase in the crystallization temperature and similar effect is noticed for sPLA-CMC biocomposites. For same crystallization temperature, the overall crystallization rate constant is enhanced when grafted CMC is added to the matrix. Several order of magnitude enhancement in the rate constant suggests that the biocomposite crystallizes much faster than sPLA at the same temperature. It also suggests the nucleation activity of the filler used. The calculated n and k value are used to measure the theoretical 't half' ($t_{1/2}$), given in the **Table 7.1**, as per the equation

$$t_{1/2} = \left(\frac{\ln 2}{k}\right)^{1/n} \qquad (7.12)$$

It is found that the experiential 't half' and calculated 't half' value is approximately same which indicates the reliability of calculated data using linear regression of Avrami equation. The activation energy for melt crystallization of biocomposite is calculated using equation 7.2 and shown in **Table 7.1**. Its activation energy for crystallization of sPLA is found to be 57 kJ.mole^{-1} and reduced to ~43 kJ.mole^{-1} for sPLA-CMC biocomposite. It shows that the crystallization is heterogeneous in nature and dominated the overall crystallization rate.

It is known that the crystallization rate is controlled by the nucleation which relates with the free energy for the formation of stable crystallites. The plot of Lauritzen and Hoffmann equation give the value of K_g which is related to the nucleation activity of fillers. The Kg value can be related and used to calculate the free energy of surface of lamella. The constants required for the calculation are taken from the literature available [13, 140, 220] as U* = 6300 J.mole^{-1}, a_o = b_o = 14.98Å, Equilibrium melting

temperature = 243°C = 516.16 K, Glass transition temperature = 61°C = 334.16 K, ρ_c = 1.27 g.cm^{-3}, Equilibrium melting enthalpy = 142 J.g^{-1}, Heat of fusion per unit volume: 180.34 J.cm^{-3}, k = 1.381×10^{-23} J.K^{-1}.

The values obtained for K_g from linear regression of the Lauritzen and Hoffmann data are given in **Table 7.2**. Nucleation constant is found to be 6.3×10^5 K^2 for sPLA which is reduced to 5.6×10^5 K^2 signifying that CMC may accelerate the crystallization process. The lower value of Kg for biocomposite compared to the pristine sPLA confirm the largely accelerated crystallization in presence of CMC due to the faster nucleation rate at the surface of grafted CMC [223]. The value of K_g can be used for the calculation of the product of lateral and folding surface free energies. It is calculated by substitution of K_g value in equation 7.4 and shown in **Table 7.2**. For sPLA, it is calculated as ~508 erg^2.cm^{-4} which is reduced to ~540 erg^2.cm^{-4} after incorporation of CMC into the matrix. Reduction in free energy also suggests that the presence of CMC may be responsible for the epitaxial growth of spherulite and facilitate for the transport of polymeric chain to the growth site from the bulk. It is also believed that the presence of CMC reduces the size of the nucleus needed for the crystal growth which can be related to the epitaxial growth of the spherulite on the surface of CMC. The formation of interface between polymer chain and surface of filler may be less hindered than the creation of individual polymer crystals. Free energy for nucleation is measured using equation 7.9 and presented in **Table 7.2**. The energy barrier for the nucleation is dropped from 7.1×10^{-13} erg for sPLA to 6.3×10^{-13} erg for sPLA-CMC biocomposite. Reduction in the nucleation energy may be due to the facility provided by the grafted CMC to polymer chains to be folded without any hindrance in comparison to pristine sPLA. From the other explanation given by Dobreva et.al. [224], lower value of K_g and nucleation energy indicate, most probably, the existence of more chain folding irregularities because of higher proportion of transcrystals developed due to epitaxial

nucleation growth on the surface of CMC. The polarizing optical microscopic images are shown in the **Table 7.3**. It can be seen that sPLA takes long time to be crystalized. However, time is significantly reduced in case of sPLA-CMC biocomposite. This POM analysis is in line with the analysis done using Avrami equation.

Table 7.1: Kinetic parameters for the isothermal crystallization of sPLA-CMC biocomposite.

T_c (°C)	$t_{1/2}$ (min) (exp.)	n	k (min^{-n})	$t_{1/2}$ (min) (cal.)	t_{max} (min)	$\tau_{1/2}$ (min^{1})	ΔE_a ($kJ.mole^{-1}$)
sPLA							
120	4.3	2.0	42.7×10^{-3}	4.0	3.4	0.248	
140	8.3	1.8	15.6×10^{-3}	8.2	6.4	0.121	-57.0
160	21.1	2.0	1.6×10^{-3}	20.8	17.7	0.048	
sPLA-0.5% CMC							
120	1.0	2.3	829.6×10^{-3}	0.9	0.9	1.08	
140	1.8	2.1	231.3×10^{-3}	1.7	1.5	0.59	-49.9
160	3.8	2.6	20.5×10^{-3}	3.9	3.7	0.26	
sPLA-2.5% CMC							
120	0.9	1.9	972.4×10^{-3}	0.8	0.7	1.20	
140	1.5	1.9	342.4×10^{-3}	1.5	1.2	0.69	-42.8
160	2.8	1.9	97.2×10^{-3}	2.8	2.3	0.36	
sPLA-5.0% CMC							
120	0.5	1.9	2540.0×10^{-3}	0.5	0.4	1.98	
140	1.4	1.9	412.5×10^{-3}	1.3	1.1	0.76	-43.9
160	1.9	1.8	264.4×10^{-3}	1.7	1.3	0.59	

T_c: Crystallization temperature, t_{max}: Time at rate of crystallization is maximum, $G=\tau_{1/2}$: Crystallization rate, exp.: Experimental, cal.: Calculated

Table 7.2: Thermodynamic parameters for sPLA and sPLA-CMC biocomposites.

Sample Name	K_g (K^2)	$\sigma\sigma_e$ ($erg^2.cm^{-4}$)	ΔG* (erg)
sPLA	6.3×10^5	507.7	7.1×10^{-13}
sPLA-0.5%CMC	5.9×10^5	475.7	6.6×10^{-13}
sPLA-2.5%CMC	5.6×10^5	451.2	6.3×10^{-13}
sPLA-5.0%CMC	5.8×10^5	467.4	6.5×10^{-13}

Table 7.3: POM images of spherulites of sPLA and sPLA-CMC biocomposites at different times.

T=140°C	sPLA	sPLA-1.0%CMC	sPLA-2.5%CMC	sPLA-5.0%CMC
0 min	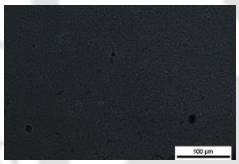	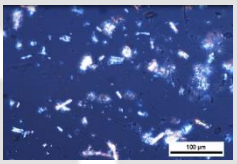	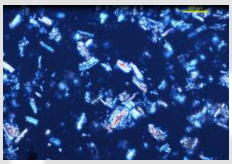	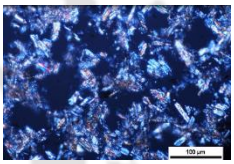
5 min	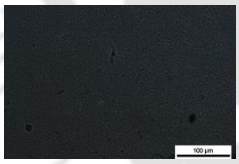	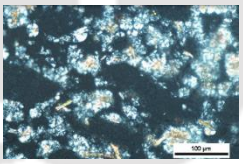	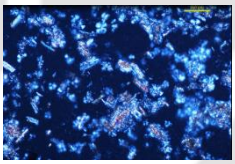	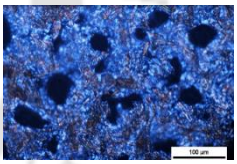
10 min	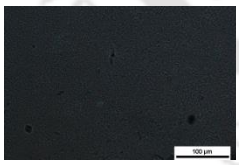	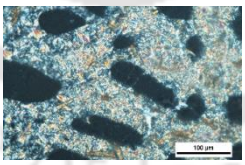	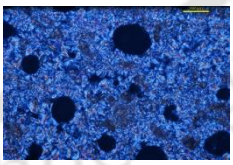	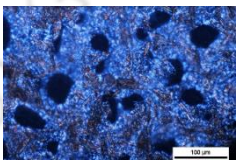
20 min	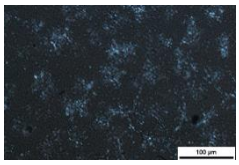	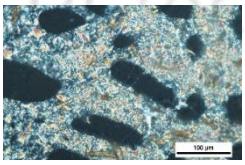	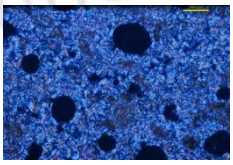	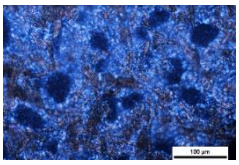
30 min	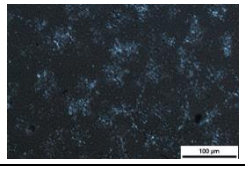	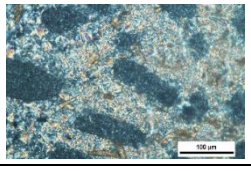	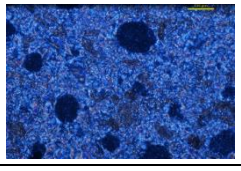	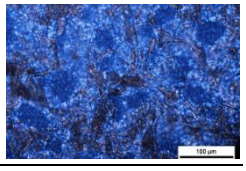

7.5.2 Effect of modified chitosan on crystallization of sPLA

Chitosan is modified by *in situ* condensation polymerization of L-lactic acid and it is incorporated with poly (D-lactic acid) in order to fabricate the stereocomplex PLA modified chitosan (MCH) biocomposite. The presence of MCH in the PLA matrix sgnificantly affects the crystallization ability of sPLA. Isothermal crystallization of prepared biocomposite is analysized at 120°C, 140°C and 160°C and heat flow against time is shown in the **Figure** 7.**8** and **Figure** 7.**9**. It is seen that the peak width reduces as the crystallization temperature decreased from 160°C to 120°C. Similar phenomenon is also observed with sPLA-MCH biocomposites. It is found that the heat flow peak shifted towards lower time side as MCH content increased which suggests the higher rate of crystallization compared to the pristine sPLA.

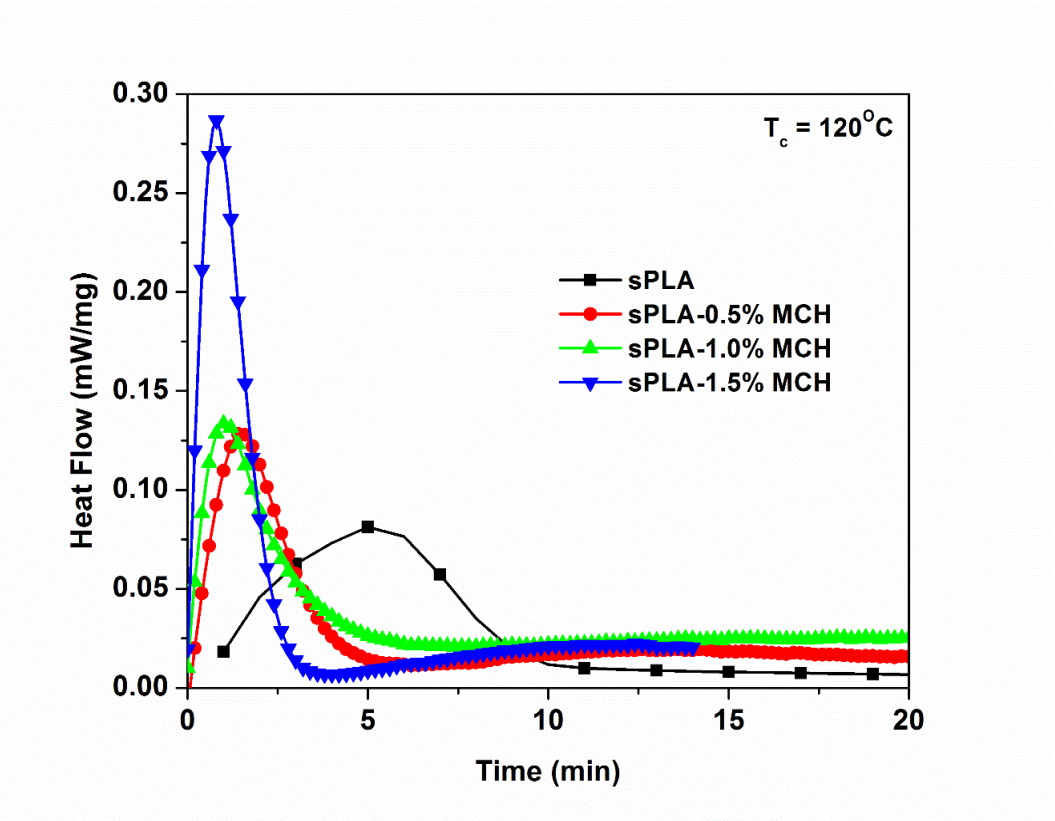

Figure 7.8: Heat flow versus time during isothermal crystallization of sPLA and sPLA-MCH biocomposites at 120°C.

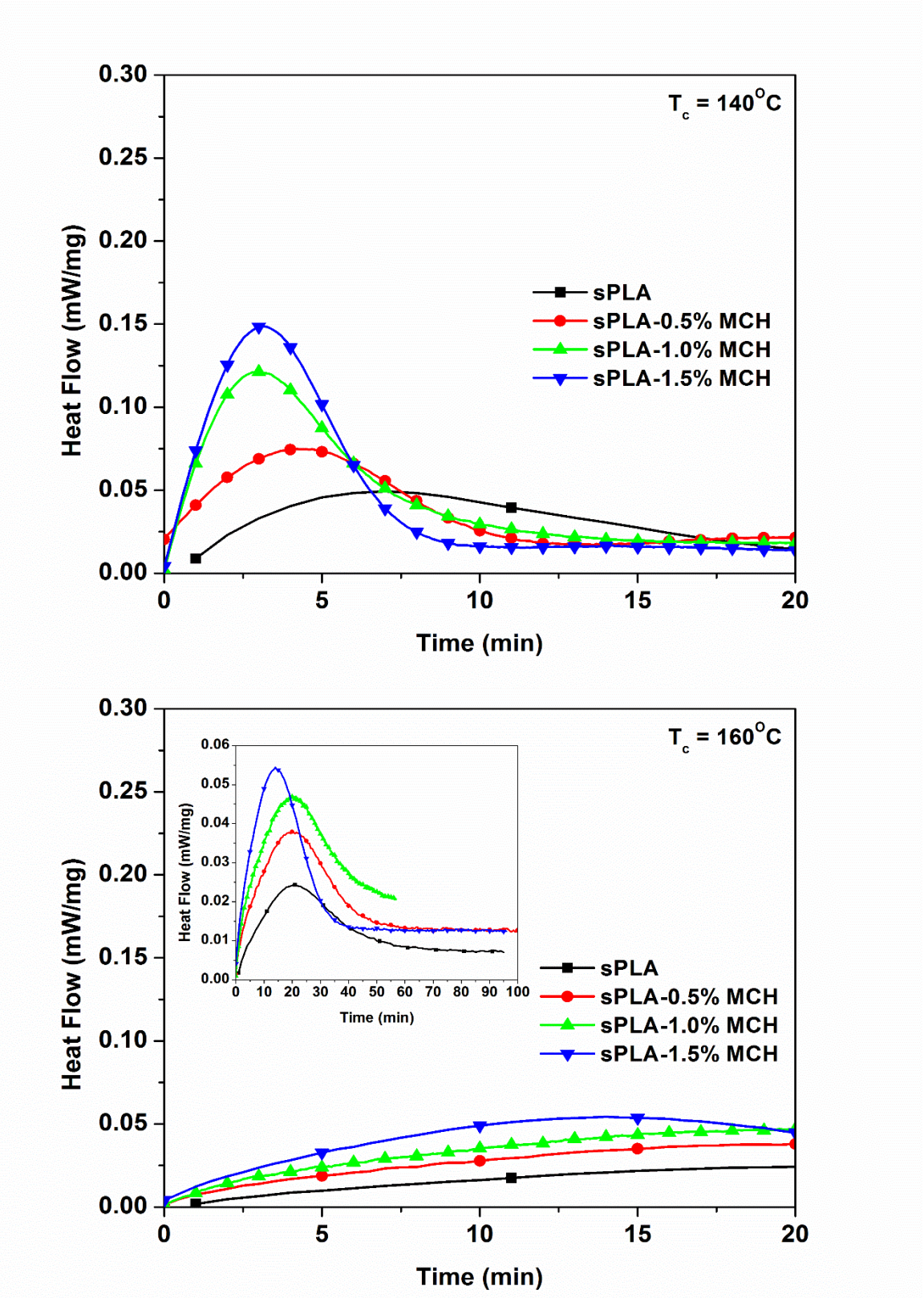

Figure 7.9: Heat flow versus time during isothermal crystallization of sPLA and sPLA-MCH biocomposites at 140°C and 160°C.

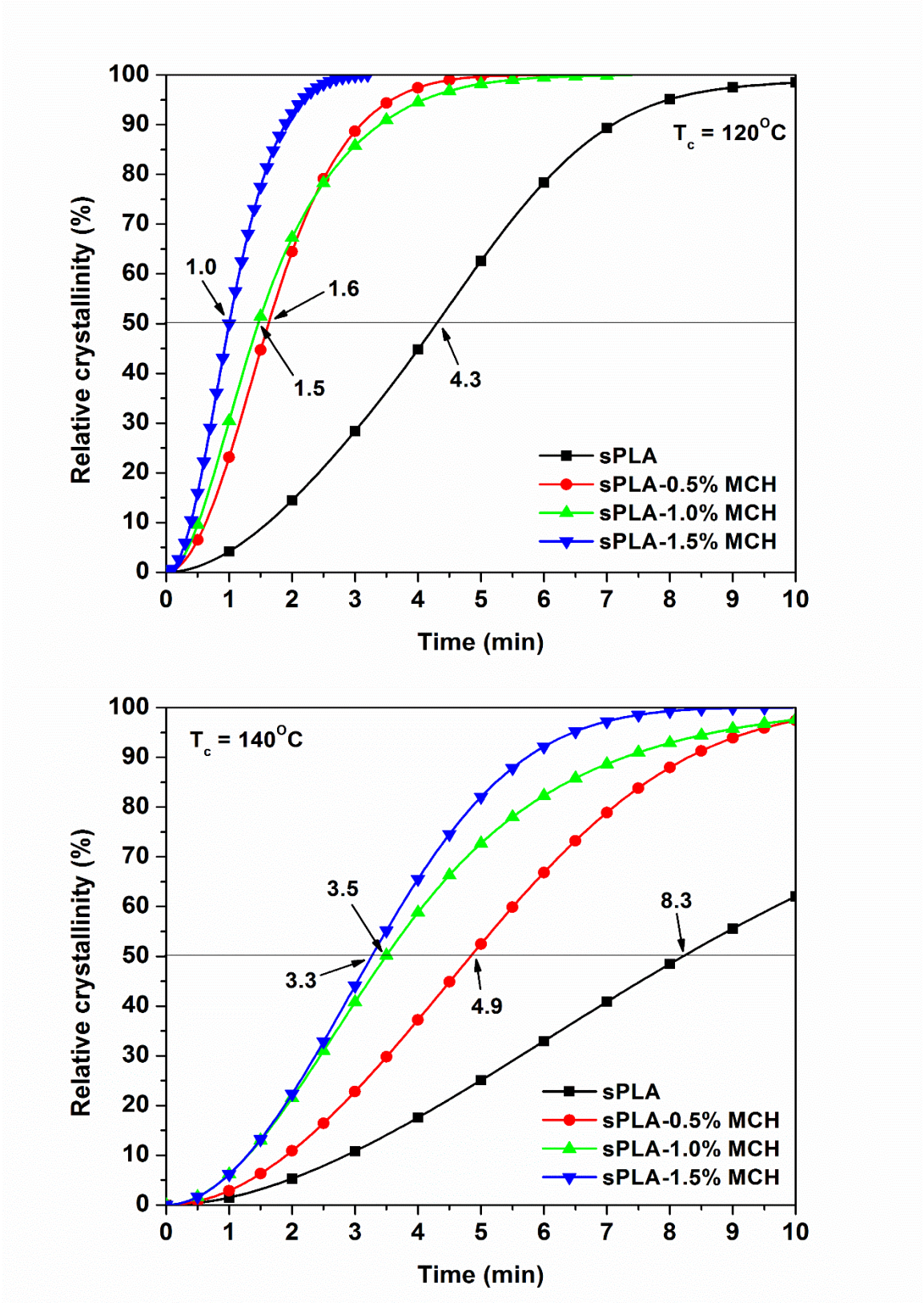

Figure 7.10: Relative crystallinity of sPLA and sPLA-MCH biocomposite at 120°C and 140°C.

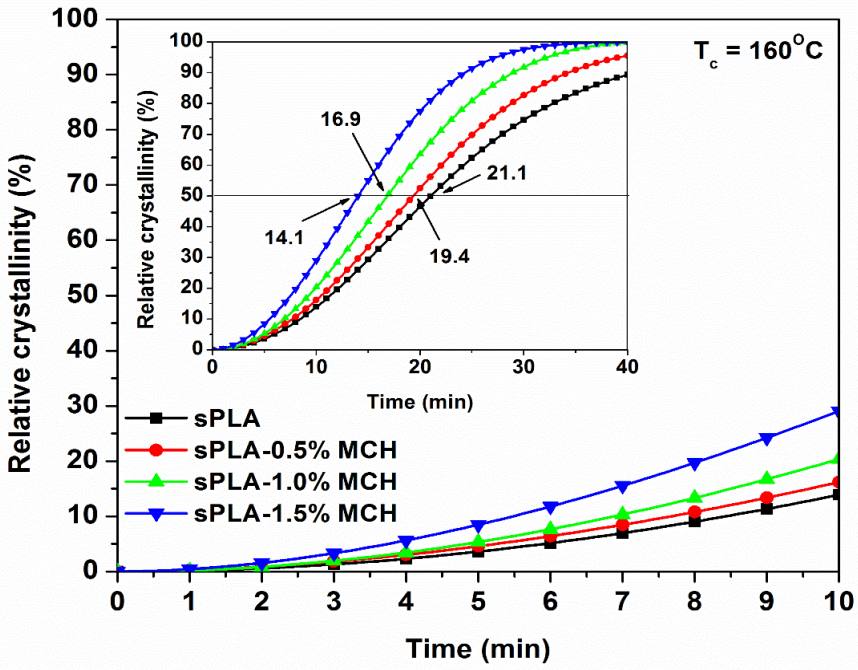

Figure 7.11: Relative crystallinity of sPLA and sPLA-MCH biocomposite at 160°C.

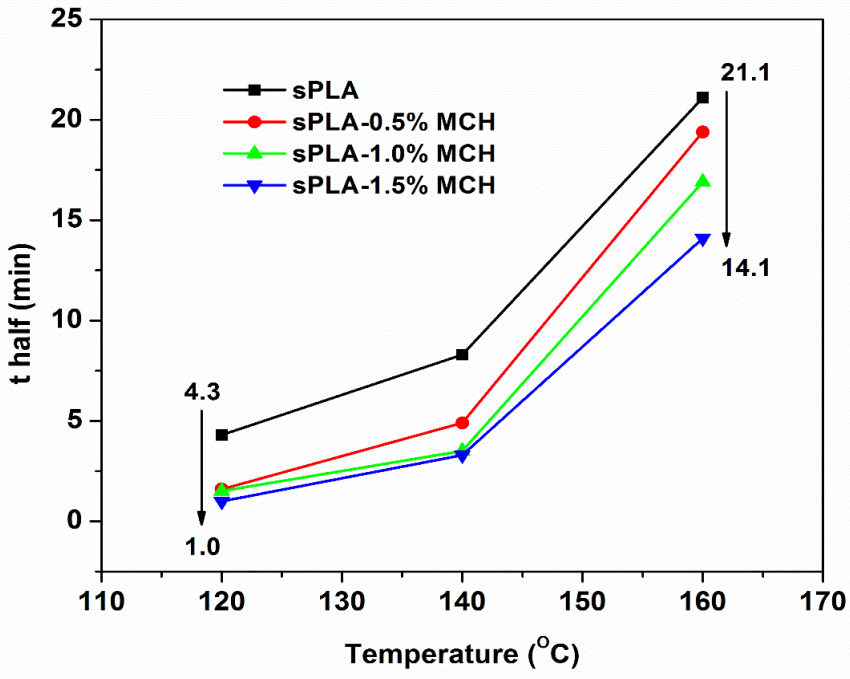

Figure 7.12: Half time of crystallization of sPLA and sPLA-MCH biocomposite against different temperatures.

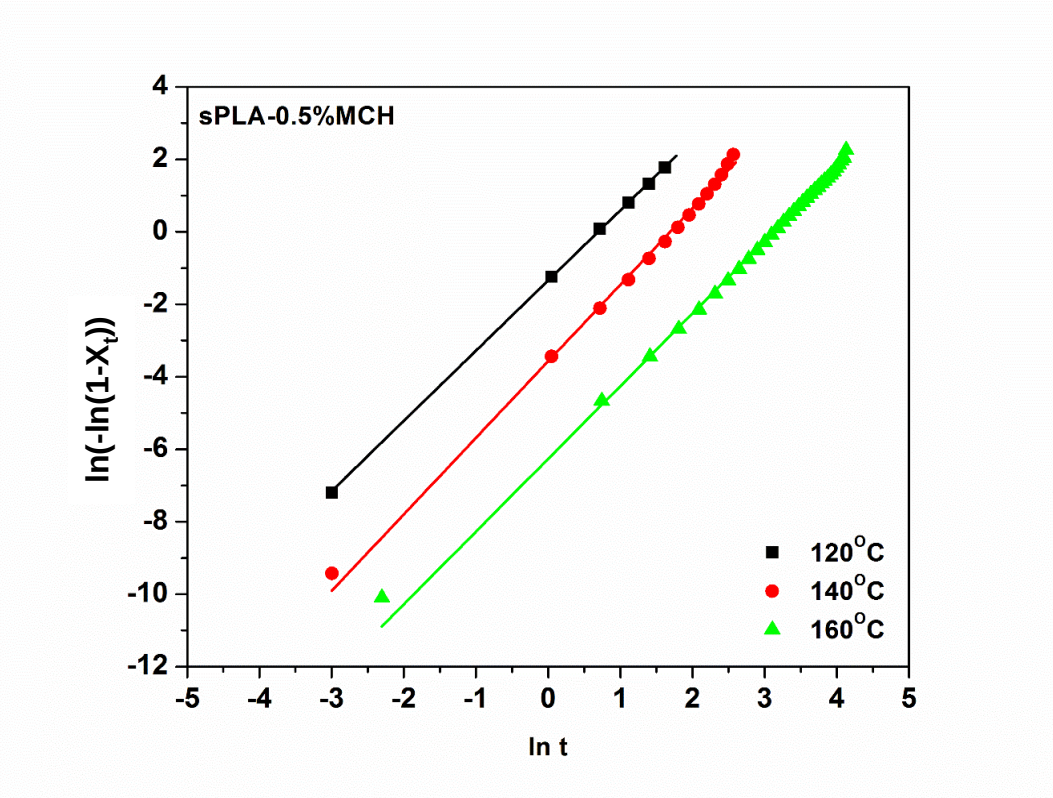

Figure 7.13: Plot of ln [-ln (1-X_t)] vs ln t for isothermal crystallization of sPLA-0.5%MCH biocomposite at different temperatures.

The relative crystallinity of sPLA and sPLA-MCH biocomposite is displayed in **Figure** 7.**10** and **Figure** 7.**11**. Proper simoidal shape is observed for the relative crystallinity which is shifted to lower time as temperature is reduced. After addition of MCH, sigmoidal shape is further shifted to lower time. The experimental 't half' calculated from the relative crystallinity of biocomposites listed in **Table 7.4**. The 't half' versus isothermal crystallization temperature is shown in **Figure** 7.**12**. The half time for sPLA at 120°C is found to be 4.1 min which is reduced to 1.0 min afted additon of 1.5% MCH. Similarly, in the case of 160°C, it is reduced from 21.1 min to 14.1 min. Reduction in the crystallization time indicates the improvement in crystallization ability of sPLA due to addtion of MCH. It is observed that the 't half' is higher for MCH in comparison to grafted CMC.

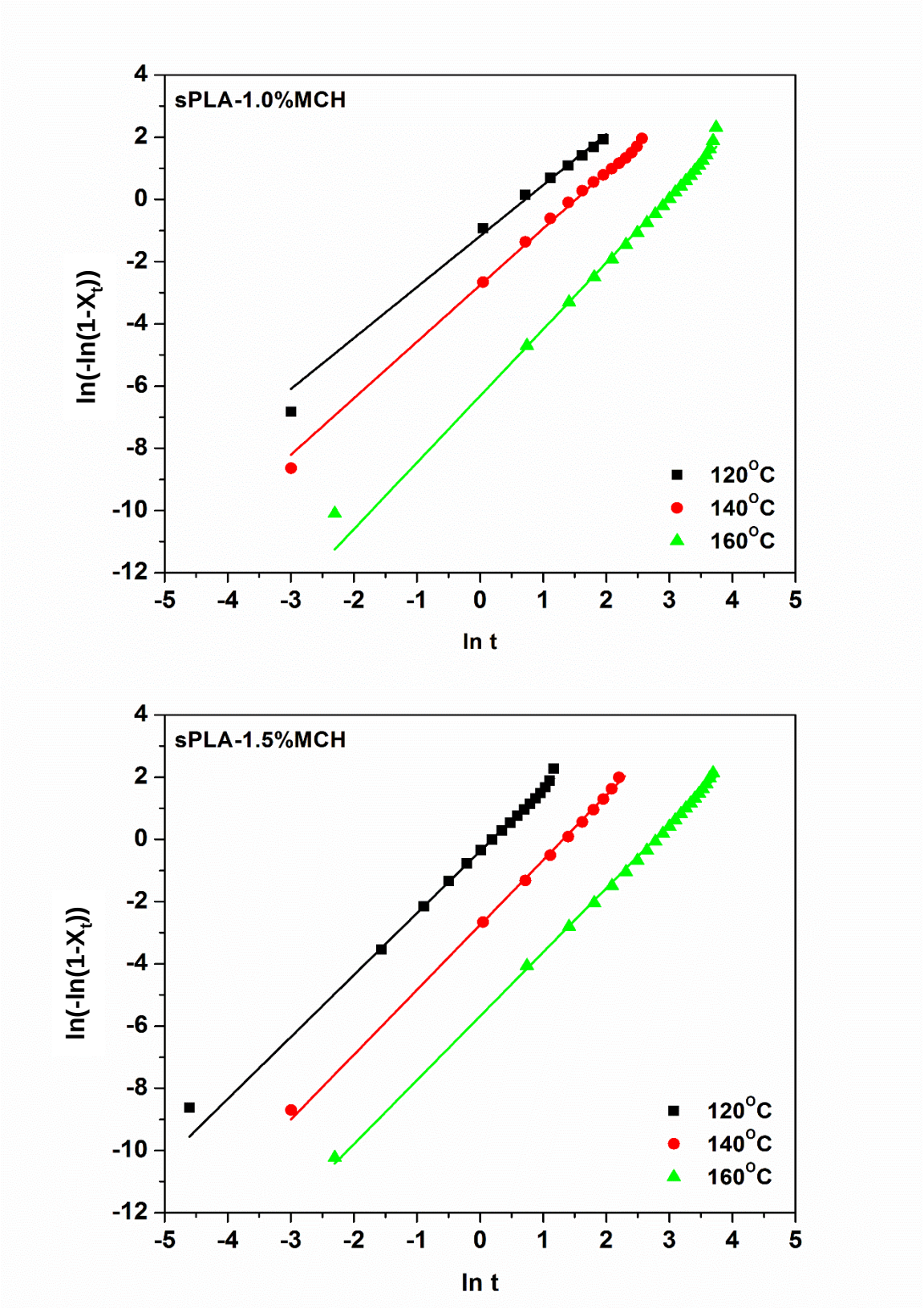

Figure 7.14: Plot of ln [-ln (1-X_t)] vs ln t for isothermal crystallization of sPLA-1.0%MCH and sPLA-1.5%MCH biocomposite at different temperatures.

The Avrami plot is shown in **Figure** 7**.13** and **Figure 7.14** and the obtained value of Avrami parameters are listed in the **Table 7.4**. It is observed that the value of 'n' is found to be more or less similar to pristine sPLA which signifies that the dimension of the spherulite remained same as for sPLA. Whereas, a significant improvement of overall crystallization rate 'k' revealed enhancement in crystallization rate after addition of MCH in the polymer matrix. The value of 'n' and 'k' is used to calculate t_{max} and calculated 't half' and listed in **Table 7.4**. The value of calculated 't half' using Avrami exponents is similar to the experimental 't half' which suggests that the calculated parameters measured best fitted the data. The activation energy for crystallization is increased to ~89 $kJ.mole^{-1}$ after addition of MCH. Increase in the energy suggests that the crystallization process need more energy with respect to sPLA. Higher activation energy for sPLA-MCH biocomposite suggests the uniform nucleation which means that the crystallites are forming due to the interaction of polymer chains and not by the presence of filler.

The nucleation constant and product of lateral and fold free energies is calculated and listed in **Table 7.5**. In case of sPLA-MCH biocomposite, the value of K_g is found to be higher than that of pristine sPLA which suggests that the presence of MCH contribute into chain mobility. The calculated value of product of lateral and fold free energies is higher for sPLA-MCH in comparison to sPLA. Enhancement in the free energy confirms that the modified chitosan is not contributed as nucleating agent but provided the extended molecular surface of PLLA to interact with PDLA. This interaction is responsible for the uniform nucleation which require higher energy of nucleation as confirmed by the increased nucleation energy (8.7×10^{-13} erg) in comparison to sPLA (7.1×10^{-13} erg). The POM images of the spherulite growth of sPLA and sPLA-MCH biocomposite at 140°C at different times is shown in **Table 7.6**.

Table 7.4: Kinetic parameters for the isothermal crystallization of sPLA-MCH biocomposite.

T_c (°C)	$t_{1/2}$ (min) (exp.)	n	k (min^{-n})	$t_{1/2}$ (min) (cal.)	t_{max} (min)	$\tau_{1/2}$ (min^{-1})	ΔE_a ($kJ.mole^{-1}$)
sPLA							
120	4.3	2.0	42.7×10^{-3}	4.0	3.4	0.248	
140	8.3	1.8	15.6×10^{-3}	8.2	6.4	0.121	-57.0
160	21.1	2.0	1.6×10^{-3}	20.8	17.7	0.048	
sPLA-0.5% MCH							
120	1.6	1.9	260.4×10^{-3}	1.8	1.4	0.597	
140	4.9	2.1	28.0×10^{-3}	4.6	4.0	0.217	-80.4
160	19.4	2.1	1.9×10^{-3}	16.6	14.5	0.060	
sPLA-1.0% MCH							
120	1.5	1.6	307.3×10^{-3}	1.7	1.1	0.602	
140	3.5	1.8	63.4×10^{-3}	3.8	3.0	0.265	-82.4
160	16.9	2.2	1.8×10^{-3}	15.0	13.4	0.067	
sPLA-1.5% MCH							
120	1.0	2.0	681.0×10^{-3}	1.0	1.0	0.991	
140	3.3	2.1	63.7×10^{-3}	3.1	2.7	0.321	-88.8
160	14.1	2.1	3.4×10^{-3}	12.6	11.0	0.079	

T_c: Crystallization temperature, t_{max}: Time at rate of crystallization is max, $G=\tau_{1/2}$: Crystallization rate

Table 7.5: Thermodynamic parameters for sPLA and sPLA-MCH biocomposites.

Sample Name	K_g (K^2)	$\sigma\sigma_e$ ($erg^2.cm^{-4}$)	ΔG^* (erg)
sPLA	6.3×10^5	507.7	7.1×10^{-13}
sPLA-0.5%MCH	7.6×10^5	616.3	8.6×10^{-13}
sPLA-1.0%MCH	7.6×10^5	612.0	8.5×10^{-13}
sPLA-1.5%MCH	7.7×10^5	624.0	8.7×10^{-13}

Table 7.6: POM image of spherulites of sPLA and sPLA-MCH biocomposites at different times.

T=140°C	sPLA	sPLA-0.5%MCH	sPLA-1.0%MCH	sPLA-1.5%MCH
0 min				
5 min		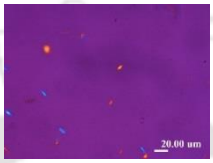	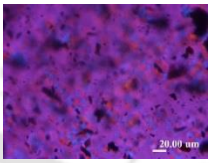	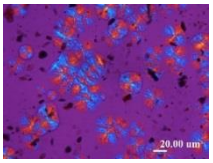
10 min		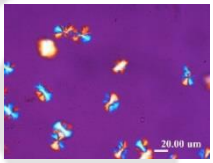	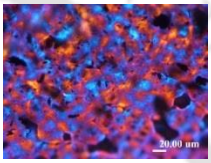	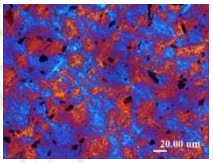
20 min	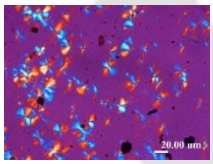	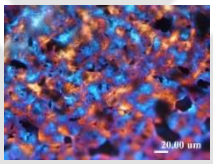	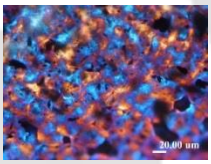	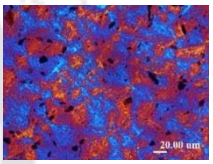
30 min	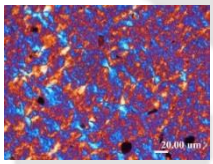	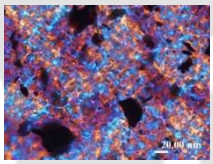	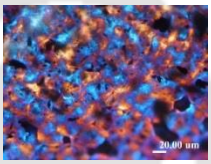	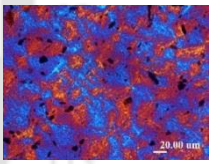

7.5.3 Effect of grafted HAP on crystallization of sPLA

Hydroxyapatite (HAP) is grafted with PDLA and blended with PLLA to fabricate the stereocomplex PLA biocomposite. The graph for heat flow versus time is shown in the **Figure** 7.15 and **Figure 7.16**. Similar phenamenon as other discussed fillers is found in for grafted HAP. The peak width is significantly reduced with the addition of grafted HAP into sPLA matrix. The peaks are shifted towords lower time range with reduction in temperature. It is also noticed that the presence of grafted HAP significantly reduced the time required for the crystallization. The relative crystallization against time is shown in

the **Figure** 7.**17** and **Figure 7.18** which confirms the relatively fast crystallization rate in comparison to sPLA.

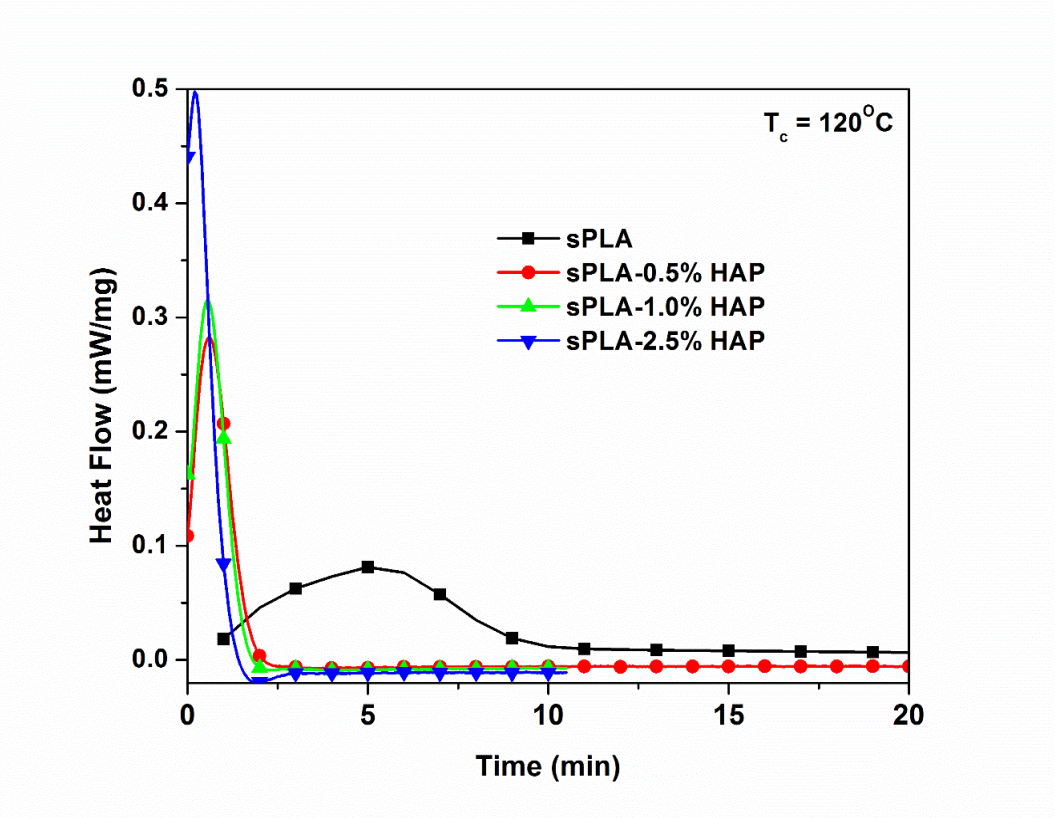

Figure 7.15: Heat flow versus time during isothermal crystallization of sPLA and sPLA-HAP biocomposites at 120°C.

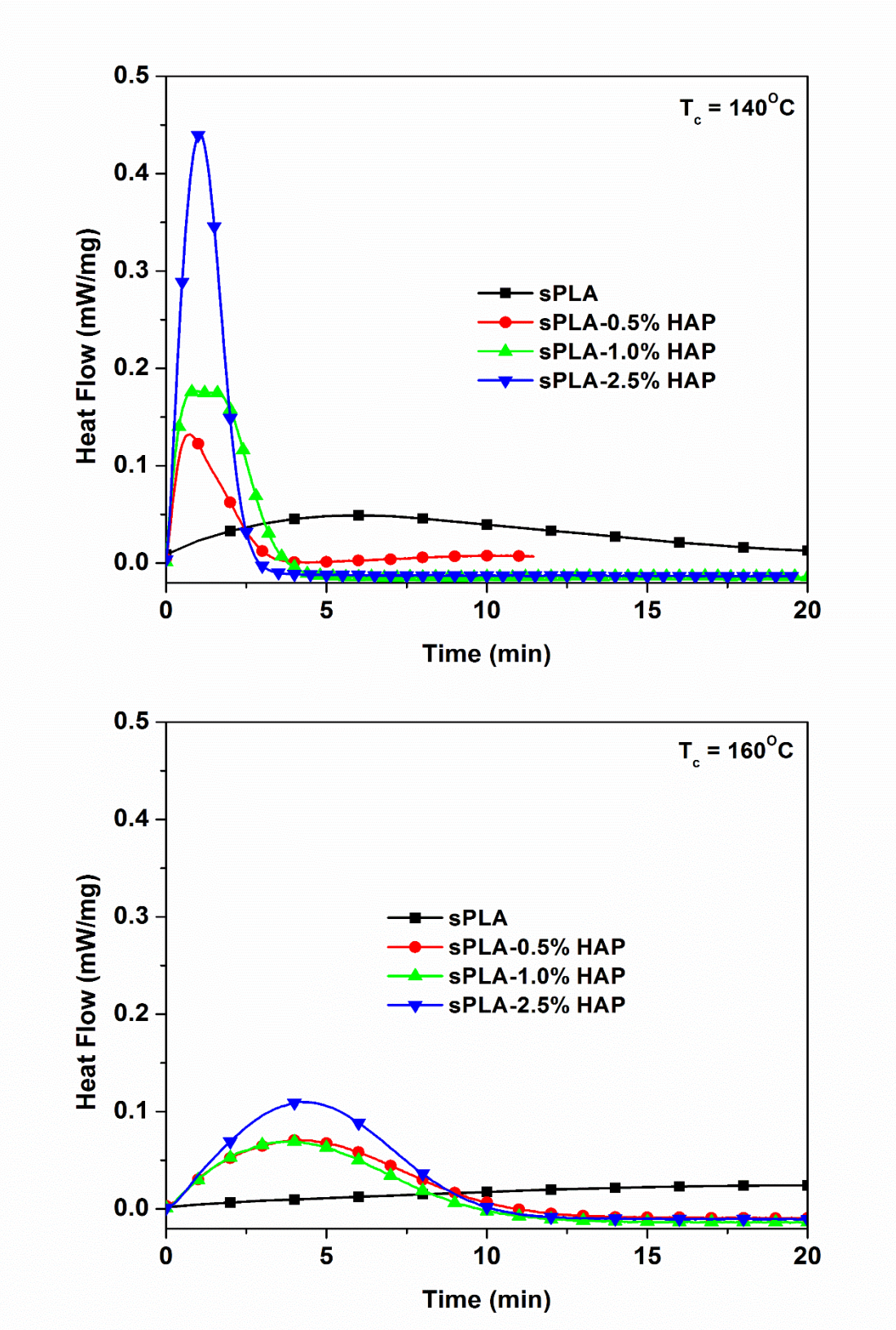

Figure 7.16: Heat flow versus time during isothermal crystallization of sPLA and sPLA-HAP biocomposites at 140°C and 160°C.

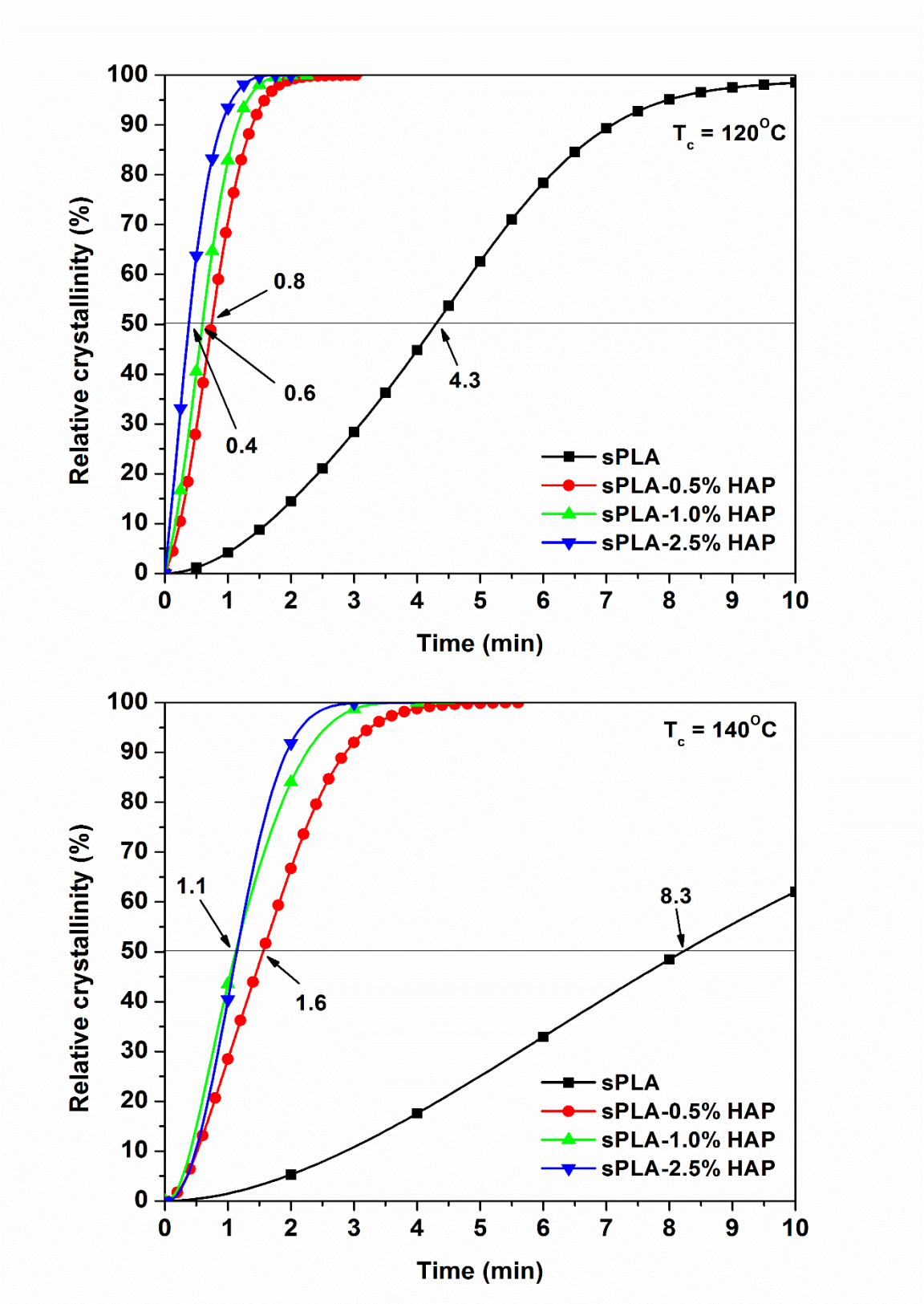

Figure 7.17: Relative crystallinity of sPLA and sPLA-HAP biocomposite at 120°C and 140°C.

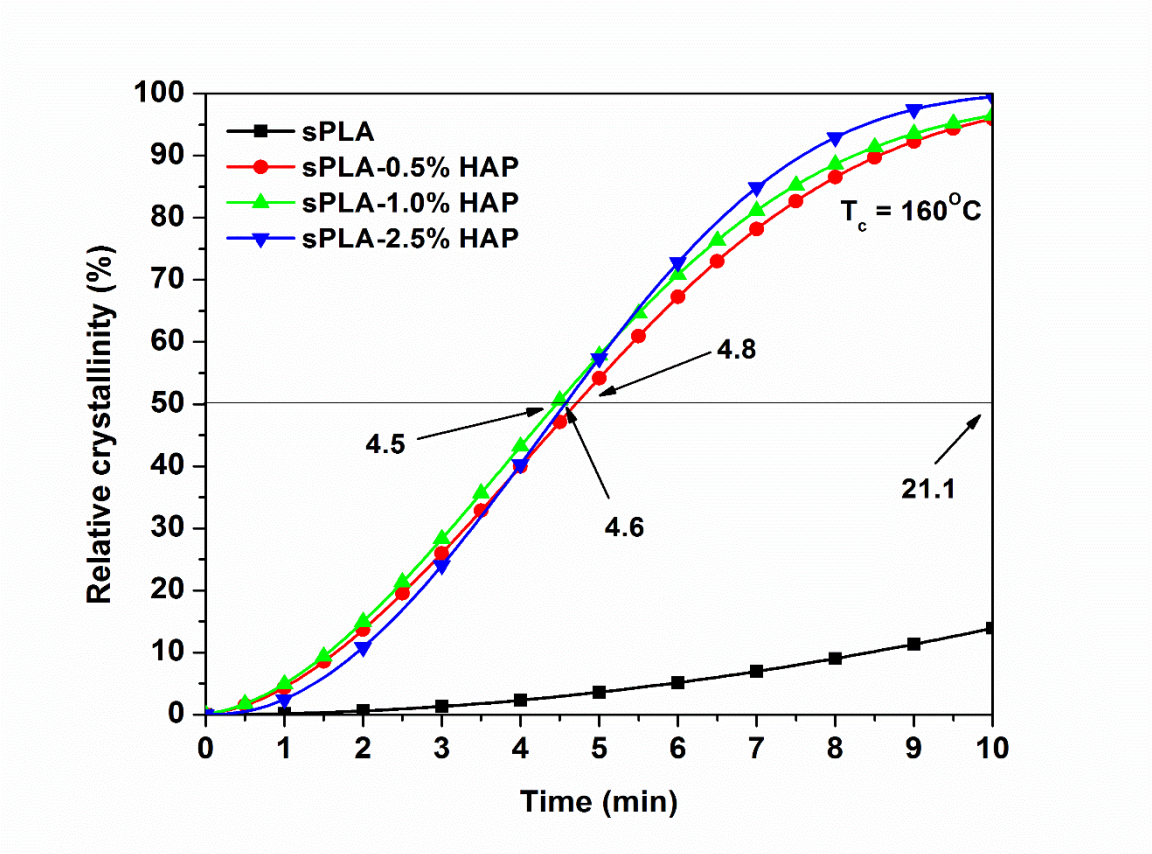

Figure 7.18: Relative crystallinity of sPLA and sPLA-HAP biocomposite at 160°C.

Figure 7.**19** represented the half time for the relative crystallinity of sPLA and sPLA-HAP biocomposite. It is found while incorporation of HAP that 't half' reduced from 4.3 min to 0.4 min from 120°C isothermal crystallization temperature and 21.1 min to 4.5 min for 160°C. Reduction in crystallization time specifically shows the higher crystallization growth rate which is calculated from the plot of Avrami equation. The plot is shown in the **Figure 7.20** and **Figure 7.21** and data of obtained 'n' and 'k' value is shown in the **Table 7.7**. The curve fitting of the Avrami equation is found to be linear. The obtained value of n is lowered in comparison to pristine sPLA but found higher in case of sPLA-2.5%HAP biocomposite. Variation in the n value suggests that the spherulite dimension is reduced in case of lower amount of grafted HAP but increased for higher loading of grafted filler which may be due to the instantaneous nucleation at lower loading and sporadic nucleation at higher loading.

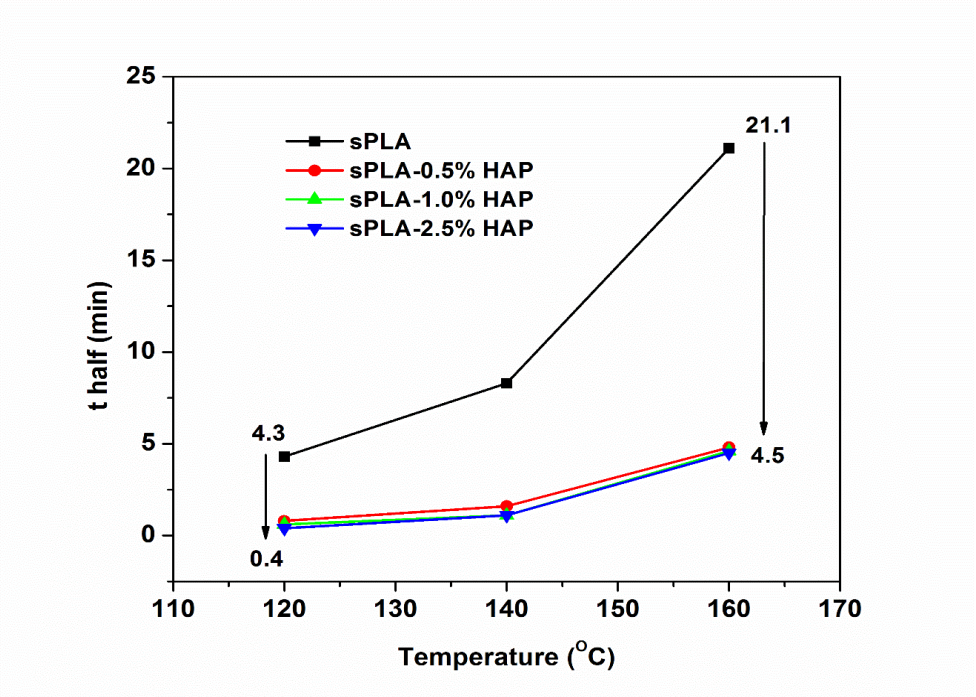

Figure 7.19: Half time of crystallization of sPLA and sPLA-HAP biocomposite against different temperature.

The overall crystallization rate constant 'k' is found higher in case of sPLA-HAP in comparison to sPLA which suggests that the crystallization rate is enhanced due to incorporation of HAP. Using Avrami exponents, the theoratical 't half' is calculted and found in line with the experimntal 't half' values. Spherulite growth rate is measured as reciprocal of 't half' and reduction is found with incrase in isothermal crystallization temperature. However, it is increased with increase in the loading of grafted HAP. The same Avrami exponent is used to calculate the activation energy for crystallization and found enhancement with respect to pristine sPLA. It is found higher in comparison to sPLA which may be due to the transition from homocrystallization to stereoomplex crystallization. In other words, the nucleation is higher which may be due to the incrased viscosity but the energy needed for the crystallization is higher which may be attributred to the result of polymorphic transition.

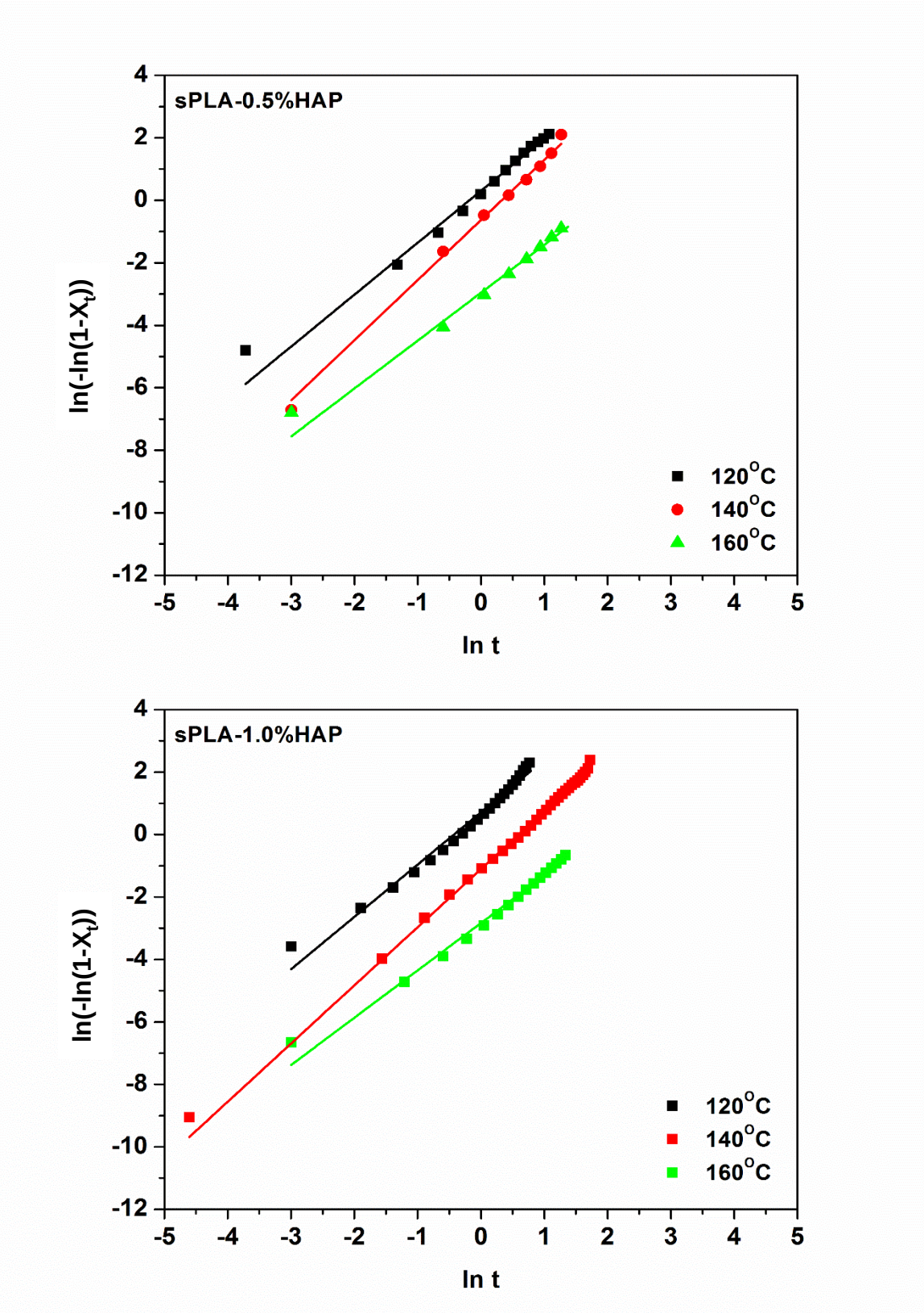

Figure 7.20: Plot of ln [-ln (1-X_t)] vs ln t for isothermal crystallization of sPLA-0.5%HAP and sPLA-1.0%HAP biocomposite at different temperatures.

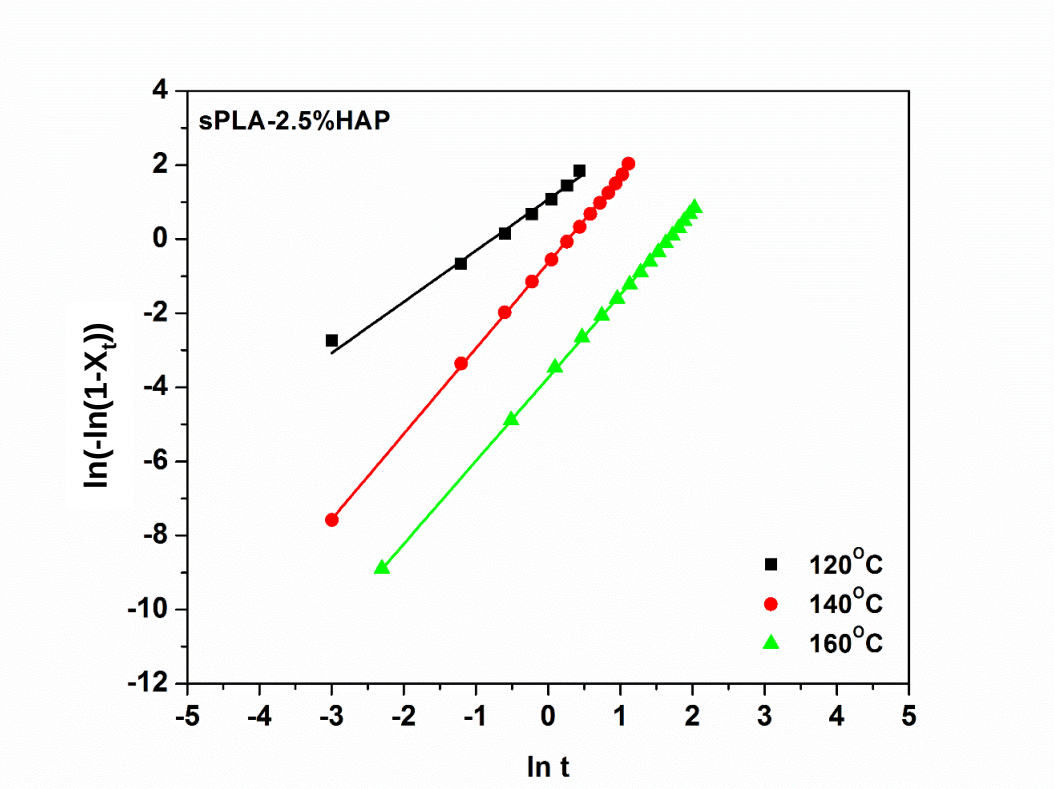

Figure 7.21: Plot of ln [-ln (1-X_t)] vs ln t for isothermal crystallization of sPLA-2.5%HAP biocomposite at different temperatures.

The 't half' value is used to calculate the nucleation constant which is related to the product of lateral and fold free energies. The calculated values are listed in **Table 7.8**. An increment is found in the Kg value with respect to sPLA which gives higher value of the free energy for nucleation. The increment in the free energies suggests that higher energy would be needed for the crystallization (i.e.) the interface development is taking high amount of energy during formation of nucleation which is also dependent on the diffusion of polymer chains from the bulk to nucleation site. The enhancement in the Kg value also confirms the regularity in the chain folding or less defects in the crystals that will need more energy as compared to pristine sPLA. It is also confirmed by the increased free energy for nucleation. The POM images related to sPLA and sPLA-HAP biocomposites are shown in **Table 7.9**.

Table 7.7: Kinetic parameters for the isothermal crystallization of sPLA-HAP biocomposite.

T_c (°C)	$t_{1/2}$ (min) (exp.)	n	k (min^{-n})	$t_{1/2}$ (min) (cal.)	t_{max} (min)	$\tau_{1/2}$ (min^{-1})	ΔE_a ($kJ.mole^{-1}$)
sPLA							
120	4.3	2.0	42.7×10^{-3}	4.0	3.4	0.248	
140	8.3	1.8	15.6×10^{-3}	8.2	6.4	0.121	-57.0
160	21.1	2.0	1.6×10^{-3}	20.8	17.7	0.048	
sPLA-0.5% HAP							
120	0.8	1.7	1356.7×10^{-3}	0.7	0.5	1.49	
140	1.6	1.9	533.4×10^{-3}	1.2	0.9	0.87	-75.4
160	4.8	1.5	52.1×10^{-3}	5.6	3.5	0.18	
sPLA-1.0% HAP							
120	0.6	1.7	2037.9×10^{-3}	0.5	0.4	1.89	
140	1.1	1.9	330.7×10^{-3}	1.5	1.2	0.68	-81.5
160	4.6	1.5	58.7×10^{-3}	5.2	3.2	0.19	
sPLA-2.5% HAP							
120	0.4	1.4	2916.6×10^{-3}	0.4	0.2	2.79	
140	1.1	2.3	526.4×10^{-3}	1.1	1.0	0.89	-84.5
160	4.5	2.3	23.7×10^{-3}	4.3	4.0	0.23	

T_c: Crystallization temperature, t_{max}: Time at rate of crystallization is max, $G=\tau_{1/2}$: Crystallization rate

Table 7.8: Thermodynamic parameters for sPLA and sPLA-HAP biocomposites.

Sample Name	K_g (K^2)	$\sigma\sigma_e$ ($erg^2.cm^{-4}$)	ΔG^* (erg)
sPLA	6.3×10^5	507.7	7.1×10^{-13}
sPLA-0.5%HAP	6.6×10^5	533.0	7.4×10^{-13}
sPLA-1.0%HAP	7.0×10^5	566.5	7.9×10^{-13}
sPLA-2.5%HAP	7.6×10^5	608.6	8.5×10^{-13}

Table 7.9: POM images of spherulites of sPLA and sPLA-HAP biocomposites at different times.

T=140°C	sPLA	sPLA-0.5%HAP	sPLA-1.0%HAP	sPLA-2.5%HAP
0 min		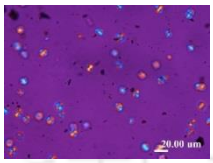	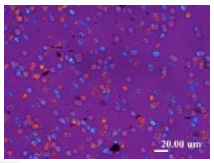	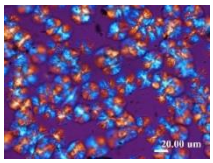
5 min		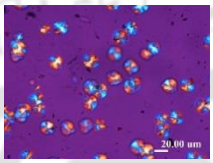	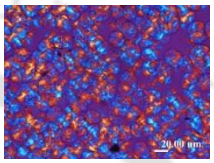	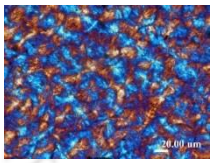
10 min	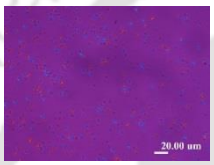	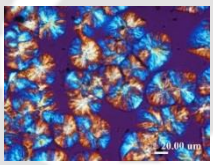	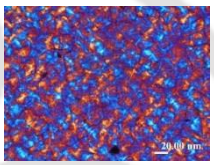	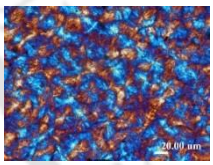
20 min	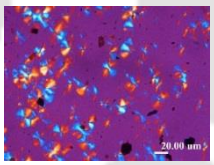	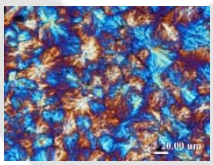	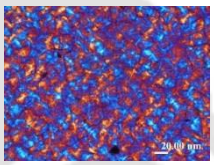	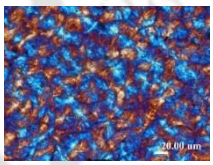
30 min	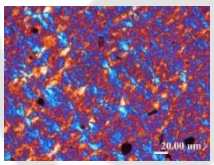	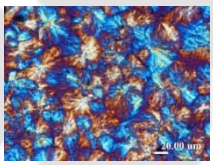	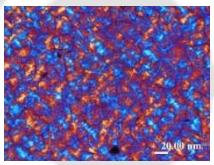	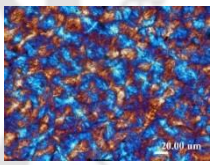

7.6. Conclusions

From the above discussion, it can be concluded that the addition of fillers significantly enhance the crystallizability of polymer matrix which ultimately helps in the formation of stereocomplex crystals. It is found that the use of different fillers affect the crystallization process differently. The dual characteristic of the fillers after modification seems to be competitive in nature. As one way they act as facilitator for the crystallization and another way they may hinder the polymer chains to be crystallized. Cellulose microcrystals are working as nucleating agent for overall crystallization where the grafted PLA chains provided the facility for the formation of stereocomplex crystallites. Whereas, as per data discussed, the modified chitosan and grafted HAP did not work as nucleating agent but helped for the formation of stereocomplex crystallites. The Avrami analysis suggested that all used fillers are responsible for the higher overall crystallization rate and the spherulite growth rate is increased which may be due to the filler content. The activation energy for sPLA-CMC biocomposite is reduced which indicate the nucleation activity due to the presence of CMC where as in the case of sPLA-MCH and sPLA-HAP, it is increased indicating that the crystallization process needs excess energy. It is found that the fold surface free energy of sPLA-CMC biocomposite decreased with increase in the grated CMC content which showed the nucleation effect of CMC. On the other hand, these energies are higher for sPLA-MCH and sPLA-HAP biocomposites which indicate that the nucleation is not facilitated by MCH or grafted HAP but done by the presence of grafted polymer chains. This difference in the results also conclude that the CMC may be responsible for the heterogeneous nucleation whereas MCH and grafted facilitate the uniform nucleation.

CHAPTER: 8

Degradation Studies of Stereocomplex PLA and Fabricated Biocomposites

Abstract

Thermal stability of the stereocomplex biocomposite is important to prove its application at elevated temperature. In this chapter, thermogravimetric analysis of the prepared biocomposites has been carried out using dynamic heating rate. The Differential Thermogravimetric analysis confirms that the decomposition is one step process and the biocomposites are stable till 300°C temperature which is significantly higher than the processing temperature of the laboratory synthesized PLA i.e. 180-220°C. The KAS and OFW isoconversional methods are used to measure the activation energy for the degradation process. The evolved gases from the TGA analysis are also studied by the coupled TGA and FTIR techniques.

8.1 Introduction

The effect of different external physical as well chemical conditions on the properties of the polymers, such as chemical structure and physical properties, due to the chemical reaction or bond breaking is responsible for the degradation of PLA which leads to the deterioration of the starting material [225]. The process of degradation involves radiation [226], oxidative [227], pyrolytic [228], mechanical [229], photocatalytic [230] catalytic [231] and biodegradation [232-234] etc. The energy generation or recycling of the polymer iste in the form of useful byproducts generated during thermal degradation is the preferred approach by the existing industries [235]. The change in the chemical structure starts at elevated temperature and generates the byproduct which is refers as thermal degradation of polymers [236].

After the synthesis of biobased polymers and development of polymer biocomposite and its application in different areas, it is extremely important to know the behavior of polymer at different conditions such as in moisture, heat, radiation, plasma, stress etc. Generally, after service life, polymers are incinerated or dumped into the soil or oceans and sometimes the energy generated by the degradation of polymers is utilized for the different purposes [237]. In case of biodegradable polymers, it is known that the biodegradable polymer, such as PLA, easily degrades in hydrolytic, enzymatic conditions and generates nontoxic byproducts [238]. The degradation occurring during elevated temperature may generate different type of gases and byproducts depending on the thermal conditions [239]. In the development of the polymer processing units/equipments, it is advantageous to know the behavior of polymers at elevated temperature. It is also very important to understand the mechanism of thermal degradation of polymers in order to develop the final product. The final products can be made out of pristine polymer or blends of polymers, additives, fillers

etc [29, 240-243]. The effect of different fillers or additives on degradation behavior of developed polymer needs to be studied in order to understand the kinetics and mechanism of degradation.

8.2 Theory

The rate of conversion or transformation in the solid state reaction is generally assumed as the product of two functions such as temperature (T) and fraction of conversion or degree of conversion (α) [244]. The relation can be shown as

$$\frac{d\alpha}{dt} = k(T)f(\alpha) \quad 8.1$$

where, f (α) is the function of conversion and k (T) is the temperature dependent function which can be given by Arrhenius equation

$$K = Ae^{-\frac{E_a}{RT}} \quad 8.2$$

The conversion factor (α) is defined as

$$\alpha = \frac{W_o - W_t}{W_o - W_f} \quad 8.3$$

where, W_o, W_t and W_f are the initial, at time t and final weight of the polymer. After combining equation 8.1 and 8.2, we get

$$\frac{d\alpha}{dt} = A\,exp\left(-\frac{E_a}{RT}\right)f(\alpha) \quad 8.4$$

Where, E_a is the activation energy, T, A and R are the temperature in Kelvin, pre-exponential factor and gas constant, respectively. The values of A, Ea and f (α) are called as kinetic triplets. For any non-isothermal investigation, the rate of reaction is governed by these kinetic triplets.

The equation is considered as general expression for the isothermal analysis condition. For the nonisothermal conditions, heating rate needs to be described in the equation and the degradation of polymer as function of temperature. Equation can be modified and written as

$$\frac{d\alpha}{dT} = \frac{A}{\beta}\exp\left(-\frac{E_a}{RT}\right) f(\alpha) \qquad 8.5$$

Where, β is the heating rate defined as $\beta = dT/dt$

Several methods have been developed by the researchers to determine the kinetic triplet. These methods can be categorized in two segments: one being isoconversional method or model free method which is based on the assumption that the conversion function is independent on the heating rate in the all range of conversion fraction and the second being the model fitting method which is grounded on reaction model and depends on the rate constant. It is believed that the model fitting method does not clearly measure the temperature dependent constant and reaction model. So, the model fitting method is considered as approximation method [245].

Several isoconversional methods such as Ozawa-Flynn-Wall (OWF) [246], Friedmann [247], Kissinger-Akahira-Sunose (KAS) [248], and Augis-Bennett [249] etc. are proposed by scientists. In case of isoconversional methods, it is believed that they give accurate activation energy. The temperature is measured corresponding to different values of conversion fraction at different heating rates. Without consideration of assumption of reaction model function, calculation of pre-exponential factor is not possible. It can also be concluded from the literature and suggested by the several researchers that for reliable kinetic evaluation one should use the models that employ kinetic curves obtained at multiple rates rather than the kinetic curve with single rate [245]. Furthermore, if the

calculated activation energy is constant irrespective of conversion factor or not dependent on the conversion factor then the reaction would be defined as one step reaction and otherwise the reaction would be called as complex or multistep reaction. In this study the kinetic analysis using two isoconversional methods i.e. Ozawa-Flynn-Wall (OWF) and Kissinger-Akahira-Sunose (KAS) has been carried out.

8.2.1 Ozawa-Flynn-Wall (OWF) method

Ozawa OWF is the isoconversional method and an integral method which utilizes the Doyle's approximation [250]. In this method, it is assumed that the temperature dependent reaction rate is governed by the Arrhenius equation. So, the equation 8.5 can be integrated and written as

$$g(\alpha) = \int_0^{\alpha} d\alpha / f(\alpha) = \frac{A}{\beta} \int_{T_o}^{T} \exp(-\frac{E_a}{RT})\, dT \qquad 8.6$$

Where, g(α) is the integral of function of conversion, T_o is the initial temperature when reaction is notified which can be assumed as zero. Equation 8.6 can be written as

$$\ln g(\alpha) = \ln(\frac{AE_a}{T}) - \ln \beta + \ln p(x) \qquad 8.7$$

where, $p(x) \approx \exp(-x)/x - \int_{\infty}^{x} \exp(-x)/x\, dx$ and $x = E_a/RT$

Using the Doyle's approximation, p(x) can be evaluated as

$$\ln p(x) \approx -5.3305 - 1.0516x \qquad 8.8$$

Combining equation 8.7 and 8.8, we get

$$\ln \beta = \ln\left(\frac{AE_a}{R}\right) - \ln g(\alpha) - 5.3305 + 1.0516\left(\frac{E_a}{RT}\right) \qquad 8.9$$

The relation between heating rate and temperature corresponds to the respective conversion (fractional weight loss) can be given as [246, 251-253]

$$\ln \beta = \ln\left(\frac{AE_a}{Rg(\alpha)}\right) - 5.3305 - 1.0516\frac{E_a}{RT} \quad 8.10$$

The activation energy can be evaluated from the slope of the plot of ln β versus 1/T which gives straight line. The activation energy (E) calculated from the TGA data is the sum of activation energies of chemical reaction and physical processes. The energy can be related to the breakage of chemical bonds. The activation energy can be defined as excess energy obtained from vibration of molecules or atom at a particular temperature. If the value of the activation energy is equal for all particular fraction of conversion, then the solid state reaction would be concluded as single step reaction otherwise it called as complex reaction mechanism.

8.2.2 Kissinger-Akahira-Sunose (KAS) method

When the change in the rate of heat occurs while other parameters are constant, the position of peak varies. This variation in the peak can be used to measure the activation energy for the reaction. Equation 8.5 is integrated with initial conditions of α = 0 at T = T_o to reach the following expression

$$g(\alpha) = \int_0^{\alpha} d\alpha/f(\alpha) = \frac{A}{\beta}\int_{T_o}^{T} \exp(-\frac{E_a}{RT})\, dT = \frac{AE_a}{\beta R} p\left(\frac{E_a}{RT}\right) \quad 8.11$$

Kissinger-Akahira-Sunose (KAS) method [248] is based on the assumption that the pre-exponential factor (A), conversion function and activation energy are independent of conversion factor. This method accounts for the Coats-Redfern approximation [254] as

$$p\left(\frac{E_a}{RT}\right) \cong \frac{\exp\left(-\frac{E_a}{RT}\right)}{\left(\frac{E_a}{RT}\right)^2} \quad 8.12$$

The relation can be written after placing equation 8.12 in equation 8.11

$$\ln\frac{\beta}{T^2} = \ln\left(\frac{AR}{E_a g(\alpha)}\right) - \left(\frac{E_a}{RT}\right) \quad 8.13$$

Thus, plot of ln (β/T^2) versus 1/T for particular fractional conversion will give straight line. The activation energy can be calculated from the slope of the line.

Thermogravimetric analysis (TGA) is the unique technique to study the thermal degradation of polymers under either isothermal or nonisothermal conditions and to evaluate their relative thermal stability. Material can be studied by TGA where weight change of specimen is recorded at a constant heating rate. Thermogravimetry or nonisothermal analysis is advantageous over the isothermal or constant temperature measurement because the sample behavior or structure may change while heating to particular temperature. The change in the initial structure of sample may complicate the data of isothermal measurement which may lead to the difficulty in data analysis or conclude in wrong analysis.

The main drawback is that alone TGA cannot give the information about the gases generated during thermal degradation of the polymers. So, it also very important to monitor the evolved gases in real time. TGA coupled with FTIR (TG-IR) is the recently developed technique using which we can monitor the gases evolved during thermal degradation investigation. In the process of thermal degradation, many volatile species can be generated and the analysis of those species can give the essential information. The TG-IR technique is an effective method to analyze the volatile component during thermal degradation and can give complete description of the mechanism of degradation. In this method, the TGA

is coupled with FTIR via a transfer line with constant temperature facility. The transfer line and the FTIR sample cells are heated at particular temperature to protect the condensation of the evolved gases. The spectra are recorded continuously at particular time interval. The FTIR spectra of the gaseous species at different stages of degradation can give the qualitative as well as quantitative analysis of the material of interest.

In this chapter, thermal degradation kinetics of the developed stereocomplex PLA is studied and the effect of different modified fillers on the degradation behaviors of sPLA is discussed.

8.3 Experimental section

The weight loss at elevated temperature is measured using thermo-gravimetric analysis (TGA, Perkin Elmer). Weight loss of sample (6-8 mg) is recorded by heating in the temperature range from 30°C to 600°C at a heating rate of 10°C.min^{-1} under an inert environment of nitrogen gas. The data generated from the TGA is processed as per the model of interest.

The volatile component generated during the thermal degradation of sPLA and its CMC, MCH and HAP biocomposite are analyzed using Perkin Elmer TGA 4000 thermo-gravimetric analyzer coupled with FTIR (Frontier 4000) through TL 8000 transfer line. High purity nitrogen gas with a flow rate of 50 mL.min^{-1} is applied to maintain the inert atmosphere. The FTIR spectra are recorded in the spectral range of 4000- 650 cm^{-1} and 8 cm^{-1} resolution is selected at an average of 4 scans.

The activation energies are calculated by using two model free methods i.e. Kissinger-Akahira-Sunose (KAS) method and Ozawa-Flynn-Wall (OWF) method. Both methods are able to give the information about the activation energy directly. Calculation

of activation energy using two different methods is adopted to confirm the reliability of the measured data. As explained in previous section, both the methods are based on the assumption that the temperature dependent reaction rate is governed by the Arrhenius equation. The difference in both the methods is that they are based on different approximation methods. The plot and analysis of such as curve fitting of the data is done using OriginPro 8.5 software.

8.4 Results and discussion

8.4.1 Thermogravimetric analysis

Figures 8.1 shows the thermogravimetric weight loss and corresponding derivative weight loss of sPLA and sPLA-CMC biocomposites, respectively, in relation to temperature at 5°C.min^{-1} heating rate. The curves obtained from TGA analysis reveal single stage weight loss profile which is also illustrated by corresponding derivative curves. The samples of all biocomposites are found to be thermally stable till ~300°C which is far higher than the required processing temperature i.e. 180°C-250°C of the laboratory synthesized PLA under identical reaction conditions. It is confirmed from the TGA analysis that the all samples had only one degradation step between 300°C to 370°C which showed there is no element degrading at a lower temperature. It is known that PLA exhibits the degradation in one step decomposition which is also shown by current analyzed samples. One step decomposition is attributed to the formation of volatile entity that generate between the temperature range of 300°C to 370°C. It is very advantageous for polymers to be degraded in single step decomposition because the component generated by degradation at lower temperature may accelerate the decomposition of polymer which may lead to the early breakage of the molecules and thus degradation starting near the processing temperature which is not desired during polymer processing.

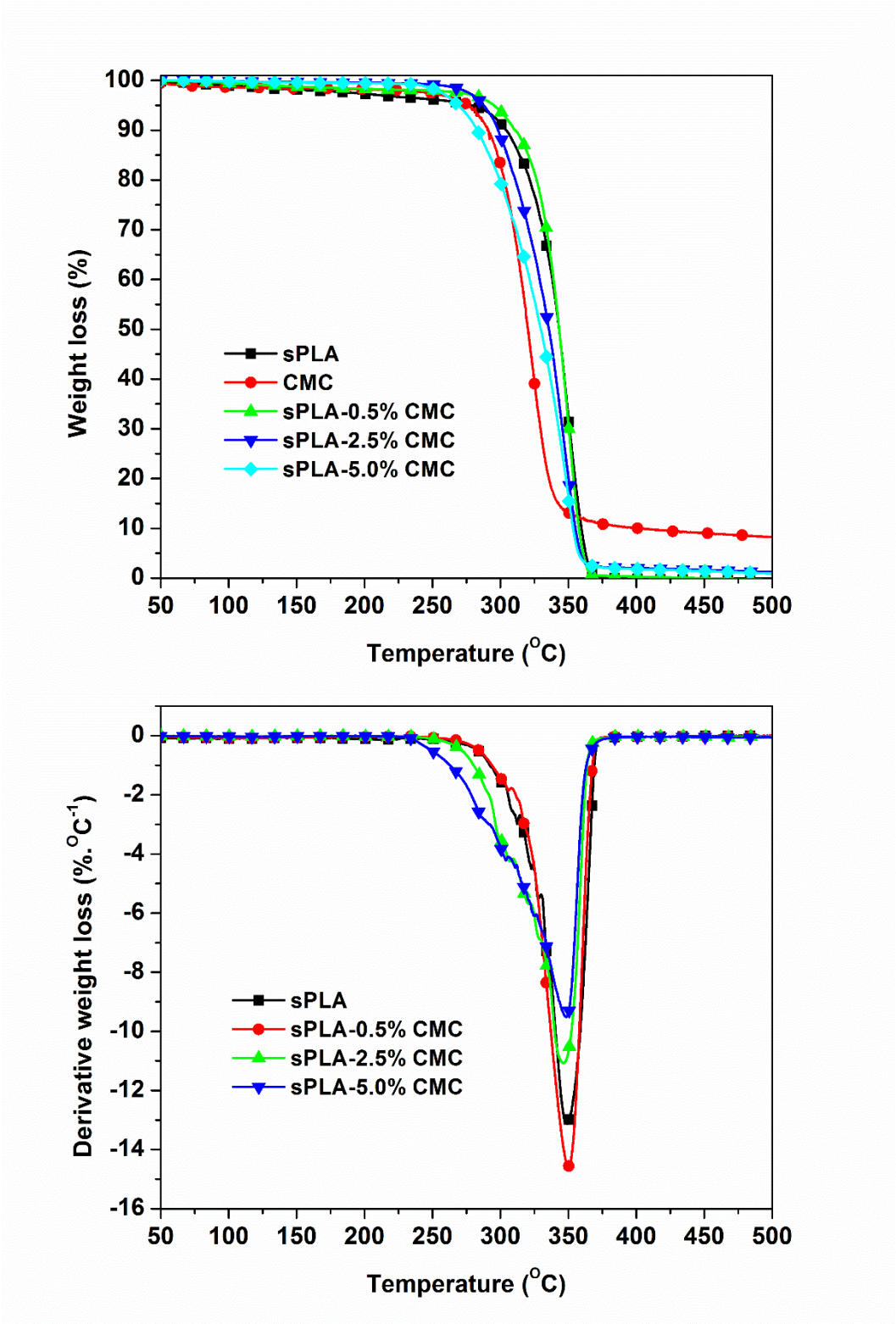

Figure 8.1: Mass loss (%) and derivative thermogravimetric graph of sPLA and sPLA-CMC biocomposite at 5°C.min^{-1}.

Table 8.1: Onset temperature, maximum degradation temperature and temperature at 50% degradation temperature of sPLA and sPLA-CMC biocomposite.

Sample Name	Heating Rate (°C.min^{-1})	T_{onset} (°C)	T_{max} (°C)	T_{50} (°C)
sPLA	**5**	304.3	348.4	371.1
	10	320.8	375.1	371.2
	15	333.5	380.0	367.1
	20	343.8	380.3	343.1
sPLA-0.5%CMC	**5**	327.3	350.4	377.8
	10	337.4	363.8	364.8
	15	346.3	370.1	357.0
	20	360.7	382.4	343.2
sPLA-2.5%CMC	**5**	313.8	346.5	367.8
	10	317.5	366.6	357.6
	15	339.0	366.4	351.8
	20	346.6	375.8	335.7
sPLA-5.0%CMC	**5**	305.2	348.1	367.0
	10	327.0	358.7	358.3
	15	336.4	367.2	347.4
	20	344.9	376.5	329.7

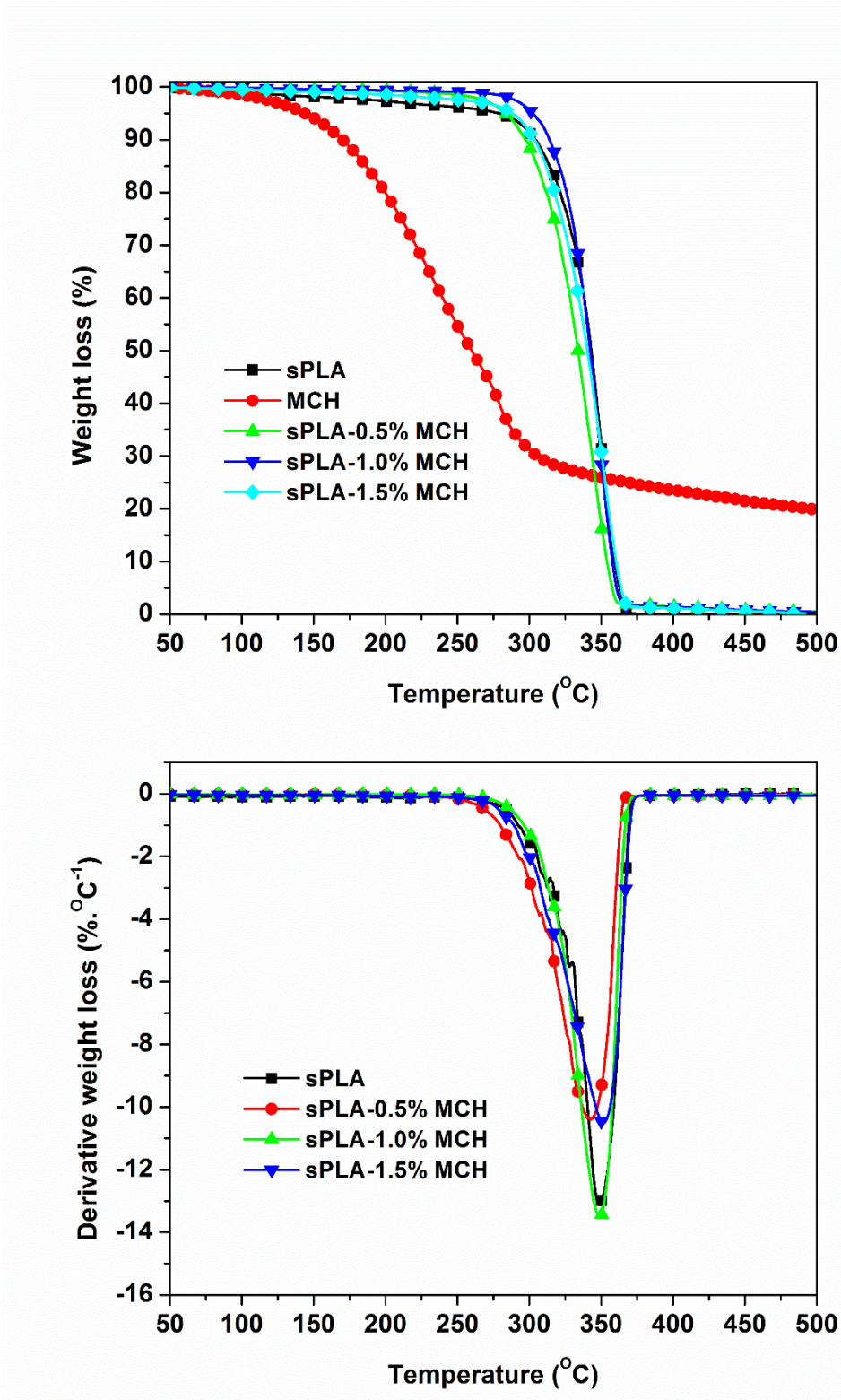

Figure 8.2: Mass loss (%) and derivative thermogravimetric graph of sPLA-MCH biocomposite at 5°C.min^{-1}.

Table 8.2: Onset temperature, maximum degradation temperature and temperature at 50% degradation temperature of sPLA-MCH biocomposite.

Sample Name	Heating Rate (°C.min^{-1})	T_{onset} (°C)	T_{max} (°C)	T_{50} (°C)
sPLA-0.5%MCH	**5**	310.3	342.1	373.5
	10	331.7	364.0	365.5
	15	342.9	375.9	352.6
	20	350.4	383.4	333.8
sPLA-1.0%MCH	**5**	322.8	348.5	371.4
	10	337.2	365.1	361.5
	15	338.5	367.9	358.4
	20	350.5	377.6	342.3
sPLA-1.5%MCH	**5**	317.8	352.3	376.6
	10	328.9	361.2	367.8
	15	345.5	371.8	351.0
	20	352.6	377.0	340.3

Maximum degradation temperature, onset degradation temperature and 50% degradation temperature of sPLA and sPLA-CMC, sPLA-MCH and sPLA-HAP are listed in **Table 8.1**. It is observed that the pristine sPLA starts decomposing at ~304°C and maximum rate of degradation is found to be ~348°C. The temperature at which 50% pristine sPLA is decomposed and the same is recorded at ~371°C. In case of sPLA-CMC biocomposites, the onset degradation temperature is 23°C higher than sPLA and recorded at 327°C for sPLA-0.5%CMC. T_{onset} is reduced to ~305°C as the content of CMC increased to 5%. The T_{onset} of the pristine CMC is ~303°C, therefore the presence of CMC may be responsible for the reduction in the degradation temperature. However, it is always higher than pristine sPLA. Similarly, the maximum degradation temperature is also first increased to ~350°C for sPLA-0.5%CMC which then reduced to ~348°C for sPLA-5%CMC. The lower degradation temperature of the CMC may be responsible for the further reduction in the T_{onset} and T_{max} with increase in the CMC content. The product formed during CMC degradation may be accelerating the decomposition of biocomposite. The temperature for 50% degradation is found to be comparable.

The gravimetric plot and degradation data of sPLA-MCH biocomposites are presented in **Figure 8.2** and **Table 8.2** respectively. It is clear from the previous chapters that the addition of modified chitosan enhances the stereocomplexation in the polymer matrix. The extended molecular surface area provided by modified chitosan is responsible for the enhancement in stereocomplexation. T_{onset} is increased to ~323°C in case of sPLA-1.0%MCH which is ~19°C higher than 304°C for sPLA and again it is reduced to 318°C for sPLA-1.5%MCH. As we know that the chitosan is modified with low molecular weight PLA which had lower decomposition temperature (~200°C) and thus it may be responsible for the reduction in the degradation temperature.

The temperature for maximum degradation rate is found to be higher than sPLA and varied between ~342°C to ~353°C which suggests that the MCH biocomposite is thermally stable compared to pristine sPLA. The temperature for the 50% weight loss is found comparable and varied between 271°C to 377°C. Increased amount of stereocomplex crystallites in the polymer matrix may be stabilizing the melt biocomposite and sustained for the longer time at elevated temperature due to which the T_{onset}, T_{max} are higher for sPLA-MCH in comparison to sPLA. Another reason for higher T_{onset} and T_{max} may be the char formation after degradation of chitosan which decelerates the degradation process and prevents the cleavage of polymer chains.

The plot and data related to percentage mass loss and derivative mass loss for sPLA-HAP biocomposites is shown in the **Figure 8.3** and **Table 8.3**. The data obtained from the TGA analysis suggests that the onset degradation temperature for sPLA-HAP biocomposite is comparable with pristine sPLA. Temperature for maximum degradation rate and 50% weight loss is also found to be comparable with sPLA and varied between ~341°C to ~345°C and ~366°C to ~371°C, respectively. There is no significant reduction in the thermal property of sPLA-HAP in comparison to sPLA.

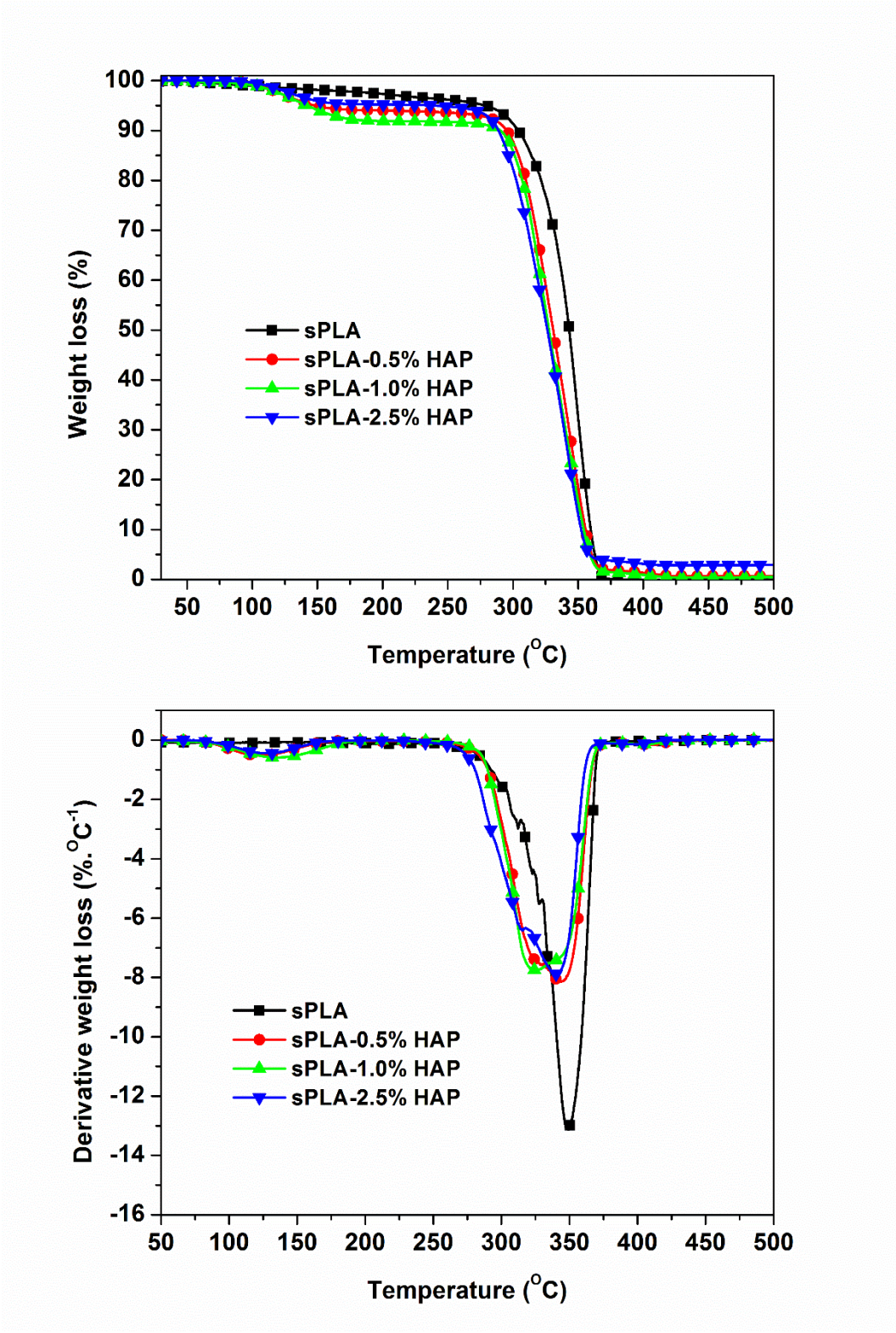

Figure 8.3: Mass loss (%) and derivative thermogravimetric graph of sPLA-HAP biocomposite at 5°C.min^{-1}.

Table 8.3: Onset temperature, maximum degradation temperature and temperature at 50% degradation temperature of sPLA-HAP biocomposite.

Sample Name	Heating Rate (°C.min^{-1})	T_{onset} (°C)	T_{max} (°C)	T_{50} (°C)
sPLA-0.5%HAP	**5**	305.5	344.8	369.6
	10	323.2	363.5	361.7
	15	335.3	370.2	352.0
	20	343.8	378.4	334.6
sPLA-1.0%HAP	**5**	300.1	339.9	367.8
	10	320.8	361.4	360.4
	15	333.4	370.1	349.5
	20	340.9	373.6	331.3
sPLA-2.5%HAP	**5**	302.5	340.6	365.5
	10	314.4	357.4	354.9
	15	326.7	362.7	344.5
	20	338.5	371.6	330.4

8.4.2 Thermal degradation kinetics

The data for weight loss of sPLA and biocomposite due to the thermal degradation at elevated temperature obtained from TGA is analyzed by isoconversional models to estimate the activation energy of decomposition. TGA analysis is done at different heating rates of 5, 10, 15 and 20°C.min^{-1} in nitrogen atmosphere. Two isoconversional methods i.e. Ozawa Flynn Wall (OWF) model and Kissinger Akahira Sunose (KAS) model are based on the assumption that the activation energy is governed by the Arrhenius equation which gives the relation between reaction rate which is temperature dependent and temperature. The difference between these two methods are that they use different approximation methods. The OWF is based on Doyle's approximation and the other is based on Coats-Redfern approximation. The KAS and OFW plots for sPLA and sPLA-CMC are presented in **Figure 8.4, 8.5** and **Figure 8.6, 8.7,** respectively. The deviation in the slope of plots against conversion factor suggests that the solid state decomposition of the biocomposite is taking place through complex reaction mechanism. The activation energy against conversion factor (α) calculated using KAS and OFW models are shown in **Table 8.4** and **Table 8.5**, respectively. The activation energies obtained from KAS and OFW models displayed identical trend. Values for sPLA obtained from KAS and OFW model, varied from ~88 kJ.mole^{-1} to ~111 kJ.mole^{-1} with average activation energy of ~103 kJ.mole^{-1} and ~93 kJ.mole^{-1} to ~116 kJ.mole^{-1} with average activation energy of ~108 kJ.mole^{-1}, respectively. There are three zone of conversion factor for activation energy variation. The activation energy is increased from 88 kJ.mole^{-1} to 103 kJ.mole^{-1} for $0.1 \leq \alpha \geq 0.3$ and reached constant 106 kJ.mole^{-1} for $0.4 \leq \alpha \geq 0.7$ which indicates that the decomposition proceeds through the breakage of linkages with similar bond energies. Further, it is increased for $0.8 \leq \alpha \geq 0.9$ from 108 kJ.mole^{-1} to 111 kJ.mole^{-1}.

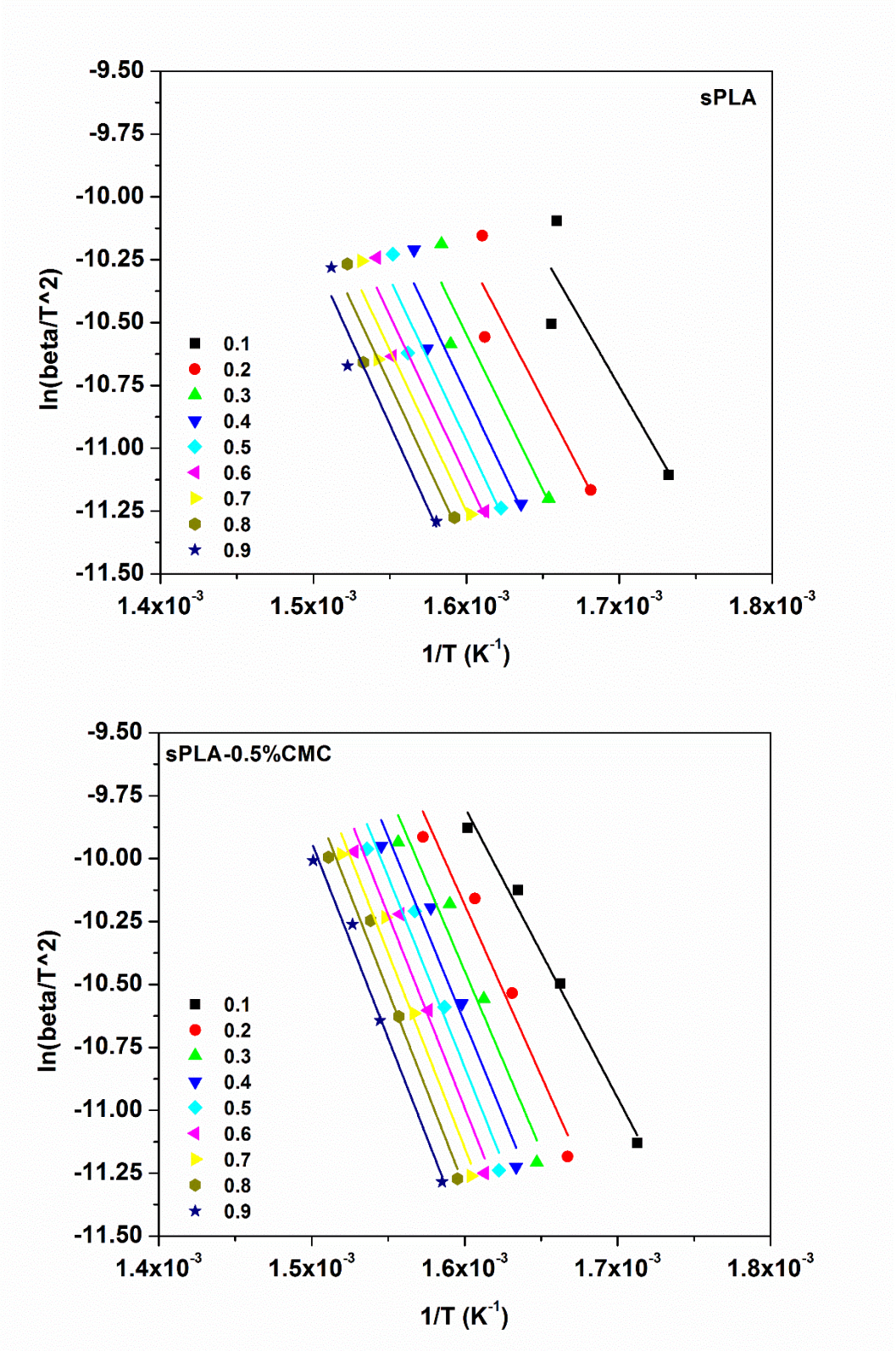

Figure 8.4: KAS plot of sPLA and sPLA-0.5%CMC.

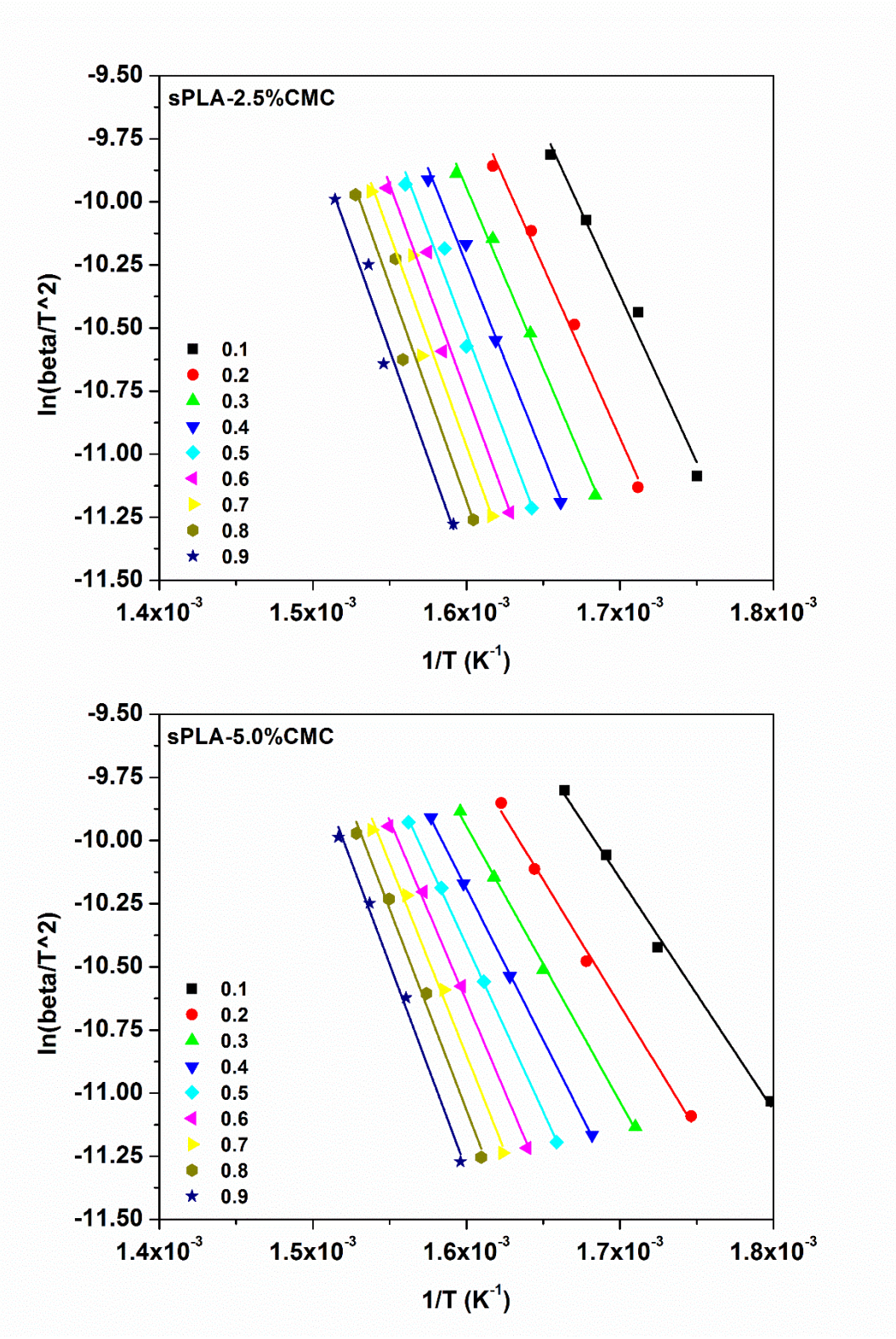

Figure 8.5: KAS plot of sPLA-2.5%CMC and sPLA-5.0%CMC.

Table 8.4: Activation energy for sPLA and sPLA-CMC biocomposite by KAS model.

alpha	Activation Energy (kJ.mole^{-1}) using KAS method			
	sPLA	**sPLA-0.5%CMC**	**sPLA-2.5%CMC**	**sPLA-5.0%CMC**
0.1	87.7	96.1	110.0	76.3
0.2	96.8	112.9	112.9	82.5
0.3	103.3	118.4	118.8	90.7
0.4	106.4	122.7	126.3	99.6
0.5	106.5	125.8	133.6	109.6
0.6	106.7	127.5	137.6	119.0
0.7	106.4	128.6	139.4	126.4
0.8	108.3	129.4	142.1	132.1
0.9	111.1	129.5	141.7	125.3
Avg.	**103.7**	**121.2**	**129.2**	**107.9**

The escalation in the activation energy with increase in conversion factor may indicate that the process of degradation is delayed because the degrading residual material became more refractory and more stable at elevated temperature [255]. In case of sPLA-CMC biocomposite, both KAS and OFW models are fit to the data meaningfully which gave the regression factor (R^2) more than 0.950. The activation energies for sPLA-CMC biocomposites are always increasing as conversion factor increased which indicate that both models sufficiently represent the thermal degradation behavior of biocomposites. Increase in the activation energy with conversion factor suggests that the material becomes more stable than pristine sPLA. For sPLA-0.5%CMC and sPLA-2.5%CMC, activation energies are found to be ~121 $kJ.mole^{-1}$ and ~129 $kJ.mole^{-1}$ which are reduced to 108 $kJ.mole^{-1}$ for sPLA-5.0%CMC.

Table 8.5: Activation energy of sPLA and sPLA-CMC biocomposite by OFW model.

alpha	Activation Energy (kJ.mole^{-1}) using OFW method			
	sPLA	**sPLA-0.5%CMC**	**sPLA-2.5%CMC**	**sPLA-5.0%CMC**
0.1	92.6	100.9	113.8	81.7
0.2	101.6	117.1	116.8	87.8
0.3	108.0	122.4	122.6	95.8
0.4	111.0	126.6	129.8	104.4
0.5	111.2	129.6	136.9	114.0
0.6	111.5	131.2	140.7	123.0
0.7	111.2	132.4	142.6	130.2
0.8	113.1	133.1	145.2	135.7
0.9	115.8	133.3	144.9	138.7
Avg.	**108.5**	**125.2**	**132.6**	**112.4**

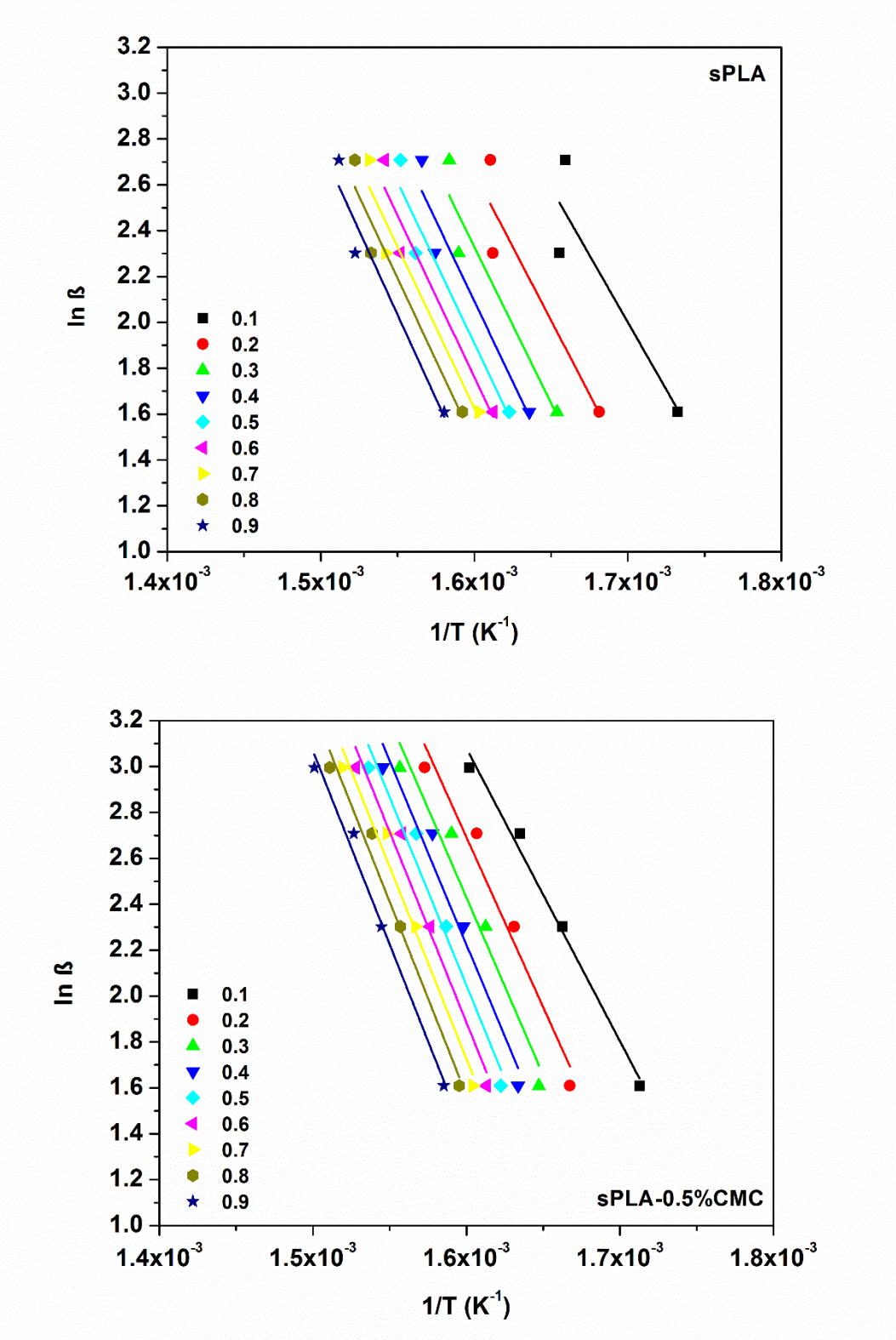

Figure 8.6: OFW plot of sPLA and sPLA-0.5%CMC.

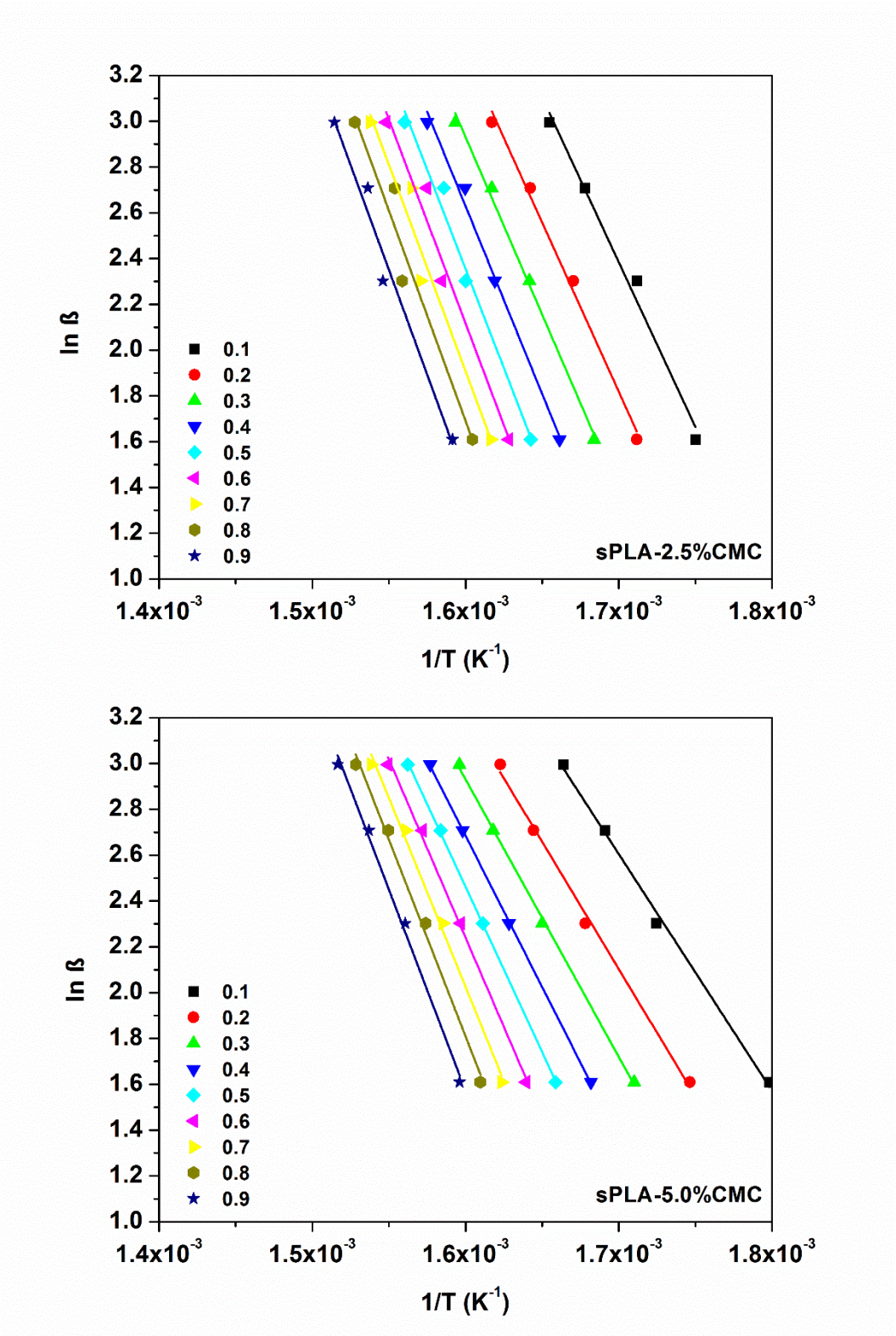

Figure 8.7: OFW plot of sPLA-2.5%CMC and sPLA-5.0%CMC.

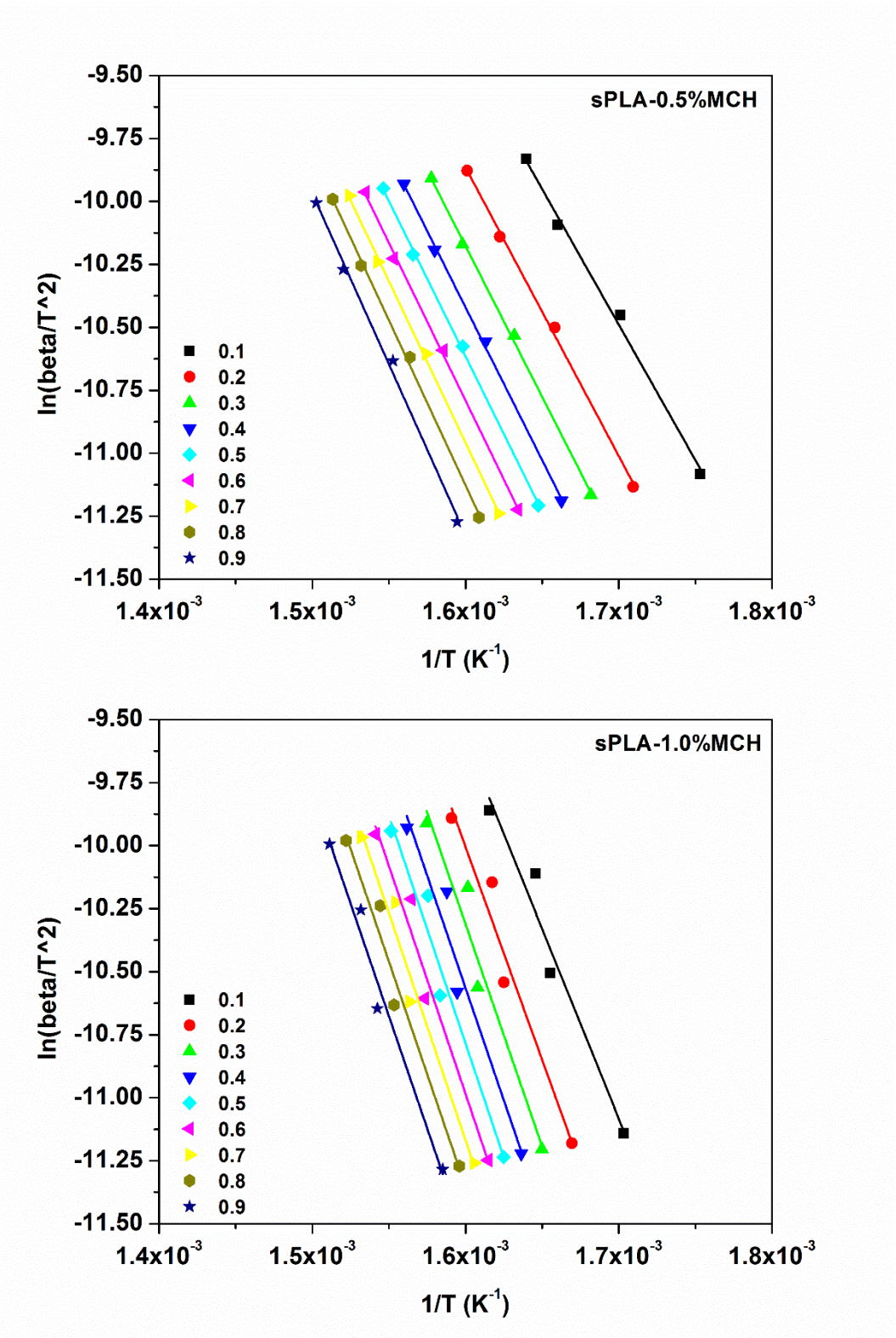

Figure 8.8: KAS plot of sPLA-0.5%MCH and sPLA-1.0%MCH.

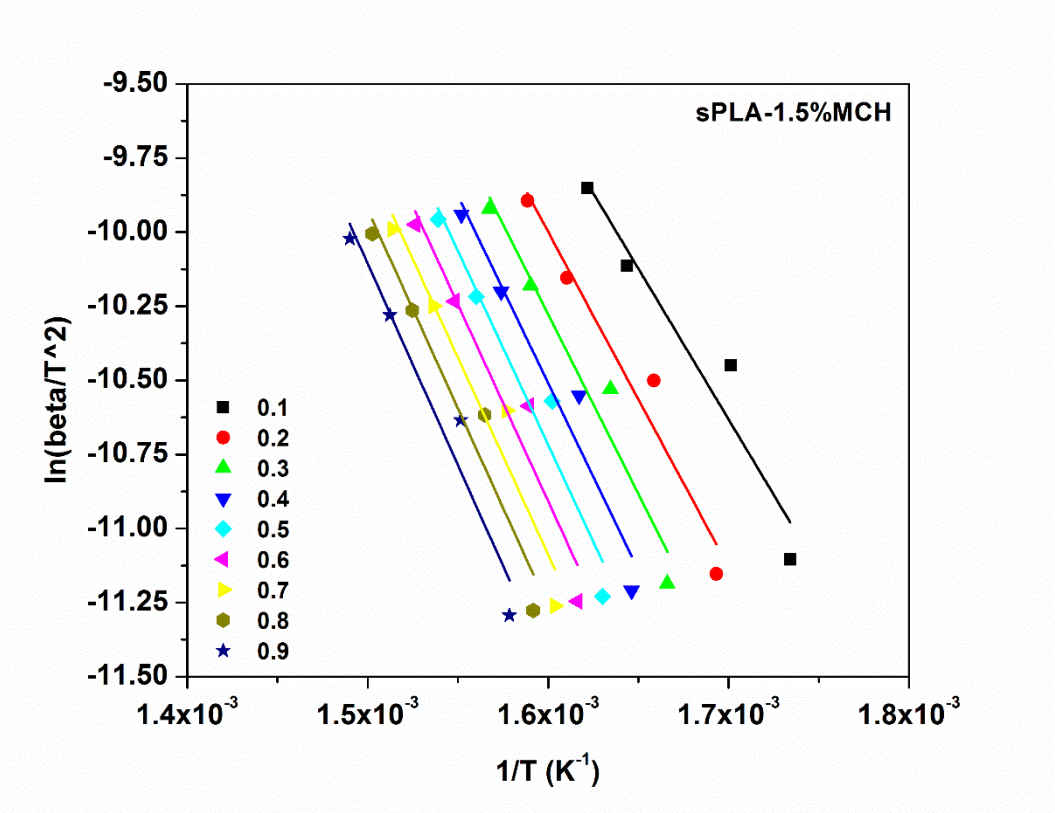

Figure 8.9: KAS plot of sPLA-1.5%MCH.

Modification of CMC via *in situ* ROP and its incorporation in the development of stereocomplex PLA biocomposite may stabilize the material which needed more energy to start breaking of bonds due to which, the activation energy is found higher as compared to pristine sPLA. The reduction in activation energy for sPLA-5.0%CMC may be due to the early degradation of unmodified hydroxyl group of CMC. The species formed due to the decomposition of CMC may accelerate the degradation of the biocomposite and thus lead to the reduction in activation energy. Similar results are found after regression with OFW model which suggest that the both models are suitable to define the degradation process of sPLA-CMC biocomposites. It is also important to note that the degradation of biocomposite is found to be similar as sPLA till 40% conversion which increased significantly thereafter suggesting that the presence of modified CMC stabilized the system.

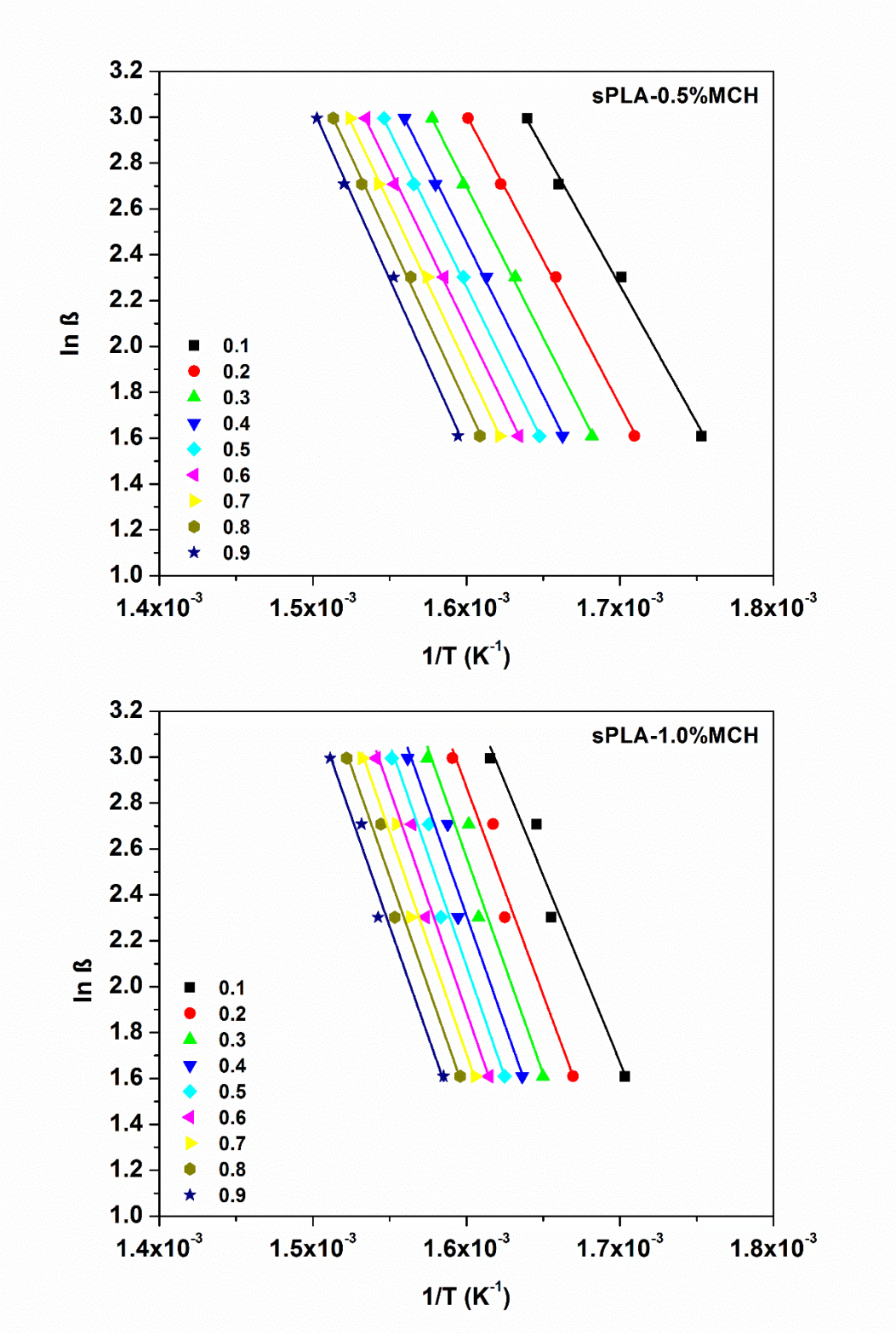

Figure 8.10: OFW plot of sPLA-0.5%MCH and sPLA-1.0%MCH.

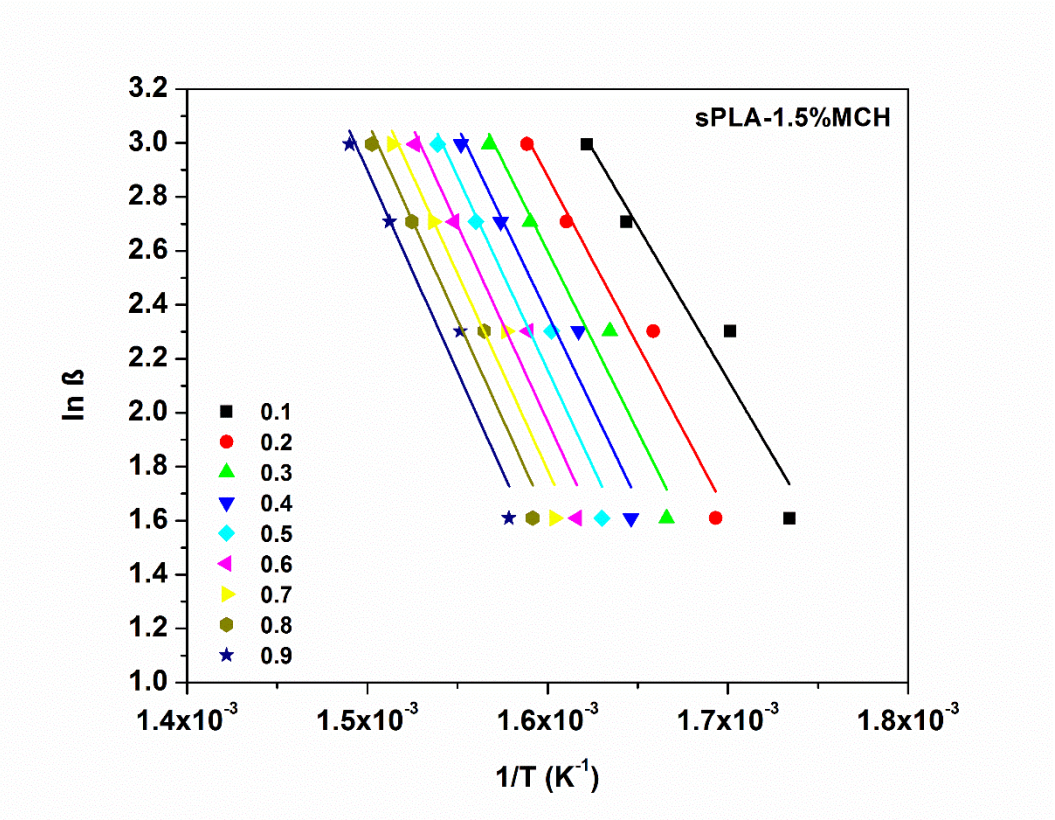

Figure 8.11: OFW plot of sPLA-1.5%MCH.

The KAS and OFW plots of sPLA-MCH and sPLA-HAP biocomposites are shown in **Figure 8.8**, **8.9**, **Figure 8.10**, **8.11** and **Figure 8.12**, **8.13**, **Figure 8.14**, **8.15** respectively. It is shown that the fitted lines are parallel to each other with some variation which suggested the complex reaction mechanism during degradation process of the polymer. The calculated activation energies from the fitted data are listed in the **Table 8.6** and **Table 8.7**. In case of sPLA-0.5%MCH, activation energies are found similar to that of pristine sPLA (~103 kJ.mole^{-1}) whereas it is significantly enhanced to ~145 kJ.mole^{-1} for sPLA-1.0%MCH. The enhancement in the activation energy may be the result of improved thermal resistance of polymer system due to the presence of modified chitosan. Reduction in α for sPLA-1.5%MCH to ~104 kJ.mole^{-1} may be attributed to the quick degradation of low molecular weight PLA molecules connected with the MCH which may act as degradation accelerator for the biocomposites.

Table 8.6: Activation energy for sPLA-MCH and sPLA-HAP biocomposite by KAS model.

alpha	Activation Energy (kJ.mole^{-1}) using KAS method					
	sPLA-0.5%MCH	**sPLA-1.0%MCH**	**sPLA-1.5%MCH**	**sPLA-0.5%HAP**	**sPLA-1.0%HAP**	**sPLA-2.5%HAP**
0.1	89.5	125.2	84.6	111.6	107.2	110.7
0.2	95.3	140.5	94.0	118.7	113.1	114.9
0.3	99.6	146.8	100.8	119.6	114.5	116.8
0.4	100.9	148.1	105.0	118.4	113.6	115.2
0.5	102.6	150.5	108.7	117.8	112.0	115.8
0.6	104.2	150.4	110.4	119.3	112.4	118.3
0.7	106.7	149.8	110.4	122.6	115.0	121.3
0.8	109.0	148.7	111.5	126.7	120.3	125.5
0.9	112.8	148.4	113.0	133.3	128.7	132.3
Avg.	**102.3**	**145.4**	**104.3**	**120.9**	**115.2**	**119.0**

Table 8.7: Activation energy for sPLA-MCH and sPLA-HAP biocomposite by OFW model.

alpha	Activation Energy (kJ.mole^{-1}) using OFW method					
	sPLA-0.5%MCH	**sPLA-1.0%MCH**	**sPLA-1.5%MCH**	**sPLA-0.5%HAP**	**sPLA-1.0%HAP**	**sPLA-2.5%HAP**
0.1	94.4	128.5	89.8	115.4	115.4	114.4
0.2	100.1	143.2	99.0	122.3	116.9	118.5
0.3	104.4	149.3	105.6	123.2	118.4	120.5
0.4	105.8	150.7	109.7	122.2	117.7	119.1
0.5	107.4	153.0	113.3	121.8	116.2	119.9
0.6	109.0	153.0	115.0	123.4	116.7	122.3
0.7	111.4	152.4	115.1	126.5	119.2	125.2
0.8	113.7	151.5	116.2	130.5	124.4	129.4
0.9	117.4	151.3	117.7	136.9	132.5	136.0
Avg.	**107.1**	**148.1**	**109.1**	**124.7**	**119.7**	**122.8**

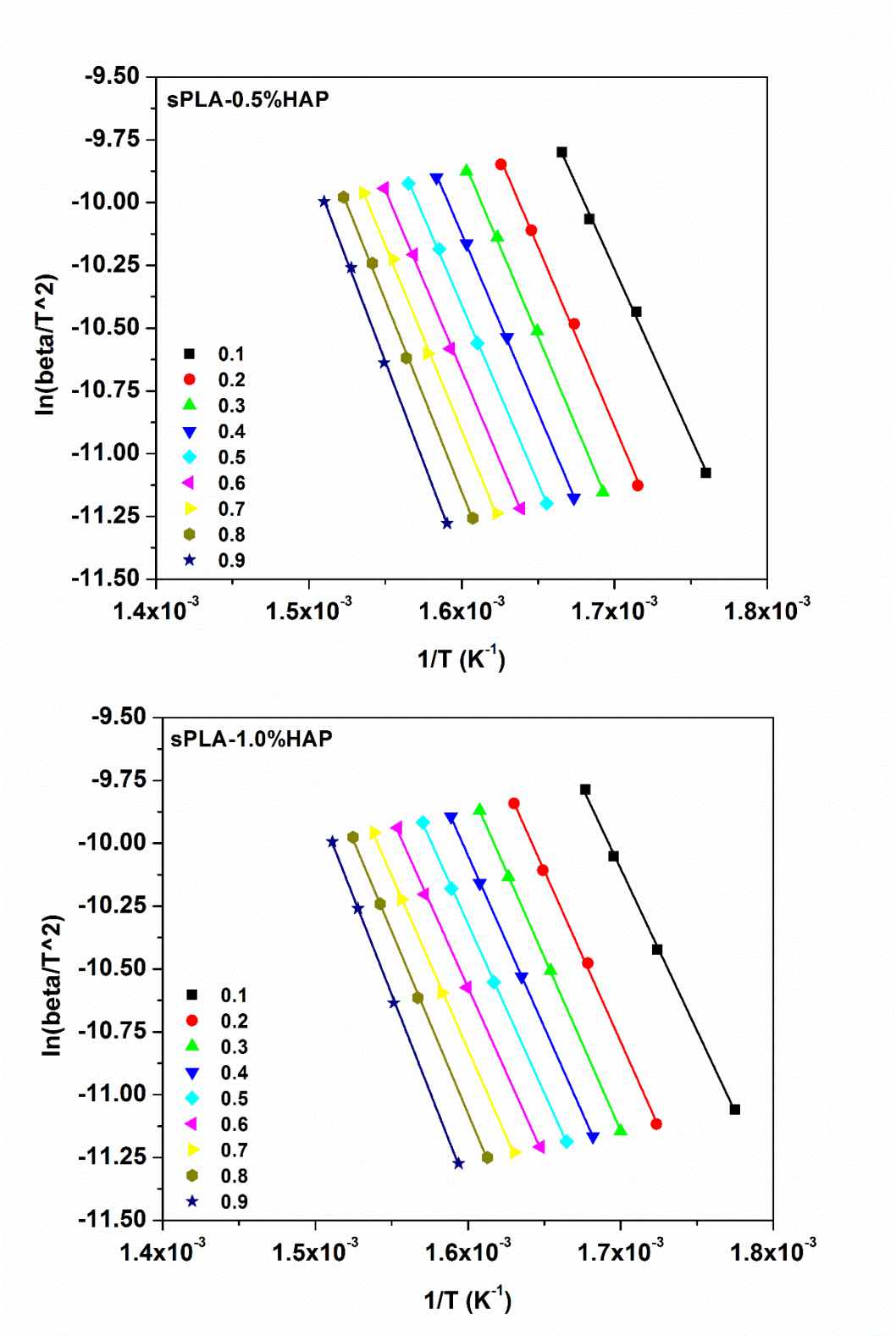

Figure 8.12: KAS plot of sPLA-0.5%HAP and sPLA-1.0%HAP.

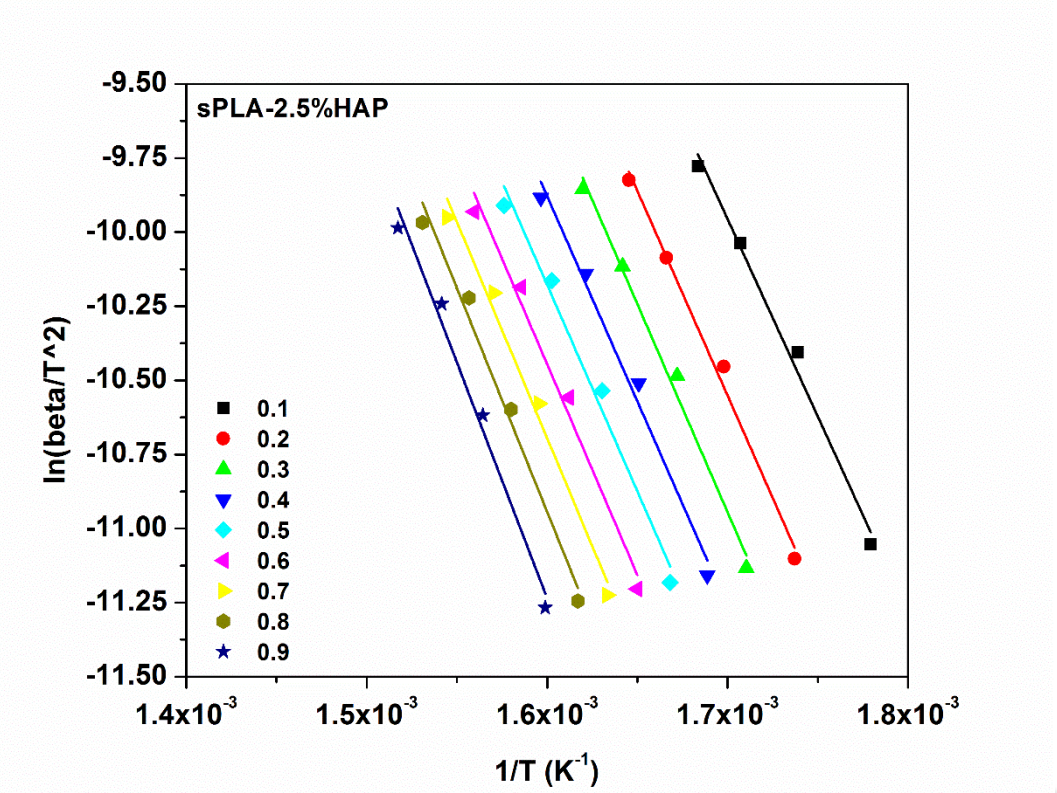

Figure 8.13: KAS plot of sPLA-2.5%HAP.

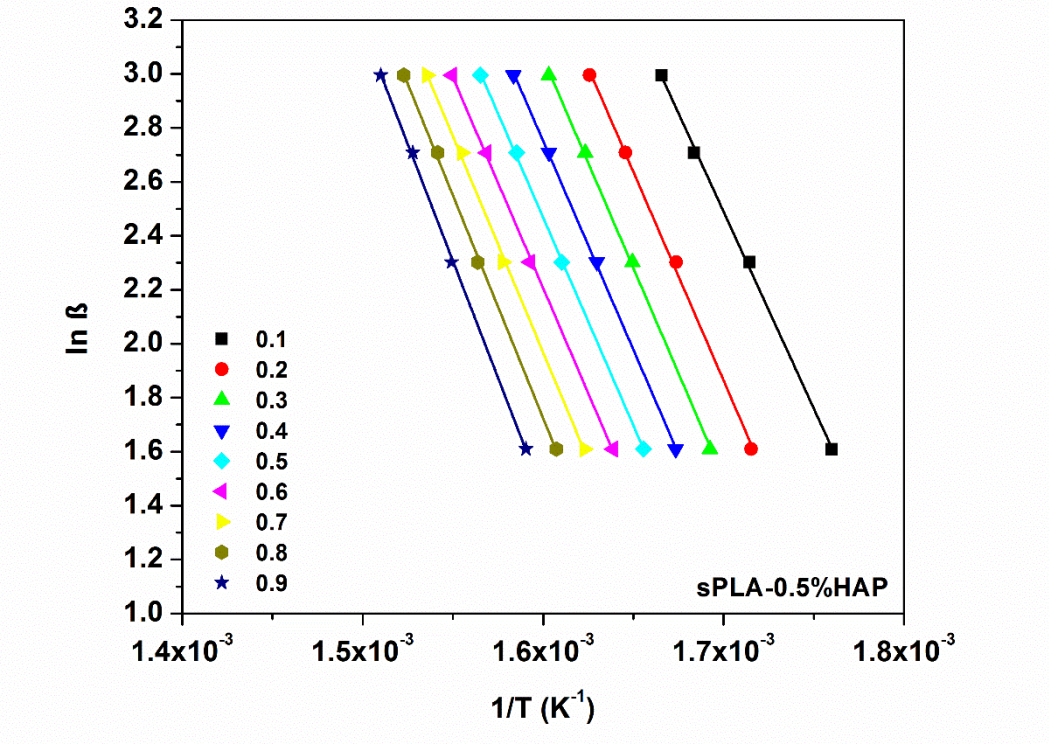

Figure 8.14: OFW plot of sPLA-0.5%HAP.

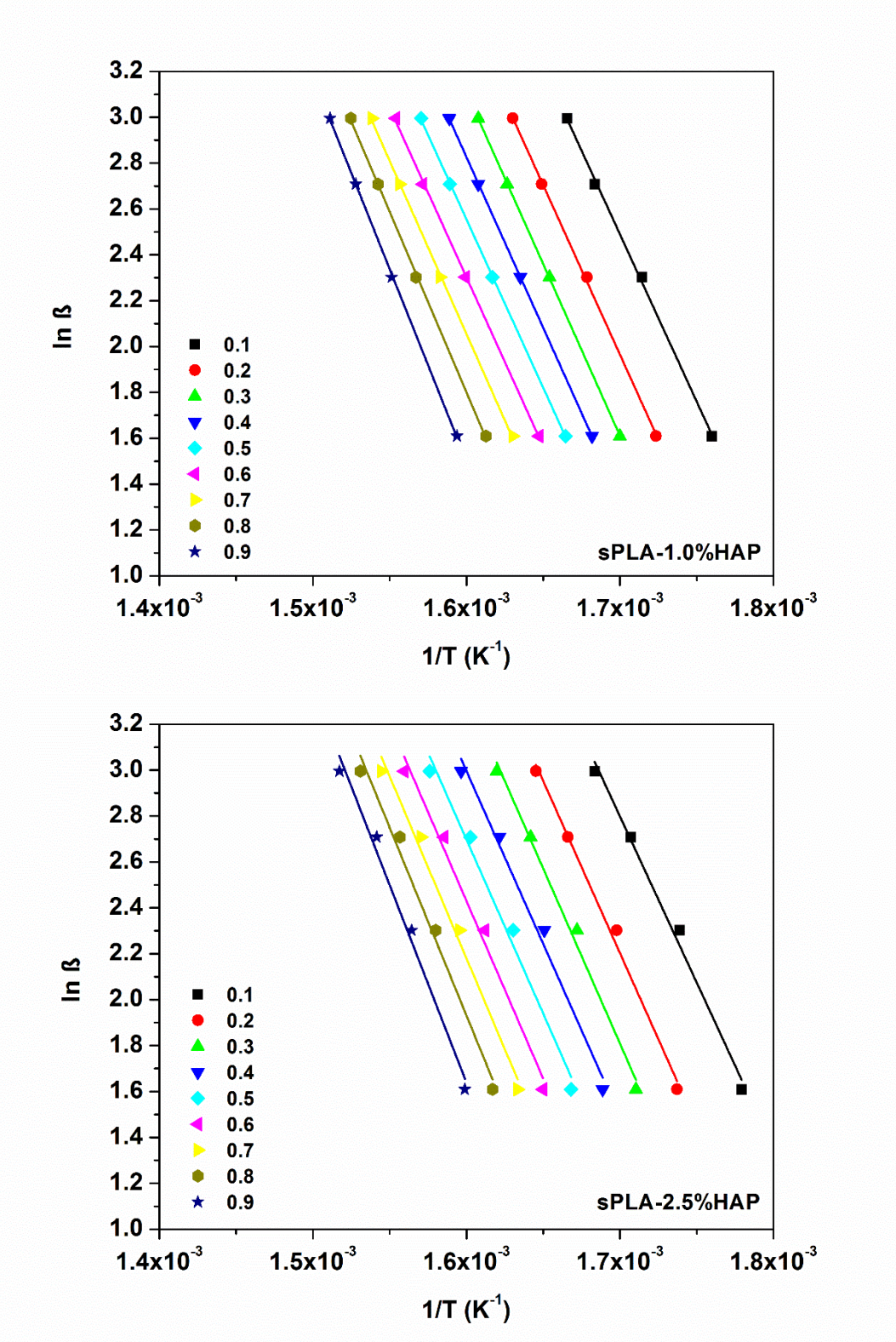

Figure 8.15: OFW plot of sPLA-1.0%HAP and sPLA-2.5%HAP.

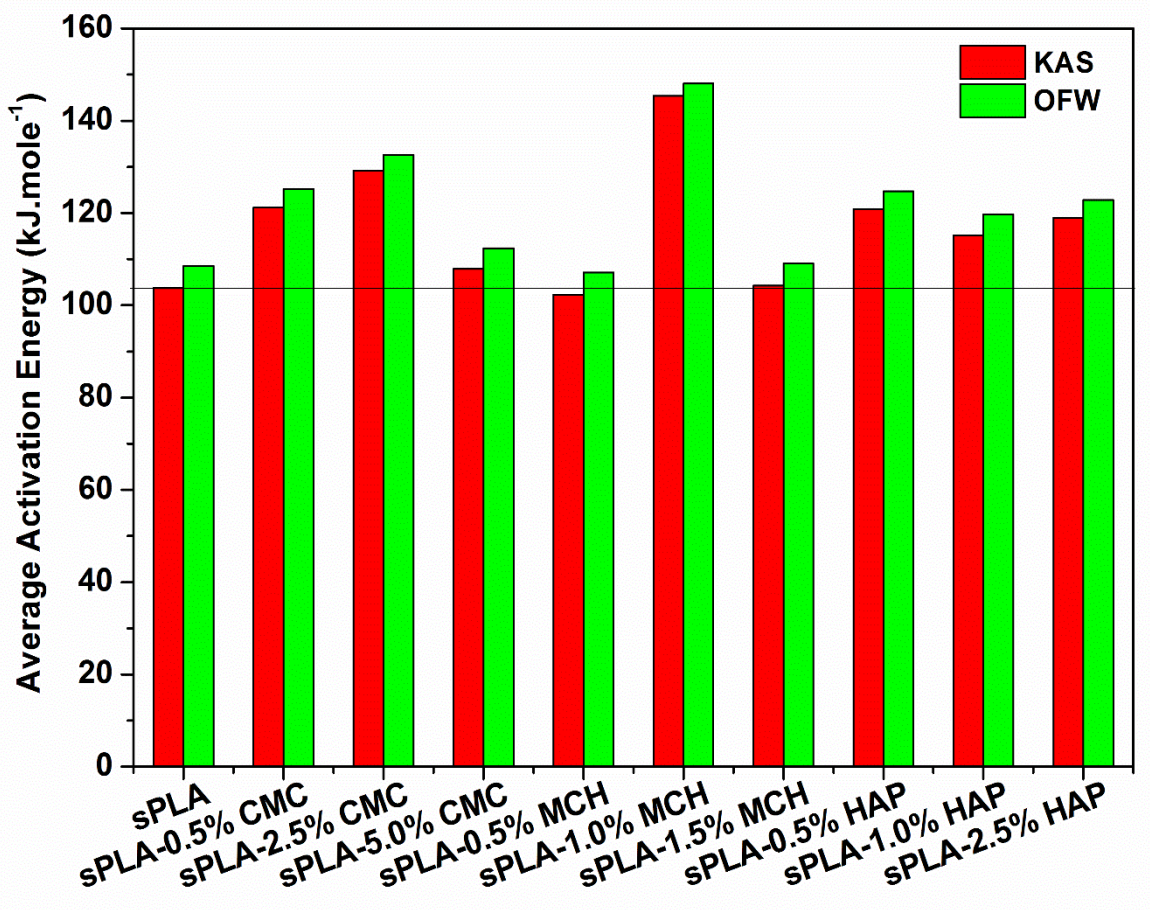

Figure 8.16: Average activation energy of sPLA and its biocomposites.

Similar trends are found for the activation energies measured using OFW model and suggested the comparable results as KAS model. The value of the activation energy is little higher in case of OFW analysis. For sPLA-1.0%MCH, the activation energy started with ~125 kJ.mole^{-1} which is significantly increased to ~147 kJ.mole^{-1}. For α = 0.3. For $0.4 \leq \alpha \geq 0.9$, E_a is similar and varied between 148-150 kJ.mole^{-1} which suggests that the decomposition is taking place through breakage of bond with similar bond energies. In case of sPLA-HAP biocomposite, it is found that the calculated average activation energy is approximately unchanged against the variation of the HAP content and varied between ~115 kJ.mole^{-1} to ~120 kJ.mole^{-1}. Higher activation energy for sPLA-HAP in comparison to sPLA can be attributed to the melt stabilization due to the presence of grafted HAP in

the matrix. The trend behavior for the variation is also similar in both KAS and OFW models. Comparative average activation energy of all samples are shown in **Figure 8.16**.

8.4.3 TGA-FTIR analysis of sPLA biocomposite

In order to understand the degradation behavior of sPLA and its biocomposite and qualitative analysis of the volatile species generated during the thermal degradation, the TG-IR analysis is performed. Representative 3D TG-IR data plots for sPLA, sPLA-2.5%CMC and sPLA-1.5%MCH are shown in **Figure 8.17**, **8.18** and **8.19**, respectively.

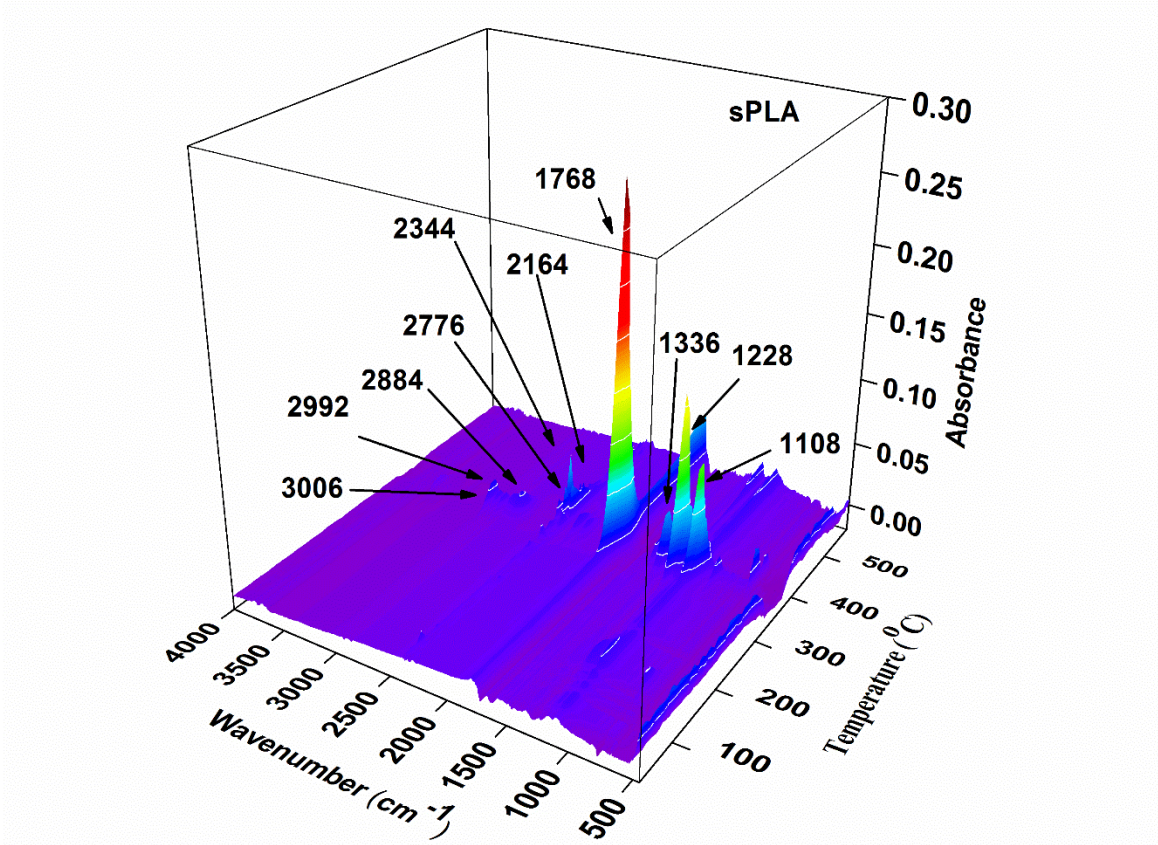

Figure 8.17: Representative 3D TG-IR data plot for sPLA (peak assignments).

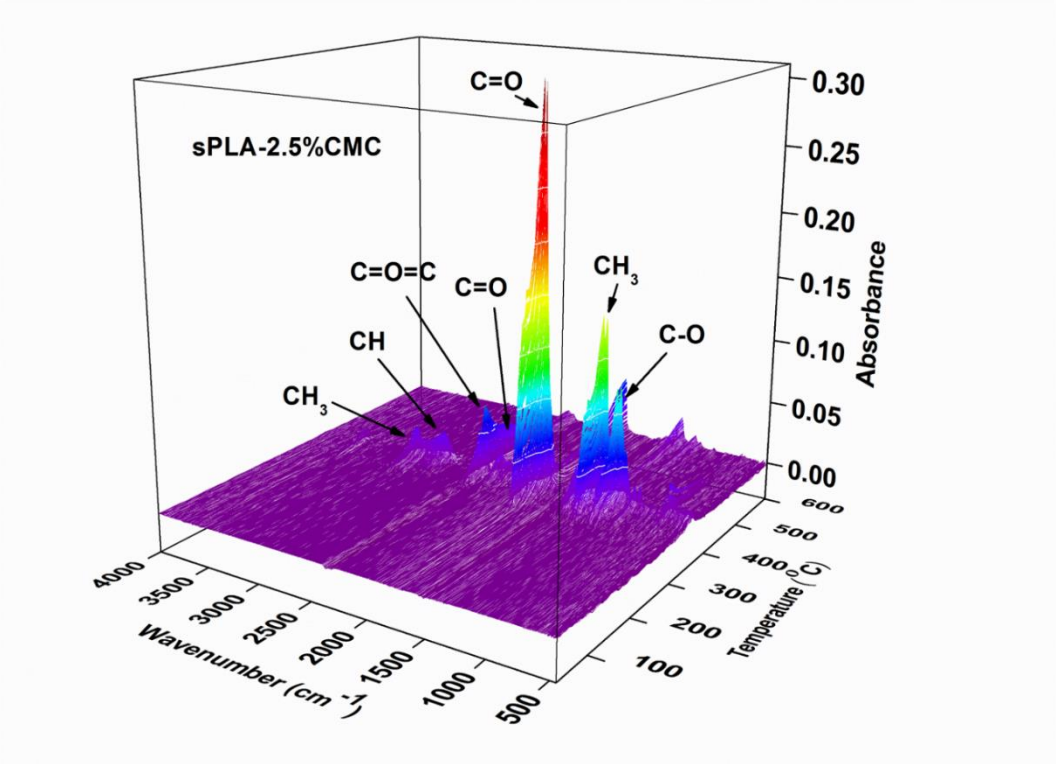

Figure 8.18: Representative 3D TG-IR data plot for sPLA-2.5%CMC.

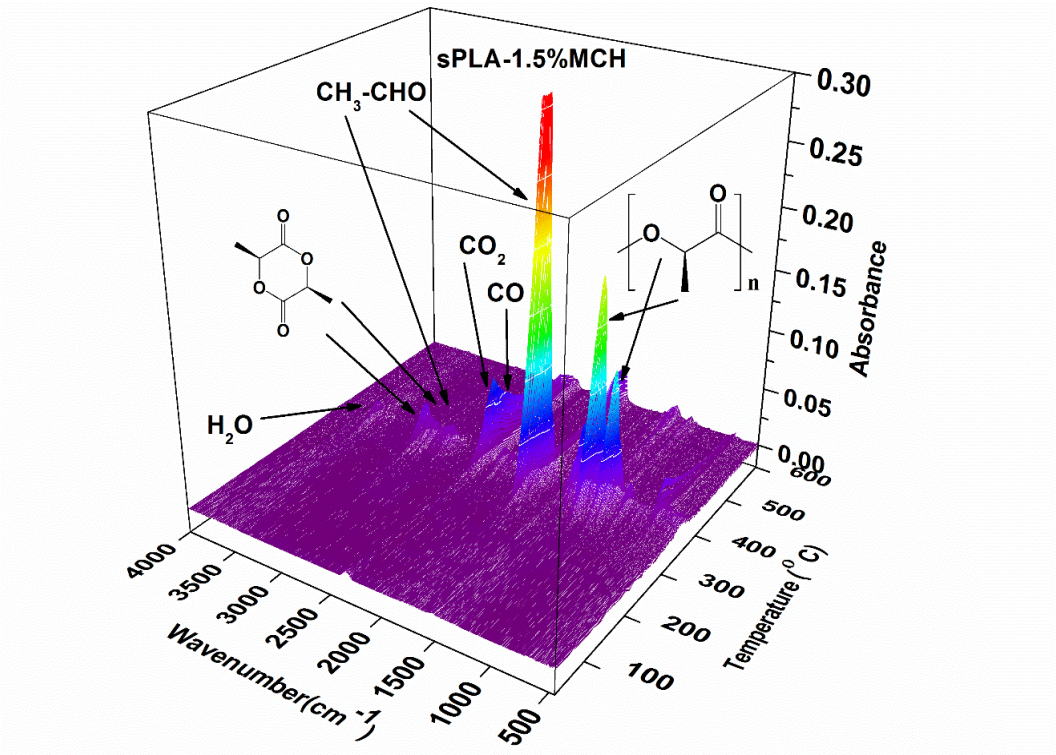

Figure 8.19: Representative 3D TG-IR data plot for sPLA-1.5%MCH.

It can be seen that the detection of the volatile component starts after 350°C for sPLA whereas for sPLA-MCH and sPLA-CMC, it starts after 400°C which suggests that the biocomposite is thermally stable at elevated temperature in comparison to the pristine sPLA. The delay in the detection of volatile component in the IR may be the result of travel time taken by the gaseous molecules through transfer line between TGA and FTIR instrument. There is no significant detection of MCH and CMC related peaks in IR spectra which may be due to the low concentration in comparison to sPLA matrix. The peak found in IR spectra at 1768 cm^{-1} is a combination of peaks related to carbonyl functional groups corresponds to different species such as acetaldehyde, lactide, dimer, trimer and short chains of PLA evolved during decomposition [255]. Other components evolved during degradation are carbon dioxide (spectra between 2365 cm^{-1} and 2344 cm^{-1}), carbon monoxide (spectra between 2185 cm^{-1} and 2164 cm^{-1}) and acetaldehyde (2802 cm^{-1} to 2776 cm^{-1}) [256]. Trace amount of water (vibration between 3900 cm^{-1} - 3450cm^{-1}) and lactide molecules (vibration at 1249 cm^{-1}, 3019 cm^{-1}) are also detected during decomposition.

8.5 Conclusions

The thermal degradation analysis of sPLA and developed biocomposite suggests that the material is stable till ~300°C which is higher than the processing temperature. Single degradation step is found for all samples. It is also noteworthy to mention that there is no adverse effect of the modified filler to the PLA matrix. The presence of grafted CMC and MCH helped to increase the thermal stability of the matrix whereas grafted HAP had lower effect due to the presence of metal oxides which are known to be de-catalysing agents for PLA. The data is analyzed using KAS and OFW methods and the activation energy is estimated. It is found that both the models can define the degradation process of the polymer. Variation in the activation energies with variation in the conversion factor suggested the complex reaction mechanism during the degradation process. It is noted that the addition of modified fillers increased the activation energy of the matrix in comparison to pristine sPLA (~103 $kJ.mole^{-1}$). Enhancement in the activation energy may be attributed to the increase in thermal stability due to the presence of modified fillers. The TG-IR analysis suggests that carbon dioxide, carbon monoxide, acetaldehyde, trace amount of water and lactide are produced during decomposition process of the biocomposites.

CHAPTER: 9

Application of Fabricated Stereocomplex PLA Biocomposites

Abstract

The motivation for this chapter is to process the fabricated biocomposites and make the objects using 3D printing technique in order to show the potential application. In this chapter, fabricated stereocomplex PLA biocomposites are melt processed to filaments and converted to the final objects in order to show the applicability of the developed materials and process. The biocomposites are transformed to gears and bones using 3D printer.

Graphical abstract

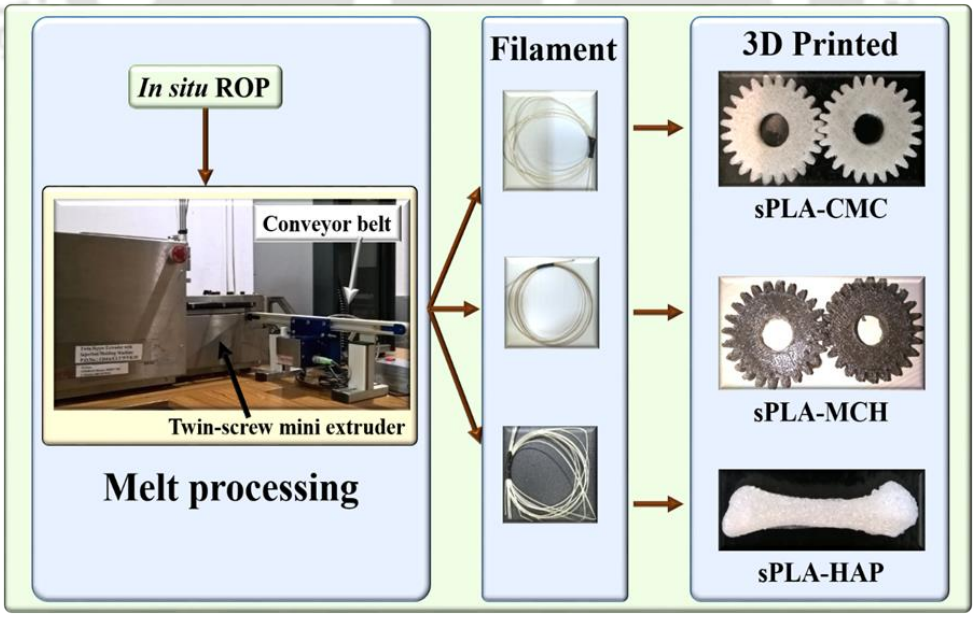

9.1 Introduction

In the previous chapters, we fabricated the stereocomplex PLA and its biocomposites such as sPLA-CMC, sPLA-MCH and sPLA-HAP which have the promising properties to be explored in several applications. The biomaterials or biofillers utilized in this research have their own significance. It is highly dependent on the application of interest for use of fillers. It is also clear that the modified fillers are having noteworthy effect on the stereocomplexation in the PLA matrix and it several properties. It is found that the modified CMC and modified chitosan improves the melting temperature as well as oxygen barrier and mechanical properties. MCH is found to be effective for the thermomechanical property of PLA. Similarly, grafted hydroxyapatite also significantly affects the stereocomplexation. All the fabricated biocomposites may be used for different applications such as high heat packaging, and other engineering application whereas the sPLA-HAP may be applicable to the biomedical applications.

Three dimensional (3D) printing is the technique in which 3D physical objects can be made from a 3D digital model by layer by layer deposition of the material in succession. Each formed layer is the sliced horizontal cross-section of the object of interest. The digital 3D models can be prepared using several software tools such as AutoCAD, Blender, Tinkercad etc. In this chapter, we have melt processed the fabricated biocomposites in order to prepare the filaments which are used for printing different prototypes for the demonstration.

9.2 Experimental section

The materials used in this chapter are developed as per the procedure given in the respective chapters. The filaments are prepared via melt processing using mini extruder and the same filaments are used in the development of the various objects by 3D printer.

9.2.1 3D printing of the objects

The object of interest is printed using 3D printer (Model: Hydra 250, Make: REDD Robotics, India) at 220°C with bed temperature of 110°C. The resolution is kept constant at 0.2 mm. Print speed is 50 $mm.sec^{-1}$, fill density 40% and bottom and top thickness kept constant 0.6 mm. Used filament has diameter of 1.6±0.2 mm.

9.2.2 Cell culture experiments

Baby Hamster Kidney fibroblasts (BHK-21) adherent cell-lines were procured from "National Centre for Cell Science (NCCS), Pune" and utilized to test the biocompatibility of the developed films. BHK-21 was maintained in 75 cm^2 tissue culture flasks at 37°C, humidified atmosphere and 5% CO_2. The culture medium is DMEM (Invitrogen) supplemented with penicillin streptomycin (Invitrogen) and fetal bovine serum (Invitrogen). The adherent cells were detached from the culture flasks by adding trypsin (Invitrogen) for 2 min at 37°C. The films were inserted in 12 well plate, along with addition of 1 ml media (DMEM) containing known concentration of cells. The cell growth was determined on the surface of the biocomposite films after 24 hours using Countess® II Automated Cell Counter (Life Technologies).

9.3 Discussion

The filaments prepared using melt processing technique are used for 3D printing of desired objects. sPLA-HAP filament is used for the fabrication of finger bone (third finger's middle phalanx) which has been successfully demonstrated. **Figure 9.1** displays the complete sequence of synthesis, processing and application of sPLA-HAP biocomposite. The prepared middle phalanx is tested for the biocompatibility with BHK-21 cell-line. The adhesion of cells on the surface of sPLA and sPLA-HAP are shown in the **Figure 9.2.** It is evident from the images that BHK-21 cells adhere to the surface of the films indicating the biocompatible nature of the developed biocomposites.

Demonstration of whole process from the synthesis to potential application of sPLA-CMC and sPLA-MCH is given in **Figure 9.3**. Synthesized materials are melt processed to form the filament with 1.6±0.2 mm diameter. The gears are 3D printed using the prepared filaments.

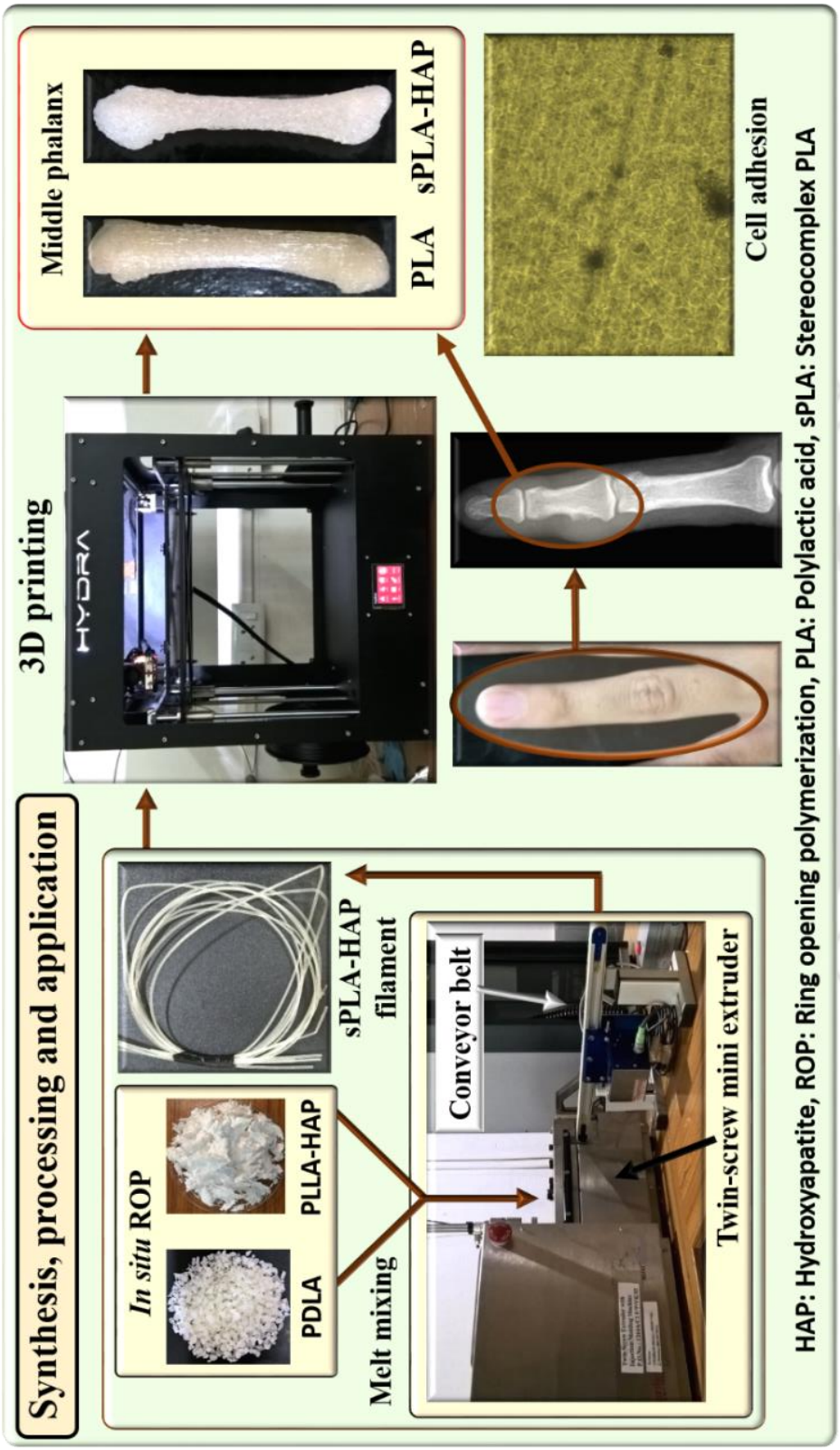

Figure 9.1: Synthesis, processing and application of stereocomplex PLA-HAP biocomposite

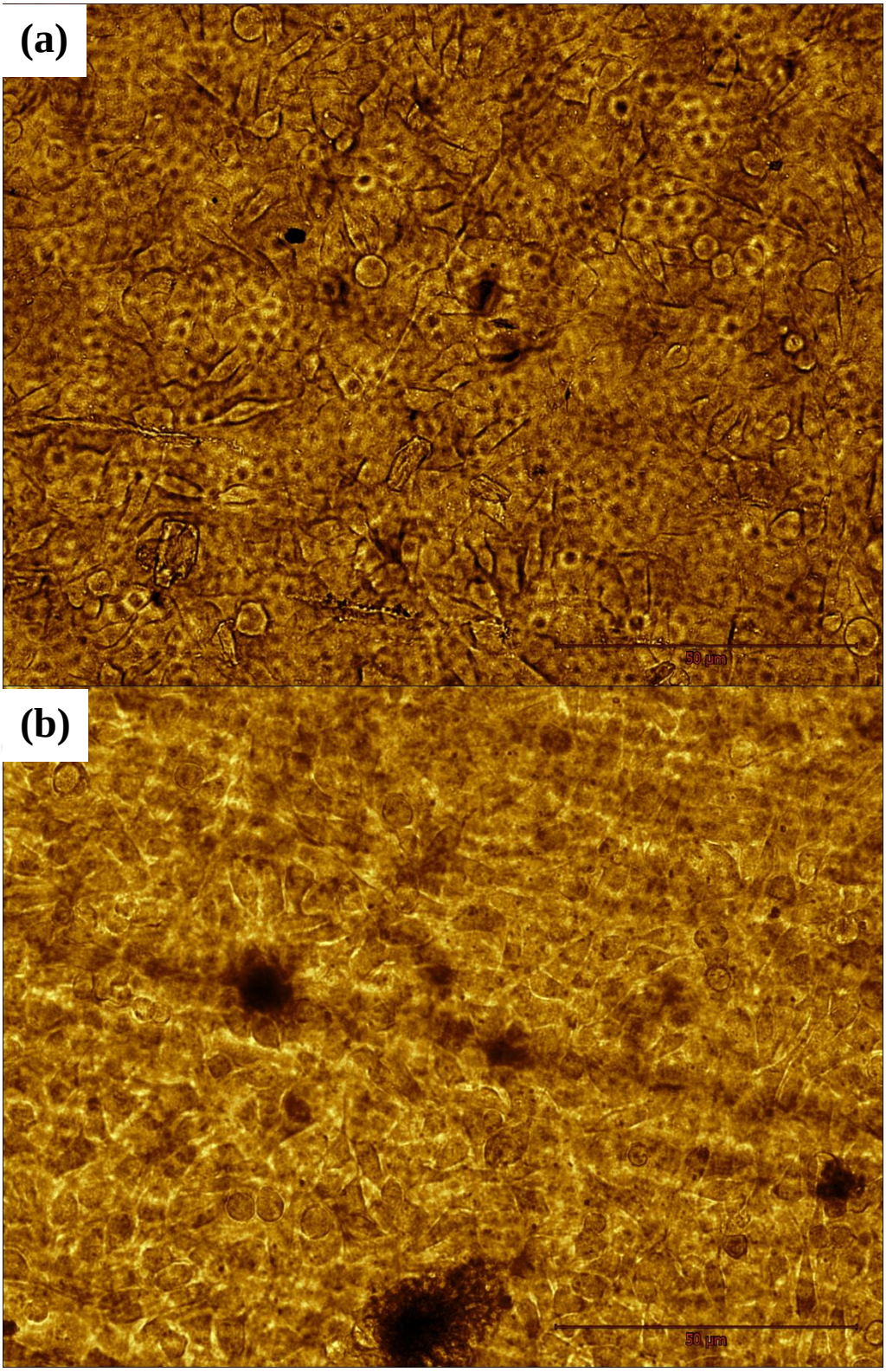

Figure 9.2: Cell (BHK-21) adhesion on (a) sPLA (b) sPLA-HAP (scale 50 µm)

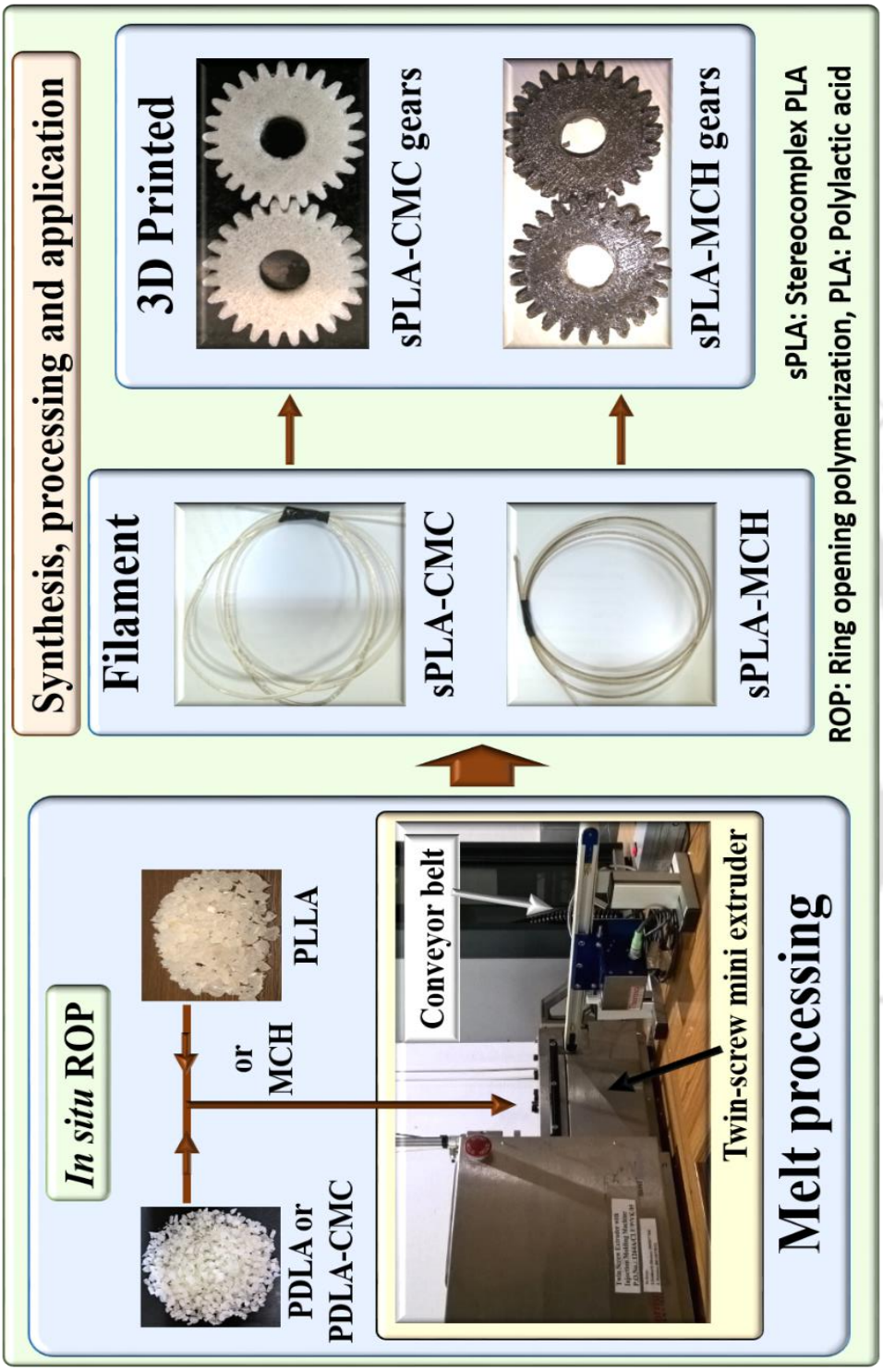

Figure 9.3: Synthesis, processing and application of sPLA-CMC and sPLA-MCH biocomposite

9.4 Conclusions

Three dimensional objects such as gears and finger bones are successfully demonstrated using 3D printing technique. It is found that the developed biocomposite can be processed as filament and 3D printed to different object for the application of interest. Adherence of BHK-21 cells on the surface of the biocomposites display the biocompatibility of the fabricated biocomposite materials.

CHAPTER: 10

Conclusions and Future Scope

10.1 Conclusions

The following major conclusions have been drawn from the current work:

- We have developed indigenous technology for the production and purification of lactide which is capable to yield high molecular weight PLA or stereocomplex PLA. The microwave assisted oligomerization is found to be an effective method which gives ~1500 Da molecular weight oligomer within the time frame of two hours which is used for the production of crude lactide. Synthesized crude lactide is purified by washing method which results in the production of PLA with ~100 kDa molecular weight using ring opening polymerization (ROP) technique whereas the lactide purified by direct crystallization process lead to the production of PLA with ~94 kDa molecular weight. The molecular weight of PLA is further increased to ~300 kDa after using the purified lactide via washing cum crystallization method.
- *In situ* modification of cellulose microcrystals (CMC) with PDLA is found to be highly effective in enhancing the dispersion of CMC into the polymer matrix. Grafted CMC provided extended molecular surface area for the formation of stereocomplex crystallites and hindered the homocrystallization phenomenon. The melting temperature is found to be ~209°C. The oxygen permeability and water vapor permeability are reduced by ~25% and ~35%, respectively. The improved storage modulus (~3500 MPa) and tensile strength (~50%) over neat stereocomplex PLA (sPLA) are the results of effective reinforcement of PLA.

- Chemically modified chitosan is successfully used for the fabrication of high molecular weight PLLA/PDLA (~200 kDa) stereocomplex biocomposite prepared using melt extrusion process. The prepared biocomposite had the melting temperature more than 207°C with ~40 $J.g^{-1}$ enthalpy in case of 1% MCH content. In case of non-isothermal cooling of biocomposite with the rate of $2°C.min^{-1}$, the degree of crystallinity is found to increase to ~70% for 1.5% MCH content and no homocrystallites is found. Heat deflection temperature is improved from ~70°C for sPLA to 145°C for sPLA with 1.5%MCH. The ultimate tensile strength enhanced from ~29 to ~63 MPa and oxygen barrier of the biocomposite films is reduced up to 56% with respect to sPLA blend.
- Stereocomplex PLA-HAP biocomposite is produced with 100% stereocomplex crystallite fractional content and melting temperature is found to be ~227°C with no trace of homocrystals. The elongation at break increased to (132%) while the tensile strength is found increased to (40.2 MPa). The storage modulus improved by ~47% at 30°C and showed the enhancement in the thermomechanical stability at elevated temperature. The enhancement in the stereocomplexation resulted 48% and 34% reduction in oxygen permeability and water vapor transmission, respectively.
- CMC is acting as a nucleating agent for overall crystallization where the grafted PLA chains provided the facility for the formation of stereocomplex crystallites. On the other hand, MCH and grafted HAP did not work as nucleating agents but helped in the formation of stereocomplex crystallites. The Avrami analysis suggested that all the used fillers are responsible for the higher overall crystallization rate and the spherulite growth rate is increased which may be due to the filler content. The activation energy for sPLA-CMC biocomposite is reduced which indicates the nucleation activity due to the presence of CMC whereas in the case of sPLA-MCH and sPLA-HAP, it is increased indicating that the crystallization process needs excess energy. This difference in the

results also conclude that CMC may be responsible for the heterogeneous nucleation whereas MCH and grafted HAP facilitate the uniform nucleation.

- The thermal degradation analysis of sPLA and developed biocomposite suggested that the material is stable till ~300°C which is higher than the processing temperature of PLA i.e. 180-200°C. Single degradation step is found for all samples. It is also noteworthy that there is no adverse effect of the modified filler to the PLA matrix. The presence of grafted CMC and MCH enhanced the thermal stability of the matrix whereas the grafted HAP had lower effect. Variation in the activation energies with variation in the conversion factor suggested the complex reaction mechanism during the degradation process. It is noted that the addition of modified fillers increased the activation energy of the matrix in comparison to pristine sPLA (~103 $kJ.mole^{-1}$). The TG-IR analysis suggests that carbon dioxide, carbon monoxide, acetaldehyde, trace amount of water and lactide are produced during decomposition process of the biocomposites.

The process for the production of purified lactide and stereocomplex PLA biocomposites is an industrially viable process and has the potential to be translated for the large scale production.

10.2 Future scope

The following studies can be carried out to further explore this area of research:

- Detailed study of crystallization mechanism of stereocomplex crystallites in biocomposites can be performed.
- The toxicological studies along with migration, biodegradation and recycling of prepared biocomposite can be carried out in order to understand the usability of the material for the different applications.
- Theoretical aspect of stereocomplexation can be explored via computational validation.
- The potential of the stereocomplexation can be explored with other chiral polymers as well as the polymers with different tacticity.
- Other fillers and additives can be explored in order to produce sPLA biocomposite.

The work presented in this thesis is just an initial understanding of stereocomplex system. From the technological point of view, it is very critical to develop the industry level process for the production of stereocomplex PLA. Production of stereoblock PLA is an emerging and promising area to understand and develop the process for its production. Processing of sPLA is highly critical task and so the study of the processing conditions and optimization to obtain stereocomplex PLA with desired properties is essential. Finding the suitable filler for the development of sPLA biocomposite to reduce the processing and development cost is essential to scale up the process for its commercialization.

Research Output

Patents

1. Vimal Katiyar, **Arvind Gupta**, "Formulation of Heat Stable Stereocomplex Poly(lactic acid) Composite", filed Indian Patent Application Number: 201631022079.
2. Vimal Katiyar, Medha Milli, **Arvind Gupta**, "Formulation of Polymer Nicotine Conjugates", filed Indian Patent Application Number: 201631034242.

Articles

1. **Arvind Gupta,** Vimal Katiyar, "Cellulose Functionalized High Molecular Weight Stereocomplex Polylactic Acid Biocomposite Films with Improved Gas Barrier, Thermomechanical Properties". ***ACS Sustainable Chemistry & Engineering*** 2017, 5 (8), 6835-6844.
2. **Arvind Gupta,** Arbind Prasad, Neha Mulchandani, Manisha Shah, M. Ravi Sankar, Sachin Kumar, Vimal Katiyar, "Multifunctional Nanohydroxyapatite-Promoted Toughened High-Molecular-Weight Stereocomplex Poly(lactic acid)-Based Bionanocomposite for Both 3D-Printed Orthopedic Implants and High-Temperature Engineering Applications". ***ACS Omega*** 2017, 2 (7), 4039-4052.
3. **Arvind Gupta,** Akhilesh Kumar Pal, Eamor M. Woo, and Vimal Katiyar, "Effects of Amphiphilic Chitosan on Stereocomplexation and Properties of Poly(lactic acid) Nano-biocomposite", submitted.
4. **Arvind Gupta,** Neha Mulchandani, Manisha Shah, Sachin Kumar and Vimal Katiyar "Modified Chitosan Facilitated Stereocomplexation of Poly(lactic acid): Influence on

Crystallization, Oxygen permeability, Wettability and Biocompatibility Behavior", submitted.

5. Melakuu Tesfaye, Rahul Patwa, **Arvind Gupta**, Manash Jyoti Kashyap, Vimal Katiyar, "Recycling of poly (lactic acid)/silk based bionanocomposites films and its influence on thermal stability, crystallization kinetics, solution and melt rheology", ***International Journal of Biological Macromolecules***, 101 (2017), 580-594.
6. Prodyut Dhar, Surendra Singh Gaur, Narendren Soundararajan, **Arvind Gupta**, Siddharth Mohan Bhasney, Medha Milli, Amit Kumar, and Vimal Katiyar, "Reactive extrusion of Poly(lactic acid)/cellulose nanocrystal films for food packaging applications: influence of filler type on thermomechanical, rheological, and barrier properties", ***Industrial & Engineering Chemistry Research***, 56 (16) (2017), 4718-4735.
7. Medha Mili, **Arvind Gupta**, Monika, Vimal Katiyar, "Designing of Poly-(L-lactide)-Nicotine Conjugates: Mechanistic, Kinetic Studies and Thermal Release Behavior of Nicotine", submitted to ***ACS Omega***.

Book Chapters

1. **Arvind Gupta**, Medha Mili, Tabli Ghosh and Vimal Katiyar, "Polylactic Acid: Potential Bio-based and Biodegradable Polymer used in Food Packaging", in book entitled "Bio-based Plastics for Food Packaging Applications by Vimal Katiyar" Smithers Rapra, 2017 (UK), **ISBN: 978-1-91024-258-2**.
2. **Arvind Gupta**, Akhilesh Kumar Pal, Rahul Patwa, Prodyut Dhar and Vimal Katiyar, "Green Composites with Excellent Barrier Properties", John Wiley & Sons, 2017 (Submitted).

Conferences/Seminars/Symposia/Workshops/Training

1. **Arvind Gupta**, Vimal Katiyar, Studies on Modified Chitosan Assisted Poly (lactic acid) Stereocomplexation, Advances in Sustainable Polymers (ASP-2016), August 4-6, 2016, Kyoto, Japan (Poster presentation).
2. **Arvind Gupta** and Vimal Katiyar, Synthesis, Characterization and Property Evaluation of Stereocomplex Poly(lactic acid) (Sc-PLA)/Cellulose Based Nanobiocomposites, CHEMCON 2015, IIT Guwahati, Guwahati, Assam, Dec. 27–30, 2015 (Oral presentation).
3. **Arvind Gupta** and Vimal Katiyar, Synthesis and Characterization of Stereocomplex PLA and Cellulose Biocomposite, Second Symposium in Sustainable Polymers (ASP-15), Guwahati, January 21 – 22, 2015 (Poster presentation).
4. **Arvind Gupta**, Dipankar Bandyopadhyay, Vimal Katiyar, "Polymer Solar Cells", Conference on Photochemistry & Luminescence, March 9-10, 2012, IIT Guwahati, Guwahati (Poster presentation).
5. Umesh Bhardwaj, **Arvind Gupta** and Vimal Katiyar, "Cellulose Hydrolysis during PLA Polymerization to Synthesize PLA-Cellulose Biocomposite", Polymer Processing Society Australia Conference (PPS-2013), Mumbai, India during December 4-7, 2013 (Oral presentation).
6. Selected as one of ten participants from India for Academia Industry Training (AIT) program in Bangalore during 01-05 Oct 2016; and EPFL, Switzerland during Nov 27, 2016 to Dec 4, 2016 organized by DST, Swissnex, Venturelab and SINE.

References

1. Thompson, R.C., et al., *Plastics, the environment and human health: current consensus and future trends.* Philosophical Transactions of the Royal Society B: Biological Sciences, 2009. **364**(1526): p. 2153-2166.
2. Brydson, J.A., *1 - The Historical Development of Plastics Materials*, in *Plastics Materials (Seventh Edition)*. 1999, Butterworth-Heinemann: Oxford. p. 1-18.
3. Paolo Fornasiero, et al., *Renewable Resources and Renewable Energy: A Global Challenge*, ed. S. Edition. 2011: CRC Press Taylor & Francis Group. 504.
4. *Material on Plastic Waste Management* in *Parivesh*. 2012: Delhi.
5. Dormer, A., et al., *Carbon footprint analysis in plastics manufacturing.* Journal of Cleaner Production, 2013. **51**: p. 133-141.
6. Wearden, G. *More plastic than fish in the sea by 2050, says Ellen MacArthur*. Davos 2016 [Web] 2016 [cited 2016 20 december].
7. Pilla, S., *Engineering Applications of Bioplastics and Biocomposites — An Overview*, in *Handbook of Bioplastics and Biocomposites Engineering Applications*. 2011, John Wiley & Sons, Inc. p. 1-15.
8. Kaplan, D.L., *Biopolymers from Renewable Resources*. Macromolecular Systems-Materials Approach, ed. 1. 1998: Springer-Verlag Berlin Heidelberg. 420.
9. *Data gathered from the Scopus Search Engine.* Keyword: Polylactic acid, Polylactide, Stereocomplex polylactic acid, Stereocomplex Polylactic acid, 2017.
10. *Potential of Plastics Industry in Northern Indian with Special Focus on Plasticulture and Food Processing, A Report on Plastics Industry*. 2014, Federation of Indian Chamber of Commerce and Industry: New Delhi.
11. Mirabal, A.S., L. Scholz, and M. Carus, *Market study on Bio-based Polymers in the World Capacities,Production and Applications: Status Quo and Trends towards 2020*. 2013, Nova Institute for Ecology and Innovation GmbH.
12. Gironi, F. and V. Piemonte, *Life cycle assessment of polylactic acid and polyethylene terephthalate bottles for drinking water*. Environmental Progress & Sustainable Energy, 2011. **30**(3): p. 459-468.
13. Garlotta, D., *A Literature Review of Poly(Lactic Acid).* Journal of Polymers and the Environment, 2001. **9**(2): p. 63-84.
14. Karak, N., *Fundamentals Of Polymers: Raw Materials To Finish Products*. 2009: Prentice-Hall Of India Pvt. Limited.
15. Ghaffar, T., et al., *Recent trends in lactic acid biotechnology: A brief review on production to purification.* Journal of Radiation Research and Applied Sciences, 2014. **7**(2): p. 222-229.
16. Scheele, C.W., *Om mjolk, och dess syra (Milk and its acid).* Kongl. Vetenskaps Academiens Nya Handlinger, Johan Georg Lange, Stockholm, 1780. **1**: p. 116-124.
17. Miller, C., et al., *3.17 - Industrial Production of Lactic Acid A2 - Moo-Young, Murray*, in *Comprehensive Biotechnology (Second Edition)*. 2011, Academic Press: Burlington. p. 179-188.
18. Masutani, K. and Y. Kimura, *Chapter 1 PLA Synthesis. From the Monomer to the Polymer*, in *Poly(lactic acid) Science and Technology: Processing, Properties, Additives and Applications*. 2015, The Royal Society of Chemistry. p. 1-36.

19. Manna, C.M., et al., *High molecular weight poly(lactic acid) produced by an efficient iron catalyst bearing a bis(amidinato)-N-heterocyclic carbene ligand.* Polyhedron, 2014. **84**: p. 160-167.
20. Peng, B., et al., *Synthesis of High Molecular Weight Poly(l-lactic acid) via Melt/Solid State Polycondensation. II. Effect of Precrystallization on Solid State Polycondensation.* Industrial & Engineering Chemistry Research, 2012. **51**(14): p. 5190-5196.
21. Nanavati, H. and V. Katiyar, *Method for producing lactic acid polymers of high crystallinity and molecular weight*. 2014, Google Patents.
22. Nanavati, H. and V. Katiyar, *Method for producing lactic acid polymers of high crystallinity and molecular weight*. 2009, Google Patents.
23. Kaihara, S., et al., *Synthesis of poly(L-lactide) and polyglycolide by ring-opening polymerization.* Nat. Protocols, 2007. **2**(11): p. 2767-2771.
24. Grueter, R. and H. Pohl, *Manufacture of lactid*. 1914, Google Patents.
25. Carothers, W.H., G.L. Dorough, and F.J.v. Natta, *STUDIES OF POLYMERIZATION AND RING FORMATION. X. THE REVERSIBLE POLYMERIZATION OF SIX-MEMBERED CYCLIC ESTERS.* Journal of the American Chemical Society, 1932. **54**(2): p. 761-772.
26. Kulkarni, R.K., et al., *Polylactic acid for surgical implants.* Archives of Surgery, 1966. **93**(5): p. 839-843.
27. Nagarajan, V., A.K. Mohanty, and M. Misra, *Perspective on Polylactic Acid (PLA) based Sustainable Materials for Durable Applications: Focus on Toughness and Heat Resistance.* ACS Sustainable Chemistry & Engineering, 2016. **4**(6): p. 2899-2916.
28. Pickering, K.L., M.G.A. Efendy, and T.M. Le, *A review of recent developments in natural fibre composites and their mechanical performance.* Composites Part A: Applied Science and Manufacturing, 2016. **83**: p. 98-112.
29. Dong, Y., et al., *Polylactic acid (PLA) biocomposites reinforced with coir fibres: Evaluation of mechanical performance and multifunctional properties.* Composites Part A: Applied Science and Manufacturing, 2014. **63**: p. 76-84.
30. Murphy, C.A. and M.N. Collins, *Microcrystalline cellulose reinforced polylactic acid biocomposite filaments for 3D printing.* Polymer Composites, 2016: doi: 10.1002/pc.24069.
31. Marra, A., et al., *Polylactic acid/zinc oxide biocomposite films for food packaging application.* International Journal of Biological Macromolecules, 2016. **88**: p. 254-262.
32. Saini, P., M. Arora, and M.N.V.R. Kumar, *Poly(lactic acid) blends in biomedical applications.* Advanced Drug Delivery Reviews, 2016. **107**: p. 47-59.
33. Pivsa-Art, W., et al., *Preparation of Polymer Blends between Poly(Lactic Acid) and Poly(Butylene adipate-co-terephthalate) and Biodegradable Polymers as Compatibilizers.* Energy Procedia, 2013. **34**: p. 549-554.
34. Ploypetchara, N., et al., *Blend of Polypropylene/Poly(lactic acid) for Medical Packaging Application: Physicochemical, Thermal, Mechanical, and Barrier Properties.* Energy Procedia, 2014. **56**: p. 201-210.
35. Zhang, M. and N.L. Thomas, *Blending polylactic acid with polyhydroxybutyrate: The effect on thermal, mechanical, and biodegradation properties.* Advances in Polymer Technology, 2011. **30**(2): p. 67-79.
36. Choudhary, P., et al., *Poly(L-lactide)/polypropylene blends: Evaluation of mechanical, thermal, and morphological characteristics.* Journal of Applied Polymer Science, 2011. **121**(6): p. 3223-3237.
37. Tsuji, H., *Poly(lactide) Stereocomplexes: Formation, Structure, Properties, Degradation, and Applications.* Macromolecular Bioscience, 2005. **5**(7): p. 569-597.

38. Darie, R.N., et al., *Effect of Nanoclay Hydrophilicity on the Poly(lactic acid)/Clay Nanocomposites Properties.* Industrial & Engineering Chemistry Research, 2014. **53**(19): p. 7877-7890.
39. Katiyar, V., et al., *Melt processing of poly(L-lactic acid) in the presence of organomodified anionic or cationic clays.* Journal of Applied Polymer Science, 2011. **122**(1): p. 112-125.
40. Katiyar, V. and H. Nanavati, *High molecular weight poly (L-lactic acid) clay nanocomposites via solid-state polymerization.* Polymer Composites, 2011. **32**(3): p. 497-509.
41. Valapa, R.B., G. Pugazhenthi, and V. Katiyar, *Effect of graphene content on the properties of poly(lactic acid) nanocomposites.* RSC Advances, 2015. **5**(36): p. 28410-28423.
42. Pal, A.K. and V. Katiyar, *Nanoamphiphilic Chitosan Dispersed Poly(lactic acid) Bionanocomposite Films with Improved Thermal, Mechanical, and Gas Barrier Properties.* Biomacromolecules, 2016. **17**(8): p. 2603-2618.
43. Tripathi, N., Monika, and V. Katiyar, *Poly (lactic acid)/modified gum arabic based bionanocomposite films: Thermal degradation kinetics.* Polymer Engineering & Science, 2017: doi: 10.1002/app.43458.
44. Dhar, P., et al., *Effect of cellulose nanocrystal polymorphs on mechanical, barrier and thermal properties of poly(lactic acid) based bionanocomposites.* RSC Advances, 2015. **5**(74): p. 60426-60440.
45. Tesfaye, M., et al., *Recycling of poly (lactic acid)/silk based bionanocomposites films and its influence on thermal stability, crystallization kinetics, solution and melt rheology.* International Journal of Biological Macromolecules, 2017. **101**: p. 580-594.
46. Dhar, P., et al., *Reactive Extrusion of Polylactic Acid/Cellulose Nanocrystal Films for Food Packaging Applications: Influence of Filler Type on Thermomechanical, Rheological, and Barrier Properties.* Industrial & Engineering Chemistry Research, 2017.
47. Bajpai, P.K., I. Singh, and J. Madaan, *Development and characterization of PLA-based green composites.* Journal of Thermoplastic Composite Materials, 2014. **27**(1): p. 52-81.
48. Aulin, C., et al., *Transparent Nanocellulosic Multilayer Thin Films on Polylactic Acid with Tunable Gas Barrier Properties.* ACS Applied Materials & Interfaces, 2013. **5**(15): p. 7352-7359.
49. Laufer, G., et al., *Clay–Chitosan Nanobrick Walls: Completely Renewable Gas Barrier and Flame-Retardant Nanocoatings.* ACS Applied Materials & Interfaces, 2012. **4**(3): p. 1643-1649.
50. Özçam, A.E., K. Efimenko, and J. Genzer, *Effect of ultraviolet/ozone treatment on the surface and bulk properties of poly(dimethyl siloxane) and poly(vinylmethyl siloxane) networks.* Polymer, 2014. **55**(14): p. 3107-3119.
51. Courgneau, C., et al., *Effect of crystallization on barrier properties of formulated polylactide.* Polymer International, 2012. **61**(2): p. 180-189.
52. Yializis, A., *Barrier film for limiting transmission of oxygen and moisture therethrough*. 2004, Google Patents.
53. Du, W., et al., *Cross-Linking Poly(lactic acid) Film Surface by Neutral Hyperthermal Hydrogen Molecule Bombardment.* Journal of Agricultural and Food Chemistry, 2015. **63**(49): p. 10604-10610.
54. Cui, Y., et al., *Gas barrier properties of polymer/clay nanocomposites.* RSC Advances, 2015. **5**(78): p. 63669-63690.
55. Armentano, I., et al., *Processing and characterization of plasticized PLA/PHB blends for biodegradable multiphase systems.*

56. Kakroodi, A.R., et al., *Tailoring poly(lactic acid) for packaging applications via the production of fully bio-based in situ microfibrillar composite films.* Chemical Engineering Journal, 2017. **308**: p. 772-782.
57. Ikada, Y., et al., *Stereocomplex formation between enantiomeric poly(lactides).* Macromolecules, 1987. **20**(4): p. 904-906.
58. Xu, H., et al., *Thermostable and Impermeable "Nano-Barrier Walls" Constructed by Poly(lactic acid) Stereocomplex Crystal Decorated Graphene Oxide Nanosheets.* Macromolecules, 2015. **48**(7): p. 2127-2137.
59. Re, G.L., et al., *Stereocomplexed PLA nanocomposites: From in situ polymerization to materials properties.* European Polymer Journal, 2014. **54**: p. 138-150.
60. Slager, J. and A.J. Domb, *Biopolymer stereocomplexes.* Advanced Drug Delivery Reviews, 2003. **55**(4): p. 549-583.
61. Mukherjee, T., et al., *Improved dispersion of cellulose microcrystals in polylactic acid (PLA) based composites applying surface acetylation.* Chemical Engineering Science, 2013. **101**(0): p. 655-662.
62. Bondeson, D. and K. Oksman, *Polylactic acid/cellulose whisker nanocomposites modified by polyvinyl alcohol.* Composites Part A: Applied Science and Manufacturing, 2007. **38**(12): p. 2486-2492.
63. Tsuji, H. and Y. Ikada, *Stereocomplex formation between enantiomeric poly(lactic acid)s. XI. Mechanical properties and morphology of solution-cast films.* Polymer, 1999. **40**(24): p. 6699-6708.
64. Saeidlou, S., et al., *Poly(lactic acid) stereocomplex formation: Application to PLA rheological property modification.* Journal of Applied Polymer Science, 2014. **131**(22): doi: 10.1002/app.41073.
65. Tsuji, H., S.H. Hyon, and Y. Ikada, *Stereocomplex formation between enantiomeric poly(lactic acids). 5. Calorimetric and morphological studies on the stereocomplex formed in acetonitrile solution.* Macromolecules, 1992. **25**(11): p. 2940-2946.
66. Rosen, T., et al., *Tailor-Made Stereoblock Copolymers of Poly(lactic acid) by a Truly Living Polymerization Catalyst.* Journal of the American Chemical Society, 2016. **138**(37): p. 12041-12044.
67. Fukushima, K. and Y. Kimura, *A Novel Synthetic Approach to Stereo-Block Poly(lactic acid).* Macromolecular Symposia, 2005. **224**(1): p. 133-144.
68. Yui, N., P.J. Dijkstra, and J. Feijen, *Stereo block copolymers of L- and D-lactides.* Die Makromolekulare Chemie, 1990. **191**(3): p. 481-488.
69. Tsuji, H., *Poly(lactide) Stereocomplexes: Formation, Structure, Properties, Degradation, and Applications.* Macromolecular Bioscience, 2007. **7**(12): p. 1299-1299.
70. Li, S.-H. and E.M. Woo, *Kinetic Analysis on Effect of Poly(4-vinyl phenol) on Complex-Forming Blends of Poly(L-lactide) and Poly(D-lactide).* Polym. J, 2009. **41**(5): p. 374-382.
71. Chang, L. and E.M. Woo, *Effects of molten poly(3-hydroxybutyrate) on crystalline morphology in stereocomplex of poly(L-lactic acid) with poly(D-lactic acid).* Polymer, 2011. **52**(1): p. 68-76.
72. Sun, Y. and C. He, *Synthesis and Stereocomplex Crystallization of Poly(lactide)–Graphene Oxide Nanocomposites.* ACS Macro Letters, 2012. **1**(6): p. 709-713.
73. Quan, H., et al., *The electrical properties and crystallization of stereocomplex poly(lactic acid) filled with carbon nanotubes.* Polymer, 2012. **53**(20): p. 4547-4552.

74. Bao, R.-Y., et al., *Enhanced Formation of Stereocomplex Crystallites of High Molecular Weight Poly(l-lactide)/Poly(d-lactide) Blends from Melt by Using Poly(ethylene glycol).* ACS Sustainable Chemistry & Engineering, 2014. **2**(10): p. 2301-2309.
75. Purnama, P. and S.H. Kim, *Bio-based composite of stereocomplex polylactide and cellulose nanowhiskers.* Polymer Degradation and Stability, 2014. **109**: p. 430-435.
76. Han, L., et al., *Stereocomplex crystallization of high-molecular-weight poly(l-lactic acid)/poly(d-lactic acid) racemic blends promoted by a selective nucleator.* Polymer, 2015. **63**: p. 144-153.
77. Bor, Y., J. Alin, and M. Hakkarainen, *Polylactide stereocomplexation leads to reduced migration during microwave heating in contact with food simulants.* Journal of Food Engineering, 2014. **134**: p. 1-4.
78. Bor, Y., J. Alin, and M. Hakkarainen, *Electrospray Ionization-Mass Spectrometry Analysis Reveals Migration of Cyclic Lactide Oligomers from Polylactide Packaging in Contact with Ethanolic Food Simulant.* Packaging Technology and Science, 2012. **25**(7): p. 427-433.
79. Ummartyotin, S. and H. Manuspiya, *A critical review on cellulose: From fundamental to an approach on sensor technology.* Renewable and Sustainable Energy Reviews, 2015. **41**: p. 402-412.
80. Kang, H., R. Liu, and Y. Huang, *Graft modification of cellulose: Methods, properties and applications.* Polymer, 2015. **70**: p. A1-A16.
81. Gregorova, A., M. Machovsky, and R. Wimmer, *Viscoelastic Properties of Mineral-Filled Poly(lactic acid) Composites.* International Journal of Polymer Science, 2012. **2012**: p. 6.
82. Liu, H. and T.J. Webster, *Mechanical properties of dispersed ceramic nanoparticles in polymer composites for orthopedic applications.* International Journal of Nanomedicine, 2010. **5**: p. 299-313.
83. Gwon, J.-G., et al., *Physiochemical, optical and mechanical properties of poly(lactic acid) nanocomposites filled with toluene diisocyanate grafted cellulose nanocrystals.* RSC Advances, 2016. **6**(12): p. 9438-9445.
84. Rinaudo, M., *Chitin and chitosan: Properties and applications.* Progress in Polymer Science, 2006. **31**(7): p. 603-632.
85. Szymańska, E. and K. Winnicka, *Stability of Chitosan—A Challenge for Pharmaceutical and Biomedical Applications.* Marine Drugs, 2015. **13**(4): p. 1819-1846.
86. Jayakumar, R., et al., *Biomedical applications of chitin and chitosan based nanomaterials—A short review.* Carbohydrate Polymers, 2010. **82**(2): p. 227-232.
87. No, H.K., et al., *Applications of Chitosan for Improvement of Quality and Shelf Life of Foods: A Review.* Journal of Food Science, 2007. **72**(5): p. R87-R100.
88. Khantayanuwong, S., C. Khemarom, and S. Salaemae, *Effects of shrimp chitosan on the physical properties of handsheets.* Agriculture and Natural Resources, 2017. **51**(1): p. 53-56.
89. No, H.K. and S.P. Meyers, *Application of Chitosan for Treatment of Wastewaters*, in *Reviews of Environmental Contamination and Toxicology: Continuation of Residue Reviews*, G.W. Ware, Editor. 2000, Springer New York: New York, NY. p. 1-27.
90. Zargar, V., M. Asghari, and A. Dashti, *A Review on Chitin and Chitosan Polymers: Structure, Chemistry, Solubility, Derivatives, and Applications.* ChemBioEng Reviews, 2015. **2**(3): p. 204-226.
91. Julià, M.R., E. Pascual, and P. Erra, *Influence of the molecular mass of chitosan on shrink-resistance and dyeing properties of chitosantreated wool.* Colouration Technology, 2000. **116**(2): p. 62-67.

92. Saeri, M.R., et al., *The wet precipitation process of hydroxyapatite.* Materials Letters, 2003. **57**(24–25): p. 4064-4069.
93. Mobasherpour, I., et al., *Synthesis of nanocrystalline hydroxyapatite by using precipitation method.* Journal of Alloys and Compounds, 2007. **430**(1–2): p. 330-333.
94. Earl, J.S., D.J. Wood, and S.J. Milne, *Hydrothermal synthesis of hydroxyapatite.* Journal of Physics: Conference Series, 2006. **26**(1): p. 268.
95. Yang, Y., et al., *Hydrothermal Synthesis of Hydroxyapatite with Different Morphologies: Influence of Supersaturation of the Reaction System.* Crystal Growth & Design, 2014. **14**(9): p. 4864-4871.
96. Rajabi, A.H., et al., *Synthesis and characterization of nanocrystalline hydroxyapatite powder via sol-gel method*, in *3rd Kuala Lumpur International Conference on Biomedical Engineering 2006: Biomed 2006, 11 – 14 December 2006 Kuala Lumpur, Malaysia*, F. Ibrahim, et al., Editors. 2007, Springer Berlin Heidelberg: Berlin, Heidelberg. p. 149-151.
97. Monma, H. and T. Kamiya, *Preparation of hydroxyapatite by the hydrolysis of brushite.* Journal of Materials Science, 1987. **22**(12): p. 4247-4250.
98. Monma, H., S. Ueno, and T. Kanazawa, *Properties of hydroxyapatite prepared by the hydrolysis of tricalcium phosphate.* Journal of Chemical Technology and Biotechnology, 1981. **31**(1): p. 15-24.
99. Kweh, S.W.K., K.A. Khor, and P. Cheang, *The production and characterization of hydroxyapatite (HA) powders.* Journal of Materials Processing Technology, 1999. **89–90**: p. 373-377.
100. Rivera, E.M., et al., *Synthesis of hydroxyapatite from eggshells.* Materials Letters, 1999. **41**(3): p. 128-134.
101. Lee, S.-W., et al., *Comparative Study of hydroxyapatite prepared from seashells and eggshells as a bone graft material.* Tissue Engineering and Regenerative Medicine, 2014. **11**(2): p. 113-120.
102. Klinkaewnarong, J., et al., *Synthesis and characterization of nanocrystalline HAp powders prepared by using aloe vera plant extracted solution.* Current Applied Physics, 2010. **10**(2): p. 521-525.
103. Akram, M., et al., *Extracting hydroxyapatite and its precursors from natural resources.* Journal of Materials Science, 2014. **49**(4): p. 1461-1475.
104. Mene, R.U., M.P. Mahabole, and R.S. Khairnar, *Surface modified hydroxyapatite thick films for CO2 gas sensing application: Effect of swift heavy ion irradiation.* Radiation Physics and Chemistry, 2011. **80**(6): p. 682-687.
105. Markov, G.G. and I.G. Ivanov, *Hydroxyapatite column chromatography in procedures for isolation of purified DNA.* Analytical Biochemistry, 1974. **59**(2): p. 555-563.
106. Tsuchida, T., et al., *Reaction of ethanol over hydroxyapatite affected by Ca/P ratio of catalyst.* Journal of Catalysis, 2008. **259**(2): p. 183-189.
107. Zahouily, M., et al., *Hydroxyapatite: new efficient catalyst for the Michael addition.* Catalysis Communications, 2003. **4**(10): p. 521-524.
108. Tamjid, E., et al., *Effect of particle size on the in vitro bioactivity, hydrophilicity and mechanical properties of bioactive glass-reinforced polycaprolactone composites.* Materials Science and Engineering: C, 2011. **31**(7): p. 1526-1533.
109. Otsuka, M., et al., *Effect of particle size of metastable calcium phosphates on mechanical strength of a novel self-setting bioactive calcium phosphate cement.* Journal of Biomedical Materials Research, 1995. **29**(1): p. 25-32.

110. Li, Z., et al., *Effects of hydroxyapatite additive content on the bioactivity and biomechanical compatibility of bioactive nano-titania ceramics.* Journal of Biomedical Materials Research Part A, 2008. **86A**(2): p. 333-338.
111. Kim, S.H. and Y.H. Kim, *Direct condensation polymerization of lactic acid.* Macromolecular Symposia, 1999. **144**(1): p. 277-287.
112. Perego, G., G.D. Cella, and C. Bastioli, *Effect of molecular weight and crystallinity on poly(lactic acid) mechanical properties.* Journal of Applied Polymer Science, 1996. **59**(1): p. 37-43.
113. Vouyiouka, S., et al., *Solid state polymerization of poly(lactic acid): Some fundamental parameters.* Polymer Degradation and Stability, 2013. **98**(12): p. 2473-2481.
114. Robert, J.L. and K.B. Aubrecht, *Ring-Opening Polymerization of Lactide To Form a Biodegradable Polymer.* Journal of Chemical Education, 2008. **85**(2): p. 258.
115. Thayer, C.A. and H.E. Bellis, *Process for the synthesis of lactide or glycolide from lactic acid or glycolide acid oligomers*. 1994, Google Patents.
116. Idage, B.B., B.S. Idage, and S. Swaminathan, *Improved process for the preparation of l-lactide of high chemical yield and optical purity*. 2011, Google Patents.
117. Yamaguchi, Y. and T. Arimura, *Method for purification of lactide*. 1996, Google Patents.
118. Mariage, P.A., D. Hottois, and P. Coszach, *Method of obtaining lactide*. 2013, Google Patents.
119. Ohara, H., et al., *Method for purifying lactide and lactide for food additives*. 2001, Google Patents.
120. Benecke, H.P., R.A. Markle, and R.G. Sinclair, *Catalytic production of lactide directly from lactic acid*. 1994, Google Patents.
121. Bhatia, K.K., *Continuous process for rapid conversion of oligomers to cyclic esters*. 1991, Google Patents.
122. Rustagi, N., S. Pradhan, and R. Singh, *Public health impact of plastics: An overview*. Vol. 15. 2011. 100-103.
123. Raquez, J.-M., et al., *Polylactide (PLA)-based nanocomposites.* Progress in Polymer Science, 2013. **38**(10–11): p. 1504-1542.
124. Rhim, J.-W., H.-M. Park, and C.-S. Ha, *Bio-nanocomposites for food packaging applications.* Progress in Polymer Science, 2013. **38**(10–11): p. 1629-1652.
125. Katiyar, V., et al., *Poly l-lactide-layered double hydroxide nanocomposites via in situ polymerization of l-lactide.* Polymer Degradation and Stability, 2010. **95**(12): p. 2563-2573.
126. Cheung, H.-Y., et al., *Biodegradation of a silkworm silk/PLA composite.* Composites Part B: Engineering, 2010. **41**(3): p. 223-228.
127. Tesfaye, M., et al., *Silk nanocrystals stabilized melt extruded poly (lactic acid) nanocomposite films: Effect of recycling on thermal degradation kinetics and optimization studies.* Thermochimica Acta, 2016. **643**: p. 41-52.
128. Li, L., S. Ding, and C. Zhou, *Preparation and degradation of PLA/chitosan composite materials.* Journal of Applied Polymer Science, 2004. **91**(1): p. 274-277.
129. Tripathi, N. and V. Katiyar, *PLA/functionalized-gum arabic based bionanocomposite films for high gas barrier applications.* Journal of Applied Polymer Science, 2016. **133**(21): doi: 10.1002/app.43458.
130. Valapa, R.B., G. Pugazhenthi, and V. Katiyar, *Fabrication and characterization of sucrose palmitate reinforced poly(lactic acid) bionanocomposite films.* Journal of Applied Polymer Science, 2015. **132**(3): doi: 10.1002/app.41320.

131. Missoum, K., M. Belgacem, and J. Bras, *Nanofibrillated Cellulose Surface Modification: A Review*. Materials, 2013. **6**(5): p. 1745.
132. Vaia, R.A., H. Ishii, and E.P. Giannelis, *Synthesis and properties of two-dimensional nanostructures by direct intercalation of polymer melts in layered silicates.* Chemistry of Materials, 1993. **5**(12): p. 1694-1696.
133. Alzari, V., et al., *In situ production of high filler content graphene-based polymer nanocomposites by reactive processing.* Journal of Materials Chemistry, 2011. **21**(41): p. 16544-16549.
134. Imre, B. and B. Pukánszky, *Compatibilization in bio-based and biodegradable polymer blends.* European Polymer Journal, 2013. **49**(6): p. 1215-1233.
135. Nishida, M., et al., *Intercalative polymerization of L-lactide with organically modified clay by a reactive extrusion method and instrumental analyses of the poly(lactic acid)/clay nanocomposites.* Journal of Applied Polymer Science, 2012. **125**(S1): p. E681-E690.
136. HAMAD, W.Y. and C. MIAO, *Nanocomposite biomaterials of nanocrystalline cellulose (ncc) and polylactic acid (pla)*. 2011, Google Patents.
137. Miao, C. and W.Y. Hamad, *In-situ polymerized cellulose nanocrystals (CNC)-poly(l-lactide) (PLLA) nanomaterials and applications in nanocomposite processing.* Carbohydrate Polymers, 2016. **153**: p. 549-558.
138. Paul, M.-A., et al., *Exfoliated Polylactide/Clay Nanocomposites by In-Situ Coordination–Insertion Polymerization.* Macromolecular Rapid Communications, 2003. **24**(9): p. 561-566.
139. Lönnberg, H., et al., *Grafting of Cellulose Fibers with Poly(ε-caprolactone) and Poly(l-lactic acid) via Ring-Opening Polymerization.* Biomacromolecules, 2006. **7**(7): p. 2178-2185.
140. Jiang, L., et al., *Stereocomplexation kinetics of enantiomeric poly(l-lactide)/poly(d-lactide) blends seeded by nanocrystalline cellulose.* RSC Advances, 2015. **5**(87): p. 71115-71119.
141. Habibi, Y., et al., *Effects of interfacial stereocomplexation in cellulose nanocrystal-filled polylactide nanocomposites.* Cellulose, 2013. **20**(6): p. 2877-2885.
142. Wu, H., et al., *Synthesis and characterization of cellulose nanocrystal-graft-poly(d-lactide) and its nanocomposite with poly(l-lactide).* Polymer, 2016. **103**: p. 365-375.
143. Purnama, P. and S.H. Kim, *Bio-based composite of stereocomplex polylactide and cellulose nanowhiskers.* Polymer Degradation and Stability, 2014. 109: p. 430-435.
144. Ma, P., et al., *Rapid Stereocomplexation between Enantiomeric Comb-Shaped Cellulose-g-poly(l-lactide) Nanohybrids and Poly(d-lactide) from the Melt.* Biomacromolecules, 2015. **16**(11): p. 3723-3729.
145. Bao, J., et al., *Preferential Stereocomplex Crystallization in Enantiomeric Blends of Cellulose Acetate-g-Poly(lactic acid)s with Comblike Topology.* The Journal of Physical Chemistry B, 2015. **119**(39): p. 12689-12698.
146. Mujica-Garcia, A., et al., *Poly(lactic acid) melt-spun fibers reinforced with functionalized cellulose nanocrystals.* RSC Advances, 2016. **6**(11): p. 9221-9231.
147. Wei, X.-F., et al., *Stereocomplex Crystallite Network in Asymmetric PLLA/PDLA Blends: Formation, Structure, and Confining Effect on the Crystallization Rate of Homocrystallites.* Macromolecules, 2014. **47**(4): p. 1439-1448.
148. Zhang, J., et al., *Infrared Spectroscopic Study of CH3···OC Interaction during Poly(l-lactide)/Poly(d-lactide) Stereocomplex Formation.* Macromolecules, 2005. **38**(5): p. 1822-1828.
149. Brizzolara, D., et al., *Mechanism of the Stereocomplex Formation between Enantiomeric Poly(lactide)s.* Macromolecules, 1996. **29**(1): p. 191-197.

150. Park, S.-H., et al., *Improvements in barrier properties of poly(lactic acid) films coated with chitosan or chitosan/clay nanocomposite.* Journal of Applied Polymer Science, 2012. **125**(S1): p. E675-E680.
151. Takács, E., et al., *Hydrophilic/hydrophobic character of grafted cellulose.* Radiation Physics and Chemistry, 2010. **79**(4): p. 467-470.
152. Dhar, P., et al., *Thermally recyclable polylactic acid/cellulose nanocrystal films through reactive extrusion process.* Polymer, 2016. **87**: p. 268-282.
153. Shi, Y. and B. Wang, *Mechanical properties of carbon fiber/cellulose composite papers modified by hot-melting fibers.* Progress in Natural Science: Materials International, 2014. **24**(1): p. 56-60.
154. Rustagi, N., S.K. Pradhan, and R. Singh, *Public health impact of plastics: An overview.* Indian Journal of Occupational and Environmental Medicine, 2011. **15**(3): p. 100-103.
155. Hofvendahl, K. and B. Hahn-Hägerdal, *l-lactic acid production from whole wheat flour hydrolysate using strains of Lactobacilli and Lactococci.* Enzyme and Microbial Technology, 1997. **20**(4): p. 301-307.
156. Mercier, P., et al., *Kinetics of lactic acid fermentation on glucose and corn by Lactobacillus amylophilus.* Journal of Chemical Technology & Biotechnology, 1992. **55**(2): p. 111-121.
157. Van de Velde, K. and P. Kiekens, *Biopolymers: overview of several properties and consequences on their applications.* Polymer Testing, 2002. **21**(4): p. 433-442.
158. Bang, G. and S.W. Kim, *Biodegradable poly(lactic acid)-based hybrid coating materials for food packaging films with gas barrier properties.* Journal of Industrial and Engineering Chemistry, 2012. **18**(3): p. 1063-1068.
159. Tawakkal, I.S.M.A., et al., *A Review of Poly(Lactic Acid)-Based Materials for Antimicrobial Packaging.* Journal of Food Science, 2014. **79**(8): p. R1477-R1490.
160. Lasprilla, A.J.R., et al., *Poly-lactic acid synthesis for application in biomedical devices-A review.* Biotechnology Advances, 2012. **30**(1): p. 321-328.
161. Furuhashi, Y., Y. Kimura, and N. Yoshie, *Self-Assembly of Stereocomplex-Type Poly(lactic acid).* Polym. J, 2006. **38**(10): p. 1061-1067.
162. Tsuji, H., S.H. Hyon, and Y. Ikada, *Stereocomplex formation between enantiomeric poly(lactic acid)s. 3. Calorimetric studies on blend films cast from dilute solution.* Macromolecules, 1991. **24**(20): p. 5651-5656.
163. Bai, H., et al., *Enhancing the melt stability of polylactide stereocomplexes using a solid-state cross-linking strategy during a melt-blending process.* Polymer Chemistry, 2014. **5**(20): p. 5985-5993.
164. Purnama, P. and S.H. Kim, *Stereocomplex Formation of High-Molecular-Weight Polylactide Using Supercritical Fluid.* Macromolecules, 2010. **43**(2): p. 1137-1142.
165. Huan, G., et al., *Fabrication and Properties of sc-PLA/SiO 2 Composites.* IOP Conference Series: Materials Science and Engineering, 2014. **62**(1): p. 012031.
166. Purnama, P., Y. Jung, and S.H. Kim, *An Advanced Class of Bio-Hybrid Materials: Bionanocomposites of Inorganic Clays and Organic Stereocomplex Polylactides.* Macromolecular Materials and Engineering, 2013. **298**(3): p. 263-269.
167. Bie, P., et al., *The properties of antimicrobial films derived from poly(lactic acid)/starch/chitosan blended matrix.* Carbohydrate Polymers, 2013. **98**(1): p. 959-966.
168. Li, Q., et al., *Applications and Properties of Chitosan.* Journal of Bioactive and Compatible Polymers, 1992. **7**(4): p. 370-397.
169. Bonilla, J., et al., *Effects of chitosan on the physicochemical and antimicrobial properties of PLA films.* Journal of Food Engineering, 2013. **119**(2): p. 236-243.

170. Gartner, H., Y. Li, and E. Almenar, *Improved wettability and adhesion of polylactic acid/chitosan coating for bio-based multilayer film development.* Applied Surface Science, 2015. **332**: p. 488-493.
171. Spiridon, I., et al., *Influence of Keratin on Polylactic Acid/Chitosan Composite Properties. Behavior upon Accelerated Weathering.* Industrial & Engineering Chemistry Research, 2013. **52**(29): p. 9822-9833.
172. Torres-Huerta, A.M., et al., *Comparative assessment of miscibility and degradability on PET/PLA and PET/chitosan blends.* European Polymer Journal, 2014. **61**: p. 285-299.
173. Hiltner, A., et al., *Oxygen transport as a solid-state structure probe for polymeric materials: A review.* Journal of Polymer Science Part B: Polymer Physics, 2005. **43**(9): p. 1047-1063.
174. Li, Y., et al., *Stereocomplex crystallite network in poly(d,l-lactide): formation, structure and the effect on shape memory behaviors and enzymatic hydrolysis of poly(d,l-lactide).* RSC Advances, 2015. **5**(31): p. 24352-24362.
175. Arias, V., et al., *Homocomposites of Polylactide (PLA) with Induced Interfacial Stereocomplex Crystallites.* ACS Sustainable Chemistry & Engineering, 2015. **3**(9): p. 2220-2231.
176. Lin, T.T., X.Y. Liu, and C. He, *A DFT study on poly(lactic acid) polymorphs.* Polymer, 2010. **51**(12): p. 2779-2785.
177. Miyamoto, T. and H. Inagaki, *The Stereocomplex Formation in Poly(methyl methacrylate) and the Stereospecific Polymerization of Its Monomer.* Polym J, 1970. **1**(1): p. 46-54.
178. Sawai, D., et al., *Crystal density and heat of fusion for a stereo-complex of poly(L-lactic acid) and poly(D-lactic acid).* Journal of Polymer Science Part B: Polymer Physics, 2007. **45**(18): p. 2632-2639.
179. Tran, H.T., et al., *Thermally resistant polylactide layer-by-layer film prepared using an inkjet approach.* Polym J, 2017. **49**(3): p. 327-334.
180. Sawai, D., M. Tamada, and T. Kanamoto, *Development of Oriented Morphology and Mechanical Properties upon Drawing of Stereo-Complex of Poly(L-lactic acid) and Poly(D-lactic acid) by Solid-State Coextrusion.* Polym. J, 2007. **39**(9): p. 953-960.
181. Tsuji, H. and T. Tsuruno, *Water Vapor Permeability of Poly(L-lactide)/Poly(D-lactide) Stereocomplexes.* Macromolecular Materials and Engineering, 2010. **295**(8): p. 709-715.
182. Pan, P., et al., *Stereocomplexation of high-molecular-weight enantiomeric poly(lactic acid)s enhanced by miscible polymer blending with hydrogen bond interactions.* Polymer, 2016. **98**: p. 80-87.
183. Fukushima, K., et al., *Stereoblock Poly(lactic acid): Synthesis via Solid-State Polycondensation of a Stereocomplexed Mixture of Poly(L-lactic acid) and Poly(D-lactic acid).* Macromolecular Bioscience, 2005. **5**(1): p. 21-29.
184. Han, L., et al., *Click chemistry synthesis, stereocomplex formation, and enhanced thermal properties of well-defined poly(l-lactic acid)-b-poly(d-lactic acid) stereo diblock copolymers.* Polymer Chemistry, 2017. **8**(6): p. 1006-1016.
185. Bibi, G., et al., *Novel Strategy of Lactide Polymerization Leading to Stereocomplex Polylactide Nanoparticles Using Supercritical Fluid Technology.* ACS Sustainable Chemistry & Engineering, 2016. **4**(9): p. 4521-4528.
186. Akagi, T., T. Fujiwara, and M. Akashi, *Inkjet Printing of Layer-by-Layer Assembled Poly(lactide) Stereocomplex with Encapsulated Proteins.* Langmuir, 2014. **30**(6): p. 1669-1676.

187. Gardella, L., et al., *On the development of a facile approach based on the use of ionic liquids: preparation of PLLA (sc-PLA)/high surface area nano-graphite systems.* Green Chemistry, 2015. **17**(7): p. 4082-4088.
188. Sun, Y. and C. He, *Synthesis, stereocomplex crystallization, morphology and mechanical property of poly(lactide)-carbon nanotube nanocomposites.* RSC Advances, 2013. **3**(7): p. 2219-2226.
189. Yang, S., et al., *Preferential formation of stereocomplex in high-molecular-weight polylactic acid racemic blend induced by carbon nanotubes.* Polymer, 2016. **105**: p. 167-171.
190. Sun, Y., et al., *Biodegradable and renewable poly(lactide)-lignin composites: synthesis, interface and toughening mechanism.* Journal of Materials Chemistry A, 2015. **3**(7): p. 3699-3709.
191. Nagahama, K., et al., *Enhanced stereocomplex formation of enantiomeric polylactides grafted on a polyrotaxane platform.* Polymer Chemistry, 2013. **4**(6): p. 1769-1773.
192. Zhang, W., et al., *Preparation and characterization of stereocomplex aggregates based on PLA-P188-PLA.* RSC Advances, 2016. **6**(56): p. 50543-50552.
193. Watanabe, J., T. Eriguchi, and K. Ishihara, *Stereocomplex Formation by Enantiomeric Poly(lactic acid) Graft-Type Phospholipid Polymers for Tissue Engineering.* Biomacromolecules, 2002. **3**(5): p. 1109-1114.
194. Salerno, A., et al., *Macroporous and nanometre scale fibrous PLA and PLA-HA composite scaffolds fabricated by a bio safe strategy.* RSC Advances, 2014. **4**(106): p. 61491-61502.
195. Dadbin, S. and Y. Kheirkhah, *Gamma irradiation of melt processed biomedical PDLLA/HAP nanocomposites.* Radiation Physics and Chemistry, 2014. **97**: p. 270-274.
196. Lin, P.-L., et al., *Effects of hydroxyapatite dosage on mechanical and biological behaviors of polylactic acid composite materials.* Materials Letters, 2007. **61**(14–15): p. 3009-3013.
197. Ishii, S., et al., *Long-term study of high-strength hydroxyapatite/poly(L-lactide) composite rods for the internal fixation of bone fractures: A 2–4-year follow-up study in rabbits.* Journal of Biomedical Materials Research Part B: Applied Biomaterials, 2003. **66B**(2): p. 539-547.
198. Sun, H., et al., *Polylactide-hydroxyapatite nanocomposites with highly improved interfacial adhesion via mussel-inspired polydopamine surface modification.* RSC Advances, 2015. **5**(116): p. 95631-95642.
199. Du, K. and Z. Gan, *Shape memory behaviour of HA-g-PDLLA nanocomposites prepared via in situ polymerization.* Journal of Materials Chemistry B, 2014. **2**(21): p. 3340-3348.
200. Qiu, X., et al., *Hydroxyapatite Surface Modified by l-Lactic Acid and Its Subsequent Grafting Polymerization of l-Lactide.* Biomacromolecules, 2005. **6**(3): p. 1193-1199.
201. Hong, Z., et al., *Grafting polymerization of l-lactide on the surface of hydroxyapatite nano-crystals.* Polymer, 2004. **45**(19): p. 6699-6706.
202. Wang, Z., et al., *Enhanced in Vitro Mineralization and in Vivo Osteogenesis of Composite Scaffolds through Controlled Surface Grafting of l-Lactic Acid Oligomer on Nanohydroxyapatite.* Biomacromolecules, 2016. **17**(3): p. 818-829.
203. Tlotleng, M., et al., *Microstructures, hardness and bioactivity of hydroxyapatite coatings deposited by direct laser melting process.* Materials Science and Engineering: C, 2014. **43**: p. 189-198.
204. Wu, C.-S., *Improving Polylactide/Starch Biocomposites by Grafting Polylactide with Acrylic Acid – Characterization and Biodegradability Assessment.* Macromolecular Bioscience, 2005. **5**(4): p. 352-361.

205. Liao, C.-J., et al., *Thermal decomposition and reconstitution of hydroxyapatite in air atmosphere*. Biomaterials, 1999. **20**(19): p. 1807-1813.
206. Oyama, H.T. and S. Abe, *Stereocomplex Poly(lactic acid) Alloys with Superb Heat Resistance and Toughness.* ACS Sustainable Chemistry & Engineering, 2015. **3**(12): p. 3245-3252.
207. Bai, H., et al., *Significantly Improving Oxygen Barrier Properties of Polylactide via Constructing Parallel-Aligned Shish-Kebab-Like Crystals with Well-Interlocked Boundaries.* Biomacromolecules, 2014. **15**(4): p. 1507-1514.
208. *Semicrystalline Polymers*, in *Electron Microscopy of Polymers*. 2008, Springer Berlin Heidelberg: Berlin, Heidelberg. p. 295-327.
209. Zhang, M., B.-H. Guo, and J. Xu, *A Review on Polymer Crystallization Theories.* Crystals, 2017. **7**(1): p. 4.
210. Glicksman, M.E., *Thermodynamics of Crystal-Melt Phase Change*, in *Principles of Solidification: An Introduction to Modern Casting and Crystal Growth Concepts*. 2011, Springer New York: New York, NY. p. 27-51.
211. Hartmann, M.H., *High Molecular Weight Polylactic Acid Polymers*, in *Biopolymers from Renewable Resources*, D.L. Kaplan, Editor. 1998, Springer Berlin Heidelberg. p. 367-411.
212. Hoffman, J.D., G.T. Davis, and J.I. Lauritzen, *The Rate of Crystallization of Linear Polymers with Chain Folding*, in *Treatise on Solid State Chemistry: Volume 3 Crystalline and Noncrystalline Solids*, N.B. Hannay, Editor. 1976, Springer US: Boston, MA. p. 497-614.
213. Muthukumar, M., *Nucleation in Polymer Crystallization*, in *Advances in Chemical Physics*. 2004, John Wiley & Sons, Inc. p. 1-63.
214. *Crystallization of a polymer on a surface.* The Journal of Chemical Physics, 1998. **109**(22): p. 10033-10041.
215. *Kinetics of Phase Change. I General Theory.* The Journal of Chemical Physics, 1939. **7**(12): p. 1103-1112.
216. *Kinetics of Phase Change. II Transformation-Time Relations for Random Distribution of Nuclei.* The Journal of Chemical Physics, 1940. **8**(2): p. 212-224.
217. *Granulation, Phase Change, and Microstructure Kinetics of Phase Change. III.* The Journal of Chemical Physics, 1941. **9**(2): p. 177-184.
218. Arrhenius, S., *Über die Reaktionsgeschwindigkeit bei der Inversion von Rohrzucker durch Säuren*, in *Zeitschrift für Physikalische Chemie*. 1889. p. 226.
219. Zhang, Q., et al., *Isothermal and nonisothermal crystallization kinetics of nylon-46.* Journal of Polymer Science Part B: Polymer Physics, 2002. **40**(16): p. 1784-1793.
220. Cartier, L., T. Okihara, and B. Lotz, *Triangular Polymer Single Crystals: Stereocomplexes, Twins, and Frustrated Structures.* Macromolecules, 1997. **30**(20): p. 6313-6322.
221. Thomas, D.G. and L.A.K. Staveley, *573. Hysteresis in transitions in solids.* Journal of the Chemical Society (Resumed), 1951(0): p. 2572-2579.
222. Naffakh, M., C. Marco, and M.A. Gómez-Fatou, *Isothermal Crystallization Kinetics of Novel Isotactic Polypropylene/MoS2 Inorganic Nanotube Nanocomposites.* The Journal of Physical Chemistry B, 2011. **115**(10): p. 2248-2255.
223. Yue, H., et al., *Macroscopic CNT fibres inducing non-epitaxial nucleation and orientation of semicrystalline polymers.* Scientific Reports, 2015. **5**: p. 16729.
224. Dobreva, T., et al., *Nonisothermal melt-crystallization kinetics of isotactic polypropylene synthesized with a metallocene catalyst and compounded with different quantities of an α nucleator*. Journal of Applied Polymer Science, 2008. **109**(2): p. 1338-1349.

225. Visakh, P.M. and O.B. Nazarenko, *Thermal Degradation of Polymer Blends, Composites and Nanocomposites*, in *Thermal Degradation of Polymer Blends, Composites and Nanocomposites*, P.M. Visakh and Y. Arao, Editors. 2015, Springer International Publishing: Cham. p. 1-16.
226. O'Donnell, J.H., *Chemistry of Radiation Degradation of Polymers*, in *Radiation Effects on Polymers*. 1991, American Chemical Society. p. 402-413.
227. Beachell, H.C. and S.P. Nemphos, *Oxidative Degradation of Polymers in Presence of Ozone*, in *OZONE CHEMISTRY AND TECHNOLOGY*. 1959, AMERICAN CHEMICAL SOCIETY. p. 168-175.
228. Yang, R., J. Zhao, and Y. Liu, *Oxidative degradation products analysis of polymer materials by pyrolysis gas chromatography–mass spectrometry.* Polymer Degradation and Stability, 2013. **98**(12): p. 2466-2472.
229. Capone, C., et al., *Thermal and mechanical degradation during polymer extrusion processing.* Polymer Engineering & Science, 2007. **47**(11): p. 1813-1819.
230. Yousif, E. and R. Haddad, *Photodegradation and photostabilization of polymers, especially polystyrene: review.* SpringerPlus, 2013. **2**: p. 398.
231. Lee, K.-H. and D.-H. Shin, *Catalytic degradation of waste polyolefinic polymers using spent FCC catalyst with various experimental variables.* Korean Journal of Chemical Engineering, 2003. **20**(1): p. 89-92.
232. Scherer, T.M., et al., *Broad-Based Screening of Polymer Biodegradability*, in *Polymers from Renewable Resources*. 2001, American Chemical Society. p. 254-280.
233. Mayer, J.M., et al., *Biodegradation of Polymer Films in Marine and Soil Environments*, in *Hydrogels and Biodegradable Polymers for Bioapplications*. 1996, American Chemical Society. p. 159-170.
234. Tokiwa, Y., et al., *Biodegradation of a Sugar Branched Polymer Consisting of Sugar, Fatty Acid, and Poly(vinyl alcohol).* Macromolecules, 2000. **33**(5): p. 1636-1639.
235. Hazrat, M.A., et al., *Utilization of Polymer Wastes as Transport Fuel Resources- a Recent Development.* Energy Procedia, 2014. **61**: p. 1681-1685.
236. Shlensky, O.F., *Thermal decomposition of polymeric materials: Characteristics of kinetics at non-isothermal heating.* Journal of thermal analysis, 1983. **28**(2): p. 421-430.
237. Huang, S.J., *Polymer Waste Management–Biodegradation, Incineration, and Recycling.* Journal of Macromolecular Science, Part A, 1995. **32**(4): p. 593-597.
238. Yew, G.H., et al., *Water absorption and enzymatic degradation of poly(lactic acid)/rice starch composites.* Polymer Degradation and Stability, 2005. **90**(3): p. 488-500.
239. Chien, Y.-C., et al., *Combustion Kinetics and Emission Characteristics of Polycyclic Aromatic Hydrocarbons from Polylactic Acid Combustion.* Journal of the Air & Waste Management Association, 2010. **60**(7): p. 849-855.
240. Oksman, K., M. Skrifvars, and J.F. Selin, *Natural fibres as reinforcement in polylactic acid (PLA) composites.* Composites Science and Technology, 2003. **63**(9): p. 1317-1324.
241. Le Duigou, A., P. Davies, and C. Baley, *Seawater ageing of flax/poly(lactic acid) biocomposites.* Polymer Degradation and Stability, 2009. **94**(7): p. 1151-1162.
242. Taib, R.M., et al., *Properties of kenaf fiber/polylactic acid biocomposites plasticized with polyethylene glycol.* Polymer Composites, 2010. **31**(7): p. 1213-1222.
243. Qian, S., et al., *Poly(lactic acid) biocomposites reinforced with ultrafine bamboo-char: Morphology, mechanical, thermal, and water absorption properties.* Journal of Applied Polymer Science, 2016. **133**(20): doi: 10.1002/app.43425.
244. Urbanovici, E. and E. Segal, *General Kinetic Equation for Solid State Reactions.* Journal of Thermal Analysis and Calorimetry, 1999. **55**(3): p. 919-924.

245. Chrissafis, K., *Kinetics of thermal degradation of polymers.* Journal of Thermal Analysis and Calorimetry, 2009. **95**(1): p. 273-283.
246. Ozawa, T., *Kinetic analysis of derivative curves in thermal analysis.* Journal of thermal analysis, 1970. **2**(3): p. 301-324.
247. Friedman, H.L., *Kinetics of thermal degradation of char-forming plastics from thermogravimetry. Application to a phenolic plastic.* Journal of Polymer Science Part C: Polymer Symposia, 1964. **6**(1): p. 183-195.
248. Kissinger, H.E., *Reaction Kinetics in Differential Thermal Analysis.* Analytical Chemistry, 1957. **29**(11): p. 1702-1706.
249. Augis, J.A. and J.E. Bennett, *Calculation of the Avrami parameters for heterogeneous solid state reactions using a modification of the Kissinger method.* Journal of thermal analysis, 1978. **13**(2): p. 283-292.
250. Doyle, C.D., *Estimating isothermal life from thermogravimetric data.* Journal of Applied Polymer Science, 1962. **6**(24): p. 639-642.
251. Flynn, J.H., *The isoconversional method for determination of energy of activation at constant heating rates.* Journal of thermal analysis, 1983. **27**(1): p. 95-102.
252. Takeo, O., *A New Method of Analyzing Thermogravimetric Data.* Bulletin of the Chemical Society of Japan, 1965. **38**(11): p. 1881-1886.
253. Flynn, J.H.F. and L.A. Wall, *General Treatment of the Thermogravimetry of Polymers.* Journal of Research of the National Bureau of Standards, 1966. **70A**: p. 487-523.
254. Coats, A.W. and J.P. Redfern, *Kinetic Parameters from Thermogravimetric Data.* Nature, 1964. **201**(4914): p. 68-69.
255. Badia, J.D., et al., *Reprocessed polylactide: Studies of thermo-oxidative decomposition.* Bioresource Technology, 2012. **114**: p. 622-628.
256. Zou, H., et al., *Thermal degradation of poly(lactic acid) measured by thermogravimetry coupled to Fourier transform infrared spectroscopy.* Journal of Thermal Analysis and Calorimetry, 2009. **97**(3): p. 929.